Experimental study and modelling of the elastoplastic behaviour of unbound granular materials under large number of cyclic loadings at various initial hydric states

Peng Jing

UNIVERSITÉ DE STRASBOURG

ÉCOLE DOCTORALE MSII (ED n°269)

INSA de Strasbourg

laboratoire des sciences de l'ingénieur, de l'informatique et de l'imagerie (ICUBE)-UMR 7357

THÈSE présentée par :

Peng JING

soutenue le : **09 Mars 2017**

pour obtenir le grade de : **Docteur de l'Université de Strasbourg**

Discipline/ Spécialité : **Mécanique, Génie Civil**

ETUDES DE L'EFFET DES FINES ET DE LA TENEUR EN EAU SUR LE COMPORTEMENT HYDROMECANIQUE DES MATERIAUX GRANULAIRES

THÈSE dirigée par :

M. CHAZALLON Cyrille	Professeur, INSA de Strasbourg
M. NOWAMOOZ Hossein	Maître de conférences (HDR), INSA de Strasbourg
M. MIGAULT Bernard	Maître de conférences (HDR), INSA de Strasbourg

RAPPORTEURS :

M. CUI YuJun	Professeur, École des Ponts ParisTech
M. HORNYCH Pierre	Chargé de recherches (HDR), IFSTTAR

AUTRE MEMBRE DU JURY :

Mme. HATTAB Mahdia	Professeur, Université de Lorraine

UNIVERSITY OF STRASBOURG

Experimental study and modelling of the elastoplastic behaviour of unbound granular materials under large number of cyclic loadings at various initial hydric states

by

Peng JING

A thesis submitted in partial fulfillment for
the degree of Doctor of Philosophy

in the

Doctoral School of MSII

March 2017

Acknowledgements

The work presented in this dissertation collected the research I have carried out during my PhD at the National Institute of Applied Science of Strasbourg (INSA-Strasbourg) and the Laboratory ICube in the University of Strasbourg, France. This research was supported by the China Scholarship Council (CSC).

Here, I am deeply grateful to my PhD supervisor, Prof. Cyrille CHAZALLON, for his guidance, assistance, understanding and patience during my PhD studies. He encouraged me to grow as an independent thinker. My sincere thanks also go to my PhD advisor, Assoc Prof. Hossein NOWAMOOZ, for his invaluable insights and careful inspection for every detail. I learned a lot from them in every discussion. I would also like to thank my co-supervisor, Assoc Prof. Bernard MIGAULT, for his continuous encouragement and invaluable assistance.

I would like to thank my colleagues in the team of Civil Engineering and Energy at INSA-Strasbourg, Assoc Prof. Saida MOUHOUBI, Assoc Prof. Georg KOVAL and Assoc Prof. Juan Carlos QUEZADA. Special thanks to my fellow PhD students, Xuan Nam HO, Ioana Maria ARSENIE, Kai LI, Quoc Tuan TRINH, Andrea THEMELI, Xiao Feng GAO, Loba SAGNOL, Gui Xian LIU, Hossein ASSADOLLAHI, Fu Jiao TANG, Laura GAILLARD and Anicet DANSOU, for all the great moments we have spent.

Finally, and most importantly, I wish to thank my parents and my brother for their endless unconditional loves, encouragements and supports throughout my life. Especially I would like to thank my wife, for her support, encouragement, quiet patience and unwavering love that made me complete my PhD research.

CONTENTS

LIST OF FIGURES

LIST OF TABLES

INTRODUCTION

Low traffic pavements with a thin bituminous surfacing, granular base and sub-base layers represent approximately 60% of the road network in France.

In low-traffic pavements, granular material layers play an important role in the overall performance of the structure, especially with the deformation behavior. Thus, in pavement design, a significant objective is to control or limit the loss of serviceability of granular material layers resulting from traffic loading and environmental related deterioration.

Among different factors, the effect of fine content as well as the water content on deformation behavior of granular materials are pretty significant.

In addition, the granular material layers located above the underground water level are in an unsaturated state. The unsaturated state of soil is described by the negative pore water pressure or suction which is strongly related to the water content (degree of saturation) and fine content. The increase of suction plays a key role in mechanical behaviour of the unsaturated soils which could strengthen the resistance of granular materials.

A world-wide interest in research on granular material in pavements in the past decades has resulted in great progresses for the evaluation or prediction of the mechanical performance of granular materials under traffic loads. However, few studies have been conducted on the coupled effects of water content, fine content (microstructure, water sensitivity) and suction (unsaturated state) on the hydromechanical behaviour of granular materials.

Objectives and scope

The effects of fine content and water content on the hydromechanical behaviour of granular material layers aren't taken into account in pavement design in France or Europe.

In this study, first we try to estimate the evolution of deformation behaviour (permanent and resilient) of granular materials under repeated loads at various water contents and fine contents through the repeated load triaxial tests (RLTTs). Subsequently, the effect of suction which is expected to represent the coupled effects of water content and fine content on deformation behaviour of granular materials, will be investigated by the soil water retention curve (SWRC). In addition, we are also interested in the shakedown behaviour of granular materials under repeated loads with the effects of water content and fine content instead of only stress level as usual.

The analytical solutions to predict permanent or resilient deformation behaviour of granular materials under repeated loads will be another main objective in this study. Based on the experimental results, the existing permanent deformation models will be improved to take into account the effects of fine content and water content or suction and the existing resilient deformation model will be modified to accommodate to broader scope of fine content and water content.

Outline of thesis

This thesis is organized into five chapters as well as an introduction and a general conclusion.

Chapter I, "Literature review", contains four parts. The first part introduces a flexible pavement structure of low traffic roads and the principle of design for this pavement structure. The second part summarizes the properties of granular material in low traffic pavement including stress state, deformation behaviour and unsaturated state. The third part reviews the permanent deformation behaviour of granular material from three aspects: influencing factors, shakedown behaviour and existing prediction models. At the end, the last part presents the resilient deformation behaviour of granular material according to influencing factors and existing prediction models.

Chapter II, "Material studied and laboratory testing" first presents the basic characteristics of studied materials: grading, methylene blue value and compaction. Subsequently, the suction measurement techniques are introduced as filter paper method and tensiometer

method. At the end, the RLTT is presented: sample preparation, experimental device and procedure.

Chapter III, "Permanent deformation behaviour of a granular material" presents the effects of fine content, water content and suction on the permanent axial deformation behavior of Missillac sand based on the results of the single-stage and multi-stage RLTTs combining with the results of suction measurement. For the analytical modelling, two new approaches based on the existing models are proposed to predict permanent axial deformation behaviour of granular materials respectively in single-stage tests and multi-stage tests: the first based on the water content and fine content and the other based on the suction value.

Chapter IV, "Resilient deformation behaviour of a granular material" first presents the resilient deformation behaviour of Missillac sand at different fine contents and water contents in RLTTs: evolution of resilient volumetric and deviatoric deformations and anisotropy effect. Subsequently, for the modelling analysis, a modified Boyce-Hornych model is proposed with the anisotropy effect to predict the resilient volumetric and deviatoric deformations. Finally, a short discussion is proposed to improve the modelling results based on the effective stress concept.

Chapter V, "Shakedown behaviour of a granular material" analyzes the shakedown behaviour of Missillac sand under repeated loads with the effects of water content, fine content and suction. Based on the classification shakedown categories, the boundary separates the stable and unstable states obtained in Δp - Δq - s/s^* space.

In the additional chapter, "Conclusions and perspectives", the findings of this study are summarized and the potential future studies are also presented.

Two Appendices are included to provide supplementary information of UGM: Appendix A presents a set of new RLTT devices for UGM samples; Appendix B presents the results of suction measurement and RLTTs for UGM Maraîchères.

The structure of this dissertation is presented in *Figure.Introduction.1*.

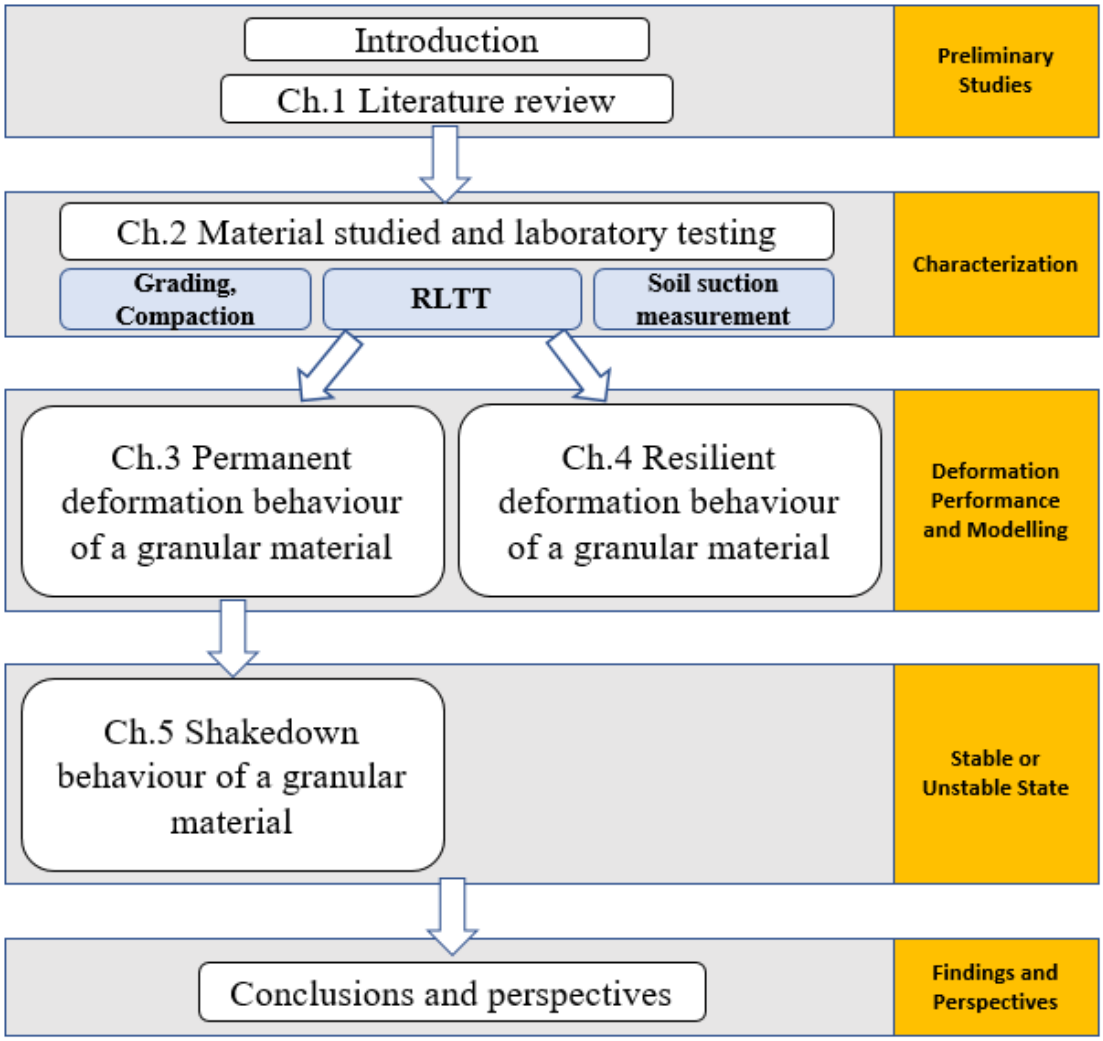

Figure Introduction.1. Structure of this dissertation

CHAPTER I. LITERATURE REVIEW

I.1. Introduction

The main objective of this chapter is to present a literature review of the properties and the hydro-mechanical behaviour of the unsaturated granular material under repeated loads in low traffic pavements. Firstly, a description of the low traffic pavement structure is introduced to understand the role of granular layers. Then, an overview of granular material properties in low traffic pavements is presented including the stress state, deformation behaviour, characterization of granular materials in laboratory and unsaturated state. Finally, the permanent deformation behaviour and resilient deformation behaviour are introduced in detail.

I.2. Description of the flexible pavement structure

I.2.1. Flexible pavement structure

A flexible pavement structure of low traffic roads represents approximately 60% of the road network in France or Europe. This low traffic pavements in general is a layered structure of selected materials placed on top of a natural or filled subgrade: a relatively thin bituminous surface layer (less than 15 cm) are supported by granular base and/or subbase layers (between 20 and 60 cm) assembly located on subgrade as shown in *Figure I.1*.

These granular layers play a key role in mechanical performance of pavement structures, which have three main functions as follows (Allou, 2006):

- The granular layers have to perform as a short-term construction platform.
- The granular layers could improve the distribution of traffic stress applied on the surface layer by optimized design to maintain the deformation at an acceptable level.
- The granular materials are good for drainage.

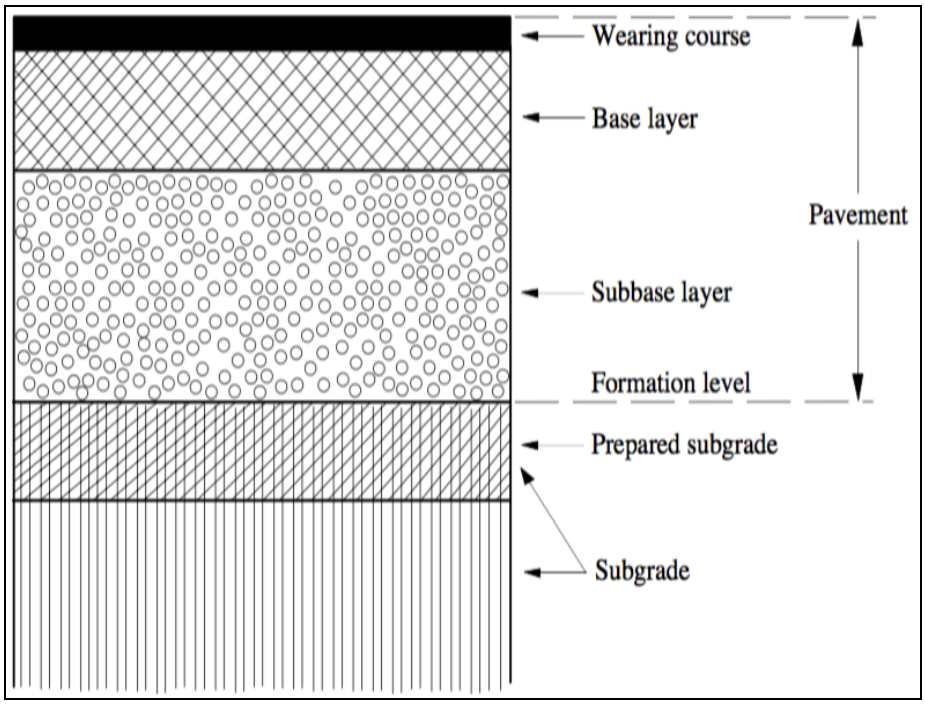

Figure I.1. Structure of flexible pavements (Lekarp, 1997)

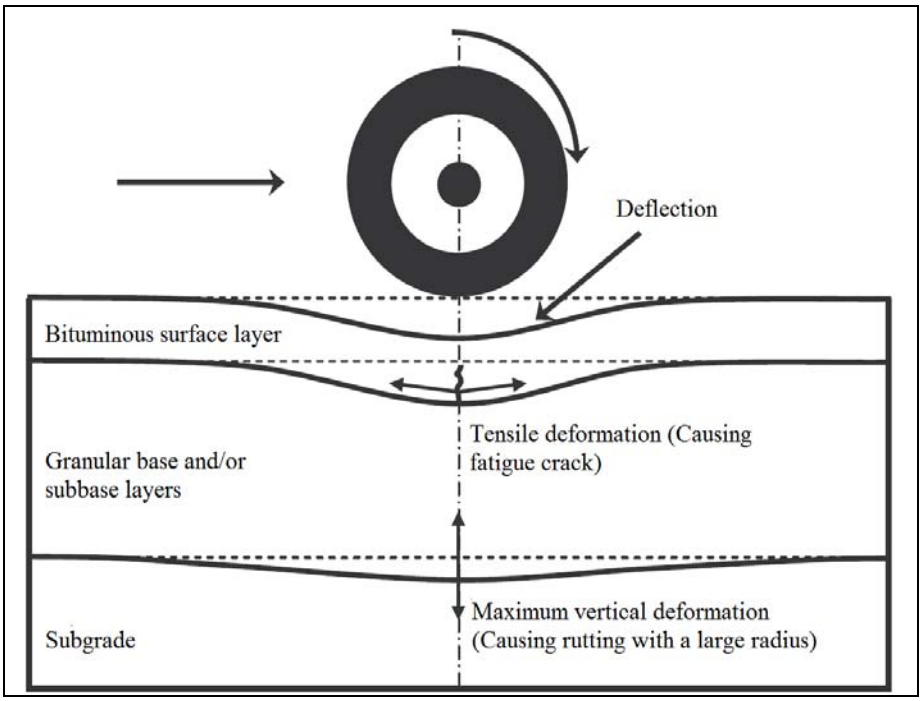

Figure I.2. Critical deformation considered in low traffic pavements (Allou, 2006)

The bituminous cover is relatively thin and these granular layers have a low rigidity. As a result, the high vertical traffic loads transmitted to granular layers with a little lateral diffusion produce permanent deformation on the surface of the pavement. The evolution of the deformation leads to two main modes of degradation: the large-radius rutting and the fatigue crack of the bituminous cover as shown in *Figure I.2*. Besides, these two modes of degradation will facilitate the infiltration of water into the pavement structure causing the acceleration of degradation.

I.2.2. Principle of design of flexible pavement structure

There are two kinds of basic methods in flexible pavement design: empirical methods and analytical methods.

The empirical methods are widely used in Europe and USA and are based on the experimental data in situ and/or the laboratory experimental results of pavement materials, like the CBR method and the AASHTO method.

However, during the service life, the pavements are subjected to complex mechanical, water, thermal and chemical effects which change the properties of pavement materials a lot. At the same time, the traffic volume is constantly increasing and new type structures are developing.

As a result, the analytical method which is based on the theoretical analysis of the stress and deformation in pavement layers, mechanical properties of pavement materials and environmental changes is necessary. This necessity has led to the development and application since the 1970s such as French analytical method (Guide technique SETRA-LCPC, 1994) and, more recently, the Super Pave method and the implementation of the AASHTO design guide in 2002 (Ho, 2013).

Empirical method

CBR method

The CBR method is the most widely known empirical pavement design method determining the total thickness of pavement. CBR method was developed by the California Division of Highways in the late nineteen-thirties.

The data required for flexible pavement design are CBR value of soil subgrade and wheel load in KG or KN. Based on the given CBR values and the thickness required to carry the wheel load value, from the below chart, an appropriate thickness design curve is selected to give the total thickness of pavement.

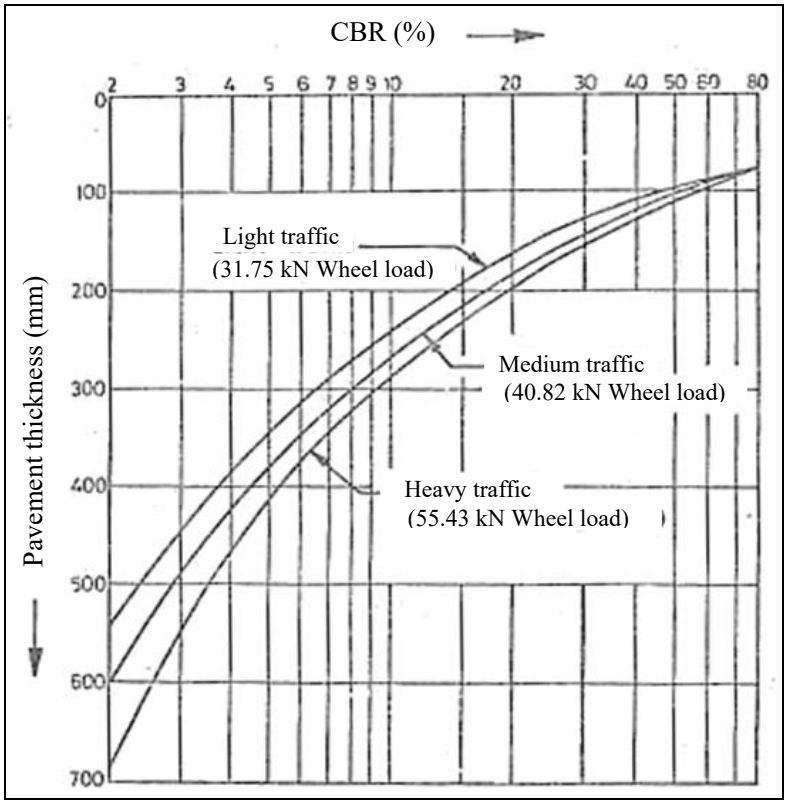

Figure I.3. CBR method - thickness design curve

The performance criterion of the design curve limits the shear stress at the top of the subgrade to a level below failure. In this method, the design criterion of unbound granular layers and the bituminous surface layer isn't taken into account.

AASHTO method

The AASHTO Guide for the flexible pavement design was developed based on the AASHTO road test in 1993. The basic philosophy of this method is achieving the specific total traffic volume and a minimum level of serviceability desired at end of the service life (Araya, 2011). In this guide, a "structural number *SN*" is introduced which could be obtained from a nomograph based on the soil support and the estimated total traffic volume, as expressed by:

$$SN = \sum a_i D_i m_i \quad \text{(I.1)}$$

where *SN* is structural number; a_i is the i^{th} layer coefficient; D_i is the i^{th} layer thickness and m_i is the i^{th} layer drainage coefficient.

The performance of the granular layers is represented by the layer coefficients which are related to resilient modulus of the layers. The resilient modulus should be determined by repeated load triaxial tests (RLTTs). Finally, the thickness of each granular layer could be estimated.

Analytical method

Guide technique SETRA-LCPC

The French analytical method for flexible pavement design, Guide technique SETRA-LCPC, (1994), is based on the calculation of pavement structure to determine the stresses produced by traffic loads and the maximum permissible strain of the structure. This method is performed as following steps:

- A pre-design of pavement structure is established for the estimated service life: the type and the thickness of the different layers of the structure are defined based on the expected traffic volume and the mechanical performances of the chosen materials.

- The stresses and deformations induced in the pavement structure and the subgrade are then calculated with the software ALIZÉ/LCPC developed by the IFSTTAR (Institut Français des Sciences et Technologies des Transports, de l'Aménagement et des Réseaux).

- The fatigue and rutting are verified in an admissible value based on the stress and deformation calculated in last step.

In the Guide technique SETRA-LCPC, (1994), pavements are classified based on their ultimate traffic capacity during the life service. The *Ti* value is defined as the traffic level estimated by the number of average daily heavy goods vehicles (poids lourds journalier moyen-MJA) (with payload > 5 tonnes). The different traffic levels are summarized in *Table I.1.* For flexible pavement, the *Ti* value is defined less or equal to T2.

Level	T5	T4	T3		T2		T1		T0		TS		TEX
			$T3^-$	$T3^+$	$T2^-$	$T2^+$	$T1^-$	$T1^+$	$T0^-$	$T0^+$	TS^-	TS^+	
MJA	0	25	50	85	150	200	300	500	750	1200	2000	3000	5000

Table I.1. Classification of the traffic level (Guide technique SETRA-LCPC, 1994)

In addition, the characteristics of the unbound granular material (UGM) in supporting layers are described simply by the Young's Modulus which is widely used in practice. *Table I.2* summarizes the values of the Young's Modulus of UGM for a low traffic pavement with a Poisson's coefficient of 0.35.

<table>
<tr><td colspan="2">Low traffic pavement : $T \leq T3$</td></tr>
<tr><td>Base layer</td><td>Category 1 : $E_{UGM} = 600$ MPa
Category 2 : $E_{UGM} = 400$ MPa
Category 3 : $E_{UGM} = 200$ MPa</td></tr>
<tr><td>Subbase layer and prepared subgrade</td><td>$E_{UGM}[1] = k\ E_{\text{Platform support}}$
$E_{UGM}[$ layer i $] = k\ E_{GNT}[$ layer (i-1) $]$
<table><tr><td>Category</td><td>1</td><td>2</td><td>3</td></tr><tr><td>k</td><td>3</td><td>2,5</td><td>2</td></tr></table>E_{UGM} limited by the corresponding values in Base layer</td></tr>
</table>

Table I.2. Young's Modulus of UGM in pavement design for the case Ti ≤ T3 (Guide technique SETRA-LCPC, 1994)

Finally, the criterion of design of the low traffic pavement structure is the limitation of the vertical deformation ε_z at the top of the prepared subgrade, which is expressed by:

$$\varepsilon_z \leq A\left(NE\right)^{-0.222} \quad \text{(I.2)}$$

where, A = 0.016 for a traffic (T <T3) and A = 0.012 for a traffic (T ≥T3); NE is the number of equivalent axles, which is expressed by:

$$NE = N.CAM \quad \text{(I.3)}$$

where, N is the cumulative number of heavy vehicles during the calculated period. CAM is the average aggression coefficient of the heavy goods vehicles compared to the reference axle weight. *Table I.3* presents the CAM values based on the traffic classification.

Level	T5	T4	T3-	T3+	≥T2
CAM	0.4	0.5	0.7	0.8	1

Table I.3. Values of the average aggression coefficient of the heavy goods vehicles (Guide technique SETRA-LCPC, 1994)

Based on the introduction of two methods of pavement design, it can be stated that both empirical method and analytical method still have insufficiencies as follows:

- Under repeated loads, the hydro-mechanical behaviour and the effect of fine content cannot be taken into account for granular materials.
- During the pavement life service, the granular materials show the anisotropic non-linear elastoplastic deformation behaviour, whereas it is simplified as isotropic linear elastic deformation behaviour in pavement design.

I.3. Granular material in low traffic pavement

I.3.1. Stress in granular material layer

Granular materials are widely used in base and subbase layers of low traffic pavements to provide load distribution and bearing capacity by the contact between particles. During their service life, a pavement structure bears a large number of stress pulses consisting of vertical, horizontal and shear stress components as shown in *Figure I.4.* These stresses change all the time. The vertical and horizontal stresses are positive in the granular layers while the shear stress is reversed as load passes producing a rotation of the principal stresses (not only the direction but also the values).

The stress state of granular materials under the repeated traffic loads is really complex and difficult to reproduce in laboratory. In the past decades, several kinds of test methods have been developed to study the mechanical behaviour of granular materials. RLTT is the most representative method even though the rotation of the direction of the principal stresses aren't taken into account. Besides, the development of hollow cylinder apparatus make it possible to simulate rotation of the direction of principal stresses.

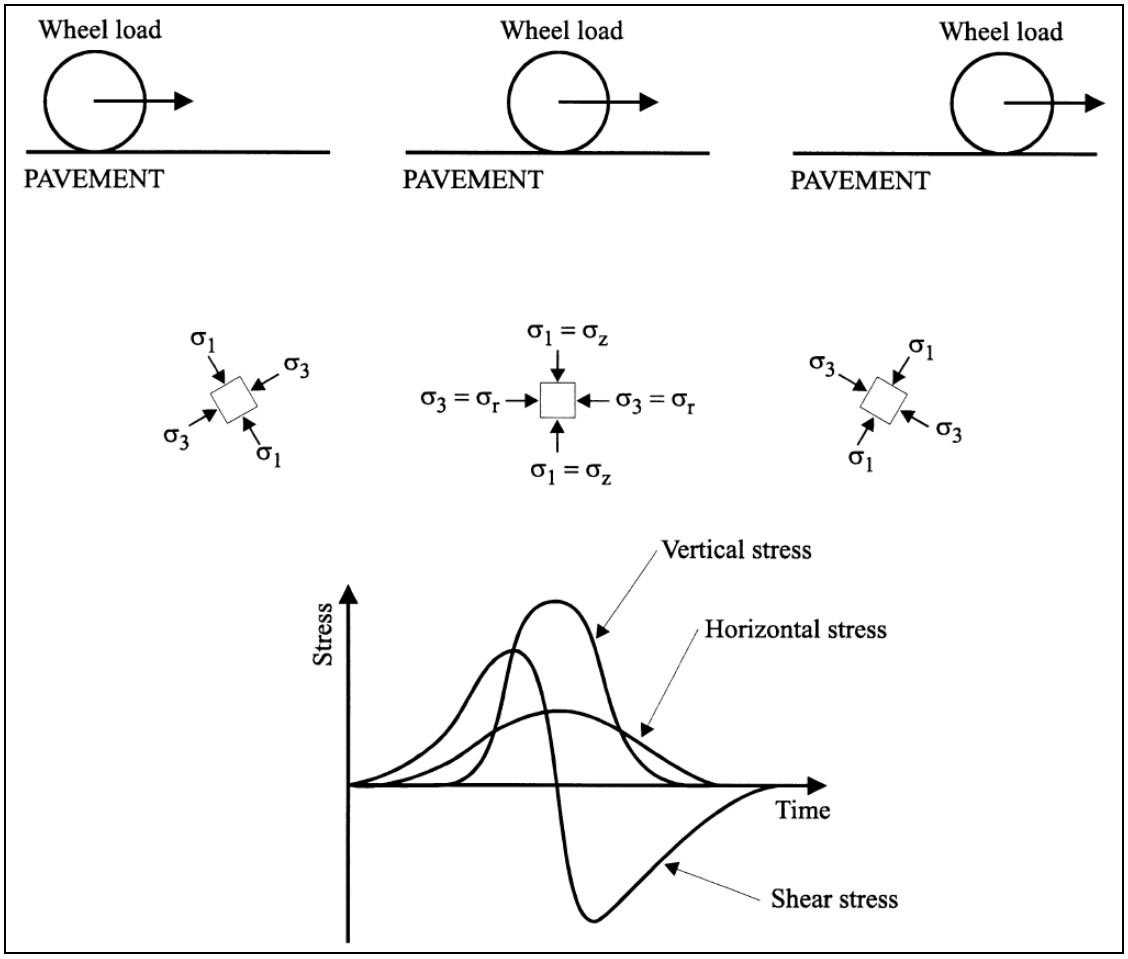

Figure I.4. Stresses beneath a rolling wheel load (Lekarp & Dawson, 1998)

I.3.2. Deformation in granular material layer

Granular materials are basically an assembly of a large number of individual cohesionless grains of different shapes and sizes. As a result, the cohesiveness of granular materials could be ignored except for the cohesion force caused by suction in unsaturated state. In general, the contact forces between particles provide the main resistance to applied loads by generating

corresponding deformation. There are two mechanisms which can be used to explain the deformation of granular materials (Davalle, 1991):

- Compressibility and rearrangement of grains (Slippage and rotation of grains).
- Breakage and crushing of grains.

It suggests that the displacement between grains causes the deformation of granular materials.

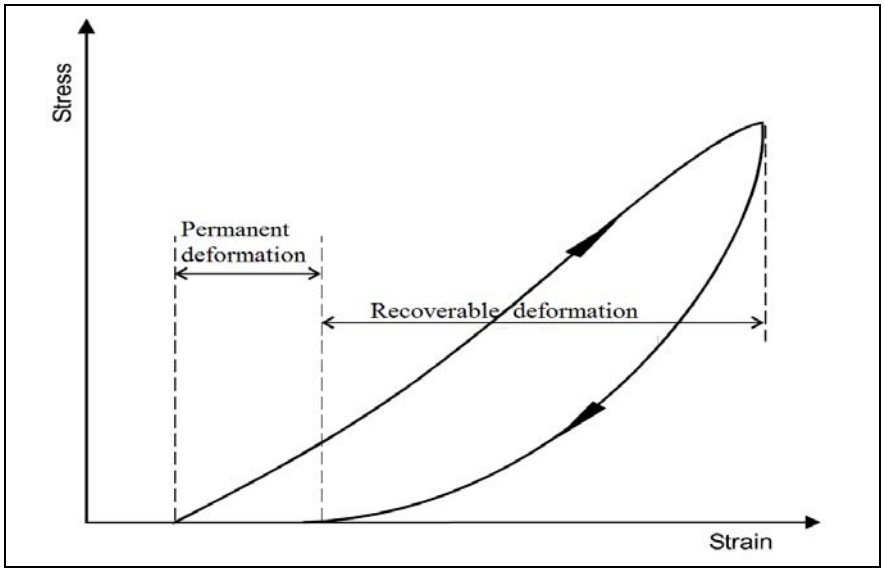

Figure I.5. Typical deformation of granular materials during one loading cycle

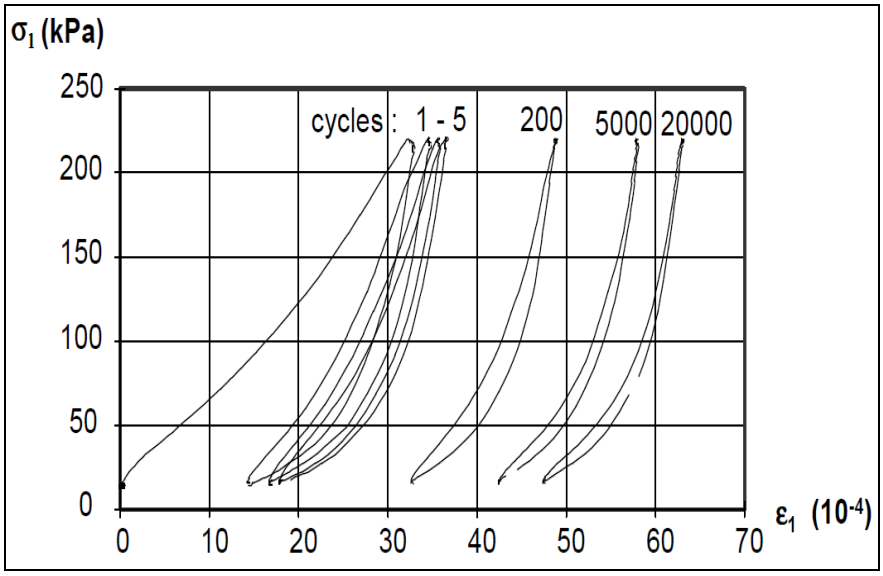

Figure I.6. Typical deformation of granular materials under cyclic loading (Hornych et al, 1998)

Figure I.5 presents the typical deformation behaviour of granular materials during one loading cycle. It can be stated that the behaviour of granular materials under compressive stresses is highly complex which exhibits both permanent deformation and recoverable deformation. Besides, the relationship between stress and strain/deformation is represented by non-linear curve with a clear hysteresis loop.

Granular materials bear a large number of cyclic traffic load during their service life. *Figure I.6* shows a typical deformation behaviour of granular materials under cyclic loads. It confirms that the recoverable deformation and permanent deformation happen in each loading cycle. The permanent deformation accumulates and lessens gradually with increase of number of cycles and reach a stable value after a sufficient amount of loading cycles.

It is noticeable that the recoverable deformation could be treated as resilient deformation only when the permanent deformation is stable. In some researches, these two concepts are not distinguished very well. In the following parts, we will use "resilient/recoverable deformation" referring to the recoverable deformation in reality which is presented as "resilient deformation" in the literatures.

I.3.3. Characterization of granular material

As introduced in section I.2, characterization of granular materials is an essential process in the empirical and analytical pavement design methods. The response of the materials to external traffic loads and environment changes can be obtained by pavement loading tests or laboratory techniques.

The pavement loading test could simulate the stress state in materials and avoid soil disturbance. However, the difficulty of reproducing the expected number of loading cycles and the cost cannot be ignored. In the past decades, many laboratory techniques have been developed to investigate bearing capacity, shear strength and degradation of pavement materials such as, CBR test (bearing capacity), K-Mould test (shear strength), Triaxial test (shear strength, cyclic performance) and Hollow Cylinder Apparatus shear test (shear strength). In this section, the RLTT, which is widely used to study the granular materials in pavement, is reviewed in detail.

Repeated load triaxial test

RLTT is a common test to investigate the mechanical behaviour of granular materials. It is used to simulate the pavement loading conditions to describe the resilient deformation behaviour (Lekarp et al., 2000a; Caicedo et al., 2009; Cary & Zapata, 2011; Nowamooz et al., 2011; Bilodeau & Doré, 2012; Nowamooz et al., 2013; Ho et al., 2014a; 2014b; 2014c; Duong et al., 2016; Salour & Erlingsson, 2015a) or permanent deformation behaviour (Hornych et al., 1993; Lekarp et al., 2000b; Gidel et al., 2001; Werkmeister et al., 2004; Puppala et al., 2009; Trinh et al., 2012; Duong et al., 2013; Salour & Erlingsson, 2015b).

Figure I.7 presents the principle of typical RLTT: a variable axial compression stress (σ_1) and a variable confining pressure (σ_3) provided by a pneumatic/liquid loading system are applied on a cylindrical sample of granular materials in a triaxial cell with a large number of loading cycles. The cylindrical samples are compacted by vibrating hammer (NF EN 13286-4, 2003) or vibrocompression (NF P 98-230-1, 1992) commonly. It is worth noting, based on the test results of Balay et al., (1998), the samples compacted in 7 layers with vibrating hammer method had a good correspondence of dry density to the vibrocompression method as shown in *Figure I.8*.

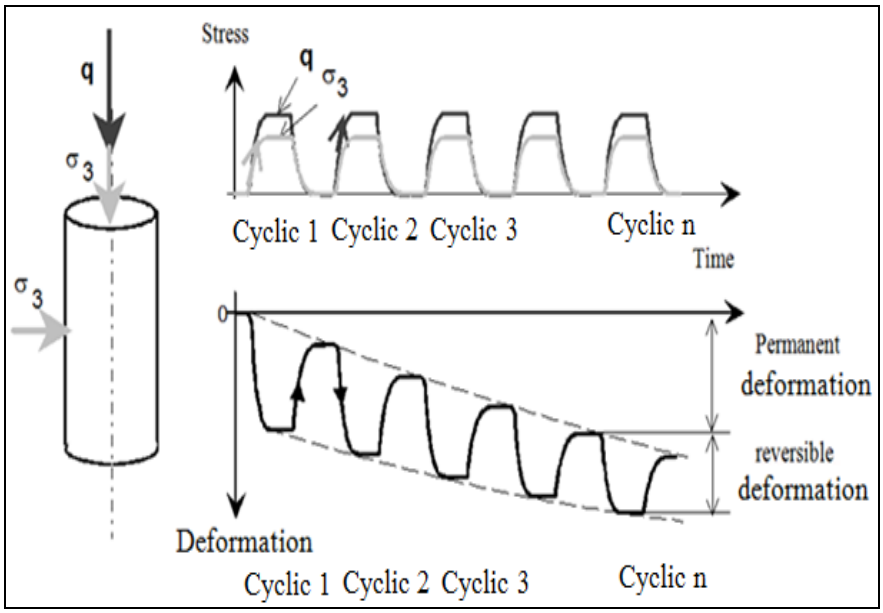

Figure I.7. Principle of typical repeated load triaxial test

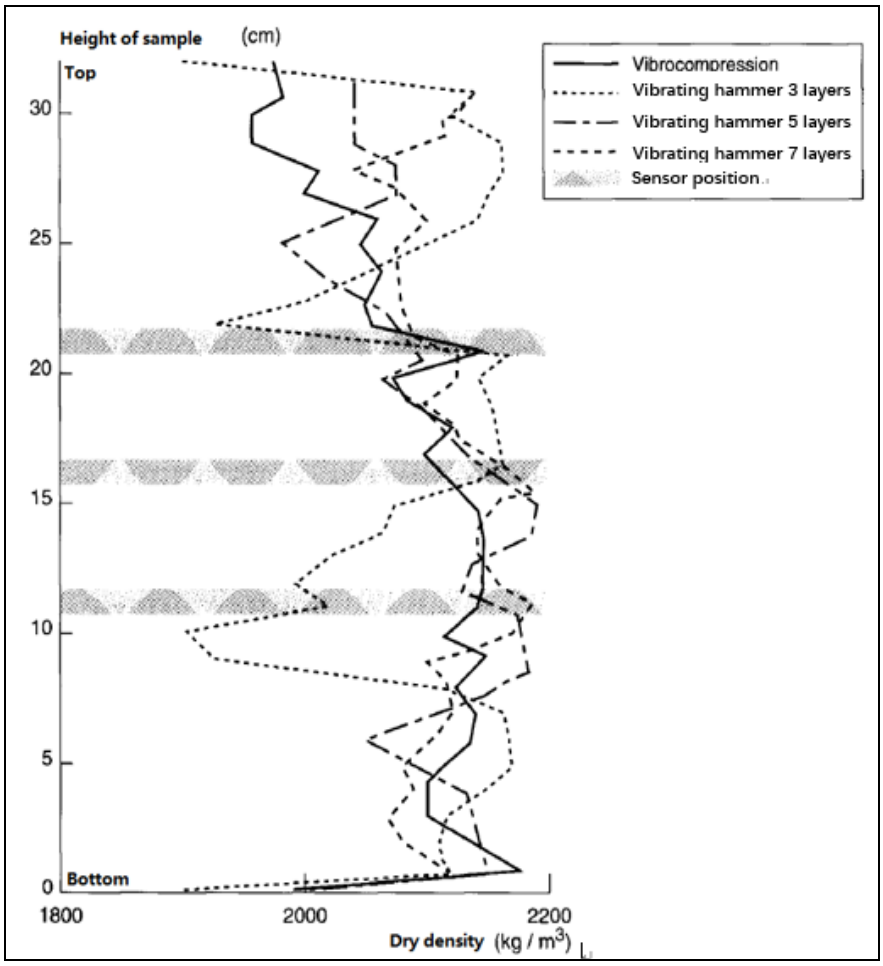

Figure I.8. Comparison of vibrating hammer method and vibrocompression method (Balay & al., 1998)

For the RLTTs, the different stress paths ($\Delta q/\Delta p$) can be applied on the samples and some improved RLTT can also control the suction condition by adjusting the air pressure and water pressure in the sample. The system can measure the axial force (q) directly by a transducer from the head of sample and a set of displacement transducer (radial and vertical) provides the measurement of radial deformation (ε_3) and axial deformation (ε_1) of the sample which make it possible to study resilient or permanent deformation behaviour.

For a triaxial test, the stress invariants are the mean normal stress (p) and the deviator stress (q) defined as:

$$p = \frac{\sigma_1 + 2\sigma_3}{3} \tag{I.4}$$

$$q = \sigma_1 - \sigma_3 \tag{I.5}$$

where, σ_1 is the axial compression stress and σ_3 is the confining pressure.

The corresponding strain invariants are the volumetric deformation (ε_v) and the deviatoric deformation (ε_q) defined as:

$$\varepsilon_v = \varepsilon_1 + 2\varepsilon_3 \tag{I.6}$$

$$\varepsilon_q = \frac{2(\varepsilon_1 - \varepsilon_3)}{3} \tag{I.7}$$

where, ε_1 is the axial deformation and ε_3 is the radial deformation.

During RLTT, the resilient deformation behaviour can be studied following the procedures defined by a French normal NF EN 13286-7. The sample is subjected to a conditioning phase to stabilize the permanent deformation, which consists of a large number of loading cycles with a given frequency. Ho et al., (2014c), investigated the behaviour of Missillac sand (a well-graded sandy soil) and noted that an equilibrium state reached after approximately 10,000 load applications. For UGM, Hornych et al., (2007), showed that the necessary number of cycles was higher than 50,000.

For the permanent deformation behaviour, due to the limitation of the consuming time and the cost of material, this is obviously not realistic to perform RLTTs on different granular material samples to determine the permanent axial deformation at different stress levels. For this reason, multi-stage tests are often performed with Gidel method (Gidel et al., 2001): One sample is subjected to several loading stages with different stress levels for a given stress path.

I.3.4. Unsaturated granular material

In soil mechanics, when the soil pores are filled by more than one fluid, e.g. water and air, the porous material is termed as unsaturated soil whose *Sr* is less than 1. There are three phases in unsaturated soil: the solid phase, the water phase and the air phase. And some theories treat air-water interface or the contractile skin (Fredlund & Morgenstern, 1977) as the fourth phase.

Soil suction

Soil suction (total suction) is composed of matric suction and osmotic suction. The matric suction depends on capillary action, soil structure and surface tension. The osmotic suction depends on the dissolved salt in soil.

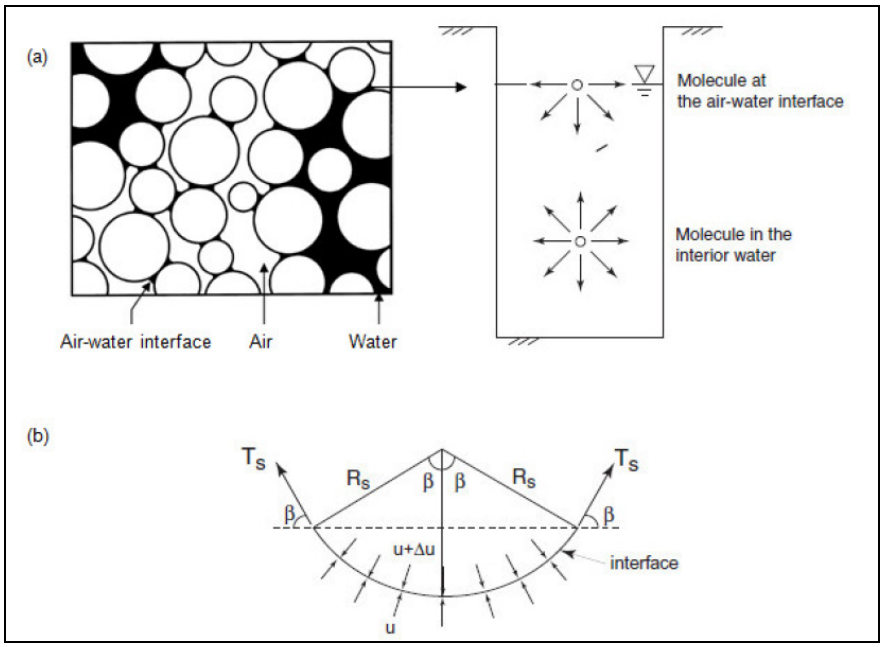

Figure I.9. Surface tension phenomenon at the air-water interface. a) Intermolecular forces on contractile skin and water; b) Pressures and surface tension acting on a curved two-dimensional surface (Fredlund & Rahardjo, 1993)

The air-water interface (contractile skin) possesses a property called surface tension. The phenomenon of surface tension results from the intermolecular forces acting on molecules in the contractile skin. When the molecule is in the interior water, there is no imbalance force. When the molecule is at the air-water interface, the molecule bears an imbalance force towards the interior water. As a result, the tensile air-water interface generates a tension force *Ts* along the interface which is named surface tension as shown in *Figure I.9*. The surface tension decreases with increasing temperature (Fredlund & Rahardjo, 1993).

In unsaturated soil, the tensile air-water interface is subjected to the pressure difference where the pore air pressure is greater than the pore water pressure. The pressure difference is defined as matric suction:

$$s_m = u_a - u_w \tag{I.8}$$

where, u_a is pore air pressure and u_w is pore water pressure.

A meniscus or the tension force *Ts* is generated to offset the imbalance and this tension force results in the capillarity phenomenon as shown in *Figure I.10*. The more matric suction, the

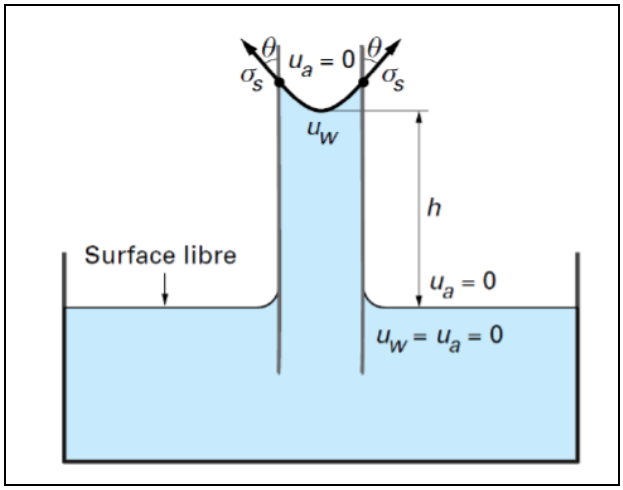

Figure I.10. Capillary rise in a tube (Delage & Cui, 2000)

smaller of radius of meniscus. When the pressure difference tends to zero, the radius of meniscus tends to infinity.

To describe the total suction, the Kelvin's Law is presented as:

$$S_T = \left(\frac{RT}{V_W}\right)\ln\left(\frac{p}{p_0}\right) \tag{I.9}$$

where, S_T is the total suction (kPa);

R is the ideal gas constant (= 8.3143 J.mol^{-1}.K^{-1});

T is the absolute temperature (k);

V_w is the volume of a mole of water (=1.8×10^{-5}m^3.mol^{-1});

p is the actual vapor pressure (kPa);

p_0 is the saturated vapor pressure(kPa).

In this study, only the matric suction s_m is taken into account termed as suction s.

Soil water retention curve

A soil water retention curve (SWRC) or soil water characteristic curve (SWCC) describes the amount of water retained in a soil (expressed as water content or degree of saturation) under an equilibrium state at a given matric suction in unsaturated soil mechanics. The SWRC is a

key property of unsaturated soil which is highly related to the soil texture and the pore structure. This relationship is not unique, it can be separated as "drying" and "wetting" curves.

Figure I.11 presents a typical SWRC including primary drying curve, primary wetting curve, scanning curves, air entry value, water entry value and residual suction value which is highly hysteresis in nature. The primary wetting curve corresponds to the wetting path for the soil starts from an oven dried state and the primary drying curve corresponds to the drying path for the soil starts from a fully saturated state. The primary wetting and drying curves enclose a possible region where soil state can exist. If the wetting path is stopped in the halfway on primary wetting curve and then a drying path is started, the new drying curve which is flatter than the primary drying curve in the possible region will be followed. The same as the wetting curve. Child, (1969) termed these new wetting and drying curve as scanning curves.

When a low suction is applied to a saturated soil, the soil remains saturated. Once a critical suction value is exceeded, the water content starts to decrease where the largest pores begin to empty. The critical suction value is commonly referred to as “air entry value”. Besides, it can be also observed that a certain amount of water can remain in the soil under a large suction. This water content is termed as “residual water content”.

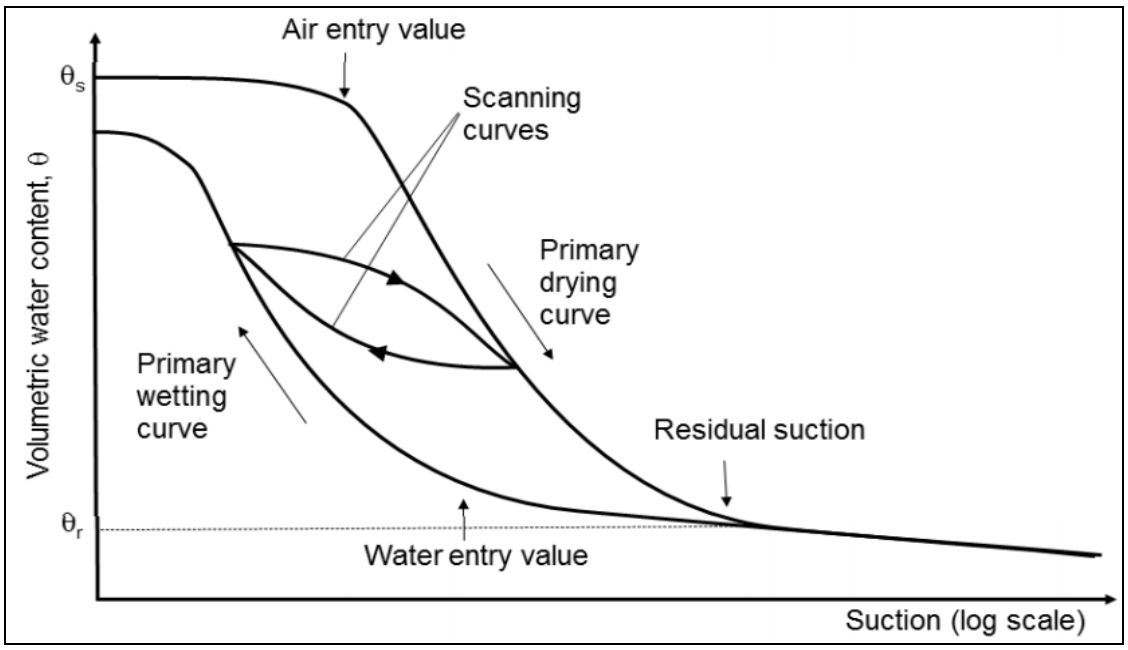

Figure I.11. Typical soil water retention curve (Toll, 2012)

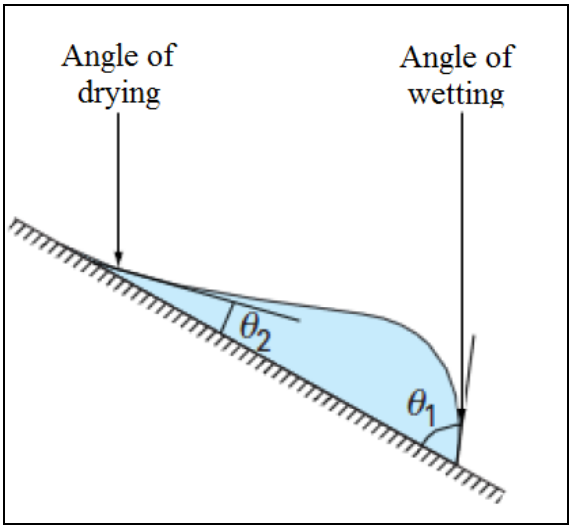

Figure I.12. The effect of contact angle

As shown in *Figure I.11*, a clear characteristic of SWRC is its hysteretic behaviour. It means the SWRC is state and history dependent (van Genuchten, 1980; Fredlund & Xing, 1994). The hysteresis could be explained by the emptying and flooding of void in soil with water. During the drying path, the large void is empty at first and it means the curvature R_d of the menisci is small corresponding to a high suction value. On the other hand, during the wetting path, the small void is flooded at first and it means the curvature R_w of the menisci is large corresponding to a low suction value. Besides, hysteresis is also attributed to the contact angles (Bear, 1969): The contact angle ($\theta 2$) caused by the air pushing the water is smaller than the angle ($\theta 1$) which caused by the water pushing the air as shown in *Figure I.12*.

Hysteresis could significantly influence the filtration, solute transport, and multiphase flow, which has been recognized for decades (Kool & Parker, 1987; Parker & Lenhard, 1987). Recently, more attention has been given to the effect of hysteresis on mechanical response, such as shear strength and deformation behaviour (Wheeler et al., 2003; Likos & Lu, 2004; Ho et al., 2014a; 2014b)

Considerable empirical equations have been developed to describe SWRC during the past several decades. *Table I.4* summarizes some common equations (Ho, 2013).

Expression	Reference	Parameters
$w = w_r + \frac{w_s - w_r}{1 + as^b}$	Gardner (1958)	a, b, w_r
$\begin{cases} \frac{w - w_r}{w_s - w_r} = \left(\frac{s_b}{s}\right)^{-\lambda} & s \geq s_b \\ w = w_s & s \leq s_b \end{cases}$	Brooks & Corey (1964)	λ, s_b, w_r
$w = w_r + \frac{(w_s - w_r)}{\left[1 + (\alpha s)^n\right]^m}$	van Genuchten (1980)	m, n, α, w_r
$\ln s = a + b \ln w$	Williams et al., (1983)	a, b
$w = w_r + (w_s - w_r) \exp\left(\frac{a - s}{b}\right)$	McKee & Bumb (1984)	a, b, w_r
$w = w_r + \frac{(w_s - w_r)}{1 + \exp\left(\frac{s - a}{b}\right)}$	McKee & Bumb (1987)	a, b, w_r
$w = w_r + \frac{(w_s - w_r)}{\left[\ln\left(e + (s/a)^b\right)\right]^c}$	Fredlund & Xing (1994)	a, b, c, w_r
$w = w_r + \frac{(w_s - w_r)}{\left[1 + \left(\frac{s}{c}\right)^b\right]^a}$	Pereira & Fredlund (2000)	a, b, c, w_r

Table I.4. Models of soil water retention curve (Ho, 2013)

where, s is suction; w_s is the saturated water content; w_r is the residual water content; s_b is the air entry value.

Effective stress concept in unsaturated soil

Terzaghi, (1923) introduced the effective stress concept in the geotechnical engineering by describing the relationship between external load and soil skeleton and soil water in saturated soil which developed soil mechanics as a new science. However, the phenomenon like unsaturated soil collapse during rewetting process shows that it is necessary to extend the effective stress to unsaturated soil.

For the saturated soils, the effective stress was expressed as (Skempton, 1961; Nur & Byerlee, 1971):

$$\sigma_{ij}^{'} = \sigma_{ij} - \left(1 - \frac{c_s}{c}\right) u_w \delta_{ij} \tag{I.10}$$

where, σ'_{ij} is effective stress tensor; σ_{ij} is total stress tensor; u_w is pore water pressure; c_s is elastic compressibility of the solid grains; c is elastic drained compressibility of the soil skeleton and δ_{ij} is Kronecker's delta.

For the unsaturated soils, Bishop and Blight, (1963) redefined the effective stress as:

$$\sigma_{ij}^{'} = \sigma_{ij} - u_a \delta_{ij} + \chi (u_a - u_w) \delta_{ij} \tag{I.11}$$

where, σ'_{ij} is effective stress tensor; σ_{ij} is total stress tensor; u_w is pore water pressure; u_a is pore air pressure; (u_a - u_w) is matric suction; χ is the effective stress parameter, attaining a value of 1 for saturated soil and zero for dry soil and δ_{ij} is Kronecker's delta.

The effective stress parameter χ is highly related to the soil saturation *Sr*, the soil structure and the cycle of wetting and drying. *Figure I.13* presents the variations of χ with *Sr* (Jennings & Burland, 1962). Khalili & Khabbaz, (1998) also showed a simple unique relationship between χ and ratio of matric suction over the air entry value (suction ratio) can be obtained for most soils as shown in Figure *I.14*

During the past several decades, various expressions of χ have been proposed by Lee, (1968); Fredlund & Rahardjo, (1993); Khalili & Khabbaz, (1998). Alonso & al., (2010) proposed an equation for the compacted clay loam as:

$$\chi = \left(S_r\right)^{\alpha} \tag{I.12}$$

where, α is the coefficient related to the porosity of macrospores against the total porosity.

$\alpha = 0$, Terzaghi effective stress expression;

$\alpha = 1$, Bishop effective stress expression;

$\alpha = \infty$, total stress expression.

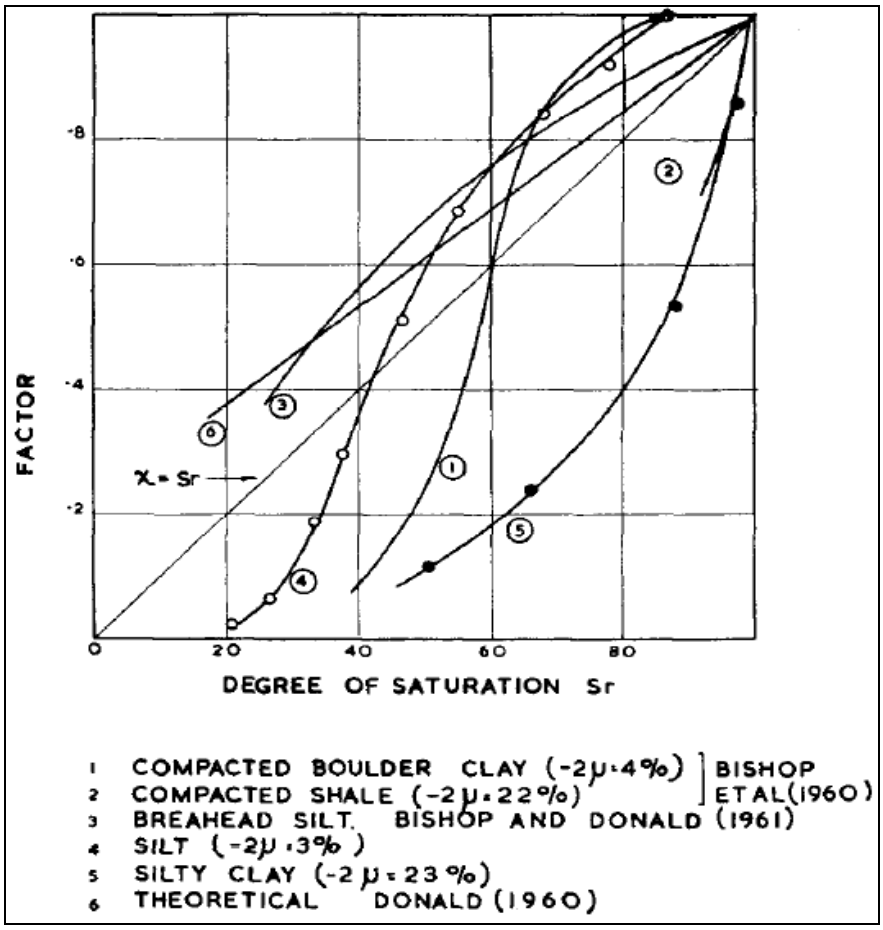

Figure I.13. The variations of χ with S_r (Jennings & Burland, 1962)

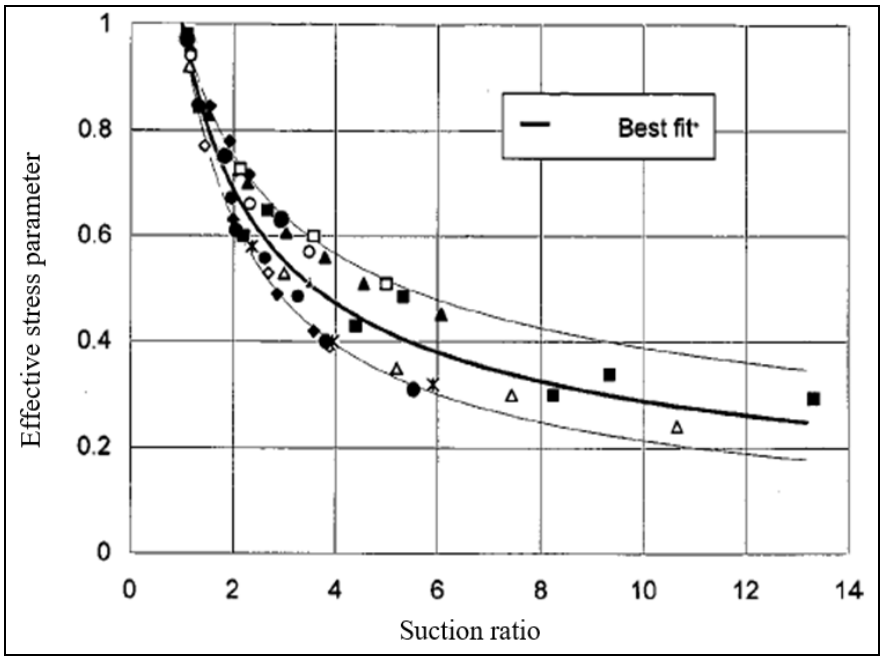

Figure I.14. Effective stress parameter χ versus suction ratio (Khalili & Khabbaz, 1998)

Pore pressure characteristics

As mentioned above, the matric suction *s* is determined by pore air and pore water pressure which is the key role in analysis of unsaturated soil. However, the distributions of pore air and pore water pressure are changing with depth of ground in practice (Tsukamoto et al., 2014). Besides, during cyclic undrained shear tests of unsaturated soil to simulate liquefaction, the continuous change of pore air and pore water pressure are observed in some researches (Unno et al., 2008; Okamura et al., 2009; Tsukamoto et al., 2014).

Tsukamoto et al., (2014) presented the distinctions of "unsaturated", "partially saturated" and "fully saturated" conditions in *Figure I.15.* In *Figure I.15,* the distributions of pore air and pore water pressure with depth are shown. With increasing depth (increasing confining pressure), the pore water pressure tends to increase faster than pore air pressure and the suction reduces continuously. At the same time, the continuous air phases reduce gradually in place of occluded bubbles which do not interact with soil structure.

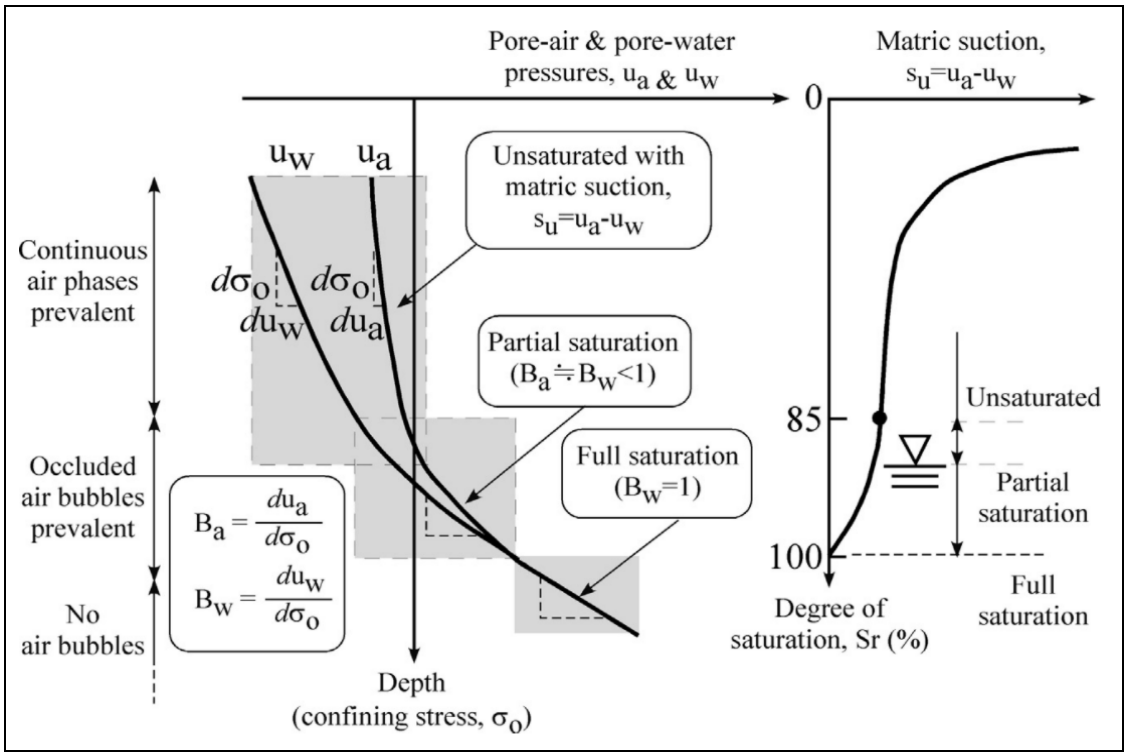

Figure I.15. Schematic interpretation of fully, partially and unsaturated soil deposits (Tsukamoto et al., 2014)

Unno et al., (2008) studied the general liquefaction state of unsaturated soils. Based on the continuous measurement of the pore water pressure, the pore air pressure and the volumetric

strain during undrained cyclic triaxial shear tests for a sandy soil, it can be observed that both the pore water pressure and the pore air pressure increase and the net stress ($\sigma_{net} = \sigma_0 - u_a$; σ_0 is confining pressure) decrease during the cyclic loading as shown in *Figure I.16.* Besides, based on the results, it can be also noted that, with the increase of the loading time or loading cycles, no significant change of the suction is observed before the pore air pressure reaches the initial confining pressure. The similar undrained shear test results have been obtained by Okamura et al., (2009) and Tsukamoto et al., (2014), as shown in *Figure I.17 and Figure I.18.*

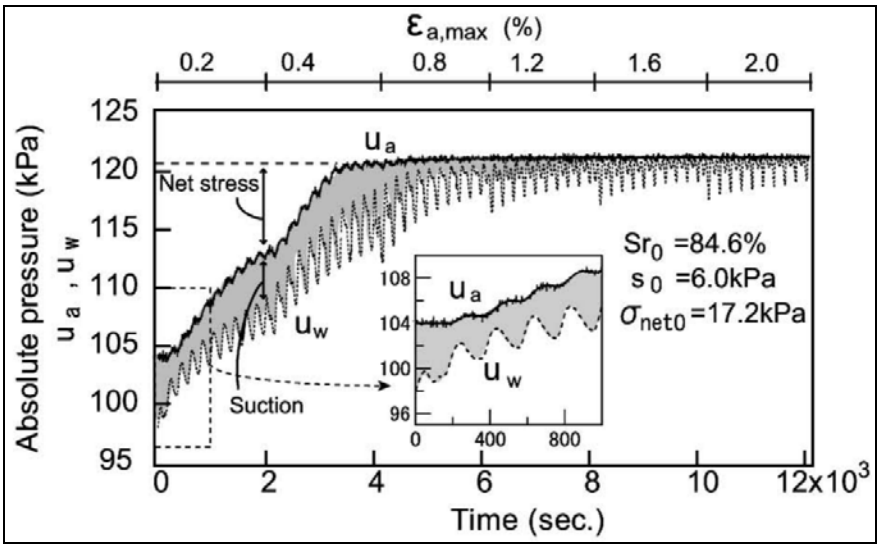

Figure I.16. Time history of pore air pressure and pore water pressure (Unno et al., 2008)

(Frequency: 0.005 Hz; Size of the sample: 50×100 mm; Dmax <0.5mm)

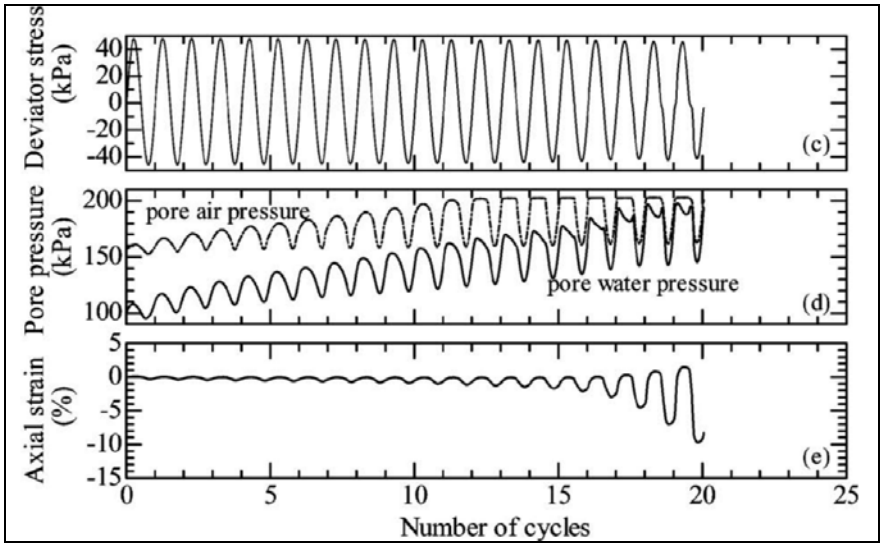

Figure I.17. Time history of pore air pressure and pore water pressure (Okamura et al., 2009)

(Frequency: 0.01Hz; Dmax <0.1mm)

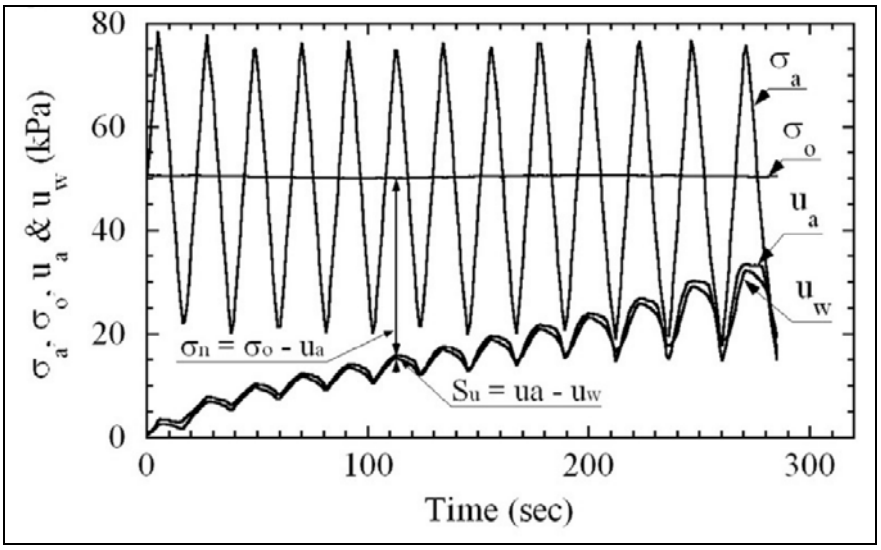

Figure I.18. Time history of pore air pressure and pore water pressure (Tsukamoto et al., 2014)

(Frequency: 0.05 Hz; Size of the sample: 60×120 mm; Dmax <1mm)

I.4. Evolution of permanent deformation behaviour of granular material

I.4.1. Factors influencing permanent deformation behaviour

As mentioned in section I.2, one of the main steps of flexible pavement design is pavement rutting control which is depended on the permanent deformation behaviour of granular materials. However, the permanent deformation behaviour is not only characterized by the material response under given traffic loads, but also influenced by a lot of factors, like: stress level; stress history; principal stress rotation; number of loading cycles; density; fine content, size distribution and aggregate type; water content and suction.

Effect of stress level

Stress level is one of the most important factors affecting the permanent deformation behaviour based on the literatures. In the early researches, Lashine et al., (1971) studied a partially saturated crushed stone under drained RLTT, the results showed that the permanent axial deformation settled down to a stable value related to the deviator stress and confining pressure. Barksdale, (1972) conducted a RLTT to a UGM with 10^5 loading cycles and found that the permanent deformation was highly affected by the stress level applied and it increased with an increase of deviator stress and decreased with an increase of confining pressure as shown in *Figure I.19.*

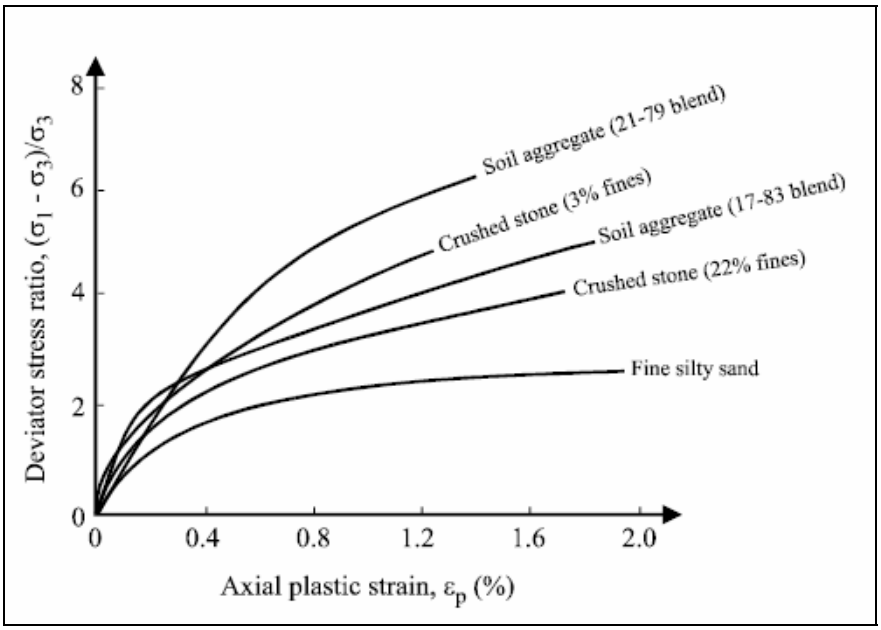

Figure I.19. Effect of stress level on permanent deformation behaviour (Barksdale, 1972)

The similar behaviour has been reported by Morgan, (1966); Pappin, (1979); Lekarp & Dawson, (1998); Trinh et al., (2012).

Effect of stress history

Brown & Hyde, (1975) investigated the effect of stress history on permanent deformation behaviour by comparing a series of successive applied stress levels with a direct highest stress level. The result showed that the permanent deformation of the latter was significantly larger than former which could be explained by the gradual material stiffening in each loading stage, as shown in *Figure I.20*.

Gidel et al., (2001) proposed a multi-stage loading procedure and confirmed that, in the multi-stage tests, the deformations at the end of several stages to reach stress level "i" stabilized at the same value as they would have been if the material had been subjected to just one stage to reach stress level "i". Absolutely, these two loading modes should be performed on the same stress path, as shown in in *Figure I.21*. This loading method could reduce the number of tests and avoid the variability of different soil specimens.

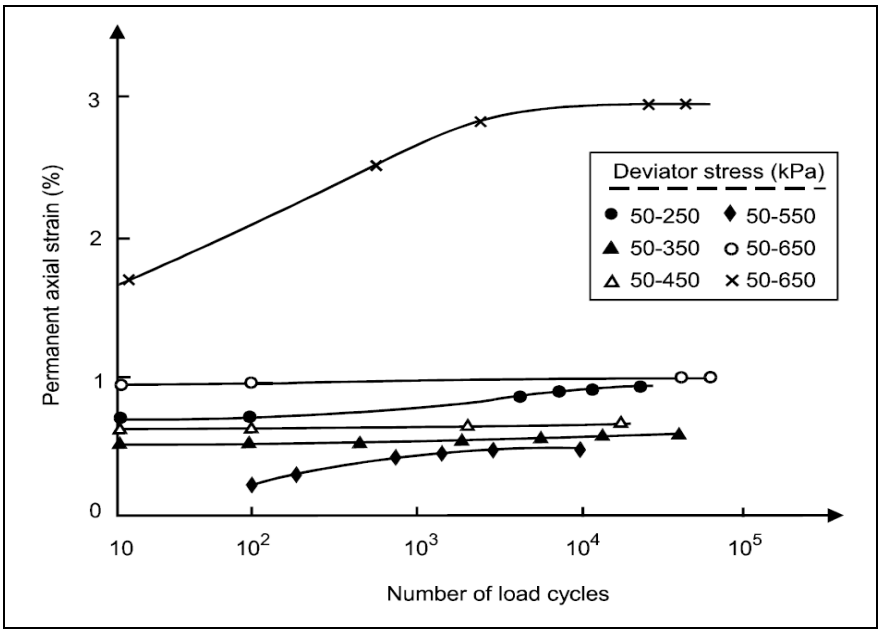

Figure I.20. Effect of stress history on permanent deformation behaviour (Brown & Hyde, 1975)

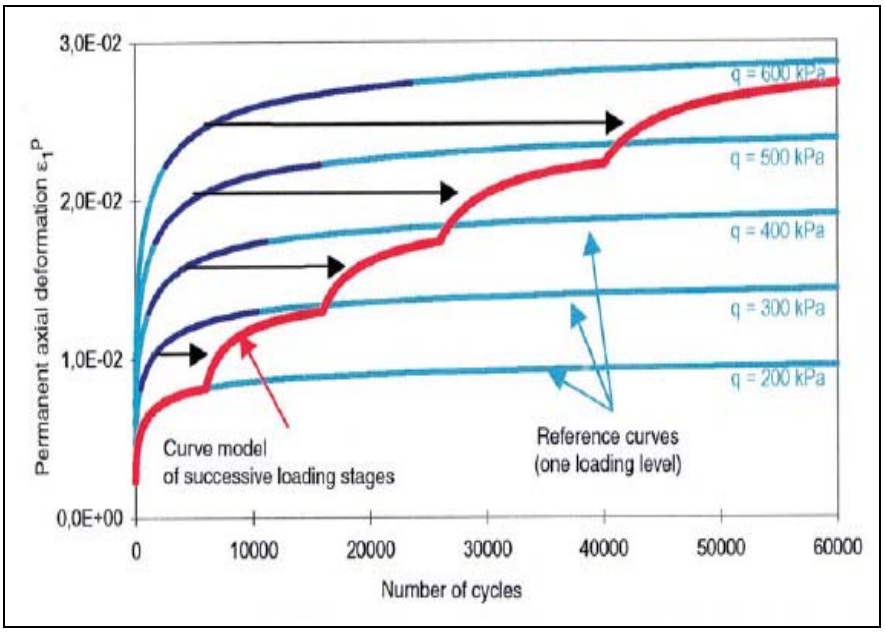

a) Construction of the curve

Figure I.21. Construction of the staged loading test curve (Gidel et al., 2001)

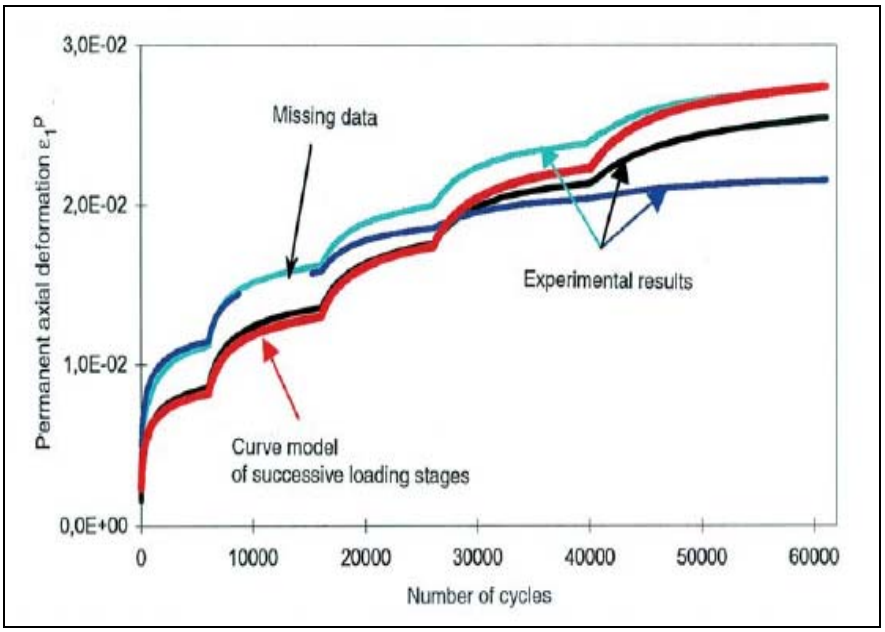

b) Comparison with experimental results

Figure I.21 -Continued

Effect of principal stress rotation

As shown in *Figure I.4,* the principal stress of one point under the pavement is changing with a distance between the horizontal axis of wheel and this point. The literatures results show that, more permanent deformation of granular materials is obtained than RLTT, taking into account of principal stress rotation.

Youd, (1972) found a significant increase in density of a sand in a cyclic shear box caused by principal stress rotation. Chan, (1990) realized a hollow cylinder shear tests with crushed limestone and observed higher permanent deformation with shear stress reversal than tests without shear stress (triaxial). Hornych, (2000) performed these two kinds loading modes with an instrumented pavement. The results showed that the permanent deformation with a rolling load was three time greater than a cyclic plate loading test.

Effect of number of loading cycles

The increase of permanent deformation in granular materials under repeated loads is a gradual process during each load application which contributes a small increment to the accumulation of strain. The number of load cycles is, therefore, one of the most important factors to consider in the analysis of the long-term behaviour of such materials (Lekarp, 2000b).

In the past several decades, many researcher have conducted a lot of tests with a large number of cycles to characterize the permanent deformation (Morgan, 1966; Barksdale, 1972; Sweere, 1990; Lekarp & Dawson, 1998). Most of literatures showed that the permanent deformation rate wound increase after a relatively large number of loading cycles. The stable permanent deformation could achieve only with a low loading stress. In fact, this is consistent with the shakedown theory which will be introduced later.

With respect to the materials used in this context, Ho et al., (2014c) investigated the resilient behaviour of Missillac sand and noted that an equilibrium state reached after a conditioning phase with approximately 10,000 load applications. For UGM, Hornych et al., (2007) showed that the necessary number of cycles was higher than 50,000.

Effect of density

The effect of density (degree of compaction) on permanent deformation of granular materials is easy to imagine based on a common sense: the lower the permanent deformation can be observed with the denser material. This behaviour has been reported by previous studies (Thom & Brown, 1988; Barksdale, 1991; van Niekirk, 2002; Uthus, 2007).

Barksdale, (1991) presented the permanent deformation of a granular material with 95% of maximum dry density was about twice the deformation with 100% of maximum compactive density as shown in *Figure I.22.* van Niekirk, (2002) demonstrated degree of compaction had more significant effect on the permanent deformation than the grading of material. Odermatt et al., (2004) addressed that the crushed aggregates had more permanent deformation than natural gravels with same degree of compaction as shown in *Figure I.23*. It meant the crushed aggregates need more compaction effort.

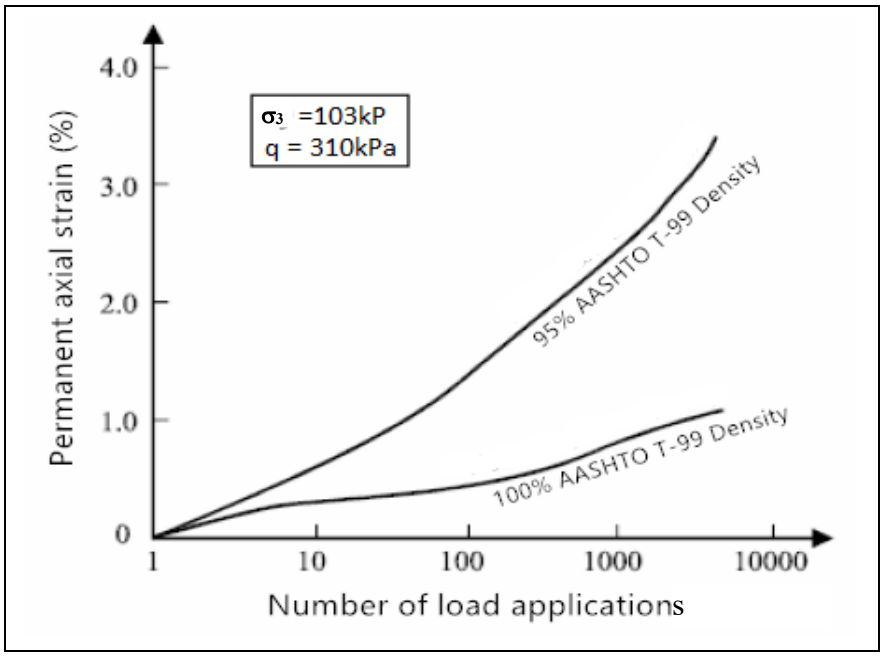

Figure I.22. Effect of density on permanent deformation behaviour (Barksdale, 1991)

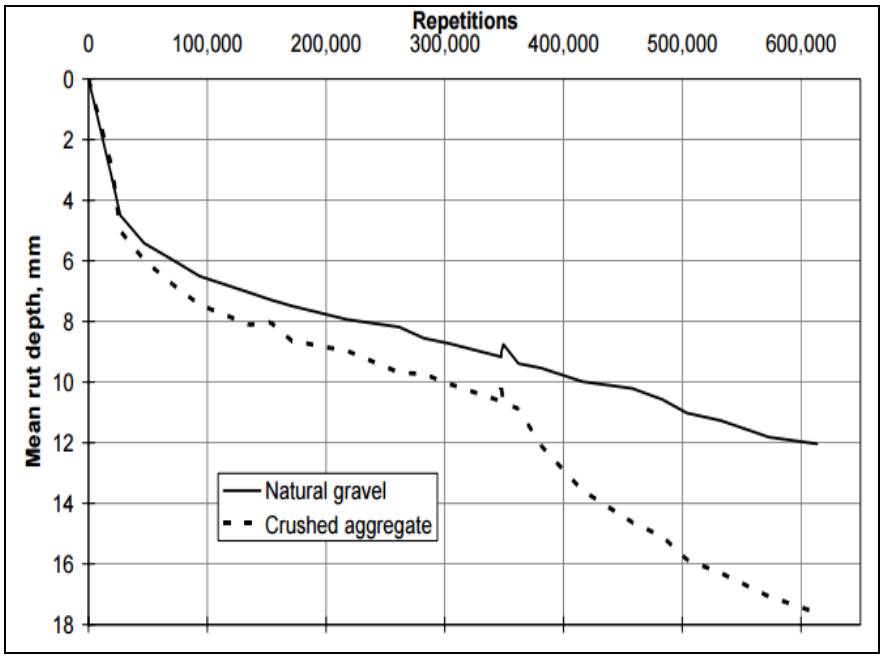

Figure I.23. Rutting of the two heavy vehicle simulator test structures (Odermatt et al., 2004)

Effect of fine content, size distribution and aggregate type

Fine content refers to an amount of particles passing through the sieve 63µm based on European, 75µm based on American classification. It can be addressed that, if the percentage of fines is not too large (lower than an experimentally defined critical value), the resistance to permanent deformation is provided by the skeleton of coarse grains. On the contrary, when the percentage of fine is high (larger than an experimentally defined critical value), the fine

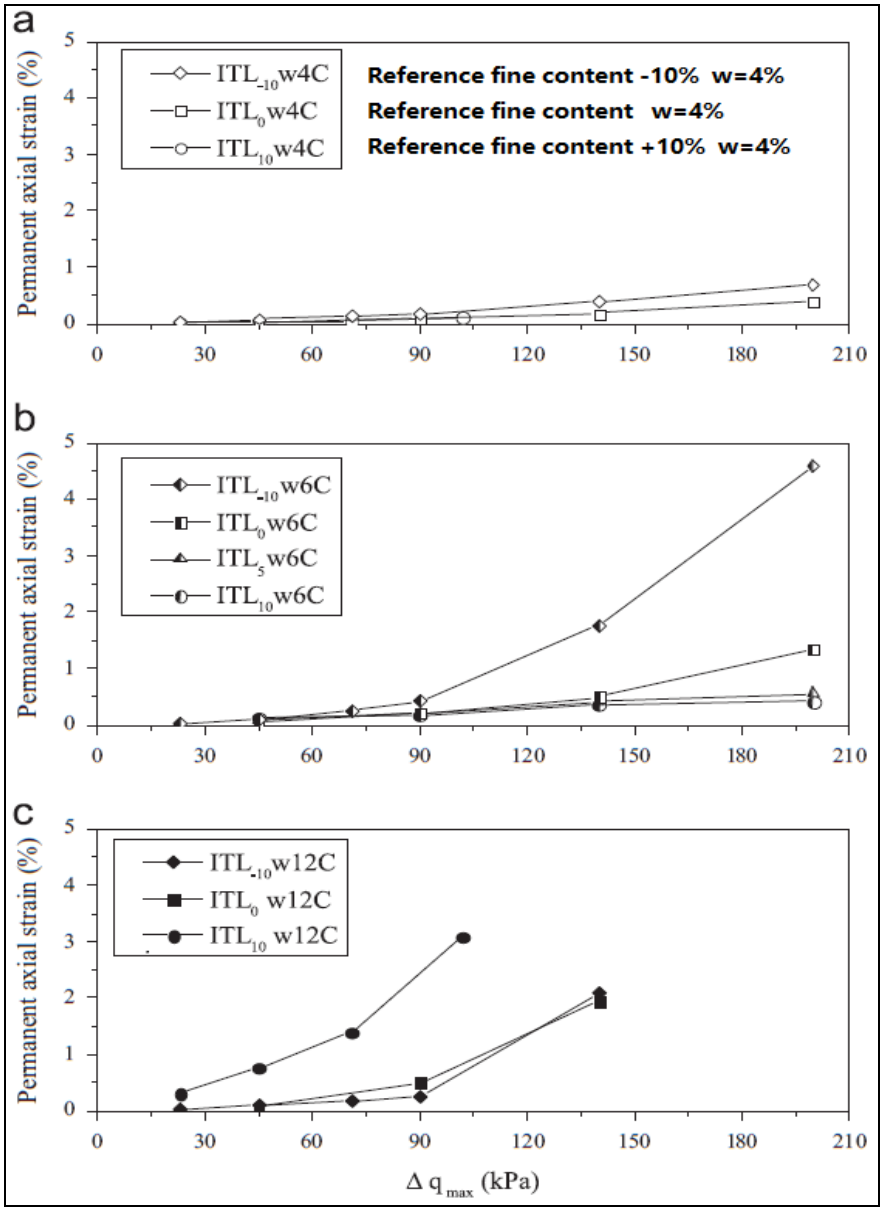

Figure I.24. Effect of fines content on the end-stage permanent axial strain at various water contents (Duong et al., 2013)

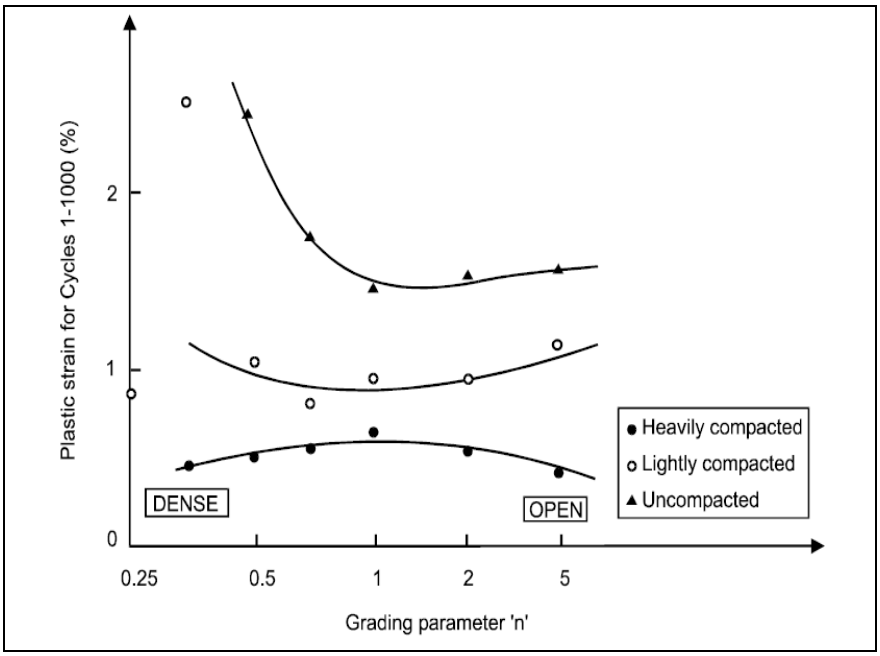

Figure I.25. Effect of grading and compaction on plastic strain (Thom & Brown, 1988)

particles take the main role and isolate the coarse grains and consequently modify the soil behaviour (Dash et al., 2010; Chang et al., 2012; Benahmed et al., 2015). And a high fine content also makes the material sensitive to high water content.

The previous studies confirmed that the resistance to permanent deformation in granular materials was reduced as the amount of fines increases (Lekarp, 2000b). However, some researches (Seif EI Dine et al., 2010; Duong et al., 2013; Jing et al., 2017) have addressed that the effect of fine content on permanent deformation was relatively complex with different moisture contents as shown in *Figure I.24*. This point will be discussed in detail in Chapter III.

The effect of size distribution or material grading was investigated by Thom & Brown (1988), and it could be observed that the uniform grading could reduce the permanent deformation only with uncompacted materials as shown in *Figure I.25*. The aggregate type is also an important role affecting the permanent deformation. Allen, (1973) addressed that the angular aggregates had more resistance to permanent deformation comparing with rounded aggregates.

Effect of water content and suction

In practice, there is always water within granular materials. The effect of water content is significantly important for the long-term behaviour of granular materials which could influence the resistance of permanent deformation. The repeated traffic loads can trigger an excessive pore pressure with too much water close to saturation and the excessive pore pressure reduces the effective stress leading to more permanent deformation.

In the past several decades, the effect of water content on permanent deformation has been reported in many researches (Dawson, 1990; Gidel et al., 2002; Werkmeister et al., 2003; Trinh et al., 2012).

Dawson, (1990) presented the positive effect of drainage on permanent deformation in a granular material as shown in *Figure I.26.* Gidel et al., (2002) studied the vertical deformation of UGM layer equipped three deformation sensors. The measurement results showed that the vertical deformation in humid season (w = 13.5%) was up to four times that measured in dry season (w = 7%) as shown in *Figure I.27.* Trinh et al., (2012) studied the permanent deformation behaviour of a fouled ballast with 3 different water contents by carrying out multi-stage RLTTs with large numbers of cycles. The results showed that the permanent axial deformation was larger for higher water contents in each loading stage.

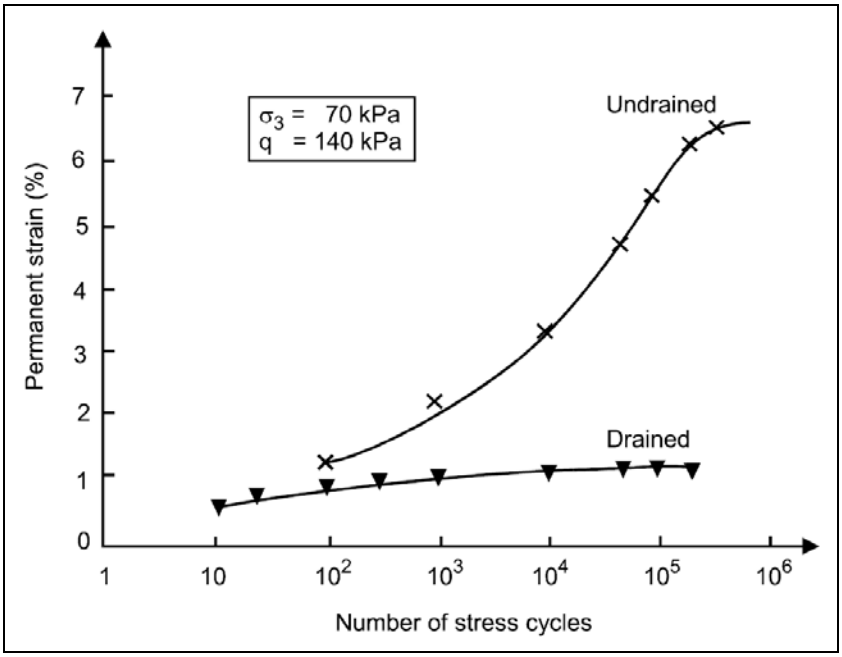

Figure I.26. Influence of drainage on permanent deformation development (Dawson, 1990)

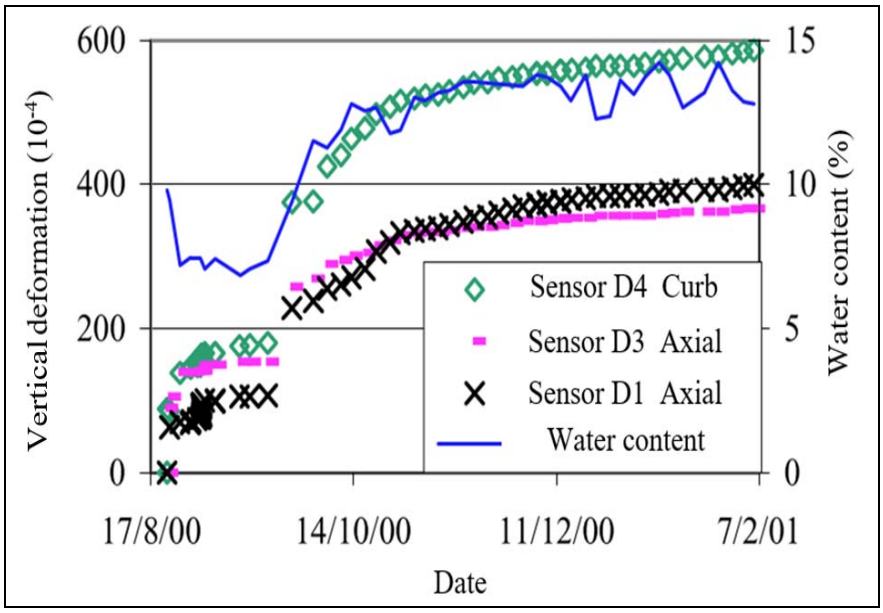

Figure I.27. Evolution of vertical deformation with water content for UGM in pavement (Gidel et al., 2002)

Generally other researchers (Uthus et al., 2006; Duong et al., 2013; Salour & Erlingsson, 2015b) have reported the same conclusion as mentioned above.

Recently, the effect of suction on material mechanical behaviour has received increased attention. Salour & Erlingsson, (2015b) mentioned that regarding the soil stress state estimations to be used in the modelling, taking into account the influence of the unsaturated state, i.e. matric suction on the material mechanical behaviour could be recommended. This is particularly favorable in subgrades with a high fine content and at low degree of saturation where soil suction effects on the material stress state is considerable.

However, in many cases, the effect of suction was regarded as water content or degree of saturation and the real role of suction in permanent deformation behaviour has been rarely studied. In fact, suction corresponds to not only the moisture state but also the fine content and further the microstructure in aggregates. Thus, the correlation between deformation behaviour and the suction could be important. This point will be discussed in detail in Chapter III.

I.4.2. Permanent deformation behaviour and shakedown theory

Pavement structures fail due to gradual accumulation of permanent deformation, or degradation in materials during their service life, and not due to rapid collapse (Sharp, 1985).

The mechanism of the failure of granular material layers can be explained by the applied traffic loads and the shakedown behaviour of the material.

The shakedown was originally developed to analyze the behaviour of pressure vessels to cyclic thermal loading. Later it was applied to analyze the behaviour of metal surfaces under repeated rolling or sliding loads (Johnson, 1986). The shakedown concept was first time drawn into the pavement engineering by Sharp & Booker (1984). In general, there are four typical categories of material response under repeated loading, as shown in *Figure I.28:*

1. Purely elastic. The applied cyclic stress is small. As a result, there is no plastic strain and all deformations are fully recovered which is purely elastic. This material response is called "Purely elastic", and the maximum applied cyclic stress level to reach this state is called "Elastic limit".

2. Elastic shakedown. The material response is plastic for a finite number of stress or strain excursions. However, the ultimate response is purely elastic. This material response is called "Elastic shakedown", and the maximum applied cyclic stress level to reach this state is called "Elastic shakedown limit".

3. Plastic shakedown. The applied cyclic stress is less than that could trigger the material collapse. After finite number of loading and unloading cycles, the significant accumulated permanent deformation could be obtained and the permanent deformation trends to stabilize with increasing number of loading cycles. Besides, it is important to note that this material response is hysteretic which means there is energy absorption during each loading cycle. This purely elastic response is called "Plastic shakedown", and the maximum applied cyclic stress level to reach this state is called "Plastic shakedown limit ".

4. Incremental collapse or ratchetting. The applied cyclic stress is relatively large that the plastic strain accumulates quickly and the material failure happens within a finite number of loading cycles. This material response is called " Incremental collapse or ratchetting ".

Based on these four typical categories material response under repeated loading, it is helpful to pavement design to ensure the pavement materials work properly in a "Elastic shakedown" or "Plastic shakedown" state with an applied stress lower than Plastic shakedown limit. In the past several decades, some researchers (Sharp & Booker, 1984; Raad et al., 1989; Collins et

al., 1993; Chazallon et al., 2009; Allou et al., 2010) have developed shakedown computational procedures for pavement analysis.

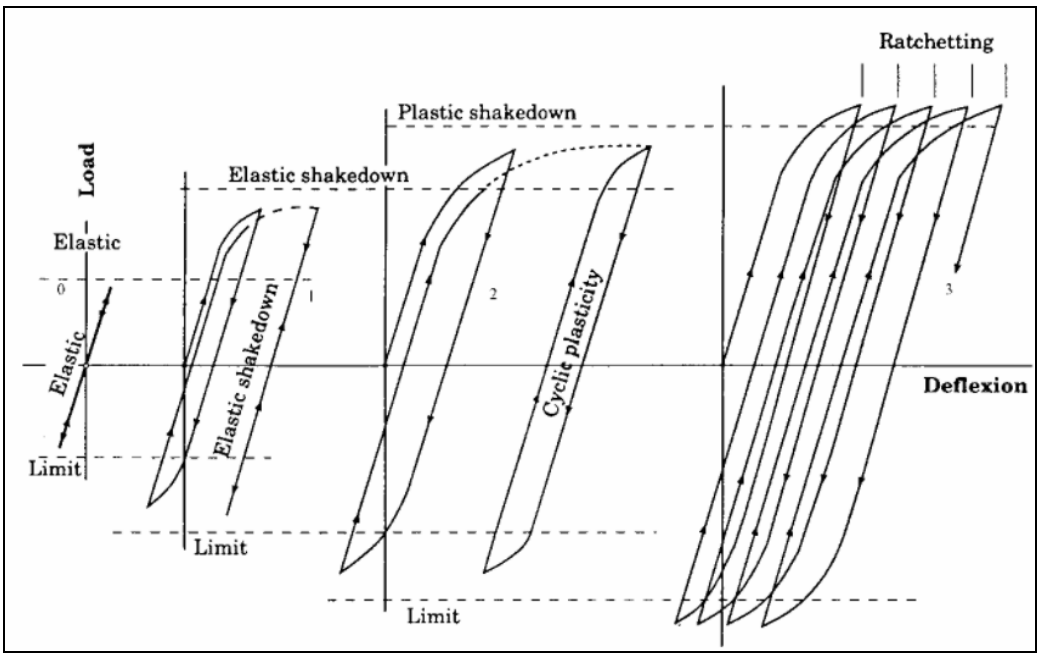

Figure I.28. Elastic/plastic behaviour under repeated cyclic pressure and tensile load (Johnson, 1986)

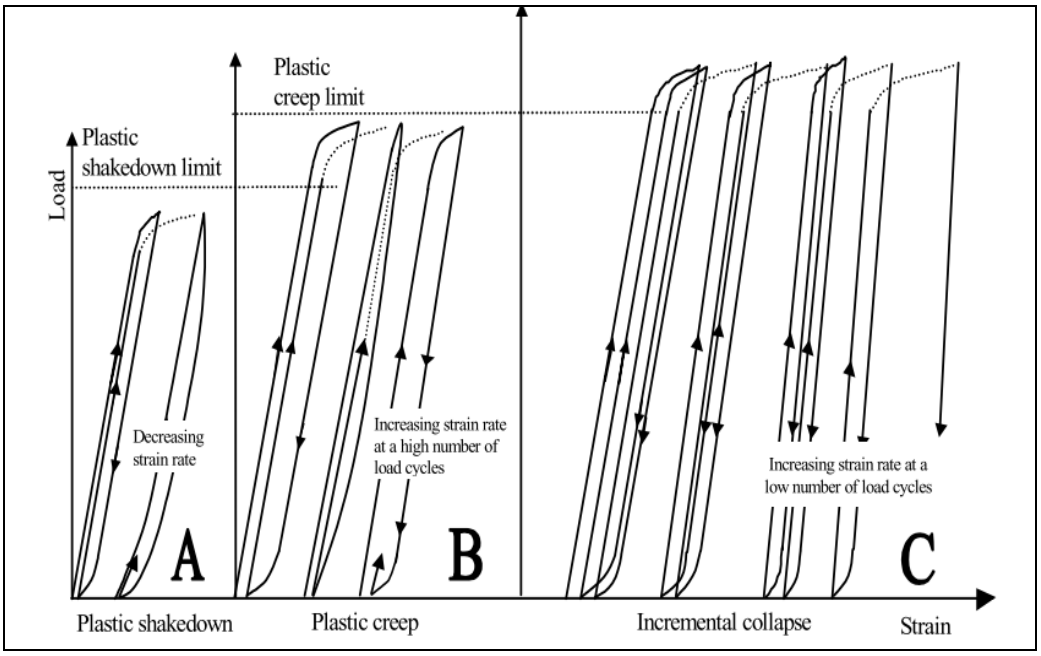

Figure I.29. Behaviour of granular materials under repeated cyclic load (Werkmeister et al., 2001)

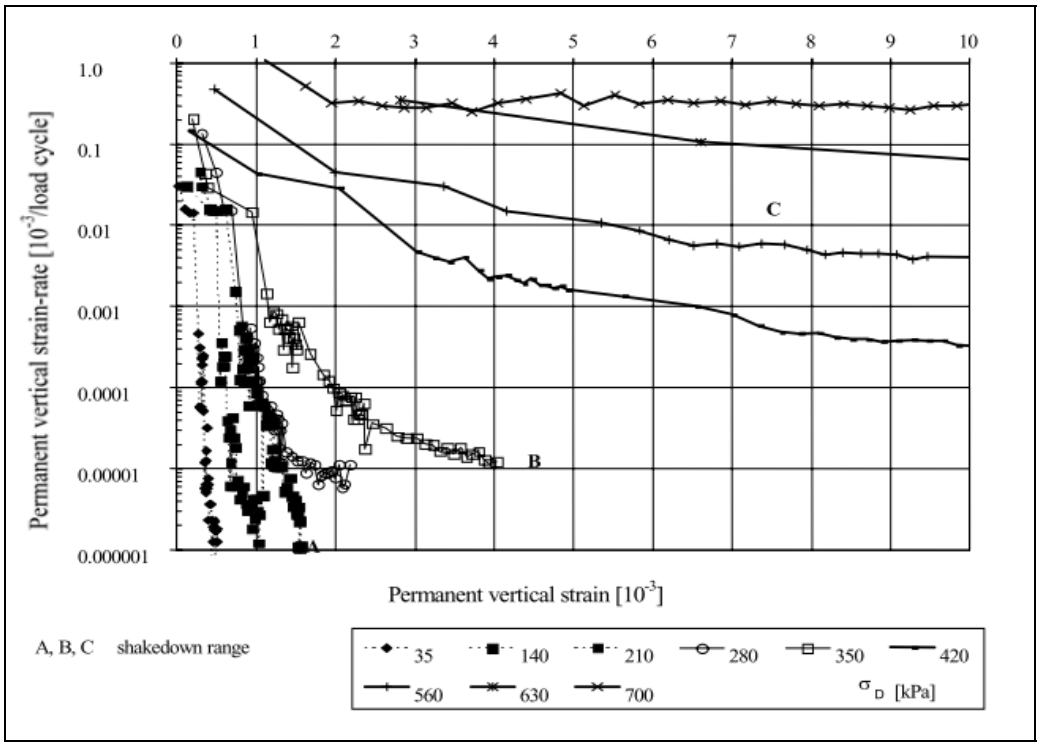

Figure I.30. Permanent vertical strain rate of Granodiorite, grading M (Werkmeister et al., 2001)

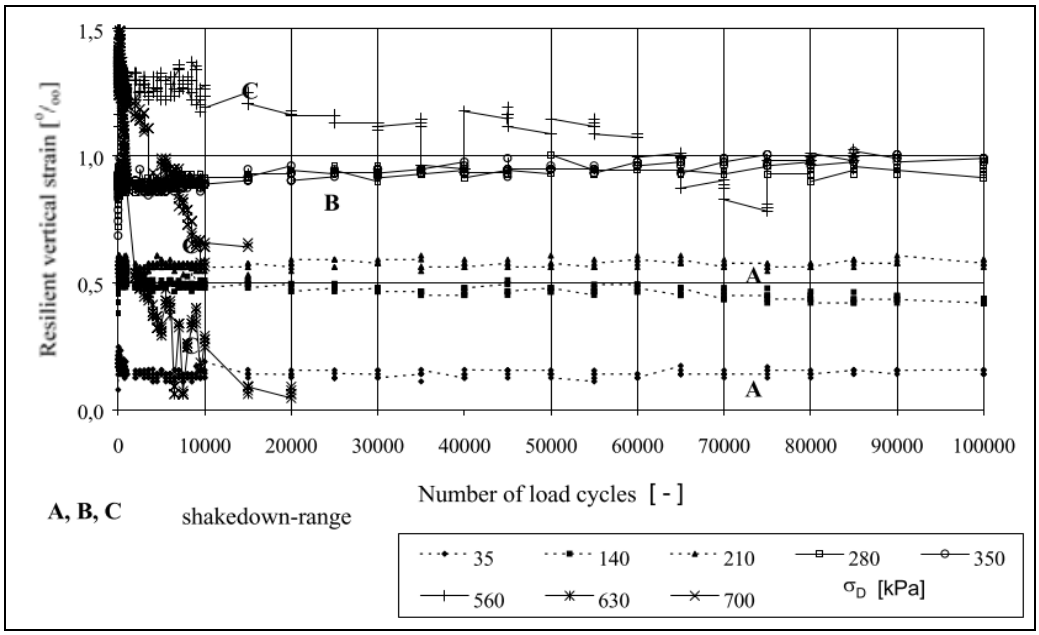

Figure I.31. Recoverable vertical strain versus number of loading cycles of Granodiorite, grading M (Werkmeister et al., 2001)

Werkmeister et al., (2001) developed the shakedown concept in laboratory tests for pavement materials and reformulated the shakedown behavior of UGM subjected to cyclic compression

loading only as shown in *Figure I.29.* In this figure, there are three categories of material response based on the permanent vertical strain rate (per cycle of loading) and the resilient vertical strain for a Granodiorite material: Range A-Plastic shakedown; Range B-Plastic creep and Range C-Incremental collapse. The variation of permanent vertical strain rate and resilient/recoverable vertical strain in three categories are illustrated in *Figure I.30* and *Figure I.31* respectively. Range A seems equivalent to "Plastic shakedown" as mentioned before, which shows a convex-downwards and fast decline curve for permanent vertical strain rate and presents a flat curve of resilient/recoverable vertical strain after an initial decline. Range C refers to "Incremental collapse or ratchetting", which shows a concavely outwards and slow decline curve (even rising curve) for permanent vertical strain rate and presents a significant decrease of resilient/recoverable vertical strain with increasing number of cycles. Range B is the intermediate behaviour, which is observed over a range of stress states. Initially behaviour is like Range A but a small residual incremental plastic strain is observed. As same as mentioned above, the desired behaviour of a good granular material layer is within plastic shakedown (Range A) or plastic creep (Range B) under repeated loads.

More recently, many studies of application of shakedown theory in characterizing the permanent deformation behaviour in laboratory have been conducted by Werkmeister, (2001; 2004; 2005); Yang & Huang, (2007); Tao et al., (2010); Song & Ooi, (2010); Chen et al., (2013); Soliman & Shalaby, (2015).

Werkmeister, (2001) defined a linear relationship between limited stress and cell pressure to separate the stable behaviour and unstable behaviour based on RLTTs, which was expressed by:

$$\sigma_{SD} = A\sigma_3 + B \tag{I.13}$$

where, A and B are regression parameters which depend on the grading, particle shape, particle surface, water content of the materials.

σ_{SD} is bound of range (kPa);

Yang, (2007) proposed an equation for predicting the critical stress with varying water contents, which was expressed by:

$$\sigma_{critical} = \sigma_{critical\_opt} + \frac{(\omega - \omega_o)}{\omega_o} \tan\theta \tag{I.14}$$

where, $\sigma_{critical}$ is critical deviator stress of subgrade soils at moisture content of ω;

$\sigma_{critical\_opt}$ is critical deviator stress of subgrade soils at optimum moisture content of ω_o;

$(\omega_o-\omega)/\omega_o$ is the normalized water content;

$tan\theta$ is decreasing rate of critical deviator stress with an increasing water content.

Tao, (2010) demonstrated the application of the shakedown theory to characterize the behaviour of traditional and recycled base materials based on laboratory RLTT and full-scaled accelerated loading tests. A novel approach was also proposed to describe the shakedown responses based on dissipated energy.

I.4.3. Models predicting permanent deformation behaviour

According to the RLTTs, various empirical-analytical models were proposed to predict the permanent deformation behaviour taking into account the number of loading cycles and the stress level.

In fact, Lekarp et al., (2000b) have summarized many computational models for permanent deformation behaviour as shown in *Table I.5.* This section will highlight some important models and add some new models.

These notations will be used in the following part:

N is the number of cycles;

p is the mean normal stress;

q is the deviator stress;

σ_1 is the axial stress;

σ_3 is the cell pressure or confining pressure;

p_a is the reference pressure (100 kPa).

Models based on number of cycles

Barksdale, (1972) found the linear relationship between permanent deformation and logarithm of number of cycles based on the RLTTs for UGM, which was expressed by:

$$\varepsilon_1^p = a + b\log N \quad \text{(I.15)}$$

Expression	No	Reference	Parameters
$\varepsilon_{1,p} = a\varepsilon_r N^b$	(1)	Veverka (1979)	$\varepsilon_{1,p}$ = accumulated permanent strain after N load repetitions
$\begin{cases} K_p(N) = \dfrac{p}{\varepsilon_{v,p}(N)} \ , \ G_p(N) = \dfrac{q}{3\varepsilon_{s,p}(N)} \\ G_p = \dfrac{A_2\sqrt{N}}{\sqrt{N}+D_2} \ , \ \dfrac{G_p}{K_p} = \dfrac{A_3\sqrt{N}}{\sqrt{N}+D_3} \end{cases}$	(2)	Jouve et al. (1987)	$\varepsilon^*_{1,p}$ = additional permanent axial strain after 100 cycles $\varepsilon_{1,p}(N_{ref})$ = accumulated permanent axial strain after a given number of cycles N_{ref}, $N_{ref} > 100$ $\varepsilon_{v,p}$ = permanent volumetric strain for N>100 $\varepsilon_{s,p}$ = permanent shear strain for N>100
$\dfrac{\varepsilon_{1,p}}{N} = A_1 N^{-b}$	(3)	Khedr (1985)	ε_N = permanent strain for load cycle N
$\varepsilon_{1,p} = a + b\log(N)$	(4)	Barksdale (1972)	ε_i = permanent strain for the first load cycle
$\varepsilon_{1,p} = aN^b$	(5)	Sweere (1990)	ε_r = resilient strain
$\varepsilon_{1,p} = (cN + a)\left(1 - e^{-bN}\right)$	(6)	Wolff & Visser (1994)	K_p = bulk modulus with respect to permanent deformation G_p = shear modulus with respect to permanent deformation
$\varepsilon^*_{1,p} = \dfrac{A_4\sqrt{N}}{\sqrt{N}+D_4}$	(7)	Paute et al. (1988)	q = deviator stress p = mean normal stress
$\varepsilon^*_{1,p} = A\left(1 - \left(\dfrac{N}{100}\right)^{-B}\right)$	(8)	Paute et al. (1996)	q^0 = modified deviator stress = $\sqrt{2/3}\cdot q$ p^0 = modified mean normal stress = $\sqrt{3}\cdot p$
$\varepsilon_{1,p} = \sum \varepsilon_N = \sum \dfrac{1}{N^h}\varepsilon_i$	(9)	Bonaquist & Witczak (1997)	p^* = stress parameter defined by intersection of the static failure line and the p-axis in p-q space p_0 = reference stress
$\varepsilon_{1,p} = \dfrac{q / a\sigma_3^b}{1 - \left[\dfrac{(R_f q)/2(C\cos\phi + \sigma_3\sin\phi)}{(1-\sin\phi)}\right]}$	(10)	Barksdale (1972)	L = stress path length σ_3 = confining pressure N = number of load applications
$\varepsilon_{1,p} = \varepsilon_{0.95S}\ln(1 - q/S)^{-0.15} + \left\{\dfrac{a(q/S)}{\left[1 - b(q/S)\right]}\right\}\ln(N)$	(11)	Lentz and Baladi (1981)	S = static strength $\varepsilon_{0.95S}$ = static strain at 95 percent of static strength C = apparent cohesion ϕ = angle of internal friction
$\varepsilon_{1,p} = 0.9\dfrac{q}{\sigma_3}$	(12)	Lashine et al. (1971)	fnN = shape factor R_f = ratio of measured strength to ultimate hyperbolic strength
$\varepsilon_{s,p} = (fnN)L\left(\dfrac{q^o}{p^o}\right)^{2.8}_{\max}$	(13)	Pappin (1979)	h = repeated load hardening parameter, a function of stress to strength ratio A_1 = a material and stress-strain parameter given (function of stress ratio and resilient modulus)
$A = \dfrac{\dfrac{q}{(p+p^*)}}{b\left(m - \dfrac{q}{(p+p^*)}\right)}$	(14)	Paute et al. (1996)	A_2-A_4, D_2-D_4 = parameters which are functions of stress ratio q/p m = slope of the static failure line
$\dfrac{\varepsilon_{1,p}(N_{ref})}{(L/p_o)} = a\left(\dfrac{q}{p}\right)^b_{\max}$	(15)	Lekarp and Dawson (1998)	a, b, c, A, B = regression parameters (A is also the limit value for maximum permanent axial strain)

Table I.5. Computational models for permanent deformation behaviour (Lekarp et al., 2000b)

where, *a* and *b* are parameters.

Veverka, (1979) proposed a relationship between the permanent and resilient deformation for UGM, which was expressed by:

$$\varepsilon_1^p = a\varepsilon_r N^b \tag{I.16}$$

where, *a* and *b* are parameters. ε_r is the resilient deformation.

Khedr, (1985) proposed a power function to predict permanent deformation with *N*, which was expressed by:

$$\frac{\varepsilon_1^p}{N} = A_1 N^{-b} \tag{I.17}$$

where, *a* and *b* are parameters.

Hornych et al., (1993) proposed the following equation which was widely used to simulate the permanent axial deformation with the variation of *N*, expressed by:

$$\varepsilon_1^p = A\left(1-\left(\frac{N}{N_0}\right)^B\right) \tag{I.18}$$

where, *A* and *B* are parameters; N_0 is the number of cycles before the first measurement.

In this equation, parameter *A* refers to the final stable permanent deformation when the number of cycles reaches to a large enough value.

Bonaquist & Witczak, (1997) developed the following equation taking into account the effect of stiffness hardening, which was expressed by:

$$\varepsilon_1^p = \sum \varepsilon_N = \sum \frac{1}{N^h}\varepsilon_i \tag{I.19}$$

where, ε_N *is* the permanent deformation for load cycle *N*; ε_i *is* the permanent deformation for the first load cycle; *h* is the hardening parameter.

Models based on stress level

The models based on number of cycles can be used to describe the evolution of permanent deformation. However, the applied stress level is important as number of cycles for

permanent deformation behaviour, which can determine the final deformation value at given stress state.

Lashine et al., (1971) observed the linear relationship between permanent deformation and q to σ_3 ratio in RLTTs. The corresponding equation was expressed by:

$$\varepsilon_1^p = a\frac{q}{\sigma_3} \tag{I.20}$$

where, a is the parameter.

Similarly, Barksdale, (1972) proposed an equation including the q to σ_3 ratio and took the strength parameters based on monotonic triaxial tests. The equation was expressed by:

$$\varepsilon_1^p = \frac{\frac{q}{a\sigma_3^n}}{1-\left[\frac{(R_f \cdot q)(1-\sin\varphi)}{2(c\cdot\cos\varphi+\sigma_3\sin\varphi)}\right]} \tag{I.21}$$

where, a and n are parameters; R_f is constant; φ is internal friction angle; c is cohesion.

Pappin, (1979) believed the permanent shear deformation was related direct to the length of the stress path in p-q plane and the q to p ratio. The number of cycles was also taken into account in this equation, which was expressed by:

$$\varepsilon_p^s = fnN \cdot L \cdot \left(\frac{q^0}{p^0}\right)_{\max}^{2.8} \tag{I.22}$$

where, $\varepsilon_p{}^s$ is permanent shear strain for N > 100; fnN is shape factor; $L = \sqrt{q^2 + p^2}$ is the length of stress path; $q^0 = \sqrt{2/3}\cdot q$ is the modified deviator stress; $p^0 = \sqrt{3}\cdot p$ is the modified mean normal stress.

Lekarp & Dawson, (1998) also assumed the permanent axial deformation was related to the length of stress path in p-q plane and the q to p ratio. The equation was expressed by:

$$\frac{\varepsilon_1^p\left(N_{ref}\right)}{\left(L/p_0\right)} = a\left(\frac{q}{p}\right)_{\max}^b \tag{I.23}$$

where, $\varepsilon_1^p(N_{ref})$ is accumulated permanent axial strain after a given number of cycles N_{ref}, $N_{ref} > 100$; $L = \sqrt{q^2 + p^2}$ is the length of stress path; p_0 is reference stress; a and b are parameters.

After that, more and more equations combining the influence of the number of cycles with the effect of stress level were developed for predicting permanent deformation.

Gidel et al., (2001) proposed a model expressed by:

$$\varepsilon_1^p = f(N) \cdot g(p_{\max}, q_{\max}) \tag{I.24}$$

The $f(N)$ is the Hornych model which has been introduced in Equation I.18. The $g(p_{max}, q_{max})$ takes the length of stress path, the q_{max} to p_{max} ratio and the parameters of failure line as:

$$g(p_{\max}, q_{\max}) = \varepsilon_1^{p0} \cdot \left(\frac{L_{\max}}{p_a}\right)^n \cdot \frac{1}{m + \frac{s_b}{p_{\max}} - \frac{q_{\max}}{p_{\max}}} \tag{I.25}$$

where, $l_{\max} = \sqrt{p_{\max}^2 + q_{\max}^2}$ is the maximum length of stress path; p_{max} and q_{max} are the maximum mean stress and the maximum deviator stress respectively for a given stress level; m and s_b are the parameters of failure line. ε_1^{p0} is model parameter.

Korkiala-Tanttu, (2005) described the development of permanent deformation using a power function of the number of cycles and the shear stress ratio, the equation was expressed by:

$$\varepsilon_1^p = CN^b \frac{R}{A - R} \tag{I.26}$$

where, C and b are the material parameters. $R=q/q_f$ is the shear stress ratio; $q_f = mp+s$ is the deviator stress at failure; A is the maximum theoretical value for the shear stress ratio ($A=R_{max} = 1.0$). Tanttu recommended $A=1.02–1.05$ to avoid the computation problems.

Trinh et al., (2012) developed an equation relating the permanent axial deformation to the number of cycles, applied deviator stress and the water content based on the results of RLTTs for a fouled ballast, which was expressed by:

$$\varepsilon_1^p = t(w, \Delta q_{\max}) \cdot f(N) \tag{I.27}$$

$$t(w, \Delta q_{\max}) = \varepsilon_1^{P0} \cdot (w + a) \cdot \left(\frac{\Delta q_{\max}}{p_a}\right)^{\alpha} \tag{I.28}$$

where, w is water content; Δq_{max} is maximum amplitude of cyclic deviator stress; ε_1^{p0}, a and α are model parameters.

As in Gidel model, the *f(N)* is the Hornych model which has been introduced in Equation I.18. This model could be used as a tool for assessing the sensitivity of the mechanical properties to changes in water content.

In addition, as Equation I.16 proposed by Veverka, (1979), some researches have also noted the strong correlation between permanent deformation behaviour and resilient deformation behaviour:

Mohammad et al., (2006) developed an equation relating the resilient modulus to the permanent axial deformation, which was expressed by:

$$M_r = 225\left(\varepsilon_1^p\right)^{-0.25} \tag{I.29}$$

where, M_r is the resilient modulus.

Yang et al., (2008a) also proposed an equation relating the permanent axial deformation to the resilient modulus, which was expressed by:

$$\varepsilon_1^p = A \cdot SL^B \cdot \left(\frac{M_r}{M_{r,j}}\right)^C \tag{I.30}$$

where, M_r is the resilient modulus; $M_{r,j}$ is the initial resilient modulus as determined by the first 5 to 10 load cycles; SL is the deviator stress level defined as the ratio of the applied deviator stress to the deviator stress at failure obtained from the static unconsolidation undrained triaxial test; A, B and C are parameters.

In general, these empirical-analytical models could provide reference deformation for rutting in pavement design with respective advantages. However, the effects of water content, fine content and suction in the modelling of permanent deformation behaviour have been seldom studied. Furthermore, as mentioned in section I.4.2, it is possible to estimate limited stresses in a granular material layers due to traffic loading based on shakedown theory. The combination between the evolution of permanent deformation and the limited stresses could improve the pavement design method for rutting.

I.5. Evolution of resilient deformation behaviour of granular material

I.5.1. Factors influencing resilient deformation behaviour

As permanent deformation behaviour, the resilient deformation behaviour is also influenced by some factors, like: stress level and history, density, fine content, water content and suction.

Effect of stress level and stress history

The previous studies of the effect of stress level on granular materials have been summarized by Lekarp et al., (2000a): The resilient modulus M_r increased with an increase of confining pressure and sum of principal stersses (Mitry, 1964; Monismith et al., 1967; Hicks, 1970; Smith & Nair, 1973; Uzan, 1985; Sweere, 1990). The deviator stress was less significant as confining pressure on material stiffness (Morgan, 1966; Hicks, 1970). The resilient Poisson's ratio of UGM increased with increasing deviator stress and decreasing confining pressure (Hicks, 1970; Brown & Hyde, 1975; Kolisoja, 1997).

Besides, in RLTTs, the difference of resilient deformation behaviour between two loading methods of constant confining pressure (CCP) and variable confining pressure (VCP) has been observed by Allen & Thompson, (1974). The results showed CCP method has higher resilient modulus M_r and Poisson's ratio ν comparing to VCP method as shown in *Figure I.32.*

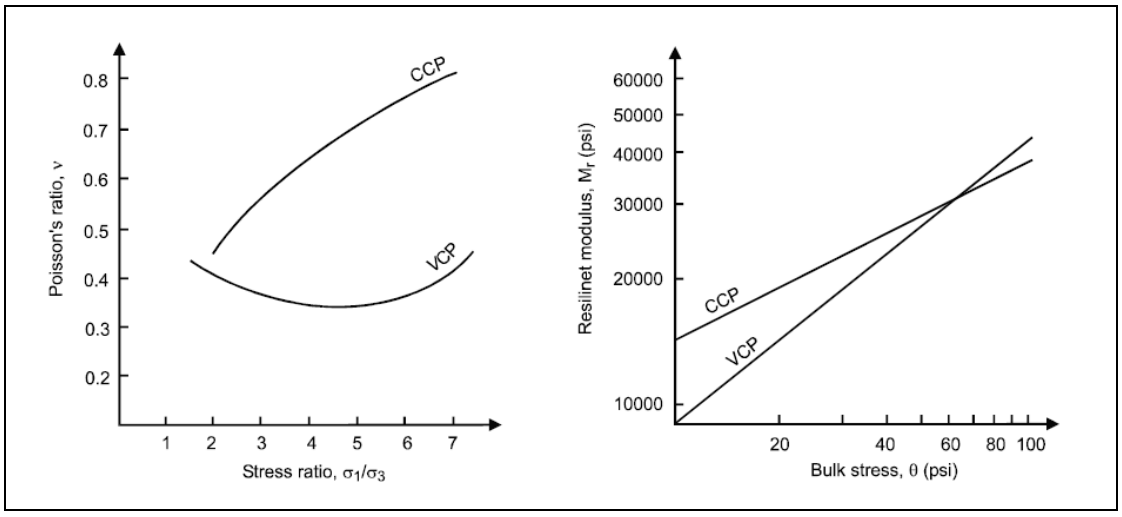

Figure I.32. Triaxial test results with CCP and VCP methods (Allen & Thompson, 1974)

It is important to note that Lekarp et al., (2000a) also addressed the different expressions of M_r and ν with these two loading methods in RLTTs.

For CCP, the M_r and ν were expressed by:

$$M_r = \frac{\Delta(\sigma_1 - \sigma_3)}{\varepsilon_1^r} \quad \text{(I.31)}$$

$$\nu = -\frac{\varepsilon_3^r}{\varepsilon_1^r} \quad \text{(I.32)}$$

where, M_r is resilient modulus; ν is resilient Poisson's ratio; σ_1, σ_3, ε_1^r and ε_3^r are major and minor principal stress and recoverable (or resilient) axial and radial deformation, respectively.

For VCP, based on generalized Hooke's law, the M_r and ν were expressed by:

$$M_r = \frac{\Delta(\sigma_1 - \sigma_3)\Delta(\sigma_1 + 2\sigma_3)}{\varepsilon_1^r \Delta(\sigma_1 + \sigma_3) - 2\varepsilon_3^r \Delta\sigma_3} \quad \text{(I.33)}$$

$$\nu = \frac{\Delta\sigma_1\varepsilon_3^r - \Delta\sigma_3\varepsilon_1^r}{2\Delta\sigma_3\varepsilon_3^r - \varepsilon_1^r \Delta(\sigma_1 + \sigma_3)} \quad \text{(I.34)}$$

In addition, the effect of stress history has been obtained in many researches which could be explained by the progressive densification and particle rearrangement under repeated loads (Dehlen, 1969). The researches showed the effect of stress history could be eliminated by the application of pre-loading to reach a stable resilient response (Hicks, 1970; Boyce, 1976; Allen, 1973). Cerni et al., (2015) reported the UGM subjected to several stress paths after an initial stress conditioning overall showed lower resilient modulus as well as higher stress dependency of the resilient properties comparing with the UGM subjected only a stress state.

Gomes-Correia, (1985) addressed that the loading time and the number of cycles had negligible effect on resilient deformation behaviour of granular materials.

Effect of density

Numerous researches (Trollope et al., 1962; Hicks, 1970; Robinson, 1974; Vuong, 1992; Kolisoja, 1997) of the effect of density (degree of compaction) on resilient deformation behaviour of granular materials showed the M_r increased with an increase of density.

Vuong, (1992) reported, a higher density and a lower water content produced higher resilient modulus and lower plastic deformation, i.e. better material performance. He observed the vertical resilient strain measured in the sample of 95 percent MDD was about 1.4 times higher than that measured in the sample of 100 percent MDD as shown in *Figure I.33*.

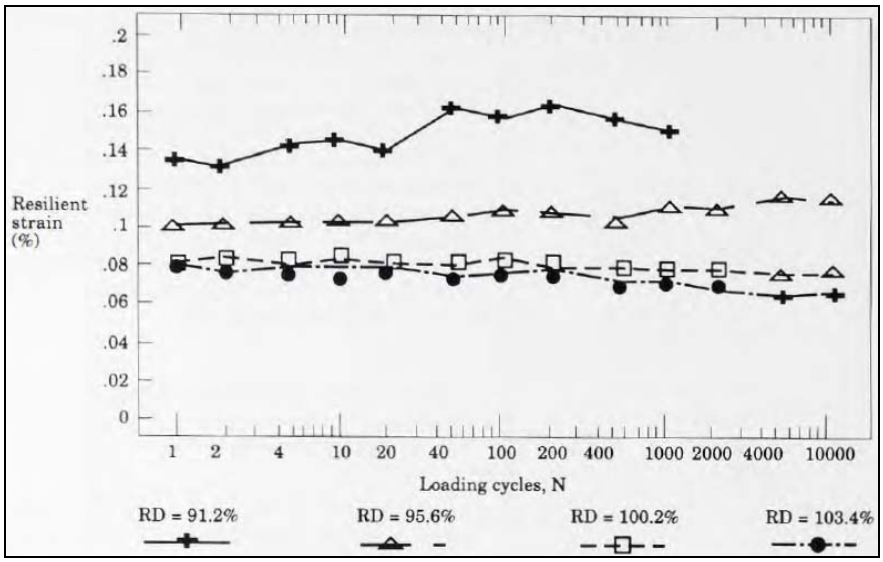

Figure I.33. Variation of resilient strains with loading cycles and relative densities for the moisture content of 5.2% (Vuong, 1992)

The resilient Poisson's ratio is influenced by the effect of density (degree of compaction) as well. This influence was reported by Hicks, (1970) and Allen, (1973). Kolisoja, (1997) found that there was a light decrease of Poisson's ratio with increasing density.

Effect of fine content

The effect of fine content on the resilient response of granular materials is very important. Many researches have showed the M_r decreased when the fine content increased (Thom & Brown, 1987; Barksdale & Itani, 1989; Kamal et al., 1993). Barksdale & Itani, (1989) observed a 60% reduction of M_r when the amount of fine content increased from 0% to 10%.

Jorenby & Hicks, (1986) addressed that the stiffness could increase with an increase of fine content in a relatively low range since the fine particles filled the space between the big grains and add more contacts. However, when the fine content was high, the increasing fine content took the main role and isolated the coarse grains and leaded to decreasing of stiffness.

More recently, the influence of fine content on resilient response has been investigated with water content or suction (Uthus, 2006; Caicedo et al., 2009; Duong et al., 2016). Caicedo et al., (2009) suggested that fine content and crushability acted on the resilient response of the materials only through their effect on the suction curve and therefore through the effect of water on the material response. Duong et al., (2016) also believed the effects of water content and fines content were linked, and it was impossible to distinguish these two effects. When

the soil was under unsaturated state, the higher fine content leaded to higher M_r due to suction effect. When the soil was close to saturated state, the fine contents showed some negative effect on the M_r.

Lekarp et al., (2000a) indicated that the well graded material could achieve a higher density leading to higher M_r. Kolisoja, (1997) showed that the resilient modulus increased with increasing maximum particle size.

Effect of water content and suction

Water in the granular materials has a significant influence on the resilient response under repeated traffic loads. Some researches (Haynes & Yoder., 1963; Hicks & Monismith, 1971) has shown the increase of water content could lead to a reduction of M_r. Haynes & Yoder, (1963) observed a 50% decrease of M_r in a gravel with an increase of the degree of saturation from 70% to 97%. Hicks and Monismith (1971) presented that the M_r decreased as water content increased above the optimum moisture content (OMC).

For a high-water content state or saturation state, it can be supposed that the generation of excessive pore water under the repeated loads could reduce the soil effective stress and leads to decrease of stiffness of soil. As a result, the decrease of M_r trends to be more obvious. Besides, the resilient response of granular materials in a dry state has been discussed by Caicedo et al., (2009) who indicated the secant modulus decreased significantly as water content decreased from 5% to 0 as shown in *Figure I.34*.

As mentioned above, in some researches (Caicedo et al., 2009; Duong et al., 2016), the effects of water content and fine content were linked usually and worked as suction form in unsaturated soil. Furthermore, the suction value (negative pore water pressure) was the key role of effective stress analysis in unsaturated state. Many researchers have shown the strong correlations between suction value and resilient response of granular materials (Coussy & Dangla, 2002; Kolisoja et al., 2002; Fleureau et al., 2003; Coronado et al., 2004; Yang et al., 2008b; Cary & Zapata, 2011; Nowamooz et al., 2011; Ng et al., 2013; Ho et al., 2014b; Han & Vanapalli, 2015; Salour & Erlingsson, 2015a; Coronado et al., 2016) as M_r increased with increasing matric suction.

Ng et al., (2013) reported that when suction increased from 0 to 250 kPa, M_r increased by up to one order of magnitude. At the same given stress and suction level, M_r measured in wetting

path was larger than that in a drying path at low cyclic stress. And the difference trend to become less with an increase of cyclic stress as shown in *Figure I.35*.

Nowamooz et al., (2011) and Ho et al., (2014b), indicated the effective stress concept based on the negative pore water pressure could improve the accuracy of evaluating the resilient deformation behaviour comparing with total stress concept.

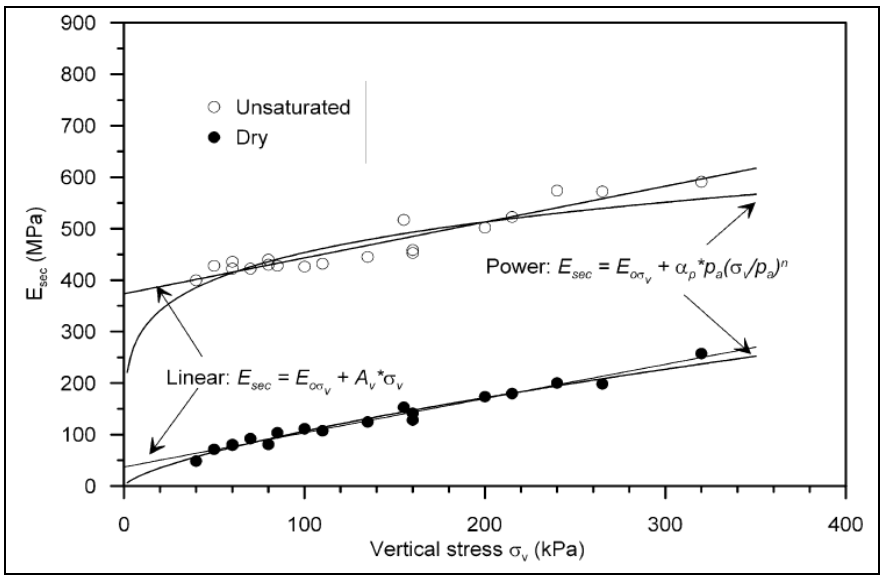

Figure I.34. Secant modulus vs. vertical stress for the unsaturated and dry materials at 5% water content and dry (Caicedo et al., 2009)

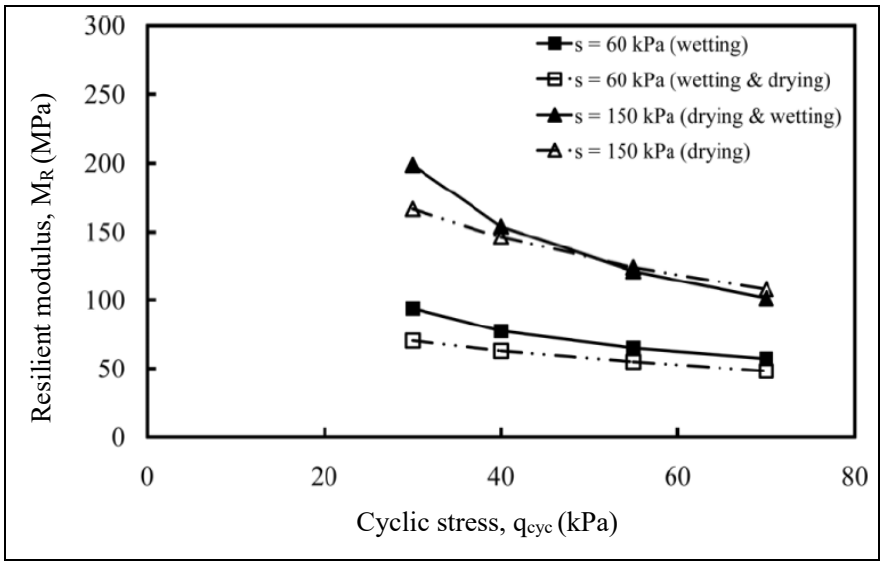

Figure I.35. Influence of wetting and drying history on resilient modulus (Ng et al., 2013)

I.5.2. Models predicting resilient deformation behaviour

The granular materials exhibit a complex non-linear response under repeated loading and reliable description of resilient behaviour using experimental methods with or without soil suction control is time-consuming and needs sophisticated equipment as well as trained personnel (Han & Vanapalli., 2016). Hence, in the past years, various empirical-analytical models have been proposed to predict the resilient deformation behaviour based on resilient modulus and Poisson's ratio or volumetric and shear stress-strain relationships.

Lekarp et al., (2000a) have summarized many computational models for resilient deformation behaviour as shown in *Table I.6 and Table I.7.* This section will highlight some important models and add some new models.

These notations will be used in the following part:

ε_1^r is the resilient axial deformation;

ε_3^r is the resilient radial deformation;

ε_v^r is the resilient volumetric deformation;

ε_q^r is the resilient deviatoric deformation.

$$K = \frac{p}{\varepsilon_v^r} \; ; \; G = \frac{q}{3\varepsilon_q^r} \tag{I.35}$$

$$\varepsilon_v^r = \left(\varepsilon_1^r + 2\varepsilon_3^r\right) \; ; \; \varepsilon_q^r = \frac{2}{3}\left(\varepsilon_1^r - \varepsilon_3^r\right) \tag{I.36}$$

Linear elastic models

Based on the Hooke's law, the linear elastic model is expressed by:

$$\begin{bmatrix} \varepsilon_v \\ \varepsilon_q \end{bmatrix} = \frac{1}{E}\begin{bmatrix} 3(1-2\nu) & 0 \\ 0 & \frac{2}{3}(1+\nu) \end{bmatrix} \cdot \begin{bmatrix} p \\ q \end{bmatrix} \tag{I.37}$$

where, E is the elastic modulus of material; ν is the resilient Poisson's ratio.

Under repeated loads, the resilient modulus and resilient Poisson's ratio of material has been defined in Equation I.31 and I.32

The bulk modulus (K) and shear modulus (G) can be expressed by M_r and ν:

$$K=\frac{M_r}{3(1-2\nu)} \quad \text{and} \quad G=\frac{M_r}{2(1+\nu)} \tag{I.38}$$

Models base on resilient modulus and Poisson's ratio

Dunlap, (1963) believed the M_r was highly related to the confining pressure and wouldn't be affected by deviator stress. An equation was proposed as:

$$M_r=k_1\cdot\sigma_3^{k_2} \tag{I.39}$$

where, k_1 and k_2 are parameters.

Seed et al., (1967); Brown & Pell, (1967); Hicks, (1970) proposed a hyperbolic equation for M_r based on mean normal stress which was called K-θ model.

$$M_r=k_1\cdot(3p/p_a)^{k_2}=k_1\cdot(\theta/p_a)^{k_2} \tag{I.40}$$

where, k_1 and k_2 are parameters.

This simple and useful model was the foundation of many other models. However, this model assumed the Poisson's ratio was constant which has been observed as a varying value and based on the applied stress by Hicks, (1970); Boyce, (1980); Sweere. (1990).

Expression	No	Reference	Expression	No	Reference
$M_r = k_1\sigma_3^{k2} \ <or>\ M_r = k_1\left(\frac{\sigma_3^{k2}}{p_0}\right)$	(1)	Dunlap (1963)	$\begin{cases} M_r = A(n_{\max} - n)p_0\left(\frac{\theta}{p_0}\right)^{0.5} \\ M_r = B(n_{\max} - n)p_0\left(\frac{\theta}{p_0}\right)^{0.7}\left(\frac{q}{p_0}\right)^{-0.2} \end{cases}$	(8)	Kolisoja (1997)
$M_r = N_1 q^{N2}\sigma_3^{N3}$	(2)	Pezo (1993)			
$M_r = k_1(\frac{p}{q})^{k2}$	(3)	Tam & Brown (1988)			
$M_r = k_1(\frac{J_2}{\tau_{\text{oct}}})^{k2}$	(4)	Johnson et al. (1986)	$M_r = A(\frac{p_m}{p_u})^B(\frac{p_u}{\delta p})^C$	(9)	Karasahin (1993)
$M_r = k_1\theta^{k2} \ <or>\ M_r = k_1\left(\frac{\theta}{p_0}\right)^{k2}$	(5)	Seed et al. (1967)	$\begin{cases} M_r = \frac{\theta}{q}(A + Bq) & \text{"CCP"} \\ M_r = \frac{\theta}{\sigma_1}(C + Dq) & \text{"VCP"} \end{cases}$	(10)	Nataatmadja & Parkin (1989)
$M_r = k_1 p_0\left(\frac{\theta}{p_0}\right)^{k2}\left(\frac{q}{p_0}\right)^{k3} <or>$ $M_r = k_1 p_0\left(\frac{\theta}{p_0}\right)^{k2}\left(\frac{\tau_{\text{oct}}}{p_0}\right)^{k3}$	(6)	Uzan (1985)	$\nu_r = A + B\left(\frac{\sigma_1}{\sigma_3}\right) + C\left(\frac{\sigma_1}{\sigma_3}\right)^2 + D\left(\frac{\sigma_1}{\sigma_3}\right)^3$	(11)	Hicks & Monismith (1971)
$M_r = k_1\frac{\theta^{k2}}{10^{A1}}$	(7)	Elliot & Lourdesnathan (1989)	$\nu_r = A\left(\frac{q_m}{p_u}\right)^B\left(\frac{p_u}{p_m}\right)^C\left(\frac{p_u}{\delta p}\right)^D$	(12)	Karasahin (1993)

M_r = resilient modulus
ν_r = Poisson's ratio
σ_1, σ_2, σ_3 = principal stresses
q = deviator stress $=\sigma_1 - \sigma_3$
p = mean normal stress $=(\sigma_1 + \sigma_2 + \sigma_3)/3$
q_m $=(q_{\max} + q_{\min})/2$
p_m $=(p_{\max} + p_{\min})/2$
δp $= p_{\max} - p_{\min}$
θ = bulk stress $=3p$
τ_{oct} = octahedral shear stress $=(2^{0.5}/3)q$

J_2 = first stress invariant
$=\sigma_1\sigma_2 + \sigma_2\sigma_3 + \sigma_3\sigma_1$
$\sigma_{1,x}$ $= \sigma_{1,\max} - \sigma_{1,\min}$
$\sigma_{3,x}$ $= \sigma_{3,\max} - \sigma_{3,\min}$
$\varepsilon_{1,x}$ = resilient axial strain
$\varepsilon_{3,x}$ = resilient horizontal strain
$n_{\max}$ = maximum porosity
n = material porosity
A_1 = mR^3
R = stress/strength

p_0 = atmospheric pressure (100kPa)
p_u = unit pressure (1 kPa)
$N_1 - N_3$ = $(10 - A), (1 - k_1)$, and $(-k_2)$, respectively, in $\log(\varepsilon_{1,x}) = A + k_1\log\sigma_1 + k_2\log\sigma_2$
k_1, k_2, k_3,
m, A - J =model parameters
CCP = constant confining pressure
VCP = variable confining pressure

Table I.6. Mathematical expressions for resilient modulus and Poisson's ratio (Lekarp et al., 2000a)

Expression	No	Reference	Parameters
$\begin{cases}\varepsilon_v = p^{\wedge}\frac{1}{K_1}\left[1-\beta\frac{q^2}{p^2}\right]\\ \varepsilon_s = p^{\wedge}\frac{1}{3G_1}\left(\frac{q}{p}\right)\end{cases}$	(13)	Boyce (1980)	
$\begin{cases}\varepsilon_v = \delta\left[\left(\frac{p}{A}\right)^n\left(1-C\left(\frac{q}{p}\right)^2\right)\right]\\ \varepsilon_s = D\delta\left[\frac{q}{p+E}\right]\left[\frac{\sqrt{p_r^2+q_r^2}}{p_m}\right]^F\end{cases}$	(14)	Brown and Pappin (1985)	ε_v = resilient volumetric strain ε_s = resilient shear strain $\sigma_1, \sigma_2, \sigma_3$ = principal stresses q = deviator stress $=\sigma_1-\sigma_3$ p = mean normal stress $=(\sigma_1+\sigma_2+\sigma_3)/3$ β = $(1-A)K_1/6G_1$ p_r = $p_{max}-p_{min}$ q_r = $q_{max}-q_{min}$ p_m = $(p_{max}+p_{min})/2$ τ = shear stress in Mohr circle plot S = normal stress in Mohr circle plot p_0 = atmospheric pressure $(100kPa)$ γ = coefficient of anisotropy (decided by regression analysis) p^* = $(\gamma\sigma_1+2\sigma_3)/3$ q^* = $\gamma\sigma_1-\sigma_3$ δ = change in A-G, K_1, G_1 = model parameters
$\begin{cases}\varepsilon_v = A(\delta\ln p)^B(\delta p)^C - D\left[\delta\left(\ln\frac{\sigma_1}{\sigma_3}\right)^2\right]^E\\ \varepsilon_s = E\left[\delta\left(\ln\frac{\sigma_1}{\sigma_3}\right)^2\right]^F\left(\delta\tau+\frac{1}{3}\delta S\right)^G\end{cases}$	(16)	Thom (1988)	
$\begin{cases}\varepsilon_v = p_0^{1-B}p^B\left[\frac{1}{A}-\frac{(1-B)}{6C}\left(\frac{q}{p}\right)^2-\frac{B}{D}\left(\frac{q}{p}\right)\right]\\ \varepsilon_s = p_0^{1-B}p^B\left[\frac{1}{3C}\left(\frac{q}{p}\right)-\frac{1}{D}\right]\end{cases}$	(17)	Elhannani (1991)	
$\begin{cases}\varepsilon_v = \frac{p^{*A}}{p_0^{A-1}}\left[\frac{\gamma+2}{3K_1}+\frac{A-1}{18G_1}(\gamma+2)\left(\frac{q^*}{p^*}\right)^2+\frac{\gamma-1}{3G_1}\left(\frac{q^*}{p^*}\right)\right]\\ \varepsilon_s = \frac{2}{3}\frac{p^{*A}}{p_0^{A-1}}\left[\frac{\gamma-1}{3K_1}+\frac{A-1}{18G_1}(\gamma-1)\left(\frac{q^*}{p^*}\right)^2+\frac{2\gamma+1}{6G_1}\left(\frac{q^*}{p^*}\right)\right]\end{cases}$	(18)	Hornych et al. (1998)	

Table I.7. Mathematical expressions for volumetric and shear stress-strain relationships (Lekarp et al., 2000a)

Uzan, (1985) introduced the deviator stress q into K-θ model which was expressed by:

$$M_r = k_1 \cdot p_a \cdot \left(\frac{3p}{p_a}\right)^{k_2} \cdot \left(\frac{q}{p_a}\right)^{k_3} \quad \text{(I.41)}$$

where, k_1, k_2 and k_3 are parameters.

Thom & Brown, (1988) indicated the M_r was related to the stress ratio. The equation was expressed as:

$$M_r = k_1 \cdot \left(\frac{p}{q}\right)^{k_2} \quad \text{(I.42)}$$

where, k_1 and k_2 are parameters.

Kolisoja, (1997) took the effect of material density into the K-θ model and the Uzan model. The new equation was expressed as:

$$M_r = A \cdot (n_{max} - n) \cdot p_a \cdot \left(\frac{\theta}{p_a}\right)^{0.5} \quad \text{(I.43)}$$

$$M_r = B \cdot (n_{max} - n) \cdot p_a \cdot \left(\frac{\theta}{p_a}\right)^{0.7} \cdot \left(\frac{q}{p_a}\right)^{-0.2} \quad \text{(I.44)}$$

where, n_{max} is maximum porosity; n is material porosity; A and B are parameters.

As mentioned in last section, M_r is influenced by the suction or degree of saturation. Several researchers proposed various equations to predict the correlation *of* M_r and suction (Yang et al., 2005; Liang et al., 2008; Cary & Zapata, 2011; Ng et al., 2013; Han & Vanapalli., 2015).

Yang et al., (2005) introduced the Bishop effective stress into an equation suggested by AASHTO T 292-91, which was expressed as:

$$M_r = k_1 \cdot (q)^{k_2} \quad \text{(I.45)}$$

Then, the new equation was expressed by:

$$M_r = k_3 \cdot (q - u_a + \chi s)^{k_4} \quad \text{(I.46)}$$

where, χ is effective stress parameter; s is suction; u_a is pore air pressure; k_1, k_2, k_3 and k_4 are parameters.

Han & Vanapalli, (2015) proposed an equation to predict the variation of the M_r with respect to the suction for compacted fine-grained subgrade soils, which was expressed by:

$$\frac{M_r - M_{rsat}}{M_{ropt} - M_{rsat}} = \frac{s}{s_{opt}} \left\{ \frac{\ln\left[2.718 + \left(\frac{s_{opt}}{a}\right)^n\right]}{\ln\left[2.718 + \left(\frac{s}{a}\right)^n\right]} \right\}^{m\xi} \quad \text{(I.47)}$$

where, M_{ropt} is the resilient modulus at optimum moisture content; M_{rsat} is the resilient modulus in saturation condition; s is suction value and s_{opt} is the suction at optimum moisture content; a, n, m and ξ are parameters.

Hicks & Monismith, (1971) developed an equation to predict ν based on the applied stress as expressed by:

$$\nu_r = A + B \cdot \left(\frac{\sigma_1}{\sigma_3}\right) + C \cdot \left(\frac{\sigma_1}{\sigma_3}\right)^2 + D \cdot \left(\frac{\sigma_1}{\sigma_3}\right)^3 \quad \text{(I.48)}$$

where, σ_1, σ_2 and σ_3 are the principal stresses; A, B, C and D are parameters.

Karasahin, (1993) related the ν to mean normal stress and proposed an equation as expressed by:

$$\nu_r = A \cdot \left(\frac{q_m}{p_u}\right)^B \cdot \left(\frac{p_u}{p_m}\right)^C \cdot \left(\frac{p_u}{\delta_p}\right)^D \quad \text{(I.49)}$$

where, $p_m = (p_{max} + p_{min})/2$;

$q_m = (q_{max} + q_{min})/2$;

$\delta_p = p_{max} - p_{min}$;

p_u is unit pressure (1kPa); A, B, C and D are parameters.

Models base on volumetric and shear stress-strain relationships

Boyce, (1980) proposed an isotropic non-linear model for predicting the resilient deformation behaviour of granular materials. The derivation of this model is introduced as follows:

First, the experimental work (Hicks & Monismith, 1971; Allen & Thompson, 1974) showed that the stiffness of a granular material was proportional to the mean normal stress raised to a

power less than one. As a result, the bulk moduli K and shear moduli G could be expressed by the functions:

$$K = K_a \cdot p^{(1-n)} \tag{I.50}$$

$$G = G_a \cdot p^{(1-n)} \tag{I.51}$$

where, K_a, G_a and n are parameters.

However, these equations didn't conform with the reciprocity theorem (Boyce, 1980) which could be applied to any linear or non-linear elastic behaviour. This reciprocity showed that the following relationship should be satisfied:

$$\frac{\partial \varepsilon_v^r}{\partial q} = \frac{\partial \varepsilon_q^r}{\partial p} \tag{I.52}$$

Hence, to conform the reciprocity, the equations were modified as following:

$$K = K_a \cdot p^{(1-n)} / \left(1 - \beta \frac{q^2}{p^2}\right) \tag{I.53}$$

$$G = G_a \cdot p^{(1-n)} \tag{I.54}$$

where, $\beta = (1-n) K_a / (6G_a)$

This indicated the bulk moduli K increased with an increase of stress ratio and shear moduli G increased only with the mean normal stress. As a result, the volumetric deformation and deviatoric deformation could be expressed as:

$$\varepsilon_v^r = \frac{1}{K_a} p^n (1 - \beta \frac{q^2}{p^2}) = \frac{1}{K_a} p^n \left[1 + \frac{(n-1) \cdot K_a}{6G_a} \left(\frac{q}{p}\right)^2\right] \tag{I.55}$$

$$\varepsilon_q^r = \frac{1}{3G_a} p^n \frac{q}{p} \tag{I.56}$$

and then the potential function was obtained by integration as:

$$W = p^{n+1} \left[\frac{1}{(n+1)K_a} + \frac{1}{6G_a} \left(\frac{q}{p}\right)^2\right] \tag{I.57}$$

Hornych and co-workers (1998) introduced the anisotropic response of granular materials into Boyce model through multiplying the axial stress by a coefficient of anisotropy γ_1. Thus, the new mean normal stress p^* and the new deviator stress q^* could be re-expressed as follows:

$$p^* = \frac{\gamma_1\sigma_1 + 2\cdot\sigma_3}{3} \tag{I.58}$$

and

$$q^* = \gamma_1\sigma_1 - \sigma_3,\ 0 < \gamma_1 < 1 \tag{I.59}$$

Then the potential function (Equation I.57) using the new p^* and q^* instead of p and q, and the homogenization parameter (Pa = 100kPa) could be rewritten as:

$$W = \frac{\left[\frac{\gamma_1\cdot\sigma_1 + 2\cdot\sigma_3}{3}\right]^{n+1}}{{p_a}^{n-1}}\left[\frac{1}{(n+1)K_a} + \frac{1}{6G_a}\left(\frac{\gamma_1\sigma_1 - \sigma_3}{\frac{\gamma_1\sigma_1 + 2\sigma_3}{3}}\right)^2\right] \tag{I.60}$$

The new equations of resilient volumetric and deviatoric deformation could be proposed by taking the derivative of potential function (Equation.I.60) as:

$$\varepsilon_v^r = \frac{{p^*}^n}{{p_a}^{n-1}}\left[\frac{\gamma_1+2}{3\cdot K_a} + \frac{n-1}{18\cdot G_a}(\gamma_1+2)\cdot\left(\frac{q^*}{p^*}\right)^2 + \frac{\gamma_1-1}{3\cdot G_a}\cdot\frac{q^*}{p^*}\right] \tag{I.61}$$

and

$$\varepsilon_q^r = \frac{2}{3}\cdot\frac{{p^*}^n}{{p_a}^{n-1}}\left[\frac{\gamma_1-1}{3\cdot K_a} + \frac{n-1}{18\cdot G_a}(\gamma_1-1).\left(\frac{q^*}{p^*}\right)^2 + \frac{2\cdot\gamma_1+1}{6\cdot G_a}\cdot\frac{q^*}{p^*}\right] \tag{I.62}$$

In the same research, Hornych et al., (1998) reported that the results of RLTTs was fitted by Boyce model with a quite poor correlation, apparently because of the cross-anisotropic behaviour of granular materials. However, the new model showed a good agreement between measured and modelling results as shown in *Figure I.36.* The modified Boyce model will be discussed in detail in Chapter IV.

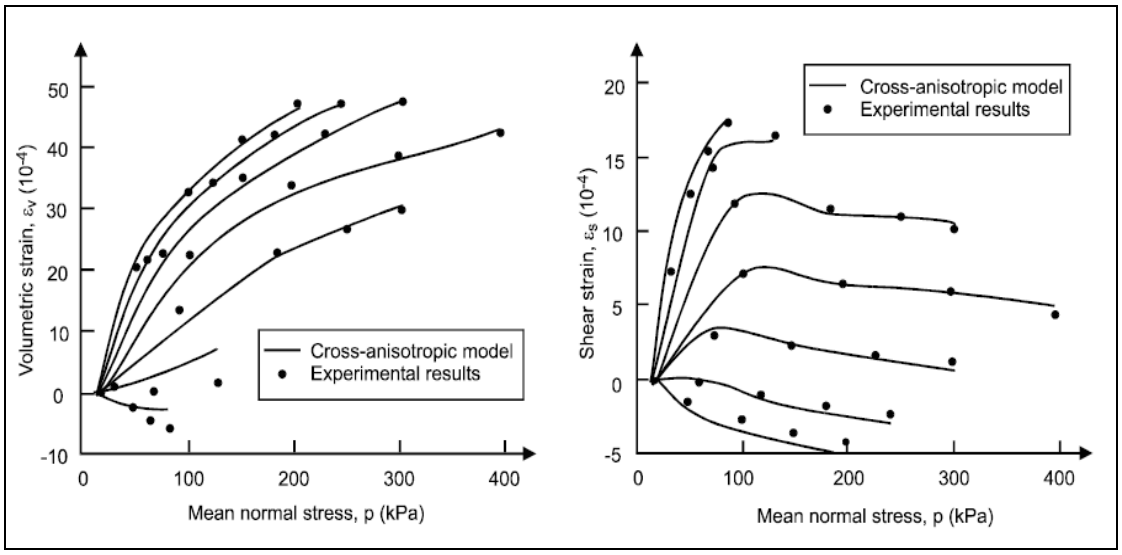

Figure I.36. Examples of fit using the cross-anisotropic model (Hornych et al., 1998)

Ho, (2013) and Ho et al., (2014b) investigated the effect of hydraulic hysteresis on the resilient behaviour of low traffic pavements based on the effective stress concept. The modified Equations I.61 & 62 were used to estimate the resilient volumetric and deviatoric deformation founded on Bishop effective stress equation (Equation I.11), which were expressed as:

$$\varepsilon_v^r = \frac{p'^n}{p_a{}^{n-1}}\left[\frac{\gamma_1+2}{3\cdot K_a}+\frac{n-1}{18\cdot G_a}(\gamma_1+2)\cdot\left(\frac{q'}{p'}\right)^2+\frac{\gamma_1-1}{3\cdot G_a}\cdot\frac{q'}{p'}\right] \tag{I.63}$$

and

$$\varepsilon_q^r = \frac{2}{3}\cdot\frac{p'^n}{p_a{}^{n-1}}\left[\frac{\gamma_1-1}{3\cdot K_a}+\frac{n-1}{18\cdot G_a}(\gamma_1-1).\left(\frac{q'}{p'}\right)^2+\frac{2\cdot\gamma_1+1}{6\cdot G_a}\cdot\frac{q'}{p'}\right] \tag{I.64}$$

where

$$p' = \frac{(\gamma_1\sigma_1-u_a)+\chi.s+2.(\sigma_3-u_a)+2\chi.s}{3} = p^*+\chi.s \tag{I.65}$$

and

$$q' = (\gamma_1\sigma_1-u_a)+\chi.s-(\sigma_3-u_a)-\chi.s = \gamma_1\sigma_1-\sigma_3 = q^* \tag{I.66}$$

The results showed that it could improve the accuracy of evaluating the resilient deformation based on effective stress concept.

I.6. Conclusion

In this chapter, we review two methods of pavement design based on the understanding of low traffic pavement structures. Both empirical method and analytical method do not take into account the hydro-mechanical behaviour and the elastoplastic deformation behaviour in granular material layers. Consequently, the behaviours of granular material in low traffic pavements are summarized including: stress state, deformation behaviour (permanent and resilient), characterization methods and unsaturated state.

Based on the literature review, it can be concluded that the permanent deformation behaviour is influenced by some factors, such as: stress level, stress history, principal stress rotation, number of loading cycles, density, fine content, size distribution, aggregate type, water content and suction. There are lots of empirical-analytical models depending on the number of loading cycles or the stress level applied and they can be used to describe the permanent deformation behaviour of granular materials. Besides, it is possible to estimate limited stresses in a granular material layers due to traffic loading based on shakedown theory.

Similarly, the resilient deformation behaviour is influenced by some factors such as: stress level and history, density, fine content, water content and suction. These models based on resilient modulus and Poisson's ratio or volumetric and shear stress-strain relationships have been proposed by different researchers.

However, the coupled effects of fine content, water content and suction on the permanent and resilient deformation behaviour of granular materials have been rarely studied, especially for the permanent deformation behaviour. For the resilient deformation behaviour, the coupled effects were only investigated for the resilient modulus rather than the volumetric and the shear stress-strain relationship.

In the following chapters, we will present the hydro-mechanical behaviour of compacted granular materials influenced by the coupled factors under repeated loading/unloading cycles.

CHAPTER II. MATERIAL STUDIED AND LABORATORY TESTING

II.1. Introduction

The first chapter has shown some principal mechanical behaviours of granular material in literatures. This chapter first presents characteristics of two studied materials named as Missillac sand and unbound granular material (UGM) Maraîchères. After that, two suction measurement techniques are introduced for these two materials. At the end, the repeated load triaxial test (RLTT) is fully presented to study the cyclic hydro-mechanical behaviour of granular materials, including: sample preparation, experimental devices, experimental procedures.

II.2. Material studied

II.2.1. Missillac sand

The studied material of Missillac fine sand is an alluvial sand coming from the quarry of Missillac in France as shown in *Figure II.1*. The particle size varies between 0 and 4 mm. This soil is used as subgrade soil in low traffic pavements for full-scale pavement tests at IFSTTAR (Institut Français des Sciences et Technologies des Transports, de l'Aménagement et des Réseaux) in Nantes, France. The specific gravity *Gs* of this soil is 2.65 g/cm^3.

Figure II.1. Missillac sand

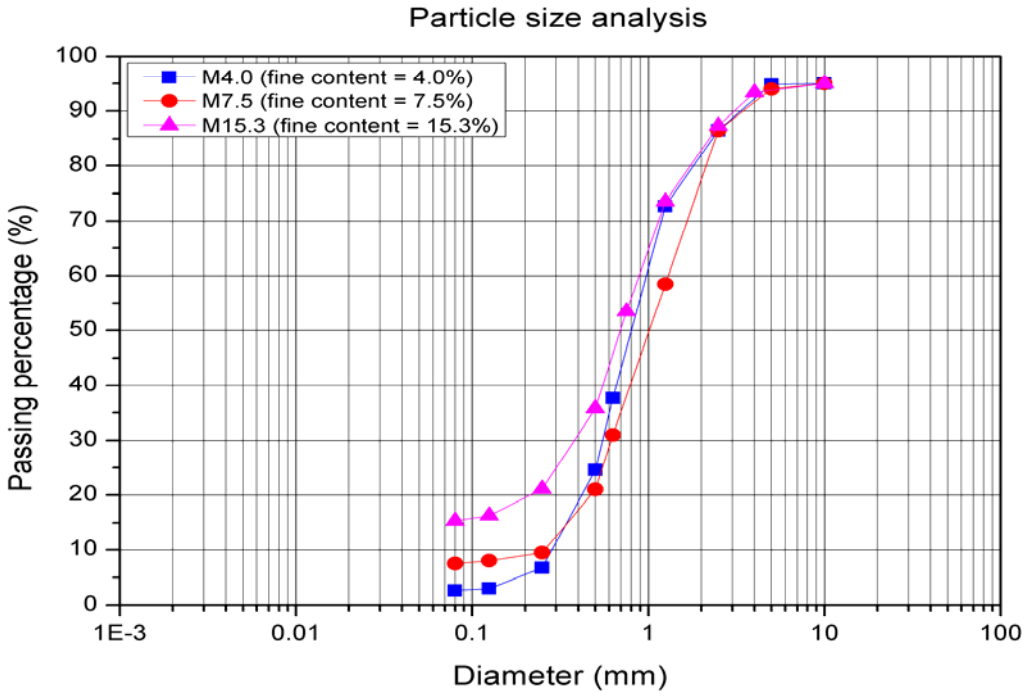

Figure II.2. Particle size distribution curves of Missillac sand (M4.0, M7.5 and M15.3)

It is sensitive to moisture and its in situ elastic modulus typically varies between 50 and 100 MPa.

In this study, the natural samples contain three different fine contents:

- M4.0 samples with 4.0% of fine content (passing through the sieve 75 µm).
- M7.5 samples with 7.5% of fine content (studied by IFSTTAR in 2002).
- M15.3 samples with 15.3% of fine content.

Material	Fraction (%)				Particle size					Blue value	Classification	
	0/80 µm	0.08/0.4 mm	0.4/2 mm	2/4 mm	d_{60}	d_{30}	d_{10}	C_u	C_c		NF	USCS
M4.0	4	10	76	5	0.95	0.55	0.30	3.17	1.06	---	B2	SP
M7.5	7.5	6.5	76	5	1.40	0.60	0.25	5.60	1.03	0.56	B2	SP-SC
M15.3	15.3	14.7	55	10	0.85	0.40	---	8.50	1.88	0.85	B5	SC

Table II.1. Characteristics of the studied materials

Figure II.2 shows the particle size distribution for the studied soils (XP P94-041,1995). *Table II.1* presents all characteristic parameters of these curves, such as C_c and C_u. The coefficients of curvature (C_c) show a well-graded composition (estimated between 1 and 3) of the studied granular materials.

Figure II.3 and *Table II.1* also show the methylene blue values (VBS) of Missillac sand M7.5 and M15.3 (NF P94-068, 1993). It states normally that the more the fine content, the larger the methylene blue value.

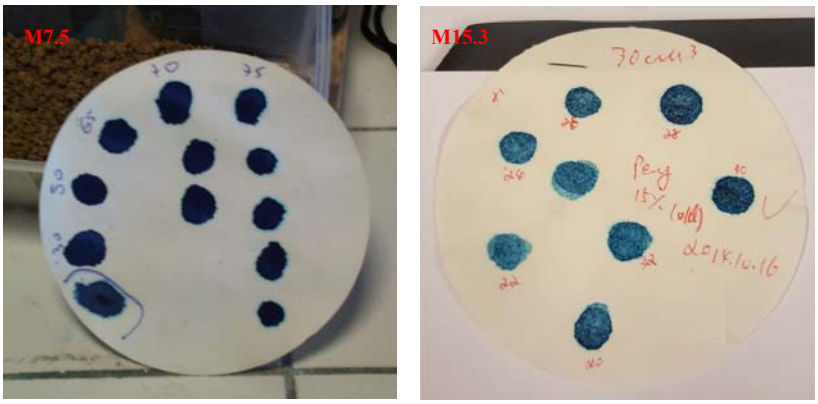

Figure II.3. Results of Methylene blue tests (M7.5 and M15.3)

Soil can be classified based on the methylene blue values and the particle size distribution (NF P11-300, 1992 or USCS ASTM D2487 - 06) as reported in *Table II.1*.

Figure II.4 presents the standard Proctor compaction curves for Missillac sand M4.0, M7.5 and M15.3. *Table II.2* shows the optimal water content (OMC) and the maximum dry density (MDD) for the different studied materials.

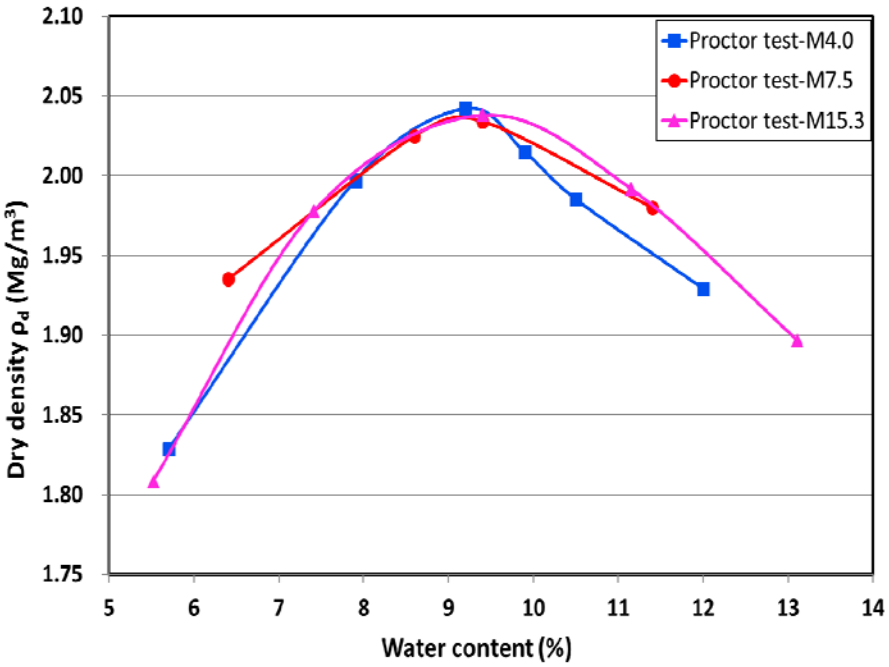

Figure II.4. Standard Proctor compaction curves (M4.0, M7.5 and M15.3)

Material	OMC	MDD
	%	Mg/m^3
M4.0	9.3	2.04
M7.5	9.1	2.04
M15.3	9.5	2.04

Table II.2. Results of standard Proctor compaction tests

Based on the standard Proctor compaction curves and the values of OMC and MDD, it can be stated that the OMC and the MDD are almost the same for these three different materials. Consequently, all the samples will be prepared in a water content range between 7% (Sr = 57.1%) and 11% (Sr = 89.7%) and a dry density close to 2.0 Mg/m^3 (e = 0.325) for the following tests.

II.2.2. UGM Maraîchères

The UGM Maraîchères are used in base layer in the annular fatigue test field by Ifsttar (L'Institut français des sciences et technologies des transports, de l'aménagement et des réseaux) in 2003. This material is a kind of Gneiss with a size of 0/20 mm as shown in *Figure II.5*.

Figure II.5. UGM Maraîchères

This material is composed of a mixture of 5 different compositions: sand 0/4 mm, gravel 2/6.3 mm, gravel 4/10 mm, gravel 10/20 mm, gravel 14/20 mm. *Figure II.6* shows the particle size distribution of UGM Maraîchères. For this material, the VBS is 0.79 and the elastic modulus is 400 MPa.

Figure II.7 also presents the modified Proctor compaction curves for UGM Maraîchères. The optimal water content (OMC) is 5.8% and the maximum dry density (MDD) is 2.20 Mg/m^3.

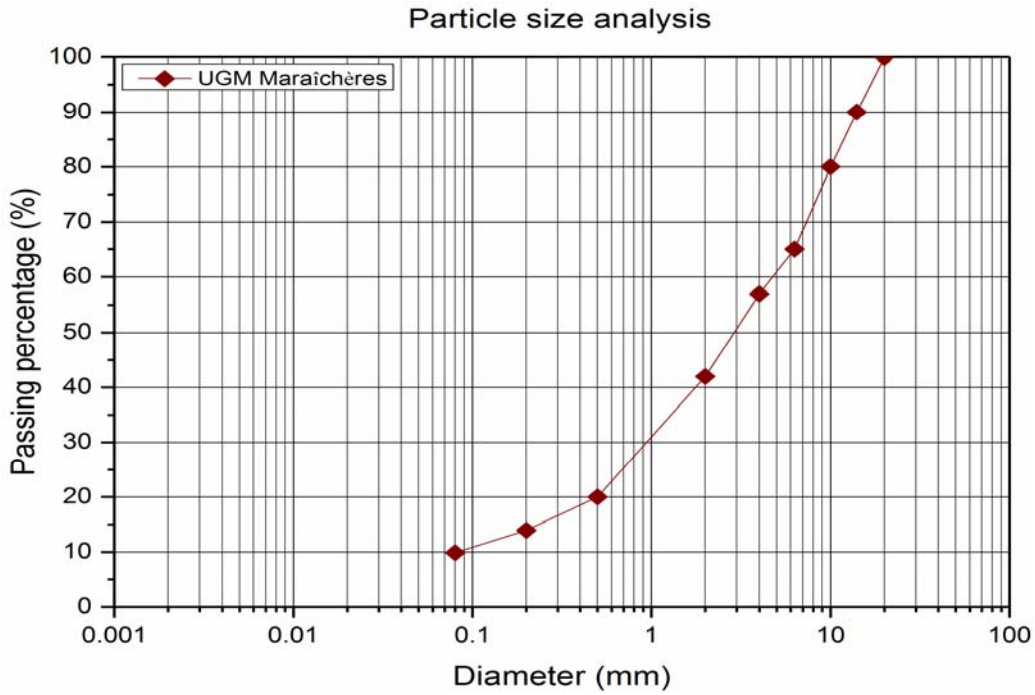

Figure II.6. Particle size distribution curves of UGM Maraîchères

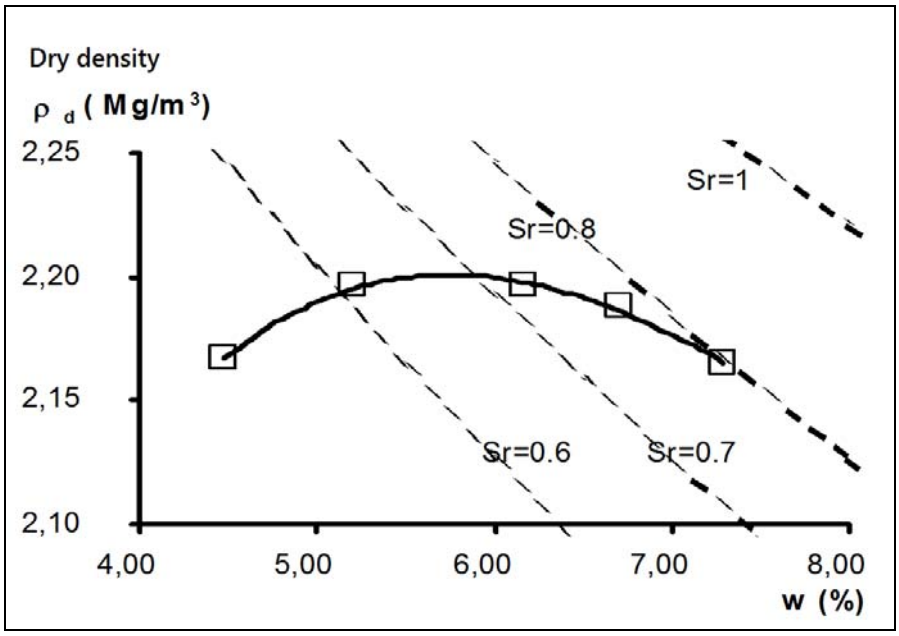

Figure II.7. Modified Proctor Compaction (UGM Maraîchères)

II.3. Soil suction measurement

II.3.1. Filter paper method

The filter paper method is widely used to measure the soil suction based on the assumption of equilibrium (moisture flow) establishment between filter paper and soil at a given suction. For

measuring a matrix suction, a filter paper sandwich is placed in direct contact with a soil sample, it is assumed that moisture flows from soil to filter paper to reach an equilibrium as shown in *Figure II.8*. For measuring a total suction, a dry filter paper is suspended above a soil sample, it is assumed that vapor flow happens through soil to filter paper. Once equilibrium arriving, the water content of filter paper is measured to calculate the suction value according to the calibration curve of filter paper (Fredlund & Rahardjo, 1993). This method can measure suctions up to 10 MPa.

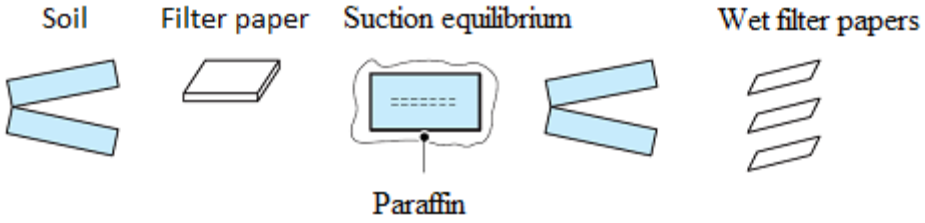

Figure II.8. Fitler paper method to measure soil matric suction (Ho, 2013)

Matric suction measurement with filter paper method (Ben Mahmoud-2010; Jing-2015)

In the present work, the matric suction of all the samples, on the wetting and drying paths, is measured by the filter paper technique (ASTM D5298-10, 1995). For the wetting path of the Soil Water Retention Curve (SWRC), the samples are prepared at a water content ranging from 7% to 12.3 % for Missillac sand (4% to 8% for UGM Maraîchères). For the drying path, the samples initially saturated (12.3% for Missillac sand and 8% for UGM Maraîchères) are dried in the ambient temperature (20°) to reach the desired water content. The samples are prepared at an initial dry density ranging of 2±0.06 Mg/m^3 for Missillac sand (2.13 Mg/m^3 for UGM Maraîchères). The soil samples are compacted in two layers with a thickness of 1.3cm to 1.6cm per layer for Missillac sand (2.5cm per layer for UGM Maraîchères). Whatman No.42 filter paper is placed between other two pieces of filter papers with a larger diameter. Three filter papers are then inserted between two soil layers. Afterwards, the samples are placed into a sealed jar and maintained for 10 days to reach the state of equilibrium. Finally, the middle piece of filter paper is weighted by a balance with an accuracy of 0.0001g to obtain the water content of filter paper and then the suction value is determined. The devices and samples of suction measurement (filter paper method) for Missillac sand and UGM Maraîchères are presented in *Figure II.9-12*.

Figure II.9. Missillac sand samples of suction measurement with filter paper method (M4.0 and M15.3)

Figure II.10. Jar containing the sample of Missillac sand and gauze-plate for drying

Figure II.11. Filter paper inserted in a sample of UGM Maraîchères

Figure II.12. Cylinder containing the sample of UGM Maraîchères

II.3.2. Tensiometer method

The tensiometer method is also commonly used to measure the negative pore-water pressure in a soil. The tensiometer consists of a high air entry, porous ceramic head connected to a pressure measuring device through a small-bore tube. The head and the tube are filled with deaired water. The head could be inserted in the soil to connect with soil water as shown in *Figure II.13*. After several hours, the equilibrium reaches and the negative pore water pressure is equal to the pressure of measuring system. The matric suction can be measured by a tensiometer limited to approximately negative 90 kPa due to the possibility of cavitation of the water in the tensiometer (Fredlund & Rahardjo, 1993). The component of soil osmotic suction will not be measured with tensiometers since soluble salts can move through the ceramic head freely.

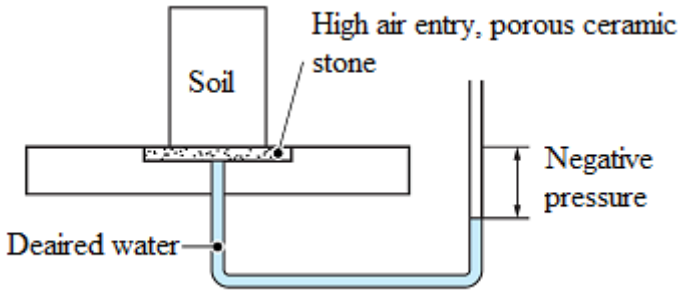

Figure II.13. Tensiometer method to measure soil matric suction (Ho, 2013)

In this study, the tensiometer method is used to calibrate the filter paper method.

Calibration of filter paper method with tensiometer method (Arsenie-2009)

The samples are prepared at an initial dry density of 2.0 Mg/m^3 with a water content ranging from 7% to 12.3 % in wetting path for Missillac sand. The dimension of height and diameter are as following: H = 3.15 cm; $Ø$ = 6.9 cm.

For Missillac sand, the time to reach equilibrium is approximate 24 hours.

Porous probes used and a sample connected with a measuring probe are shown in *Figure II.14*.

Figure II.14. Porous probes and the sample connected with a measuring probe

Figure II.15 presents the suction measurement results of Missillac sand with two methods. The results measured by tensiometer are consistent with the results measured by filter paper method. As a consequence, in this study, the filter paper method, which is supposed to be less time consuming, is used to measure the matric suction of studied materials.

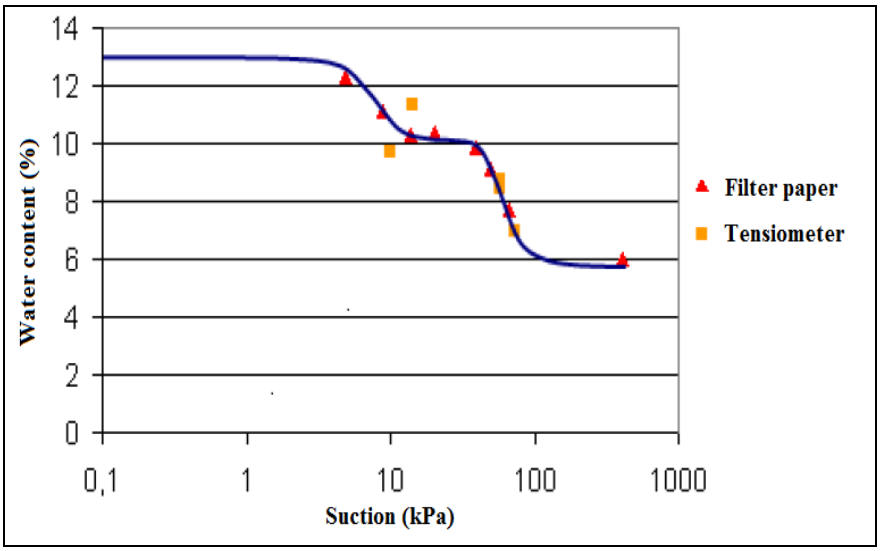

Figure II.15. Suction measurement results of Missillac sand M4.0 with two methods (Arsenie, 2009)

II.4. Repeated load triaxial tests

The RLTT is a common test to investigate the repeated mechanical behaviour of granular materials. In this study, RLTTs are carried out following the French standard (NF EN 13286-7), which defines the test procedures for characterizing resilient and permanent deformation behaviours of granular materials. All the procedures and equipments of our RLTT are presented in this section.

II.4.1. Sample preparation

Soil is first dried in the oven for 48 hours in a temperature of 55°C to achieve a dry state as shown in *Figure II.16*. The oven temperature of 55°C is selected to prevent the distress of fine particles in high temperatures.

After cooling, soil is mixed with a given water content by a mixer in the homogeneous manner (*Figure II.17*). To avoid water loss and reach the homogeneous state, the mixed soil is sealed in a plastic bag for 24 hours.

The samples Missillac sand M4.0 and M15.3 and the samples UGM Maraîchères are compacted following the method of vibrating hammer (*Figure II.18*, NF EN13286-4, 2003) in 7 layers with a height of 285±5 and a diameter 150 mm. The samples Missillac sand M7.5 are compacted following the method of vibrocompression (NF P98-230-1, 1992) in 1 layer with a height of 320±5 mm and a diameter 160 mm. Using the vibrating hammer, it can be stated that the compaction time (per layer) decreases with the increase of the fine content for Missillac sand: 45s-55s for M4.0 and 25s-35s for M15.3 (>60s for UGM Maraîchères).

As mentioned in literature review, based on the study of Balay, (1998) on a UGM, it can be stated that the dry density with the vibrating hammer method in 7 layers is approximately same with the vibrocompression method.

Figure II.16. Soil drying in oven

Figure II.17. Mixer

All the samples are prepared at a water content range between 7% and 11% with a dry density of 2±0.06 Mg/m^3 for Missillac sand. However, for UGM Maraîchères, we are still adjusting the new devices of RLTT and we have only tried the water content of 4%.

Samples of Missillac sand with two different fine contents and the sample of UGM Maraîchères are presented in *Figure II.19*.

Figure II.18. Vibrating hammer

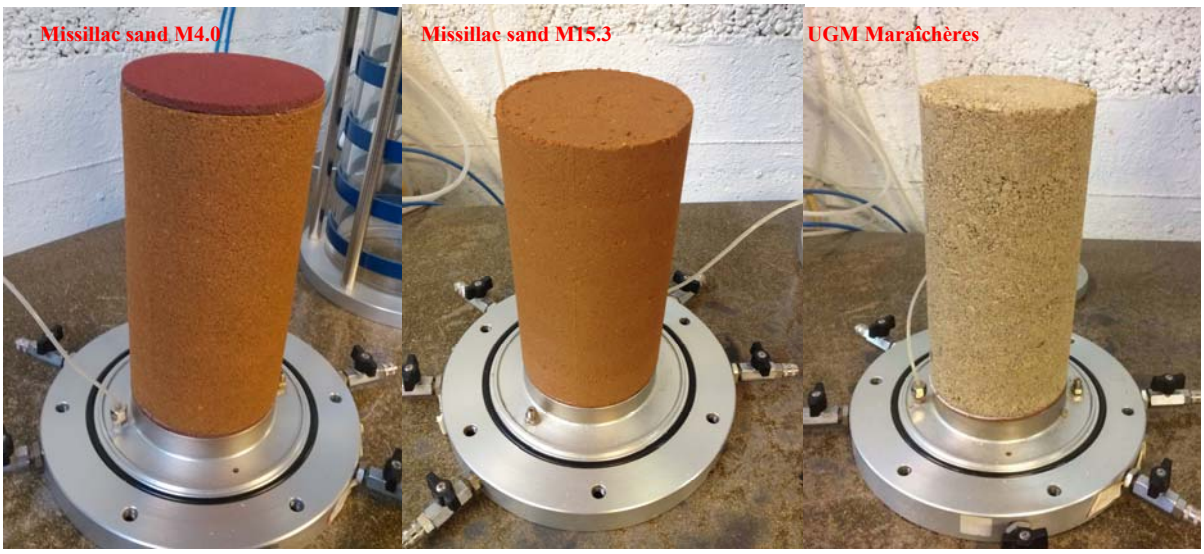

Figure II.19. Samples of Missillac sand and UGM Maraîchères

II.4.2. Experimental devices

RLTT devices have been remarkably developed during past decades. Representative firms, like GDS and CONTROLS, have widespread users all over the world. In this study, our devices are assembled by Wykeham Farrance and GDS and this is a part of European project INTERREG IV A, Upper Rhine Programme (Project B20, TEM3).

Our triaxial device is a composite of an elevated worktop, a triaxial cell, a pneumatic loading system, a stress and strain measurement system and a controlling computer (*Figure II.20*).

Loading and Measurement systems

During a triaxial test, an axial stress (σ_1) and a confining pressure (σ_3) are applied on the soil sample in the triaxial cell simulating the loading state under pavement to measure the vertical strain (ε_1) and the radial strain (ε_3). Both the axial stress and the confining pressure are supplied by the pneumatic servo loading system.

The principal measurement system is a composite of stress/pressure transducers and displacement transducers. The typical transducers used in such test are:

- An axial force transducer. The axial force transducer is placed on the head of sample which allows an accurate real-time measurement of the force applied by the piston.
- A cell pressure transducer. The cell pressure transducer is placed on the bottom of triaxial cell.

Figure II.20. RLTT devices

- Two axial displacement transducers based on Hall effect. The measured values are used to characterize axial deformation of samples.
- A radial displacement transducers based on Hall effect. It can measure the variation of sample diameter.

The three Hall effect displacement transducers are fixed on the central part of sand samples by needles (screws for UGM samples, as introduced in Appendix A) and strong adhesive as shown in *Figure II.21*. After that, the silicone glue is used to reinforce transducers and prevent water getting into the sample. During the RLTT, for accuracy, the axial deformation and radial deformation are measured by these two axial transducers and a radial transducer with local ways, in the central part of the sample, to overcome shrinking phenomenon. The range of these three transducers is ±3 mm and the precision is 1%.

Figure II.21. Samples of RLTT with axial displacement transducers and radial displacement transducer a) Missillac sand b) UGM Maraîchères

Controlling system

The cyclic loading signals are provided by a compact dynamic controller and ordered by a computer using a software designed for RLTTs by CONTROLS. Meanwhile, the acquired tension signals can be turned into usable values by a data acquisition card and the computer (*Figure II.22*).

Figure II.22. Compact dynamic controller, data acquisition card and controlling computer

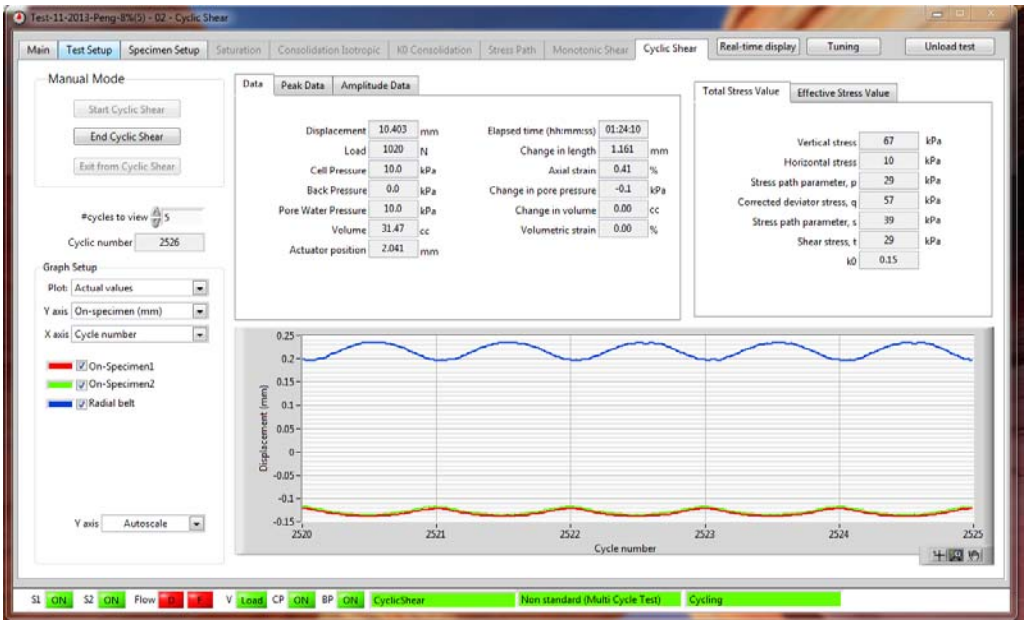

Figure II.23. CONTROLS software

Using this software, we can set the test parameters such as number of cycles, stress paths, loading frequency etc. The software can be also used to monitor the loading cycles, the stress paths, the resilient deformation, the permanent deformation and other loading information in real-time (*Figure II.23*).

II.5. Repeated load triaxial test procedures

In this section, the influence of stress path and the frequency are first introduced. Then, the RLTT procedures for studying the cyclic deformation behaviour are presented in two parts: resilient deformation test and permanent deformation test (multi-stage).

The resilient deformation test consists of a conditioning phase and a following resilient phase. The function of conditioning phase is to stabilize the permanent deformation which also can be named as permanent deformation test (single-stage).

II.5.1. Influence of stress path and frequency

During loading procedures, the deviatoric stress and the cell pressure, these two-applied sinusoidal cyclic loads, should synchronize with each other. Based on the former work of Ho, (2013), it can be noticed that tests in stress path of $\Delta q/\Delta p = 3$ can be carried out with any frequency, because the confining pressure is constant (*Figure II.24.c)*. Nevertheless, when the frequency is higher than 0.1 Hz, the confining pressure does not synchronize with the

deviatoric stress for any stress path of $\Delta q/\Delta p \neq 3$ with an obvious hysteresis (*Figure II.24.a & b*).

As a consequence, in this study, the stress path of $\Delta q/\Delta p = 3$ and frequency of $f = 0.5$ Hz are chosen for conditioning phase in resilient deformation tests and permanent deformation tests. The stress paths of $\Delta q/\Delta p \neq 3$ and frequency of $f = 0.1$ Hz are used to characterize the resilient deformation behaviour in different stress paths.

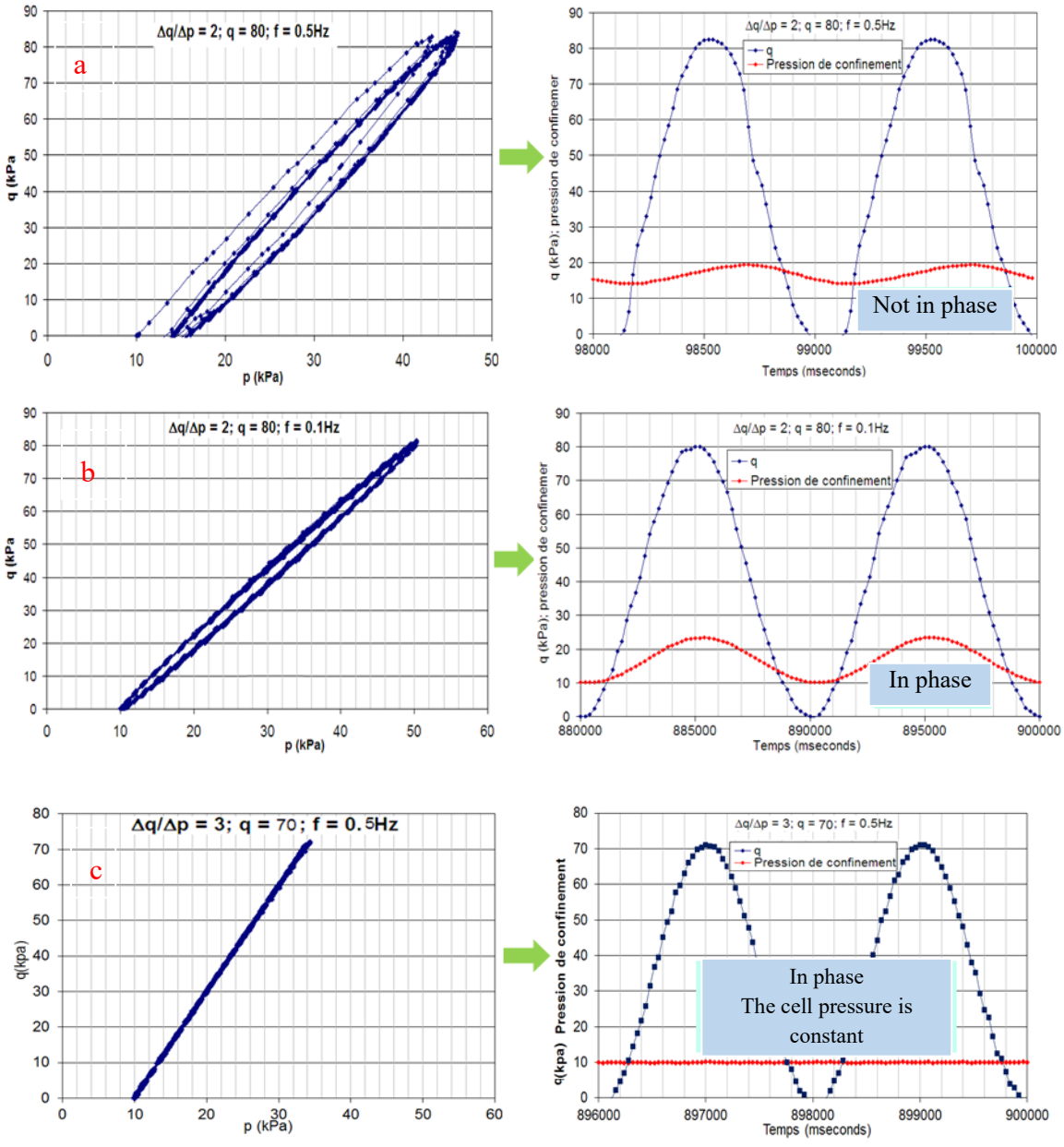

Figure II.24. Influence of stress path and frequency (Ho, 2013)

II.5.2. Resilient deformation tests

- **Conditioning phase (permanent deformation test (Single-stage)):**

As mentioned in above, the stress paths used in conditioning phase is $\Delta q/\Delta p$ = 3 (p = 33,33 kPa et q = 70 kPa) from an initial stress state (p_0 = 10 kPa, q_0 = 0 kPa) at a frequency of f = 0.5 Hz for samples of Missillac sand M4.0 and M15.3. For UGM Maraîchères, the samples are applied with the same stress slope of $\Delta q/\Delta p$ = 3 but a higher stress level (p = 95 kPa et q = 235 kPa) from an initial stress state (p_0 = 20 kPa, q_0 = 10 kPa) at a frequency of f = 0.5 Hz.

It is also important to note that, the samples of Missillac sand M7.5 are applied in stress path of $\Delta q/\Delta p$ = 2 (p = 50 kPa et q = 85 kPa) from an initial stress state (p_0 = 10 kPa, q_0 = 5 kPa) at a frequency of f = 1 Hz. The loading system is supplied by a liquid servo apparatus and as a result, there is no synchronization problem.

Ho et al., (2014c) investigated the behaviour of Missillac sand and noted that an equilibrium state reached after approximately 10,000 load applications. For UGM, Hornych et al., (2007) showed that the necessary number of cycles was higher than 50,000. Thus, the number of cycles is chosen as N = 10,000 cycles for Missillac sand samples and N = 50,000 cycles for UGM samples. When the permanent axial deformation rate $\Delta\varepsilon/\Delta N$ is lower than 1×10^{-7}, we can state that the permanent axial deformation achieves the equilibrium state.

- **Complete resilient test:**

After the conditioning, a series of loads are applied to each sample with different stress paths of $\Delta q/\Delta p$ = 0; 0.5; 1; 2; 3 (NF EN 13286-7 or AASHTO T 307-99). For each stress path (100 cycles), as mentioned in above, frequency of f = 0.1 Hz (1Hz for M7.5 specially) is used to keep deviatoric stress and cell pressure synchronizing with each other. The last cycle in each stress path is used to determine the resilient behaviour. For Missillac sand, the different stress paths are presented in *Table II.3 and Figure II.25 & 26.* For UGM Maraîchères, the different stress paths are also presented in *Table II.4* and *Figure II.27.*

Material	$\Delta q/\Delta p$	Δp (kPa)	Δq (kPa)
Missillac sand	0	80	0
	0.5	80	40
	1	80	80
	2	40	80
	3	20	60

Table II.3. Stress paths applied in complete resilient test for Missillac sand

Material	$\Delta q/\Delta p$	Δp (kPa)	Δq (kPa)
UGM Maraîchères	0	250	0
	1	400	400
	1.5	400	600
	2	300	600
	2.5	90	225

Table II.4. Stress paths applied in complete resilient test for UGM Maraîchères

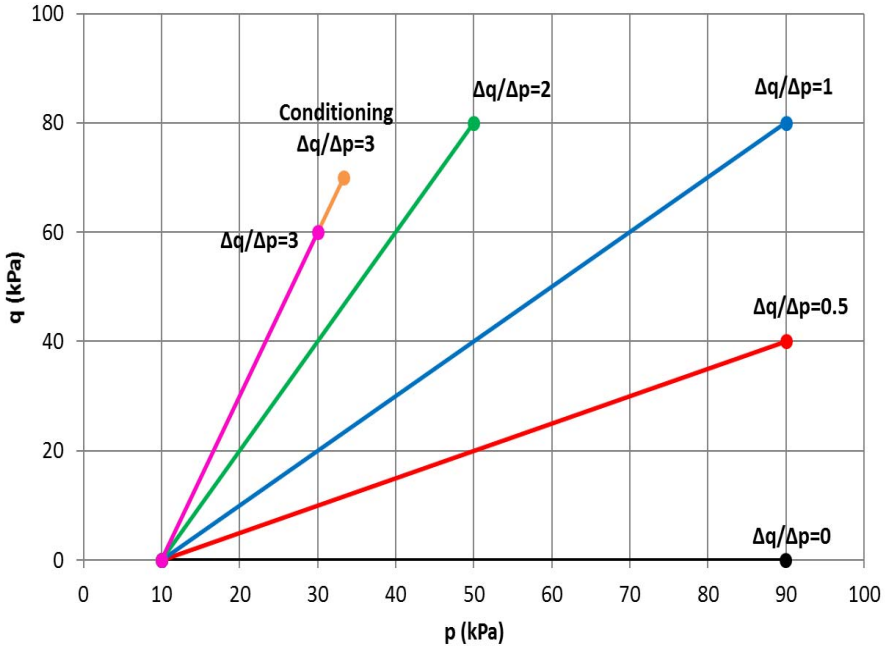

Figure II.25. Stress paths applied in complete resilient tests (Missillac sand M4.0 and M15.3)

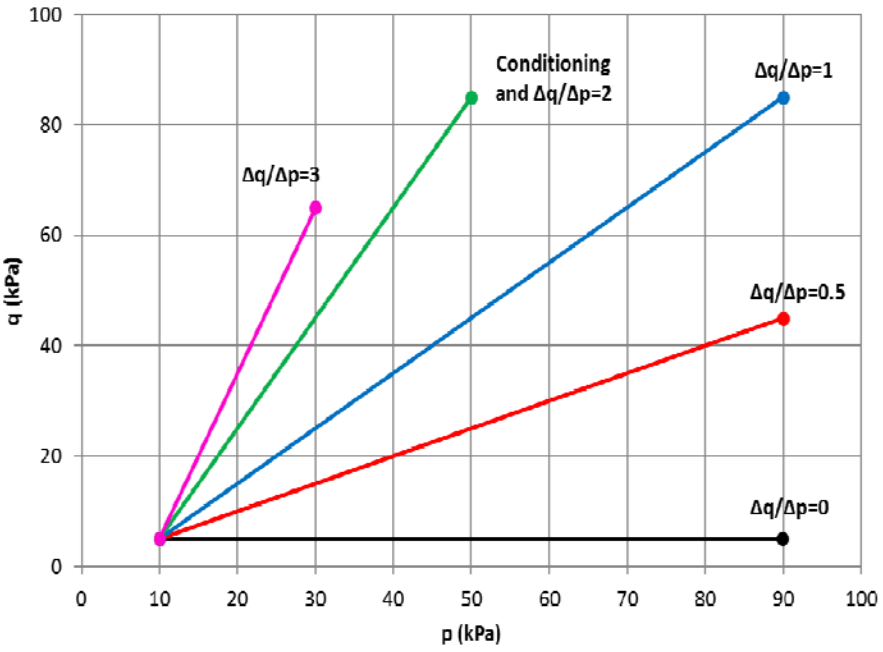

Figure II.26. Stress paths applied in complete resilient tests (Missillac sand M7.5)

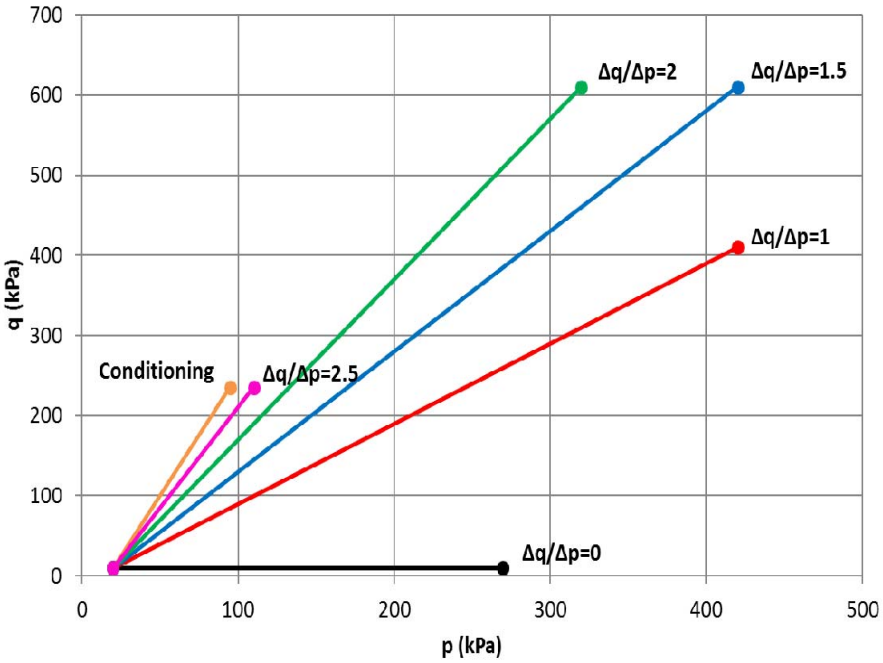

Figure II.27. Stress paths applied in complete resilient tests (UGM Maraîchères)

II.5.3. Permanent deformation tests (multi-stage)

As mentioned in literature review, Gidel et al., (2001) found that, in the multi-stage tests, the deformations at the end of several stages to reach stress level “i” stabilized at the same value as they would have been if the material had been subjected to just one stage to reach stress level "i". Absolutely, these two loading modes should be performed on the same stress path. This procedure could reduce thus the number of tests and avoid the variability of soil specimens.

In the present study, the multi-stage loading procedure proposed by Gidel et al., (2001) is adopted. During the test, one sample at a given water content is subjected to a series of loading stages with different deviatoric stresses on a given stress path and each loading stage includes 10000 cycles. The water content and the stress state applied to Missillac sand M7.5 and M15.3 are shown in *Table II.5* and *Table II.6* respectively and Figure *II.28*.

For M7.5, the different stress paths ($\Delta q/\Delta p$ = 1; 1.5; 2; 3) are applied to different samples with a constant water content (w = 11%) from an initial stress state of (p_0 = 10 kPa, q_0 = 5 kPa) at the frequency of 1 Hz.

For M15.3, the different samples are prepared with different water contents (w = 7.7%, w = 9.4%, w = 9.9% and w = 11.1%), and then a constant stress path ($\Delta q/\Delta p$ = 3) is applied to the samples from an initial stress state of (p_0 = 10 kPa, q_0 = 0 kPa) at the frequency of 0.5 Hz.

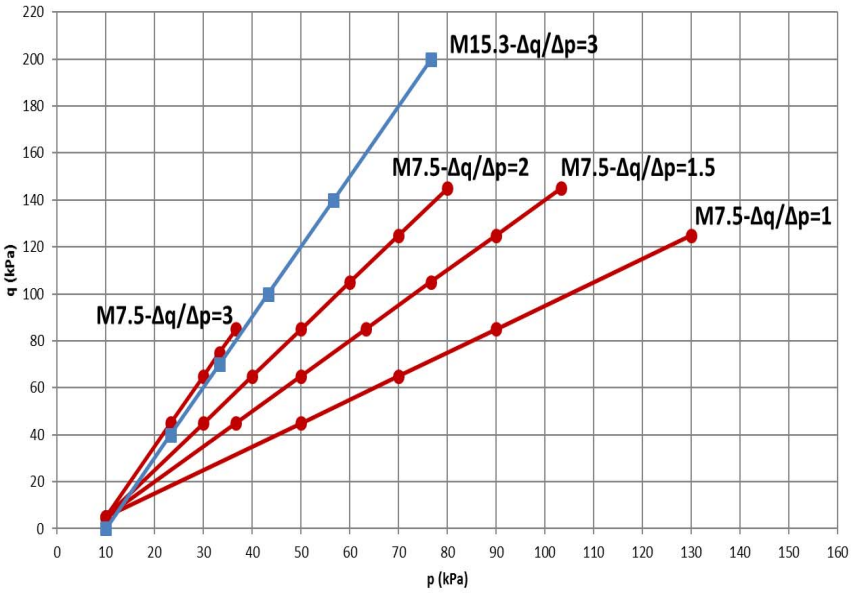

Figure II.28. Stress paths applied in multi-stage tests (Missillac sand M7.5 and M15.3)

w (%)	11.0		11.0		11.0		11.0	
Sr(%)	89.79		89.7		89.7		89.7	
Stress path	**Initial stress state (p_0, q_0) = (10, 5 kPa); Frequency f = 1 Hz**							
	$\Delta q/\Delta p$ = 3		**$\Delta q/\Delta p$ = 2**		**$\Delta q/\Delta p$ = 1.5**		**$\Delta q/\Delta p$ = 1**	
	Δq (kPa)	**Δp (kPa)**	**Δq (kPa)**	**Δp (kPa)**	**Δq (kPa)**	**Δp (kPa)**	**Δq (kPa)**	**Δp (kPa)**
Level 1	40	13.3	40	20	40	26.6	40	40
Level 2	60	20	60	30	60	40	60	60
Level 3	70	23.3	80	40	80	53.3	80	80
Level 4	80	26.7	100	50	100	66.6	120	120
Level 5	---	---	120	60	120	80	---	---
Level 6	---	---	140	70	140	93.3	---	---

Table II.5. Cyclic stress paths in the multi-stage test for Missillac sand M7.5

w (%)	7.7		9.4		9.9		11.1	
Sr (%)	62.8		76.6		80.7		90.5	
Stress path	**Initial stress state (p_0, q_0) = (10, 0 kPa); Frequency f = 0.5 Hz**							
	$\Delta q/\Delta p$ = 3		**$\Delta q/\Delta p$ = 3**		**$\Delta q/\Delta p$ = 3**		**$\Delta q/\Delta p$ = 3**	
	Δq (kPa)	**Δp (kPa)**	**Δq (kPa)**	**Δp (kPa)**	**Δq (kPa)**	**Δp (kPa)**	**Δq (kPa)**	**Δp (kPa)**
Level 1	40	13.3	40	13.3	40	13.3	40	13.3
Level 2	70	23.3	70	23.3	70	23.3	70	23.3
Level 3	100	33.3	100	33.3	100	33.3	100	33.3
Level 4	140	46.7	140	46.7	140	46.7	---	---
Level 5	200	66.7	200	66.7	200	66.7		

Table II.6. Cyclic stress paths in the multi-stage test for Missillac sand M15.3

In addition, it is important to note that all the samples are cut into 9 parts to measure the water content after test. The maximum difference of water content between different parts in a sample is less than 1% for all the studied materials in this study. As a result, we consider all the tested samples as a homogeneous state and then the permanent and resilient behaviours can be analyzed.

II.6. Conclusion

This chapter introduces the material characteristics and the procedures of suction measurement and RLTTs for Missillac sand and UGM Maraîchères. In the following chapters, using these experimental procedures, we will study the influence of water content, fine content mainly on the evolution of the permanent and resilient deformations for Missillac sand. The results of suction measurement and RLTTs for UGM Maraîchères will be shown in Appendix B.

CHAPTER III. PERMANENT DEFORMATION BEHAVIOUR OF A GRANULAR MATERIAL

III.1. Introduction

In this chapter, the effects of fine content, water content and suction on the permanent axial deformation of Missillac sand is studied with the repeated load triaxial tests (RLTTs) for both single-stage and multi-stage tests. For the analytical modelling, we use principally the framework proposed by Hornych et al., (1993) for single-stage tests and the framework proposed by Gidel et al., (2001) for multi-stage tests to estimate the variation of permanent axial deformation of Missillac sand during several loading and unloading cycles. Two approaches are proposed through these two frameworks: the first based on the water content and fine content and the other based on the suction value.

III.2. Soil water retention curve (SWRC)

The soil water retention curve gives the indispensable data to understand the hydraulic behaviour of the unsaturated granular material used in pavement structures. As introduced in Chapter II, in this study, the matric suction of Missillac sand samples, on the wetting and drying paths, is measured by the filter paper technique (ASTM D5298-10, 1995).

Figure III.1 shows the variation of matric suction with water content for both wetting and drying paths for M4.0 and M15.3. It can be stated that both wetting and drying paths move towards the left side when the fine content decreases. In other words, the higher the fine content, the higher the suction value. Similar observations are reported by Caicedo et al., 2009 and Duong et al., 2014.

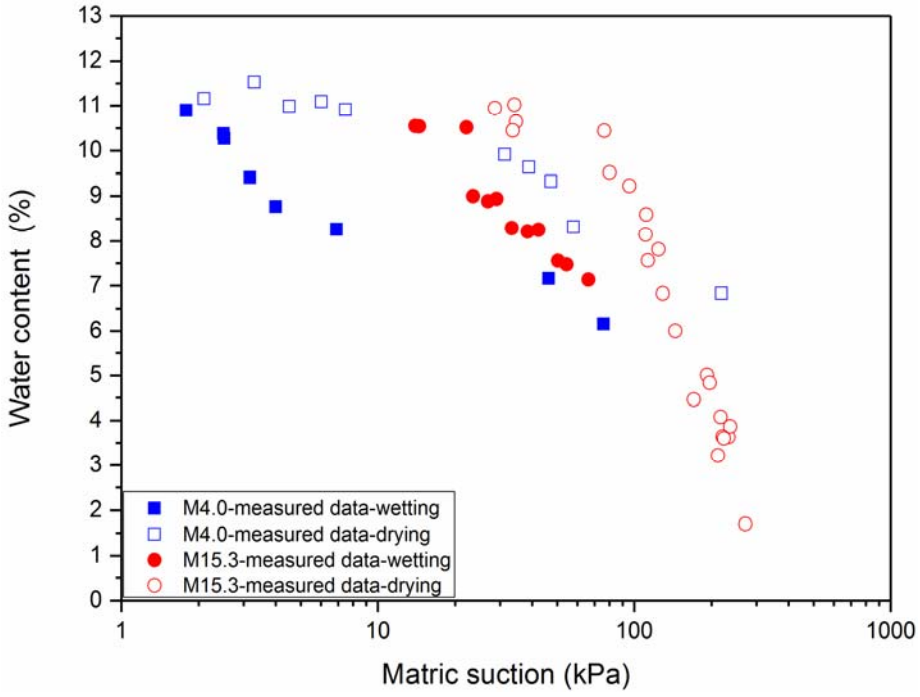

Figure III.1. Matric suction obtained by the filter paper method for Missillac sand (M4.0 and M15.3)

Based on experimental results, various empirical equations have been suggested to describe the SWRC. Among these equations, the relationships proposed by Brooks & Corey, (1964); van Genuchten, (1980) and Fredlund & Xing, (1994) have been widely used in geotechnical engineering. In this study, we use the van Genuchten model, because of its simplicity and its meaningful parameters. The van Genuchten equation is written as follows:

$$w = w_r + \frac{(w_s - w_r)}{\left[1 + (\alpha s)^n\right]^m} \quad \text{(III.1)}$$

where w is the actual soil water content at the suction s (kPa); w_s (%) and w_r (%) are the saturated water content and the residual water content; α is a parameter related to the air entry suction; m and n are the model parameters with the relationship: $m=1-1/n$.

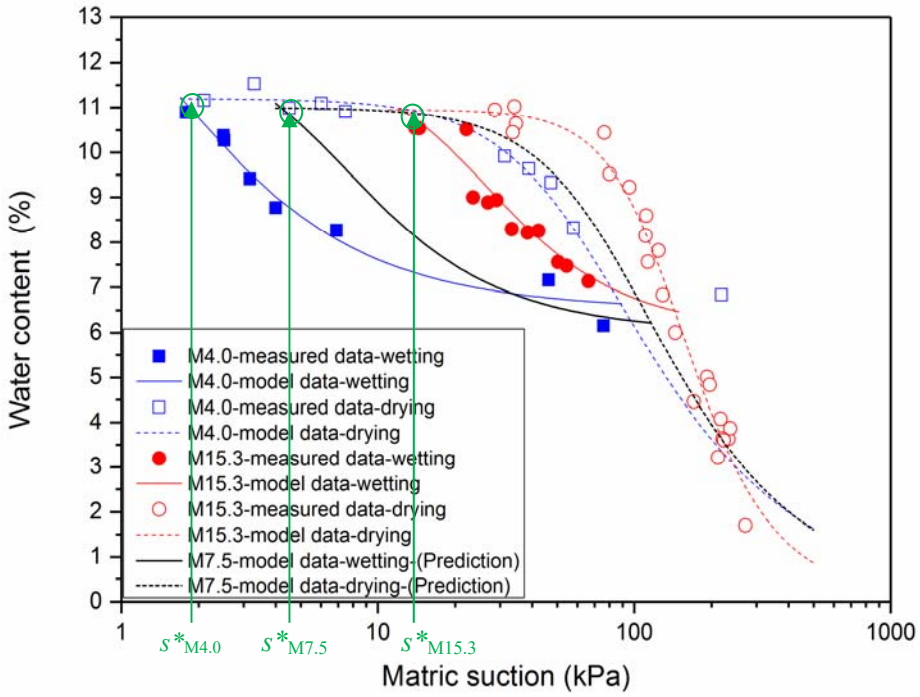

Figure III.2. Matric suction obtained by the filter paper method as well as the model prediction (M4.0, M7.5 and M15.3)

Parameters of VG model	M4.0		M15.3		M7.5 (Prediction)	
	Wetting	Drying	Wetting	Drying	Wetting	Drying
α	0.803	0.016	0.049	0.007	0.180	0.012
n	1.929	1.947	2.261	3.025	2.100	2.100
m	0.482	0.486	0.558	0.669	0.524	0.524
w_s (%)	14.3	11.2	11.8	11.0	12.3	11.0
w_r (%)	6.5	0.1	6.0	0.1	6.0	0.1
s^* (kPa)	1.8±0.18		12±1.2		4.2±0.42	

Table III.1. Parameters of van Genuchten model

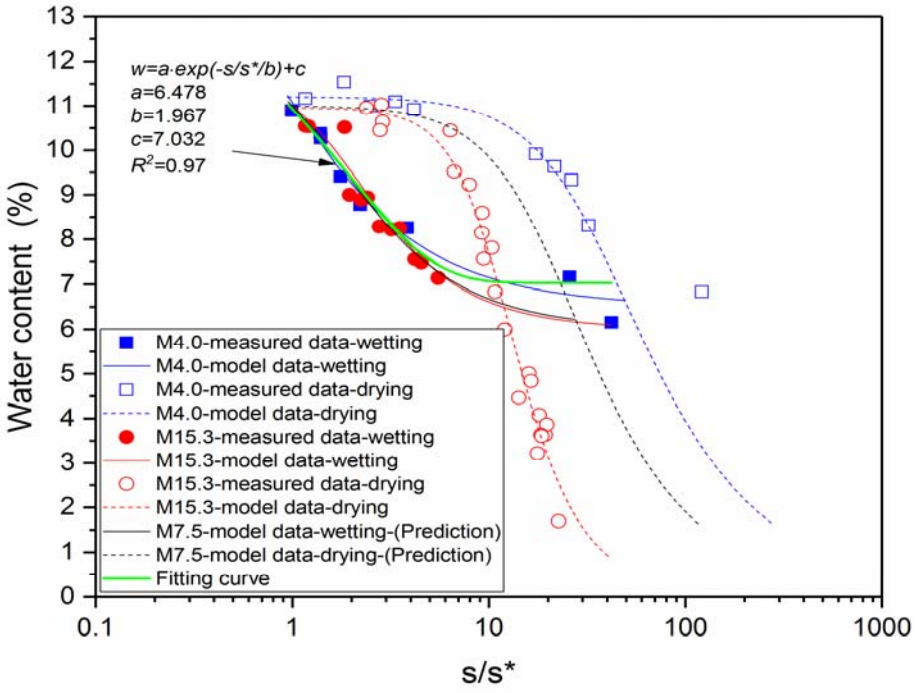

Figure III.3. Evolution of water content w as a function of s/s (M4.0, M7.5 and M15.3)*

Figure III.2 shows the measured matric suction as well as the model estimations. It presents that the van Genuchten model fits well with the measured values for both studied materials. The parameters are summarized in *Table III.1*. *Figure III.2* also shows that the wetting and drying paths join together at a low suction value. We may consider that the wetting and drying paths are unique in this suction range. We define *s** as the suction value corresponding to the intersection point of wetting and drying paths. It is significantly related to fine content. *Table III.1* summarizes the *s** values for different samples.

Based on the parameters of van Genuchten model for the samples M4.0 and M15.3, the model parameters and the *s** values are predicted for M7.5 presented in *Table III.1*. *Figure III.2* also shows the prediction SWRC for M7.5 both wetting and drying paths.

Figure III.3 also presents that the SWRCs for three different materials coincide together in wetting path by using *s/s** value instead of suction value. As a result, the evolution of water content could be described as an exponential function of *s/s** in wetting path for all three materials, which is defined as:

$$w = a \cdot e^{(-s/s*/b)} + c \qquad \text{(III.2)}$$

where a, b and c are constant.

III.3. Permanent axial deformation behaviour in single-stage test

Based on the RLTTs in single-stage test, the mechanical characteristics of Missillac sand are studied. Afterwards, two approaches are applied to experimental results to predict the permanent axial deformation.

III.3.1. Sample preparation and stress paths

For the experimental procedure, as introduced in Chapter II, all the samples of Missillac sand M4.0 and M15.3 are compacted following the method of vibrating hammer (NF EN13286-4, 2003) in 7 layers with a height of 285±5 mm and a diameter of 150 mm. The samples of Missillac sand M7.5 are compacted following the method of vibrocompression (NF P98-230-1, 1992) in 1 layer with a height of 320±5 mm and a diameter 160 mm.

All the samples are prepared at a water content range between 7% and 11% with a dry density of 2±0.06 Mg/m^3. For the three studied materials, the cyclic stress paths during the conditioning phase (single-stage test) are summarized in *Table III.2*.

Sample	$\Delta q/\Delta p$	Initial stress state (p_0, q_0)	Final (Δp, Δq)	Frequency
M4.0	3	10 kPa, 0 kPa	23.33 kPa, 69.99 kPa	0.5Hz
M7.5	2	10 kPa, 5 kPa	40 kPa, 80 kPa	1Hz
M15.3	3	10 kPa, 0 kPa	23.33 kPa, 69.99 kPa	0.5Hz

Table III.2. Cyclic stress paths in single-stage tests

III.3.2. Experimental results

Figure III.4, Figure III.5 and *Figure III.6* present the evolution of permanent axial deformation ε_1^p and permanent radial deformation ε_3^p for Missillac sand M4.0, M7.5 and M15.3 respectively in conditioning phase.

Permanent axial deformation

For permanent axial deformation, the results show that ε_1^p increases with an increase of number of cycles at different water contents as illustrated in *Figure III.4.a* for M4.0, *Figure III.5.a* for M7.5 and *Figure III.6.a* for M15.3. The values of $\Delta\varepsilon/\Delta N$ at end of each test are less than or close to 10^{-7} for three materials. We can state that the permanent axial deformation has

achieved the equilibrium state after 10,000 cycles. This value will be later taken as *A* value in Equation.I.18 in the following analytical approaches.

The permanent axial deformation of samples M7.5 with a lower stress path of $\Delta q/\Delta p = 2$ easily stabilizes after 2000 cycles in all of water contents. The ε_1^p values of M7.5 are less than M4.0 and M15.3 which have a higher stress path of $\Delta q/\Delta p = 3$ obviously.

In the same stress path of $\Delta q/\Delta p = 3$, we can observe that the permanent axial deformation increases significantly as the water content increases and the deformation hardly stabilizes with the highest water content, such as samples M4.0-11.0% (*Figure III.4.a*) and M15.3-11.1% & 11.3% (*Figure III.6.a)*. It suggests that more cycles are required to reach the stabilized permanent axial deformation at a water content which is close to the saturated state. When the water content is lower than 10% for M4.0 or 11% for M15.3 included, the permanent axial deformation stabilizes more quickly with an increase of fine content (for M4.0 after 4000 cycles in *Figure III.4.a* and for M15.3 after 2000 cycles in *Figure III.6.a*).

Permanent radial deformation

For permanent radial deformation, the results show that the ε_3^p also increases with an increase of number of cycles at different water contents as illustrated in *Figure III.4.b* for M4.0, *Figure III.5.b* for M7.5 and *Figure III.6.b* for M15.3. Based on the value of $\Delta\varepsilon/\Delta N$ at end of each test, it can be also stated that the permanent radial deformation of all tested samples achieves the equilibrium state after 10,000 cycles.

In general, the permanent radial deformation should have the almost same trend with permanent axial deformation with an increase of water content. However, in these tests, some samples seem to have inaccurate ε_3^p values at given water contents, such as samples M4.0-9.0% & 9.3%, M7.5-9.6% and M15.3-11.0%. It can be related to the measurement of permanent radial deformations.

Since the permanent axial deformation is more popularly employed in the pavement engineering, the permanent axial deformation will be mainly studied in this chapter.

Final permanent axial deformation

Figure III.7 shows the variation of the final permanent axial deformation with the water content for samples M4.0 and M15.3. In this section, we are not able to compare the

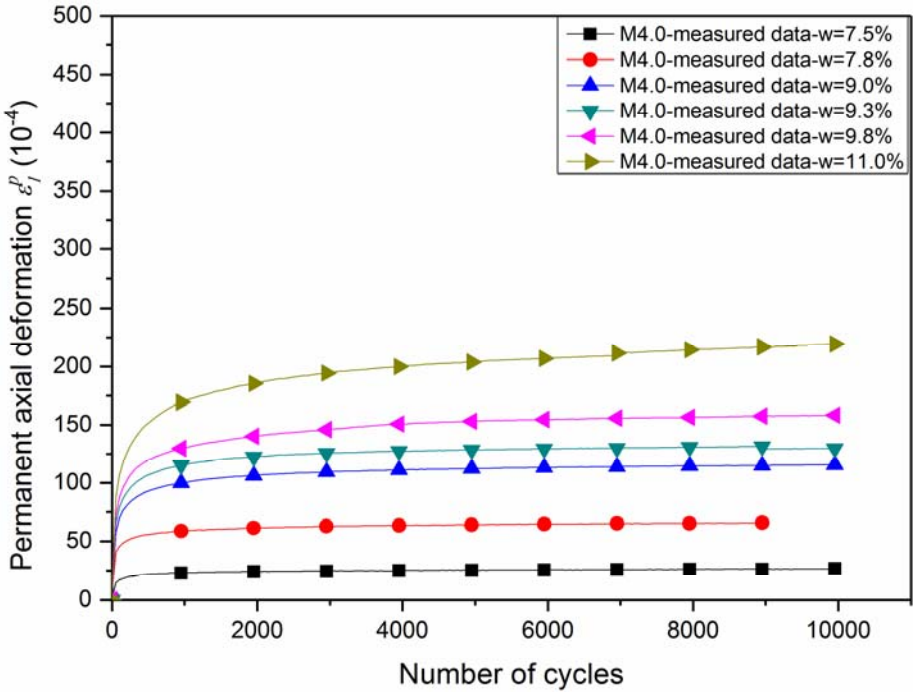

a)

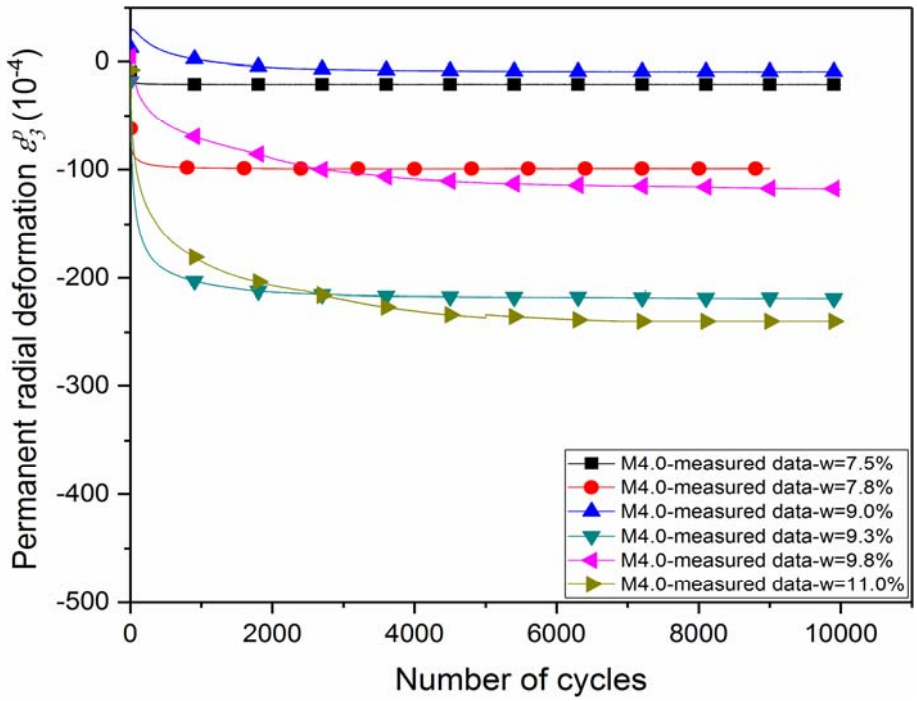

b)

Figure III.4. Evolution of permanent axial deformation ε_1^p (a) and permanent radial deformation ε_3^p (b) for Missillac sand M4.0 in conditioning phase

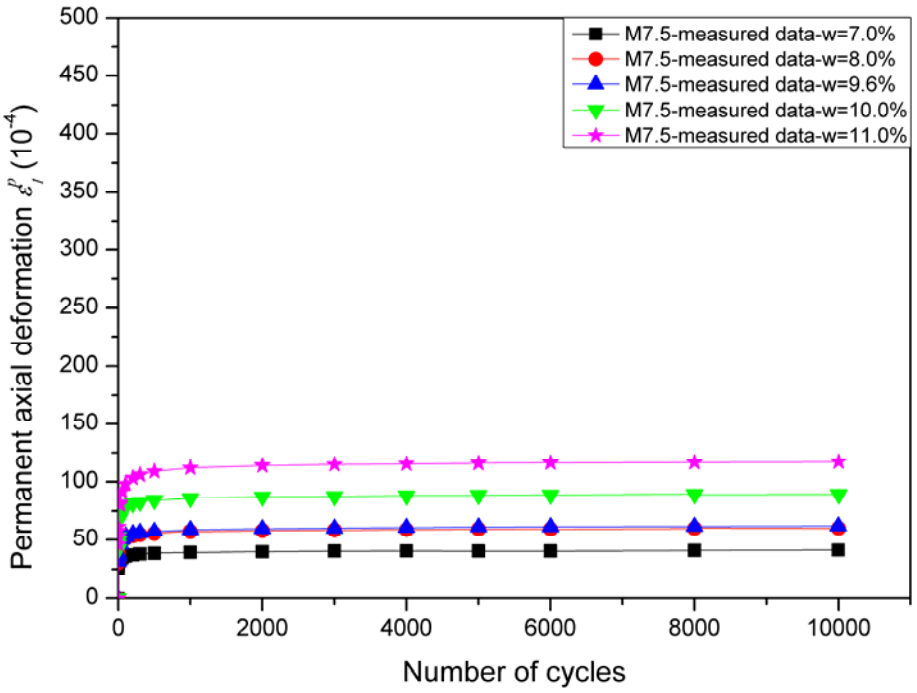

a)

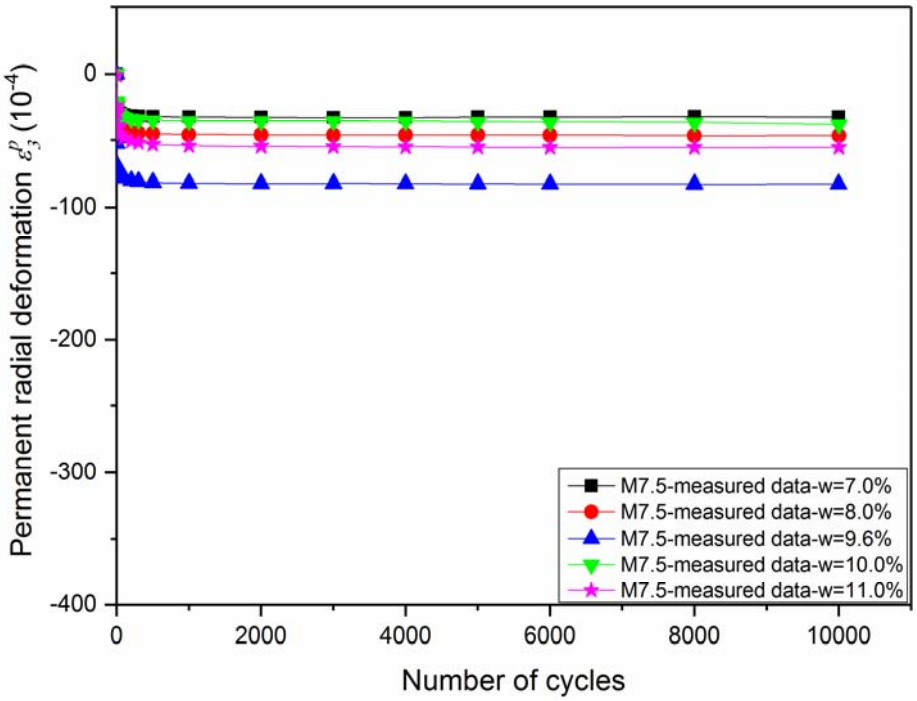

b)

Figure III.5. Evolution of permanent axial deformation ε_1^p (a) and permanent radial deformation ε_3^p (b) for Missillac sand M7.5 in conditioning phase

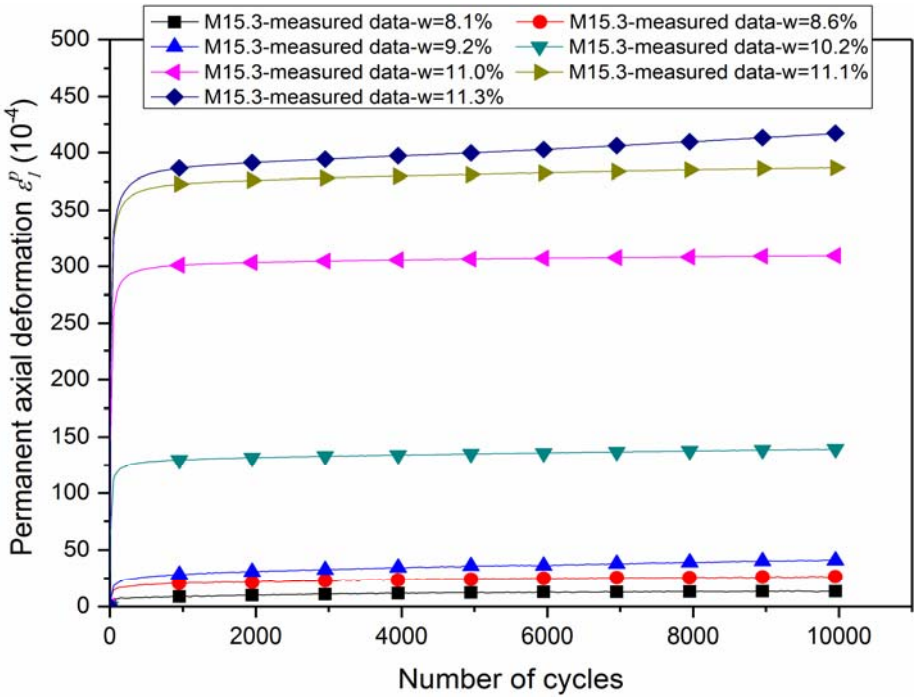

a)

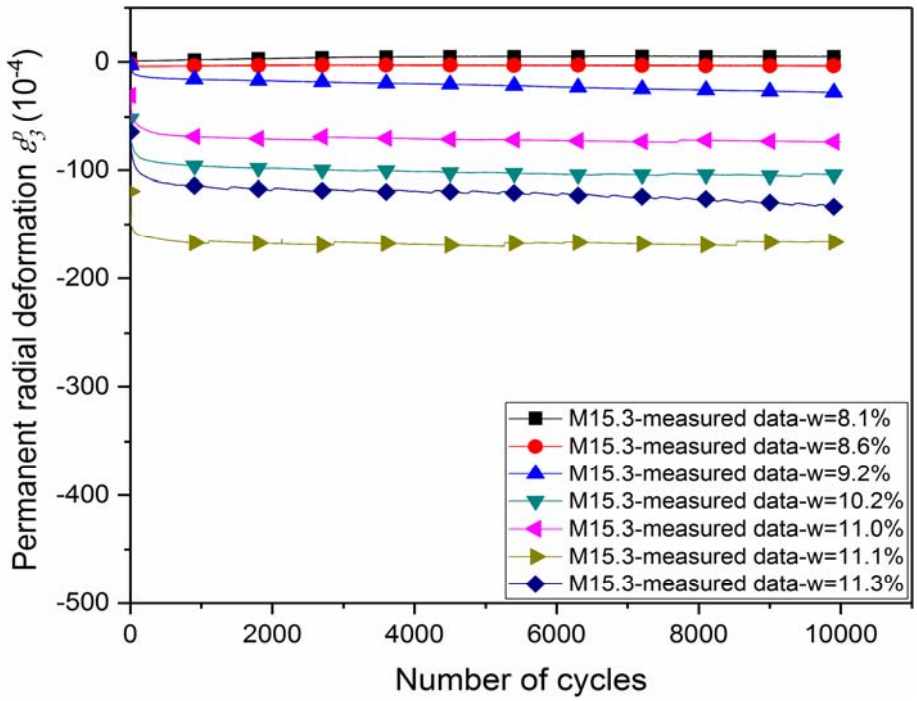

b)

Figure III.6. Evolution of permanent axial deformation ε_1^p (a) and permanent radial deformation ε_3^p (b) for Missillac sand M15.3 in conditioning phase

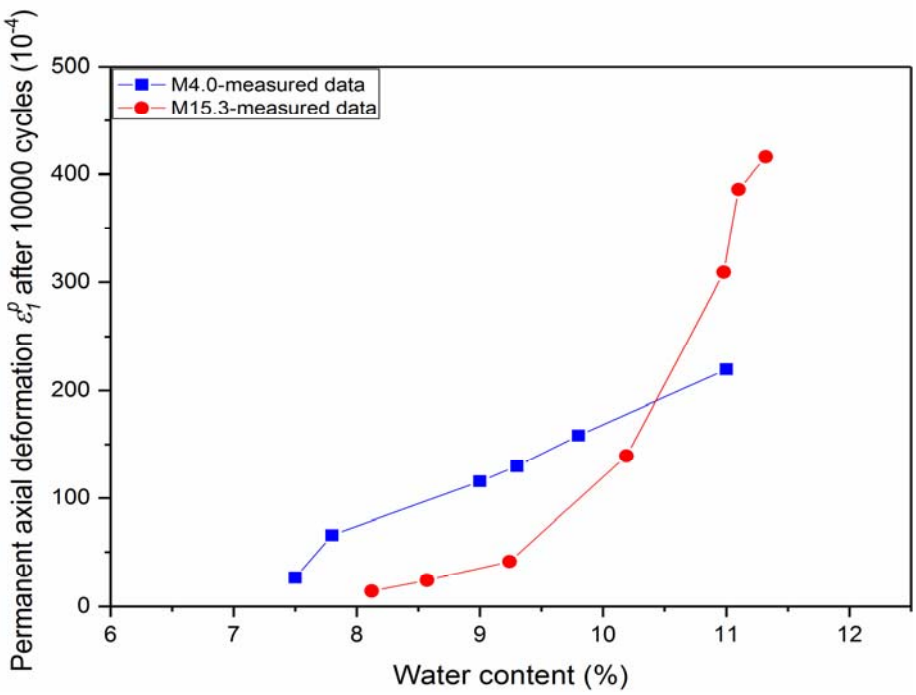

Figure III.7. Final permanent axial deformation after 10,000 cycles versus water content (M4.0 and M15.3)

permanent axial deformation of M7.5 with others (M4.0 and M15.3) because the single-stage tests for this material are performed at a different stress path ($\Delta q/\Delta p = 2$).

It shows that the influence of the fine content is relatively complex: For the water contents between 7% and 10%, the lower the fine content, the higher the permanent axial deformation. Even, the samples M15.3 at a water content less than 8% are very stiff and consequently the deformations are very small and negligible. For the water content higher than 10.3 % (close to the saturated state), the effect of fine content is inversed and the soil with a higher fine content (M15.3) exhibits the higher permanent axial deformation.

These observations can be related to the unsaturated states of samples at different fine contents and water contents. The fine content influences the suction significantly as shown above in SWRC (*Figure III.1* and *Figure III.2*) and the suction increases with the increase of the fine content, which makes the soil particles closer. As the result, the unsaturated soil is more resistant to deformation. On the contrary, close to saturated state, the suction value is almost zero and the fine particles are mainly clay, which decrease the resistance of soil after its combination with water. Similar observations were presented by Seif EI Dine et al., (2010) and Duong et al., (2013). Besides, it is considered that with a content of fine particles below

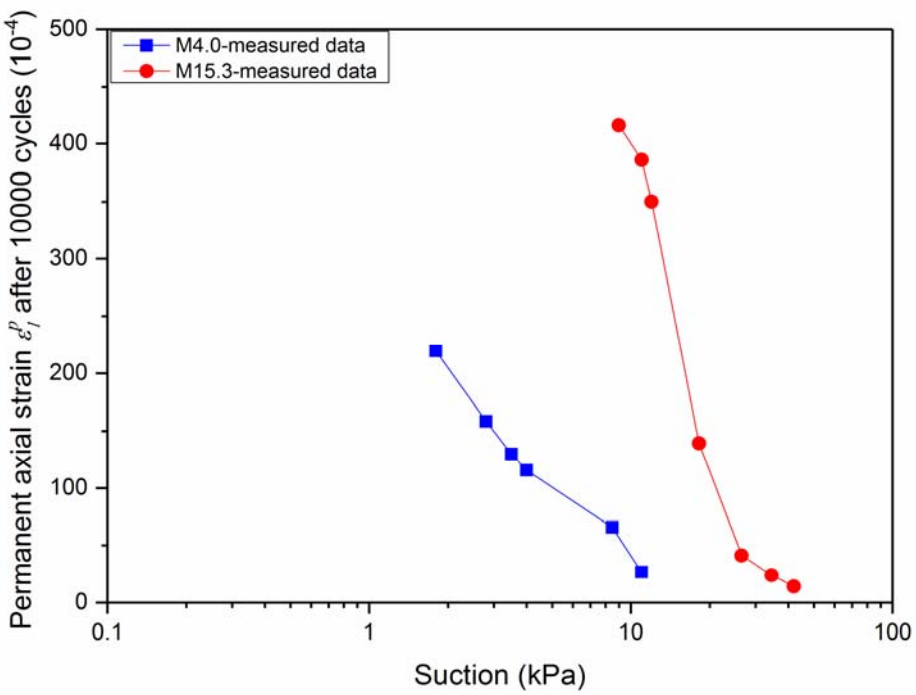

Figure III.8. Final permanent axial deformation after 10,000 cycles versus suction (M4.0 and M15.3)

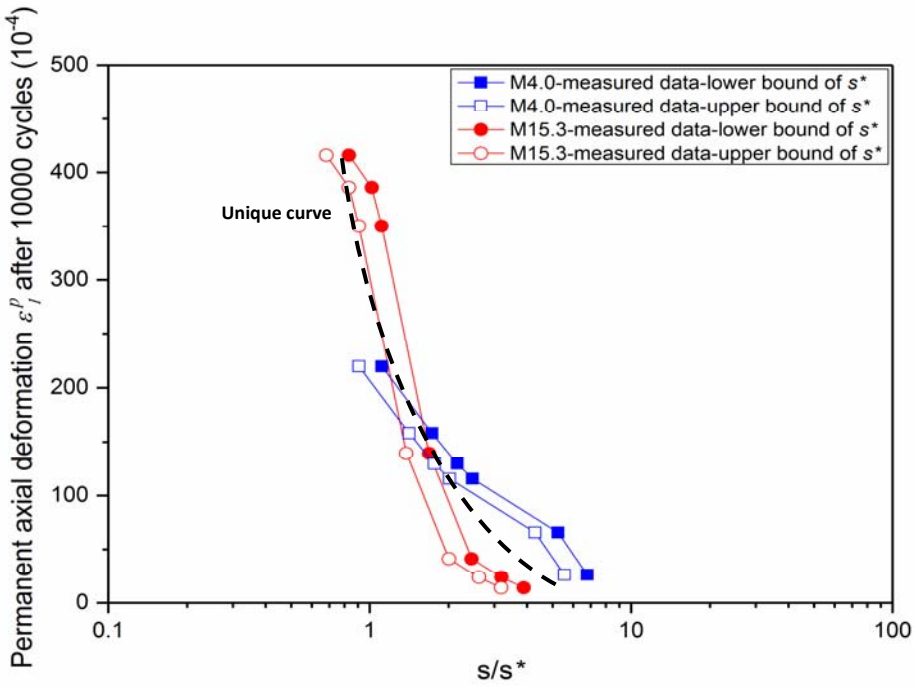

Figure III.9. Final permanent axial deformation after 10,000 cycles versus s/s (between s/(110%·s*) and s/(90%·s*)) (M4.0 and M15.3)*

a limit value, the mechanical behaviour is dominated by the skeleton of sand grain and the soil structure could be denser owing to fine particles. Then, when the fine content is higher than this limit value, the mechanical behaviour is governed by fine particles (Dash et al., 2010; Chang et al., 2012; Benahmed et al., 2015).

From SWRC, it is possible to relate the final permanent axial deformation to suction value. *Figure III.8* shows the final permanent axial deformation versus *s* (suction) in single-stage tests for samples with two different fine contents. It can be stated that the permanent axial deformation decreases significantly with the increases of suction as explained above. From the results shown in *Figure III.8*, we can observe that the influence of the water content and the fine content cannot be represented by the suction value. With the same suction value, for instance, we can also observe that the higher the fine content, the larger the final permanent axial deformation.

In the last section, we defined a new parameter s^* which is the suction value of the intersection point of wetting and drying paths in SWRC. Since the s^* value is very sensitive to any variation of the model parameters, this value is presented in *Table III.1* in a range of between 90%•s^* and 110%•s^* for the lower bound and the upper bound of s^* respectively. *Figure III.9* shows the final permanent axial deformation versus s/s^* for both studied materials.

These findings are interesting for the following calculation since only one curve presented in *Figure III.9* can be used to describe the variation permanent axial deformation with s/s^*. An exponential equation will be proposed for this unique curve in the section III.3.4.

III.3.3. Modelling results based on water content and fine content

Several researchers considered the influence of the water content or the fine content on the mechanical behaviour of granular materials under cyclic loading in their models as shown in introduction. However, no relationship was proposed to relate the permanent axial deformation to the water content and fine content in literature.

In this section, based on the test results presented in *Figure III.7*, a power function, which represents the "*A*" value in Equation.I.18, relates the final permanent axial deformation to the water content. The equation can be written as follows:

$$A = a \cdot \left(\frac{w}{k} \right)^{o \cdot (cc)^u} \quad \text{(III.3)}$$

where, A is the final permanent axial deformation (10^{-4}); w is the water content (%); cc is the fine content (%); a, k, o and u are constant.

Figure III.10 compared the estimated A value with the measured axial deformation after 10000 cycles versus water content. It can be stated that this model fits well the experimental results.

Another required parameter in Equation.I.18 is the power B. Parameter B controls the shape of evolution of permanent axial deformation with number of cycles. The variation curve of permanent axial deformation becomes flatter when B (absolute value) increases. The test results presented in *Figure III.4.a* and *Figure III.6.a* show that the higher the water content, the smaller the B value, and the higher the fine content, the larger the B value. Based on these results, we propose the following equation for B:

$$B = \left(\frac{k'}{w} \right) + o' \cdot cc \quad \text{(III.4)}$$

where, k' and o' are constant.

Combining Equation.III.3 and Equation.III.4, the modified Equation.I.18 can be written as follows:

$$\varepsilon_1^p = a \cdot \left(\frac{w}{k} \right)^{o \cdot (cc)^u} \cdot \left(1 - \left(\frac{N}{N_0} \right)^{\left(\frac{k'}{w} \right) + o' \cdot cc} \right) \quad \text{(III.5)}$$

Figure III.11 shows the comparison between the proposed model for ε_1^p (Equation.III.5) and the experimental results. Generally, it can be stated that the proposed model fits very well qualitatively and quantitatively with most the experimental results. The parameters of the proposed model are summarized in *Table III.3*. *Table III.3* also shows that only one set of parameters required to take into account the number of cycles, the water content and the fine content with a good global correlation coefficient.

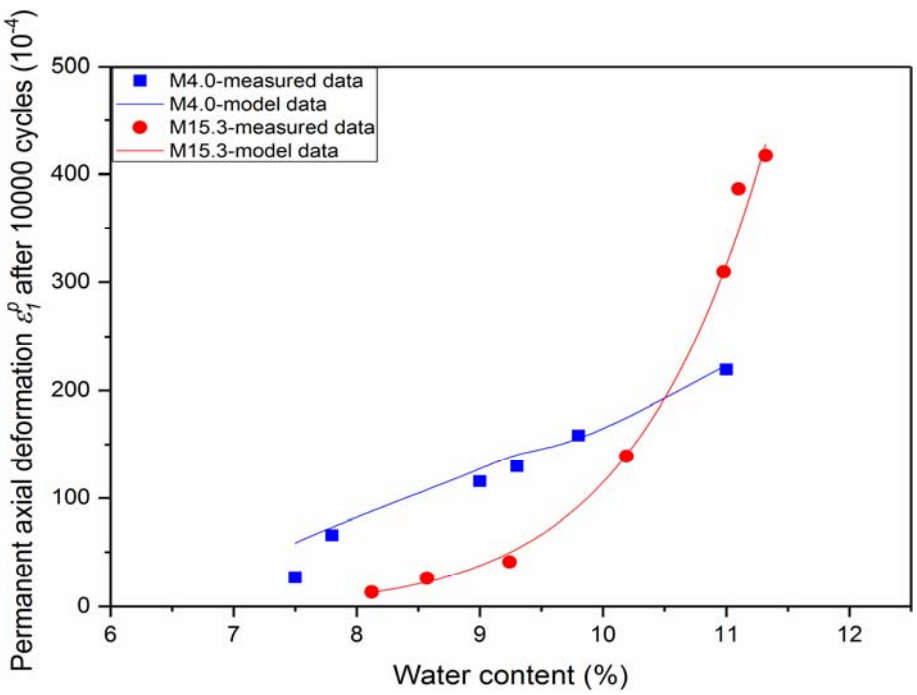

Figure III.10. Test results as well as the model prediction for ε_1^p after 10,000 cycles versus water content (M4.0 and M15.3)

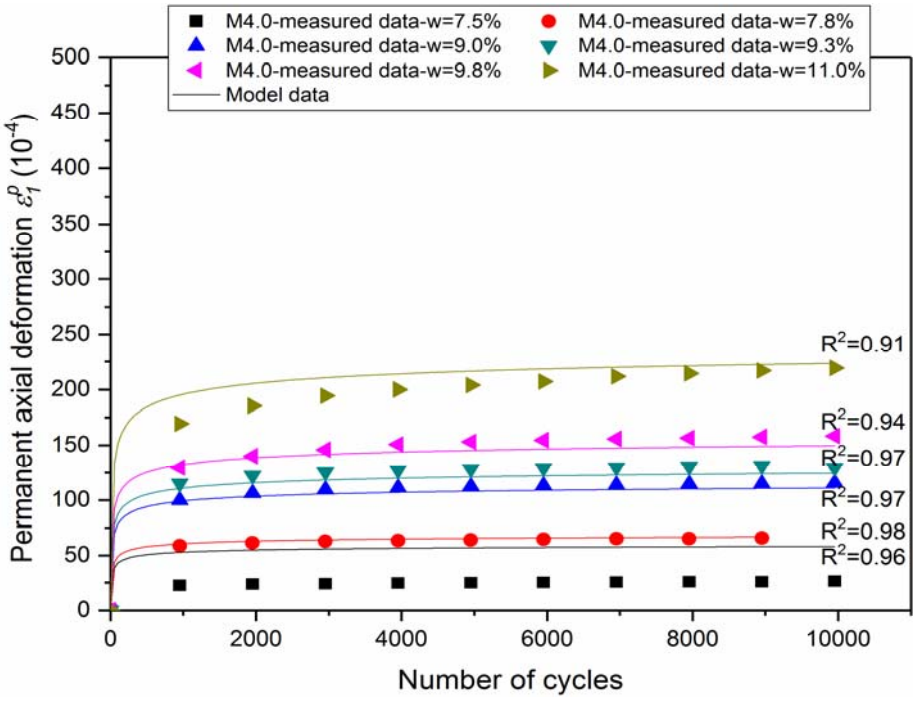

a)

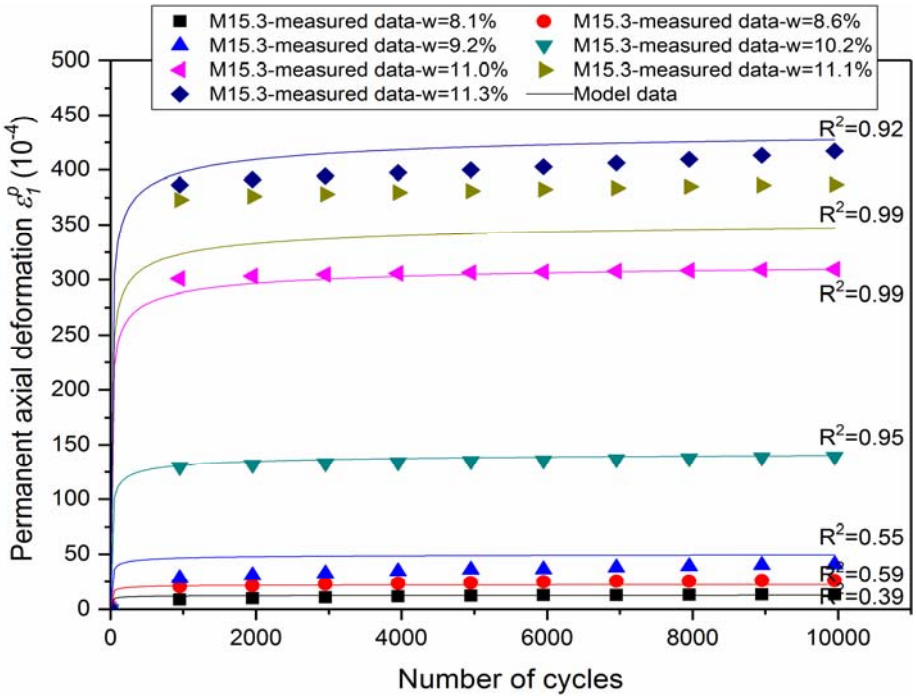

b)

Figure III.11. Test results as well as the model prediction for ε_1^p based on water content and fine content, a) M4.0 and b) M15.3

Missillac sand	*a*	*k*	*o*	**R^2**
	238.058	10.661	1.264	
	u	*k'*	*o'*	0.94
	0.782	-1.800	-0.012	

Table III.3. Parameters of the model for the single-stage tests (M4.0 and M15.3) based on water content and fine content

Based on the simulation results in *Figure III.11*, the proposed model can describe correctly the permanent axial deformation of Missillac sand. However, 6 parameters are necessary to be calibrated in these calculations if the water content and the fine content are considered in the proposed approach. Therefore, in the next section the fine content and water content will be replaced by suction to reduce number of parameters affecting the mechanical soil behaviour.

III.3.4. Modelling results based on suction value

In view of the pervious results presented in *Figure III.9*, a simple power function relationship is proposed between final permanent axial deformation *A* and *s/s** value:

$$A = b \cdot \left(\frac{s}{s^*} \right)^d \quad \text{(III.6)}$$

where, s is suction value (kPa); b and d are constant.

Figure III.12 compares the measured and predicted permanent axial deformation after 10000 cycles versus s/s^*. It can be stated that Equation.III.6 can predict correctly the final permanent axial deformation.

As shown in *Figure III.11*, Equation.III.5 describes the B value (the curve shape) well. In order to relate the B value with suction value, *Figure III.13* shows calculated B values by Equation.III.5 versus variations of the suction value for M4.0 and M15.3. It can be observed that there is a linear relationship between the B value and the $ln(s/s_a)$ value (s_a is equal to 100kPa).

Based on *Figure III.13*, we propose a following equation for B:

$$B = e \cdot \ln\left(\frac{s}{s_a} \right) + f \quad \text{(III.7)}$$

where, s_a is equal to 100kPa; e and f are constant.

As a result, a modified Equation.I.18 can be written as follows:

$$\varepsilon_1^p = b \cdot \left(\frac{s}{s^*} \right)^d \cdot \left(1 - \left(\frac{N}{N_0} \right)^{e \cdot \ln\left(\frac{s}{s_a} \right) + f} \right) \quad \text{(III.8)}$$

Figure III.14 shows the comparison between the proposed model for ε_1^p (Equation.III.8) and the experimental results. For M4.0, the model values are close to the measured value at the lowest water content (7.5%) and the highest water content (11%). The model values are lower than the measured values for the other four water contents, which shows the obvious difference between model values and measured values. For M15.3, the model value is close to the measured value at the water content of 10.2% and the highest water content of 11.3%. The model values are higher than the measured values at water contents lower than 10.2% and are lower than measured values at water contents higher than 10.2%. Generally, it can be stated that the proposed model fits right with the experimental results. The parameters of the proposed model are summarized in *Table III.4*.

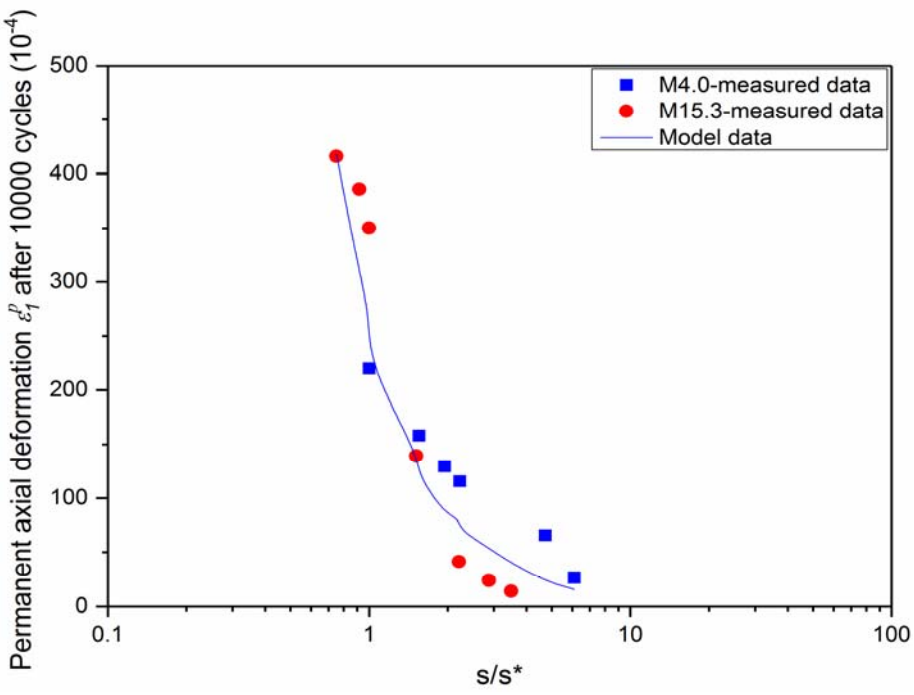

Figure III.12. Test results as well as the model prediction for ε_1^p after 10000 cycles versus s/s (M4.0 and M15.3)*

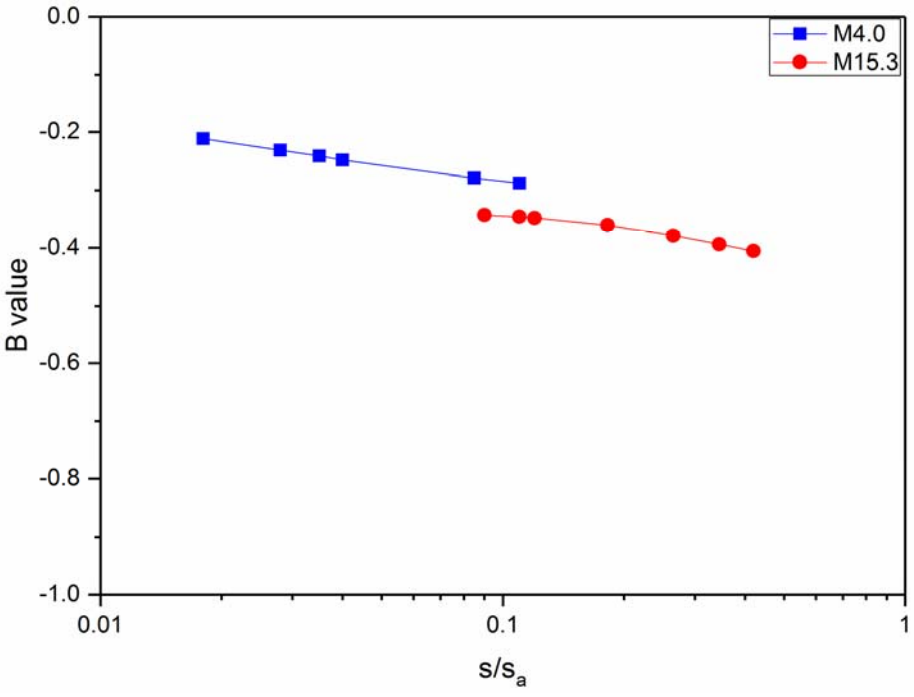

Figure III.13. Calculated B values by Equation.III.5 versus s/s_a (M4.0 and M15.3)

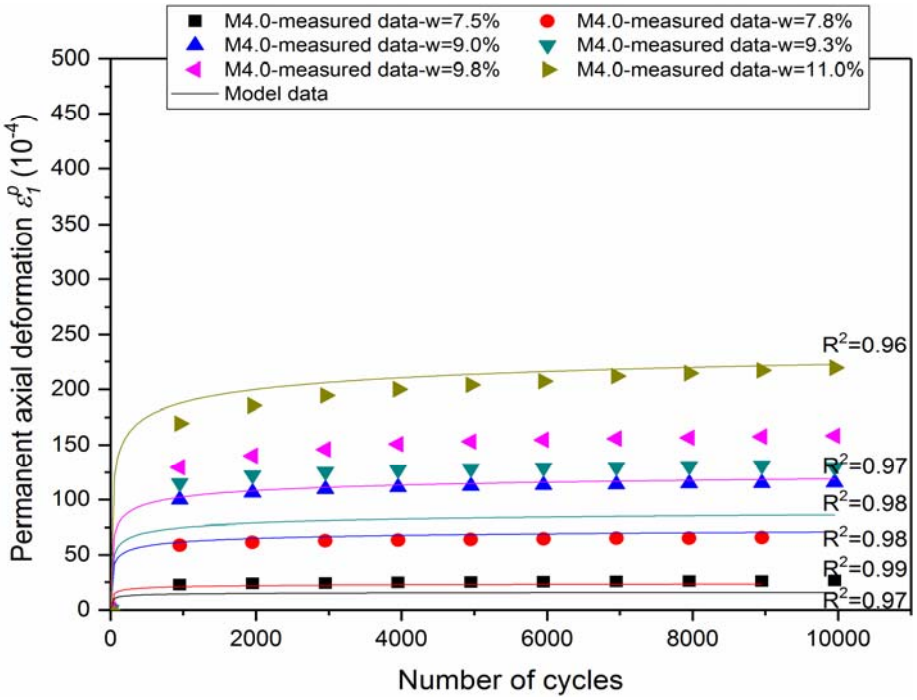

a)

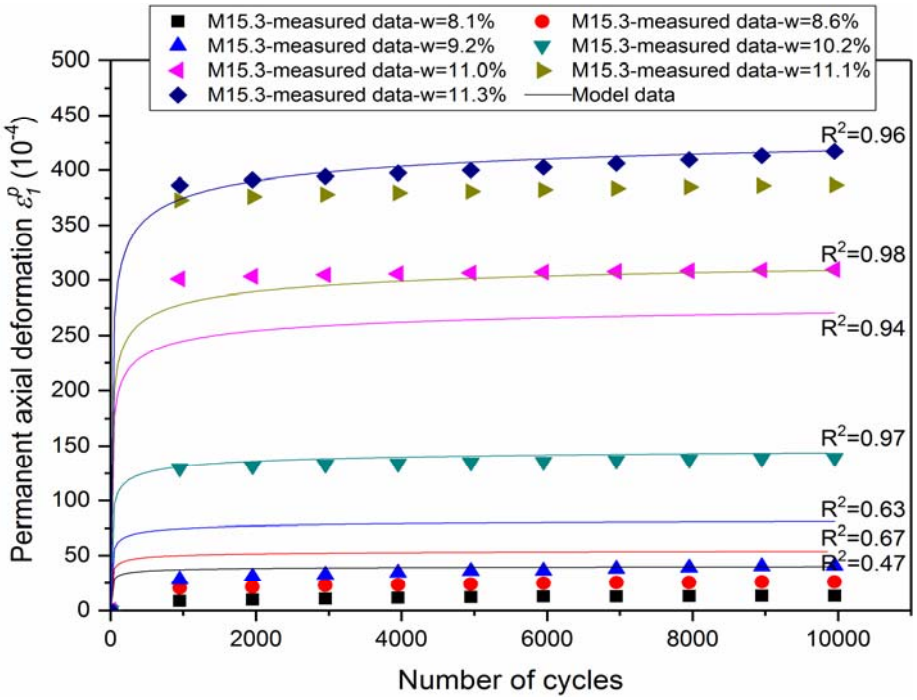

b)

Figure III.14. Test results as well as the model prediction for ε_1^p based on suction value, a) M4.0 and b) M15.3

Missillac sand	*b*	*d*	**R^2**
	300.000	-1.569	
	e	*f*	0.90
	-0.060	-0.400	

Table III.4. Parameters of the model for the single-stage tests (M4.0 and M15.3) based on suction value

III.3.5. Discussion

Generally, it can be observed that there is an optimum fine content, which corresponds to the minimum permanent axial deformation at a given water content. It is difficult to estimate this optimum fine content because it changes drastically with the variation of water content.

For the water contents, less than 10.3% (or maybe the optimum proctor water content), the increase of fine content reduces the permanent axial deformation. In other words, the optimum fine content corresponds to the highest studied fine content.

On the other hand, for the water content higher that 10.3%, the decrease of fine content reduces the permanent axial deformation (*Figure III.7*). In other words, the optimum fine content reaches its minimum value at a water content close to the saturated state. However, we need more experiments particularly at one or two other fine contents to determine accurately the minimum optimum fine content at the saturated state of our studied materials. This point will be further investigated in our future studies.

To solve the problem of dual variation of the permanent axial deformation with the water content and the fine content and to avoid the determination of the optimum fine content, the permanent axial deformation is related to suction values. A unique curve may define the variation of the permanent axial deformation with $s/s*$ value. These findings are helpful for an easier interpretation of the results. Besides, it can be stated that the model based on the suction value has less parameters (*b, d, e, f)* than the model based on the water content and fine content which has two more parameters (*a*, *k*, *o*, *u*, *k'*, *o'*).

III.4. Permanent axial deformation behaviour in multi-stage test

The same as the single-stage tests in section 3, the previous two approaches are applied to model the results of RLTT in multi-stage test.

III.4.1. Sample preparation and stress paths

For sample preparation, the samples M15.3 are compacted following the method of vibrating hammer (NF EN13286-4, 2003) in 7 layers with a height of 285 ± 5 and a diameter 150 mm, the same as the single-stage tests. The samples M7.5 are compacted following the method of vibrocompression (NF P98-230-1, 1992) in 1 layer with a height of 320 ± 5 mm and a diameter 160 mm.

During the test procedure, one sample at a given water content is subjected to a series of loading stages with different deviatoric stresses on a given stress path and each loading stage includes 10000 cycles. For M7.5, the different stress paths ($\Delta q/\Delta p$ = 3, $\Delta q/\Delta p$ = 2, $\Delta q/\Delta p$ = 1.5 and $\Delta q/\Delta p$ = 1) are applied to different samples with constant water content (11%) from an initial stress state of (p_0, q_0) = (10, 5 kPa) at the frequency of 1 Hz. For M15.3, the different samples are prepared with different water contents (w = 7.7%, w = 9.4%, w = 9.9% and w = 11.1%), and then a constant stress path ($\Delta q/\Delta p$ = 3) is applied to the samples from an initial stress state of (p_0, q_0) = (10, 0 kPa) at the frequency of 0.5 Hz.

The water content and the stress state applied to M7.5 and M15.3 in multi-stage tests are shown in *Table II.5* and *Table II.6* respectively.

III.4.2. Experimental results

Figure III.15.a and *Figure III.15.b* present the permanent axial deformation versus the number of cycles at different stress levels in multi-stage tests for M7.5 and M15.3 respectively. It implies that the evolution of the permanent axial deformation is also related to the stress state: the higher the stress path or the higher the stress level, the larger the permanent axial deformation. The Influence of the water content is the same as the single-stage tests: the higher the water content, the larger the permanent axial deformation.

Besides, comparing the results of M7.5 with M15.3 for stress path $\Delta q/\Delta p$ = 3, stress levels Δq = 40 kPa and Δq = 70 kPa and a water content w = 11%, it can be also observed that the sample close to saturated state with a higher fine content exhibits less mechanical resistance as it has been shown in single-stage test.

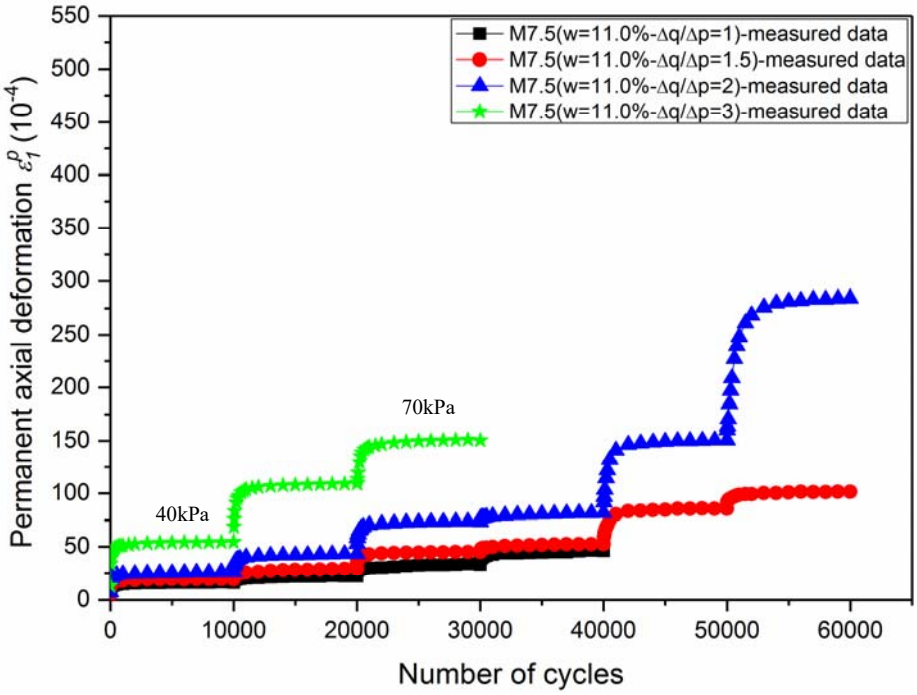

a)

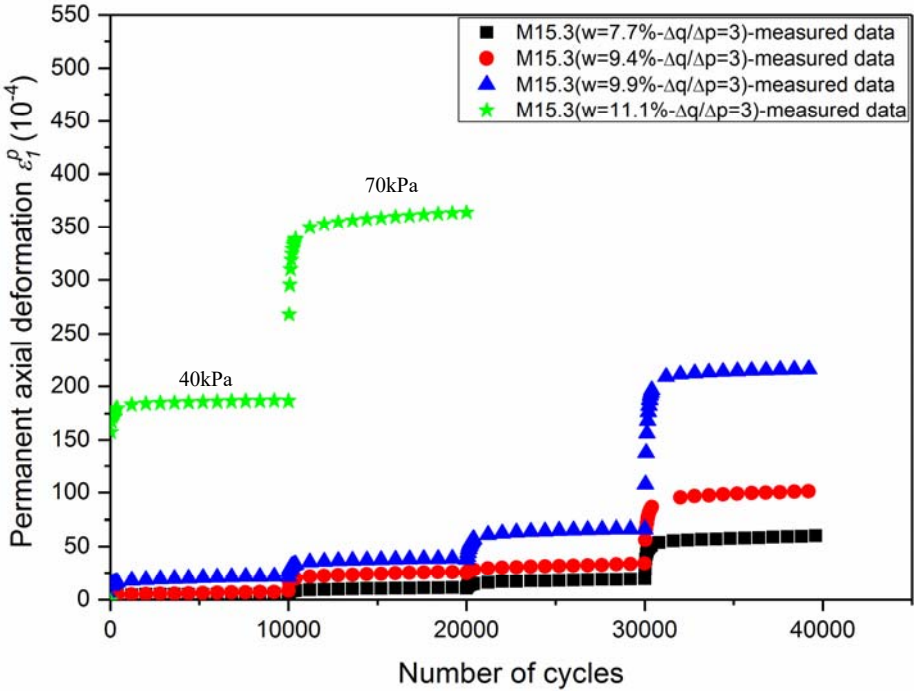

b)

Figure III.15. Test results of the multi-stage tests, a) M7.5 and b) M15.3

III.4.3. Modelling results based on water content and fine content

Based on Equation.I.24 and Equation.III.5, a new equation is proposed for estimating multi-stage RLTTs as follow:

$$\varepsilon_1^p = R \cdot \left(1 - \left(\frac{N}{N_0}\right)^{\left(\left(\frac{k'}{w}\right)+o'\cdot cc\right)}\right) \cdot \left(a \cdot \left(\frac{w}{k}\right)^{o\cdot(cc)^u}\right) \cdot \left(\frac{l_{\max}}{p_a}\right)^n \cdot \frac{1}{m + \frac{s_b}{p_{\max}} - \frac{q_{\max}}{p_{\max}}} \quad \text{(III.9)}$$

where, w is the water content (%); cc is the fine content (%); $l_{\max} = \sqrt{{p_{\max}}^2 + {q_{\max}}^2}$; p_{max} (kPa) and q_{max} (kPa) are the largest mean stress and the largest deviatoric stress respectively per load cycle; P_a = 100kPa; R, a, k, o, u, k', o', m, s_b and n are constants.

In this context, all multi-stage test results are used to determine the model parameters by following the next two steps:

Step 1: Determine parameters a, k, o, u, m, s_b and n by fitting $g(q_{max}, cc, w)$ in Equation.III.9.a for the cumulated permanent axial deformation obtained at the end of each loading stage as shown in *Figure III.16.a* and *Figure III.17.a*:

$$g\left(q_{\max}, cc, w\right) = \left(a \cdot \left(\frac{w}{k}\right)^{o\cdot(cc)^u}\right) \cdot \left(\frac{l_{\max}}{p_a}\right)^n \cdot \frac{1}{m + \frac{s_b}{p_{\max}} - \frac{q_{\max}}{p_{\max}}} \quad \text{(III.9.a)}$$

Equation.III.9 could be rewritten as:

$$\varepsilon_1^p = R \cdot \left(1 - \left(\frac{N}{N_0}\right)^{\left(\left(\frac{k'}{w}\right)+o'\cdot cc\right)}\right) \cdot g\left(q_{\max}, cc, w\right) \quad \text{(III.9.b)}$$

Step 2: Determine parameters R, k', o' by fitting Equation.III.9.b to the permanent axial deformation evolution with the number of cycles, as shown in *Figure III.16.b & 17.b*.

All these parameters were summarized in *Table III.5* and the simulation results were presented in *Figure III.16.b & 17.b*. However, the accuracy is less than the single-stage test because of the different stress paths and the different stress levels to be taken into account in the calibration, the results show a good capacity of the model to estimate the permanent axial deformation behaviour for Missillac sand.

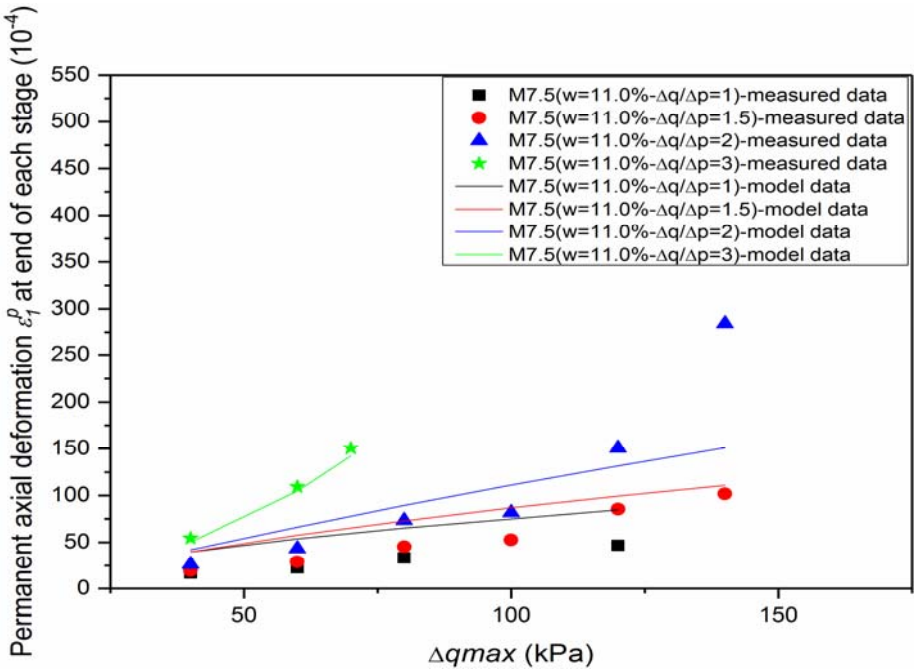

a)

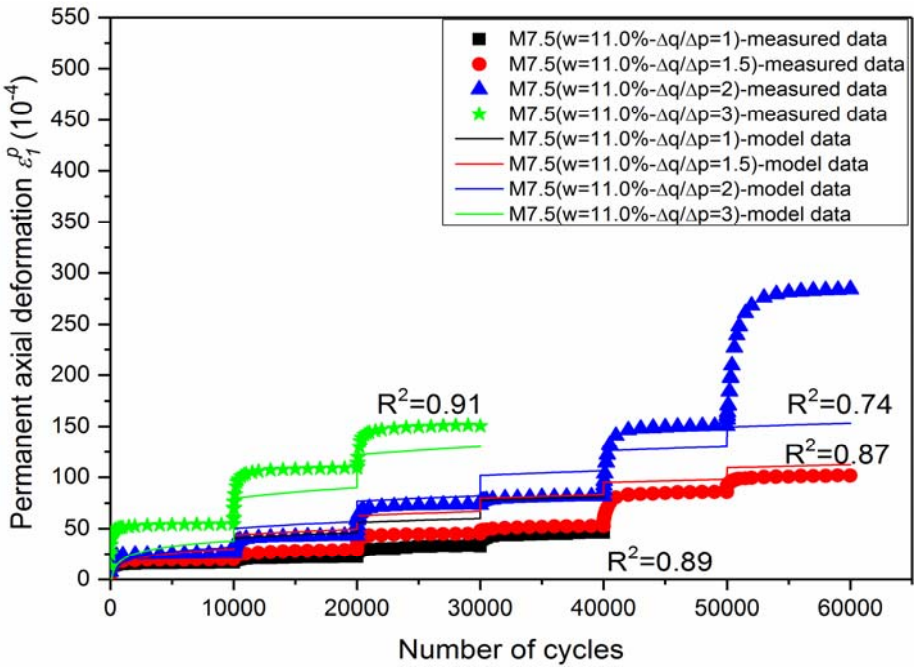

b)

Figure III.16. Test results as well as the model prediction for ε_1^p based on water content and fine content for M7.5

a) Cumulated permanent axial deformation at the end of each loading stage

b) Variation of the permanent axial deformation with the number of cycles

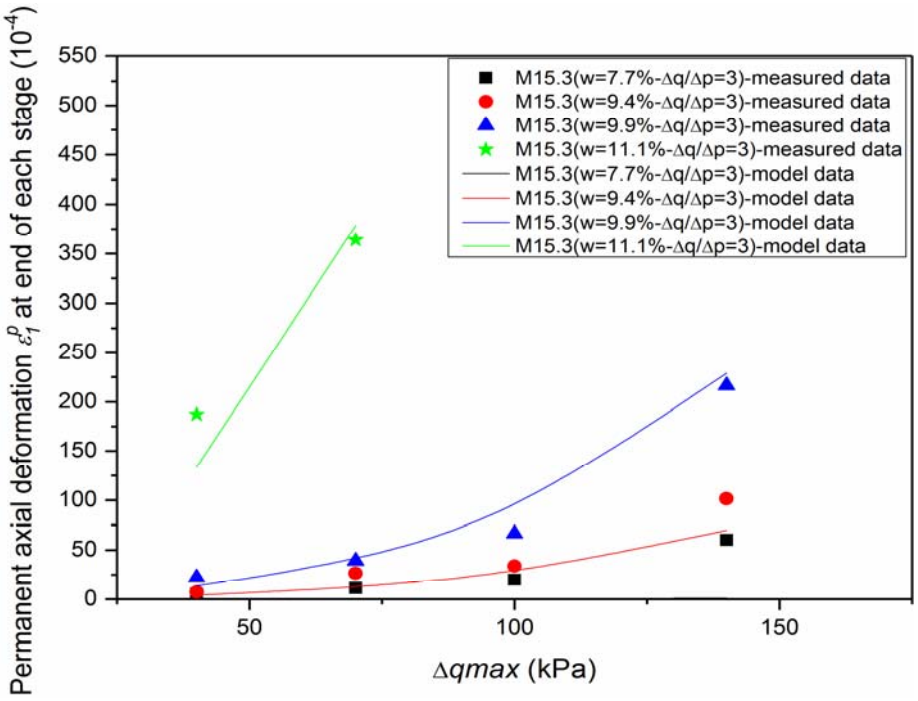

a)

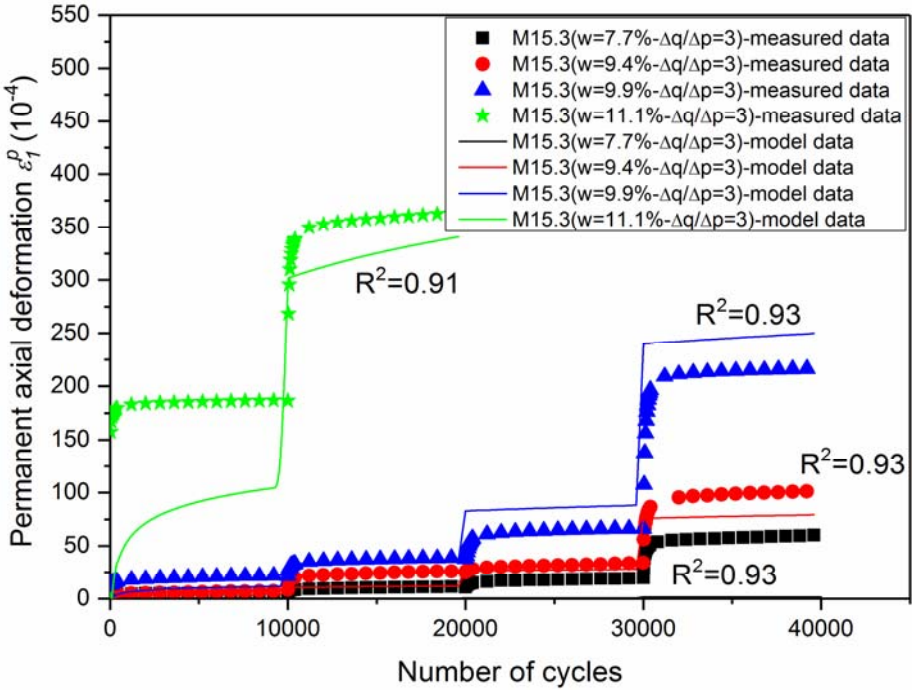

b)

Figure III.17. Test results as well as the model prediction for ε_1^p based on water content and fine content for M15.3

Missillac sand	*a*	*k*	*o*	*u*	*m*	R^2
	51.111	10.140	1.377	1.003	2.620	
	s_b	*n*	*R*	*k'*	*o'*	0.74
	25.693	0.500	4.235	-0.443	-0.0003	

Table III.5. Parameters of the model for the multi-stage tests (M7.5 and M15.3) based on water content and fine

Application of the proposed model on permanent deformation of the material from literature

Duong et al., (2013) applied multi-stage cyclic triaxial tests on an interlayer soil used in ancient railway sub-structure in France. These tests were performed at a stress path ($\Delta q/\Delta p$ = 3), at three different water contents (4.0%, 6.0% and 12.0%) and at three different fine contents (7.0%, 15.0% and 23.0%). The materials are defined as $M7.0_{Duong}$, $M15.0_{Duong}$ and $M23.0_{Duong}$.

The test results were shown in *Figure III.18.b*, *Figure III.19.b* and *Figure III.20.b*, which implied that in unsaturated state and for the same water content, increasing fine content makes the suction higher and thus strengthening the soil. On the contrary, in saturated state, suction becomes zero and the shear strength decreases accordingly. The same results were previously observed for the Missillac sand.

The same procedure was used to simulate the permanent axial deformation of the studied soils during the multi-stage tests. The results are also shown in *Figure III.18.b*, *Figure III.19.b* and *Figure III.20.b*. *Table.III.6* presents also the fitted parameters of the proposed model. It can be stated that the proposed model performs well.

Missillac sand	*a*	*k*	*o*	*u*	*m*	R^2
	71.540	11.393	0.191	0.992	2.535	
	s_b	*n*	*R*	*k'*	*o'*	0.85
	38.389	0.300	1.731	-0.225	-0.0066	

Table III.6. Parameters of the model for the multi-stage tests (Duong et al., 2013) based on water content and fine content

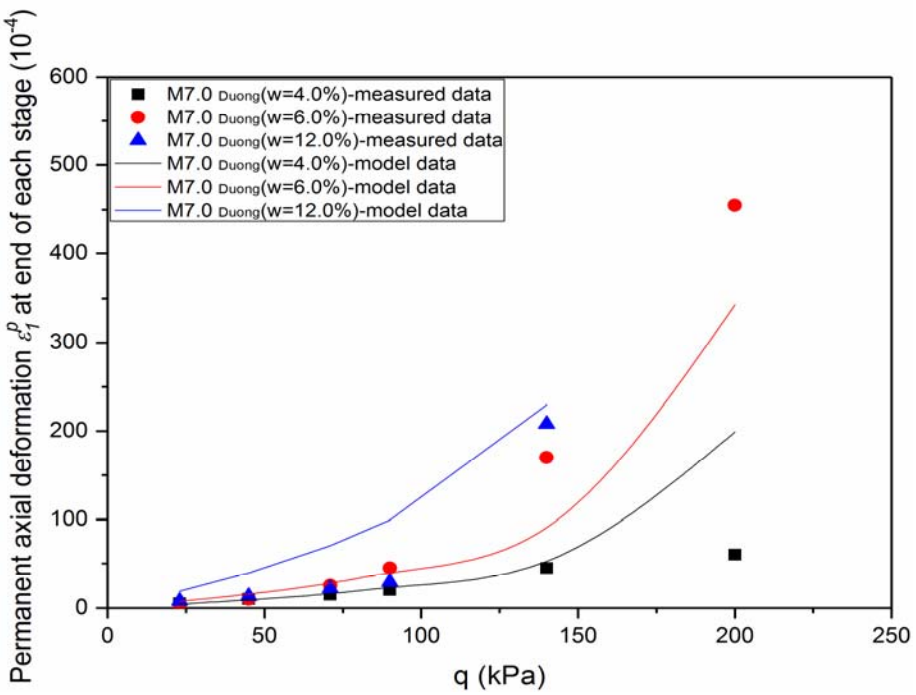

a)

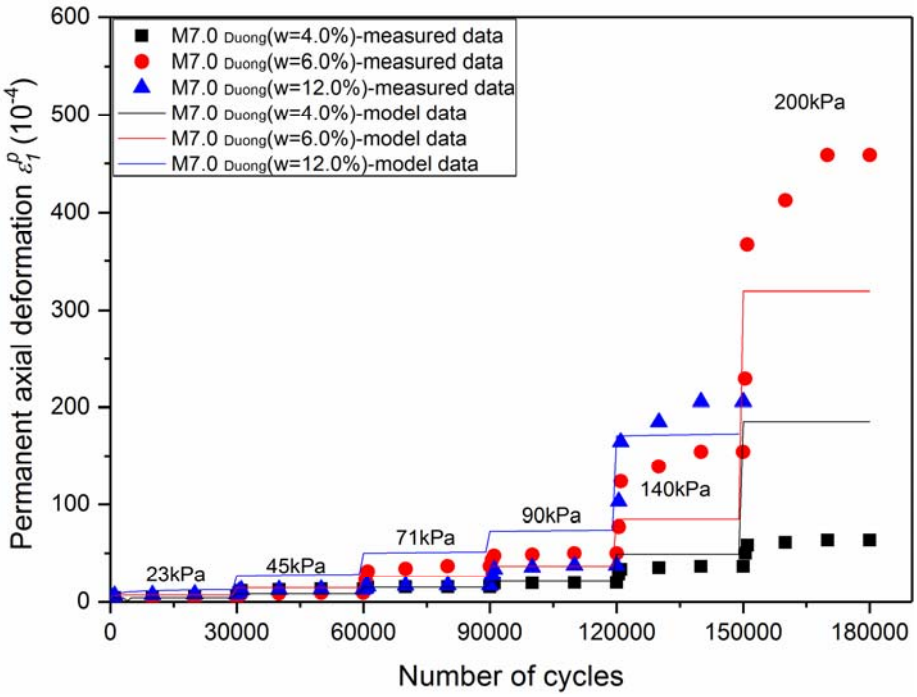

b)

Figure III.18. Test results as well as model prediction for ε_1^p based on water content and fine content for $M_{Duong}7.0$

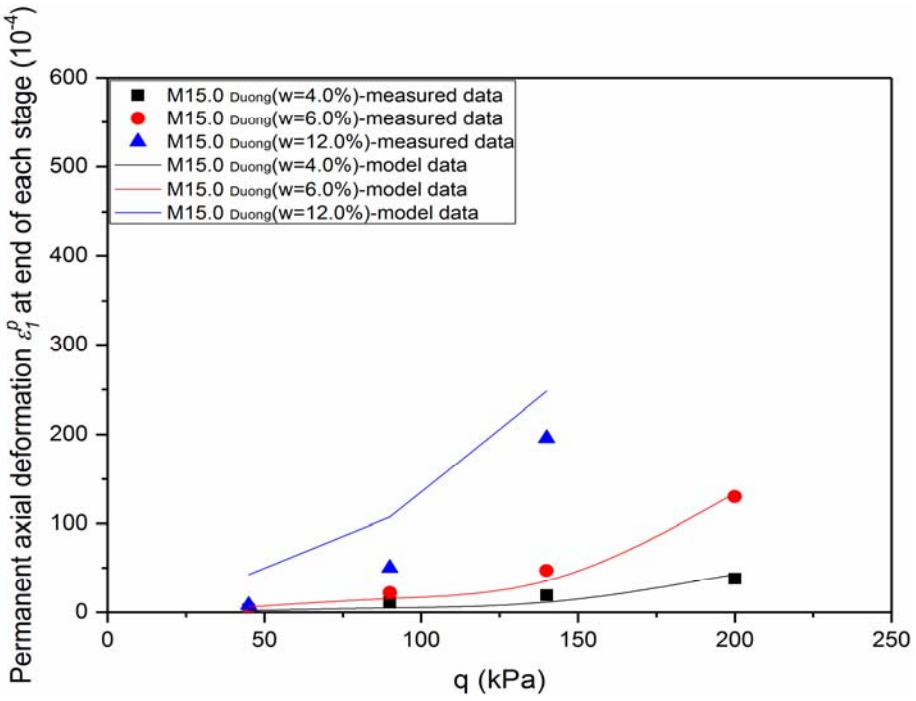

a)

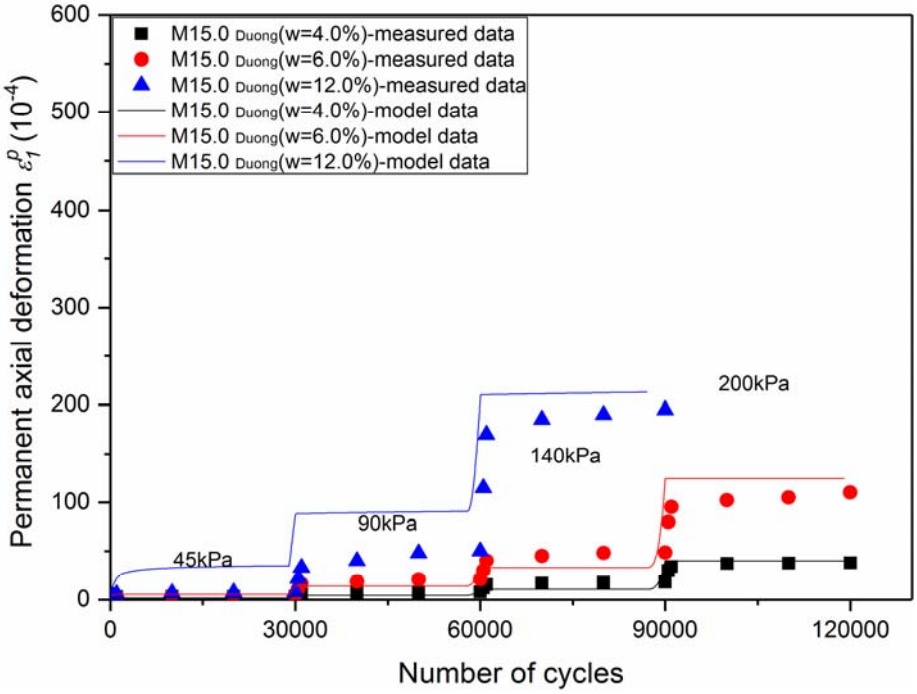

b)

Figure III.19. Test results as well as model prediction for ε_1^p based on water content and fine content for $M_{Duong}15.0$

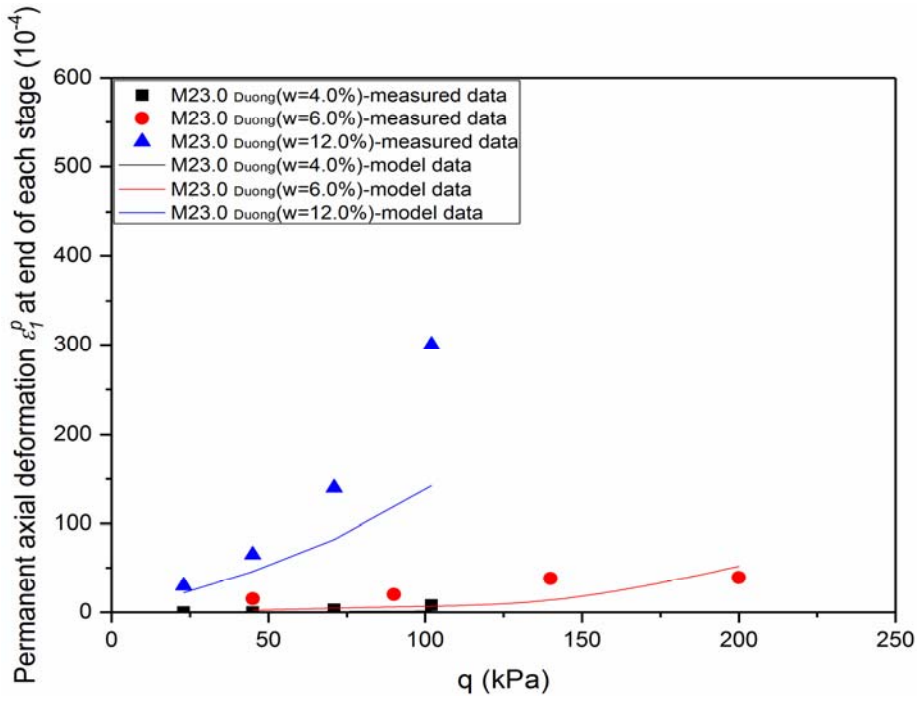

a)

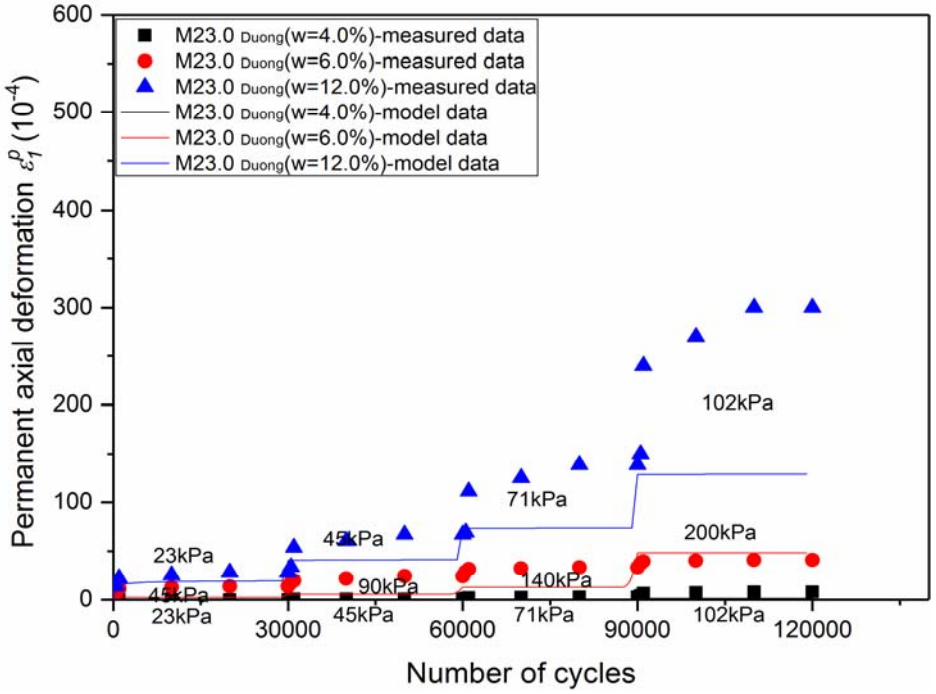

b)

Figure III.20. Test results as well as model prediction for ε_1^p based on water content and fine content for $M_{Duong}23.0$

III.4.4. Modelling results based on suction value

The permanent axial deformation in the multi-stage tests can be also related to suction value. Based on the Equation.I.24 and Equation.III.8, a new equation, which is considering the different stress states, is also proposed to estimate the permanent axial deformation behaviour, as follow:

$$\varepsilon_1^p = T \cdot \left(1 - \left(\frac{N}{N_0}\right)^{e \cdot \ln(s/s_a)+f}\right) \cdot b \cdot \left(s/s^*\right)^d \cdot \left(\frac{l_{\max}}{p_a}\right)^n \cdot \frac{1}{m + \frac{s_b}{p_{\max}} - \frac{q_{\max}}{p_{\max}}} \quad \text{(III.10)}$$

where, s is suction value (kPa); s^* is the suction value (kPa) of the intersection point of wetting and drying paths in SWRC; s_a is equal to 100 kPa; $l_{\max}=\sqrt{{p_{\max}}^2+{q_{\max}}^2}$; p_{max} (kPa) and q_{max} (kPa) are the largest mean stress and the largest deviatoric stress respectively per load cycle; P_a = 100kPa. T, b, d, e, f, m, s_b, and n are constant.

The same procedure is used to determine the model parameters:

Step 1: Determine parameters b, d, m, s_b and n by fitting $g(q_{max}, s)$ in Equation.III.10.a for the cumulated permanent axial deformation obtained at the end of each loading stage as shown in *Figure III.21.a* and *Figure III.22.a*.

$$g\left(q_{\max}, s\right) = b \cdot \left(s/s^*\right)^d \cdot \left(\frac{l_{\max}}{p_a}\right)^n \cdot \frac{1}{m + \frac{s_b}{p_{\max}} - \frac{q_{\max}}{p_{\max}}} \quad \text{(III.10.a)}$$

Equation.III.10 could be rewritten as:

$$\varepsilon_1^p = T \cdot \left(1 - \left(\frac{N}{N_0}\right)^{e \cdot \ln(s/s_a)+f}\right) \cdot g\left(q_{\max}, s\right) \quad \text{(III.10.b)}$$

Step 2: Determine parameters T, e, f by fitting Equation.III.10.b to the permanent axial deformation evolution with the number of cycles as shown in *Figure III.21.b* and *Figure III.22.b*.

All these parameters were summarized in *Table III.7*. *Figure III.21.b* and *Figure III.22.b* show the test results and the modelling results. Generally, it suggests that the simulation is in

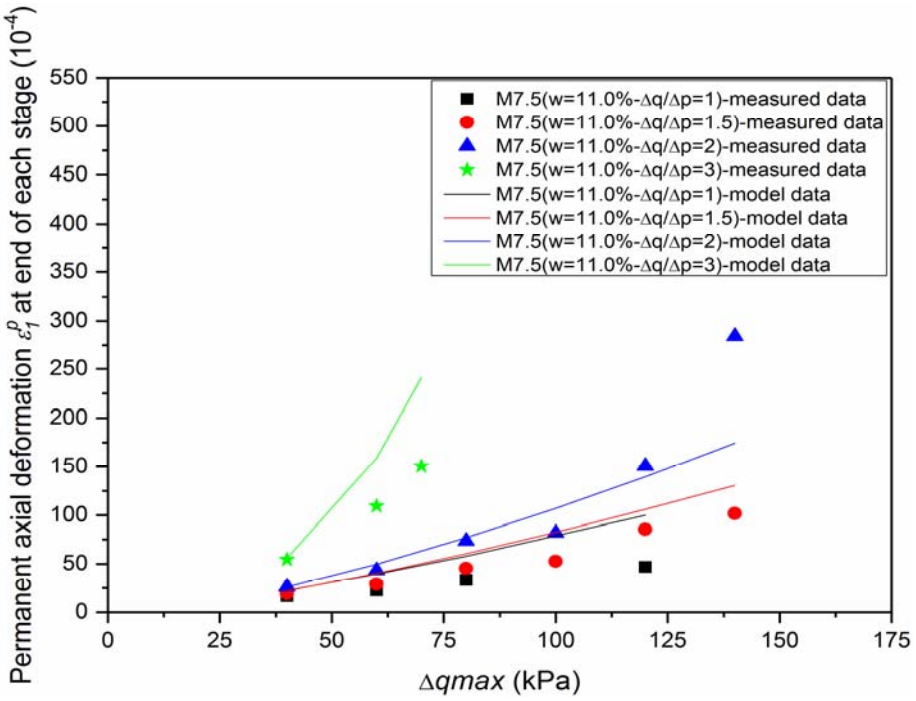

a)

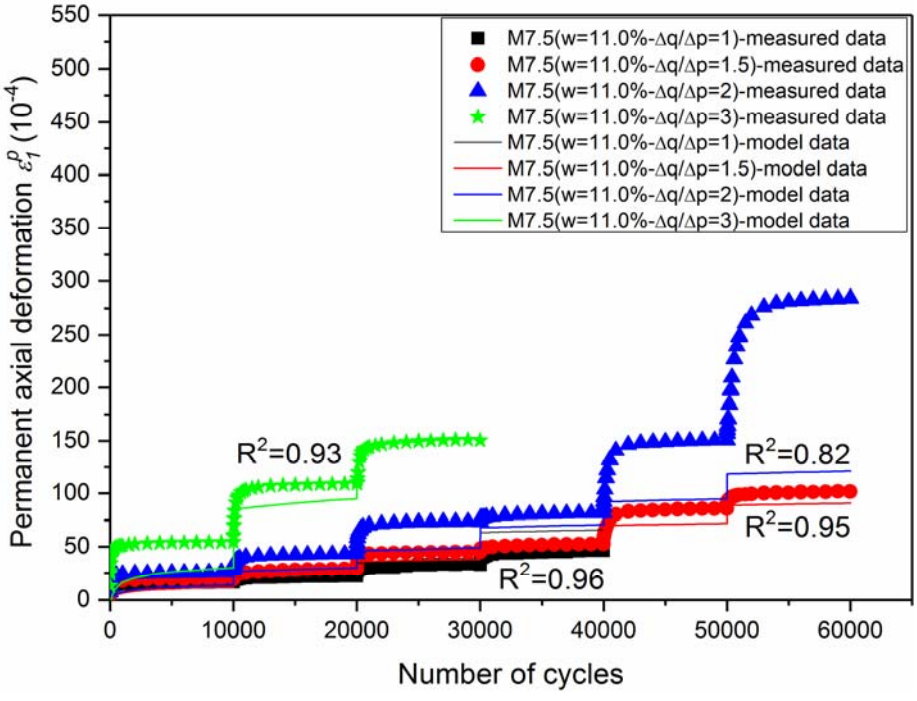

b)

Figure III.21. Test results as well as the model prediction for ε_1^p based on suction value for M7.5

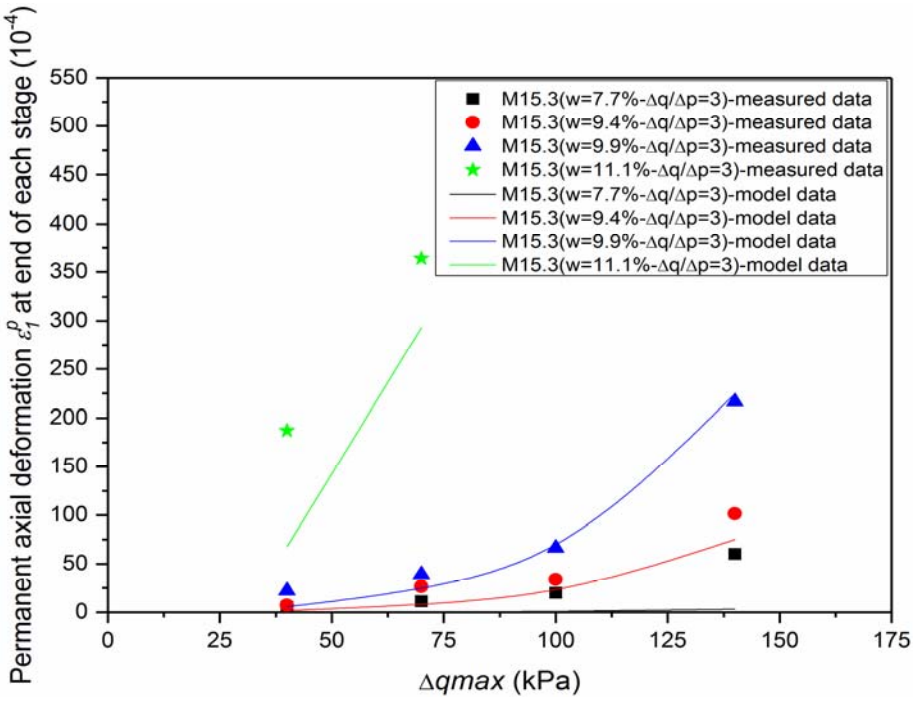

a)

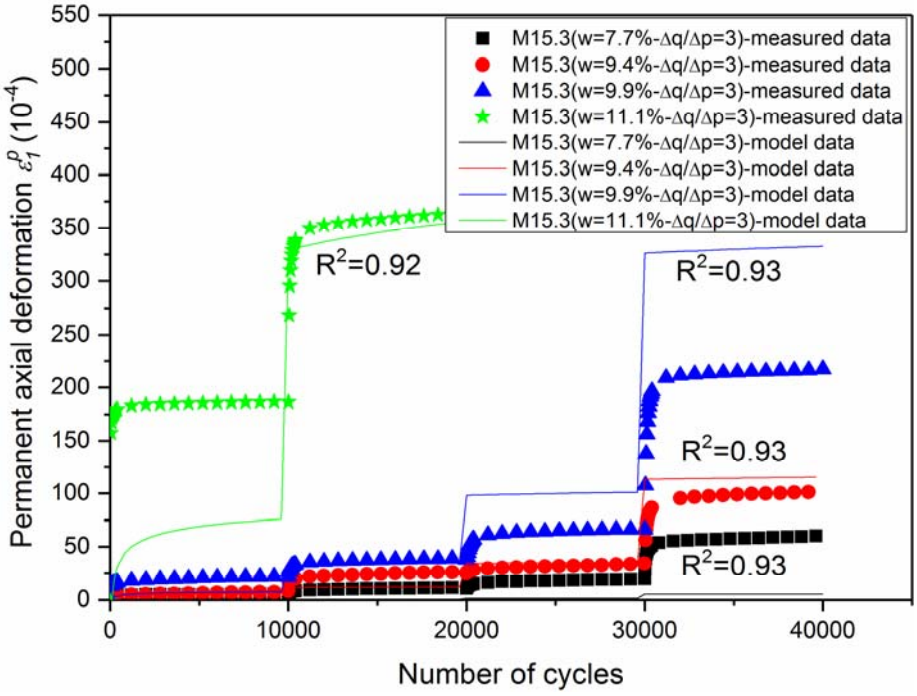

b)

Figure III.22. Test results as well as the model prediction for ε_1^p based on suction value for M15.3

good agreement with the experimental results. Moreover, the accuracy is not far from the model based on the fine content and the water content.

Missillac sand	*b*	*d*	*m*	s_b	R^2
	98.421	-4.547	2.873	9.392	
	n	*T*	*e*	*f*	0.67
	1.291	1.812	-0.134	-0.499	

Table III.7. Parameters of the model for the multi-stage tests (M7.5 and M15.3) based on suction value

III.4.5. Discussion

As it was mentioned for the single-stage tests, the comparison of these two series of modelling results shows that the model (Equation.III.9) based on water content and fine content is moderately more accurate (R^2 = 0.74) than the model (Equation.III.10) based on suction value (R^2 = 0.67). However, the number of parameters of the proposed model is obviously decreased when it is based on suction value: Equation.III.10 with 8 parameters (*T*, *b, d, e, f, m, s,* and *n*) compared to Equation.III.9 with 10 parameters (*R, a, k, o, u, k', o', m, s* and *n*).

III.5. Conclusion

This chapter investigates the permanent axial deformation of the Missillac sand in low traffic pavements under cyclic loading at various initial moisture states. A series of RLTTs are applied on the different remolded soil samples at different water contents and different fine contents in single-stage procedure. Another series of tests are carried out at different fine contents, different water contents and different stress states in multi-stage procedure. Both in single-stage tests and multi-stage tests, the results show that the permanent axial deformation increases with the increase of the water content, while the influence of fine content depends on the initial water content and the water sensitivity of fine particles. Increasing the stress path and the stress level leads to an increase of the permanent axial deformation in multi-stage test.

To describe the permanent axial deformation of Missillac sand, we propose a new empirical-analytical model considering the effect of the water content, the fine content, the number of

cycles and the stress state based on the Hornych model (Equation.I.18) and Gidel model (Equation.I.24). The simulation results show a good capacity of this proposed model to evaluate the permanent axial deformation in both single-stage tests and multi-stage tests.

Besides, the SWRCs are obtained by filter paper method for Missillac sand at different fine contents. To solve the problem of dual variation of the permanent axial deformation with the water content and the fine content and to avoid the determination of the optimum fine content (which is complicated in this study), the permanent axial deformation is related to suction values. A unique curve may define the variation of the permanent axial deformation with s/s^* value. These findings are helpful for an easier interpretation of the results. Besides, it can be stated that the model based on the suction value has two less parameters than the model based on the water content and fine content with the same accuracy approximately.

These two proposed models can reduce the number of tests required to predict the soil permanent axial deformation.

CHAPTER IV. RESILIENT DEFORMATION BEHAVIOUR OF A GRANULAR MATERIAL

IV.1. Introduction

In this chapter, we present the resilient test results of repeated load triaxial tests (RLTTs) for Missillac sand with three different fine contents: the stabilization of the permanent deformation; the resilient deformations; the maximum volumetric deformation and the maximum deviator deformation in s/s^* plane and the anisotropy effect on the resilient behaviour. For the modelling analysis, a modified Boyce-Hornych model is proposed with the anisotropy effect predicting correctly volumetric deformation and deviatoric deformation. A discussion is introduced at the end of the chapter to improve the model based on effective stress concept.

IV.2. Experimental results and analysis of RLTTs

IV.2.1.Sample preparation and test procedures

As introduced in Chapter III, all the samples of Missillac sand M4.0 and M15.3 are compacted following the method of vibrating hammer (NF EN13286-4, 2003) in 7 layers with a height of 285±5 mm and a diameter of 150 mm and the samples of Missillac sand M7.5 are compacted following the method of vibrocompression (NF P98-230-1, 1992) in 1 layer with a height of 320±5 mm and a diameter 160 mm. All the samples are prepared at a water content range between 7% and 11% with a dry density of 2±0.06 Mg/m^3.

Conditioning phase

The samples are first subjected to a conditioning phase that consisted of 10,000 loading/unloading cycles to stabilize the plastic strains. At the end of the conditioning phase, the increase in permanent axial deformation as presented in the last chapter was lower than 10^{-7} per cycle confirming the stabilized plastic deformation.

For the three studied materials, the cyclic stress paths during the conditioning phase has been summarized in *Table III.2*.

Resilient test phase

After the conditioning phase, 5 different stress paths ($\Delta q/\Delta p$ = 0; 0.5; 1; 2; 3) are applied to each sample, as shown in *Table IV.1* and each stress path consists of 100 loading/unloading cycles. An initial stress state of (p_0, q_0) = (10, 0 kPa) is applied to samples M4.0 and M15.3 and another initial stress state of (p_0, q_0) = (10, 5 kPa) is applied to samples M7.5. For each stress path, the last loading/unloading cycle is used to determine the resilient behaviours.

$\Delta q/\Delta p$	Missillac sand M4.0, M15.3		Missillac sand M7.5	
	p (kPa)	q (kPa)	p (kPa)	q (kPa)
0	90	0	90	5
0.5	90	40	90	45
1	90	80	90	85
2	50	80	50	85
3	30	60	30	65

Table IV.1. Cyclic stress paths in resilient test phase

IV.2.2.Stabilization of permanent deformation

Based on the results of the conditioning phase shown in Chapter III, we can observe that the permanent deformation increases significantly as the water content increases and the deformation hardly stabilizes with the highest water content (≥ 11%) for Missillac sand M4.0 and M15.3 with the stress path of $\Delta q/\Delta p$ = 3. For the water contents close to the saturated state, more cycles are required to reach the stabilized permanent axial deformation. It can be also stated that, in unsaturated state, the permanent deformation stabilizes more quickly when the fine content increases, if we compare the results of M4.0 at the water content less than 10% to M15.3 at the water content less than 11%.

In general, for the three materials, both the permanent axial deformation ε_1^p and the permanent radial deformation ε_3^p have achieved the equilibrium state after 10,000 cycles, because the values of $\Delta\varepsilon/\Delta N$ at end of each test are less than $10^{-7.}$

In this section, the stabilization of permanent deformation will be studied by overall axial deformation ε_1 and radial deformation ε_3 in the last 10 cycles of resilient test phase. The evolution of axial deformation and the radial deformation of the Missillac sand M4.0 and M15.3 in stress paths of $\Delta q/\Delta p$ = 0, 0.5 and 3 at two water contents of w = 8% and 11.0% in the last 10 cycles of resilient test are shown in *Figure IV.1*, *Figure IV.2, Figure IV.3* and *Figure IV.4* respectively. As the same time, the evolution of volumetric deformation ε_v and deviatoric deformation ε_q are also presented with same water content and same stress path in the same Figures. The following points can be concluded based on the results:

- The results confirm that even following a conditioning phase, the small evolution of ε_1^p and ε_3^p between initial state (0 deformation) to the last 10 cycles can be still observed for some samples in some stress paths, principally for ε_3^p as shown in *Figure IV.1.a & 1.e*; *Figure IV.2.a & 2.e*; *Figure IV.3.a & 3.c* and *Figure IV.4.a*, *4.c & 4.e*. For the M15.3 material with a high water content of 11% with the stress paths of $\Delta q/\Delta p$ = 0 and 0.5, both evolutions of ε_1^p and ε_3^p can be detected as shown in *Figure IV.4.a & 4.c*.

- The variation of ε_1 and the ε_3 between the last cycle and 91 th to 99 th cycles cannot be detected, except for the M15.3 material with a high-water content of 11% in stress paths of $\Delta q/\Delta p$ = 0 and 0.5, where the variation of ε_3 is more significant than ε_1. It suggests that the axial deformation ε_1 and the radial deformation ε_3 in the last 10 cycles for these

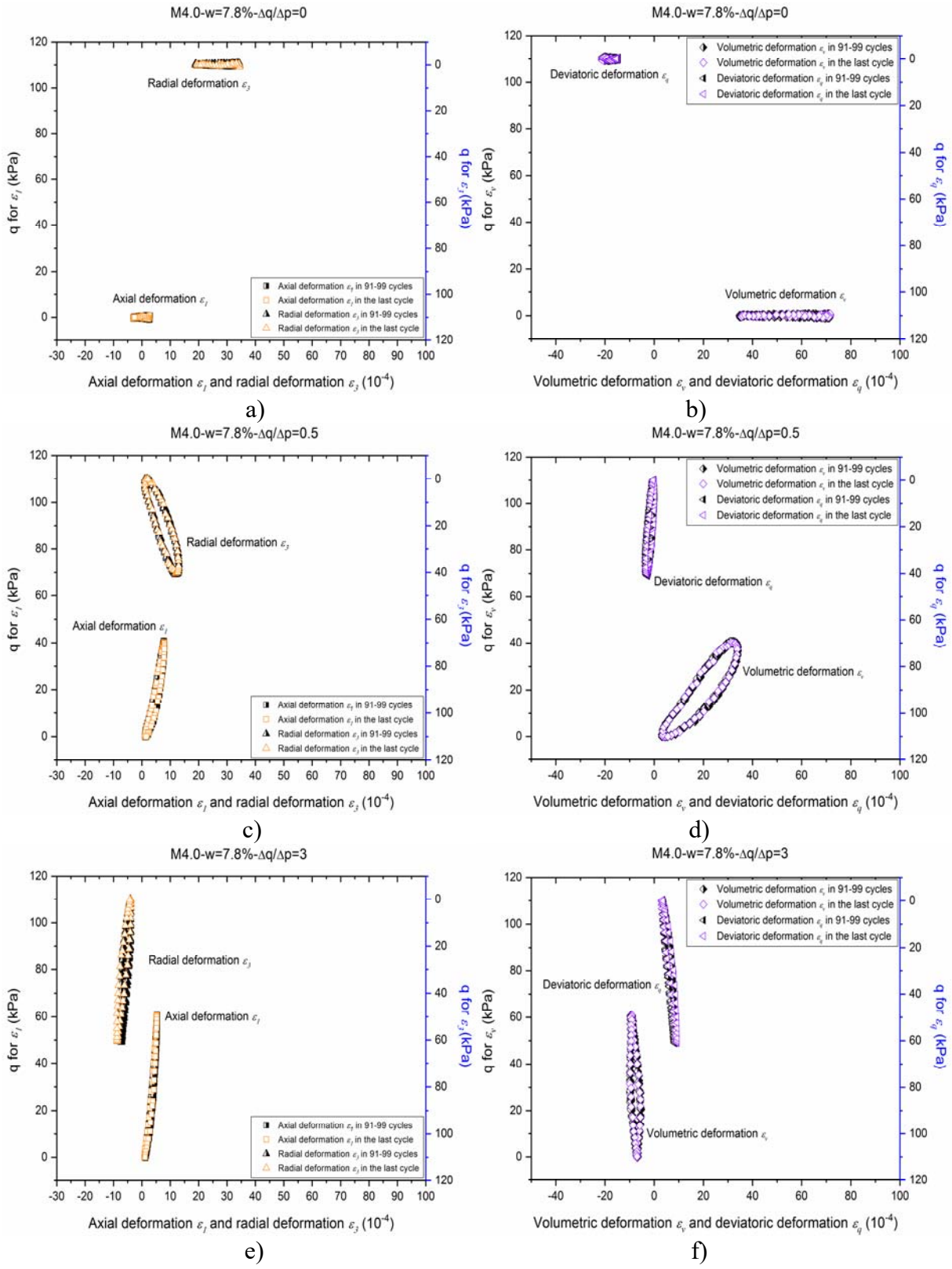

Figure IV.1. Evolution of axial deformation ε_1, radial deformation ε_3, volumetric deformation ε_v and deviatoric deformation ε_q in the last cycle and 91 th to 99 th cycles for M4.0 in stress paths of $\Delta q/\Delta p$ = 0; 0.5 and 3 with water content of 7.8%

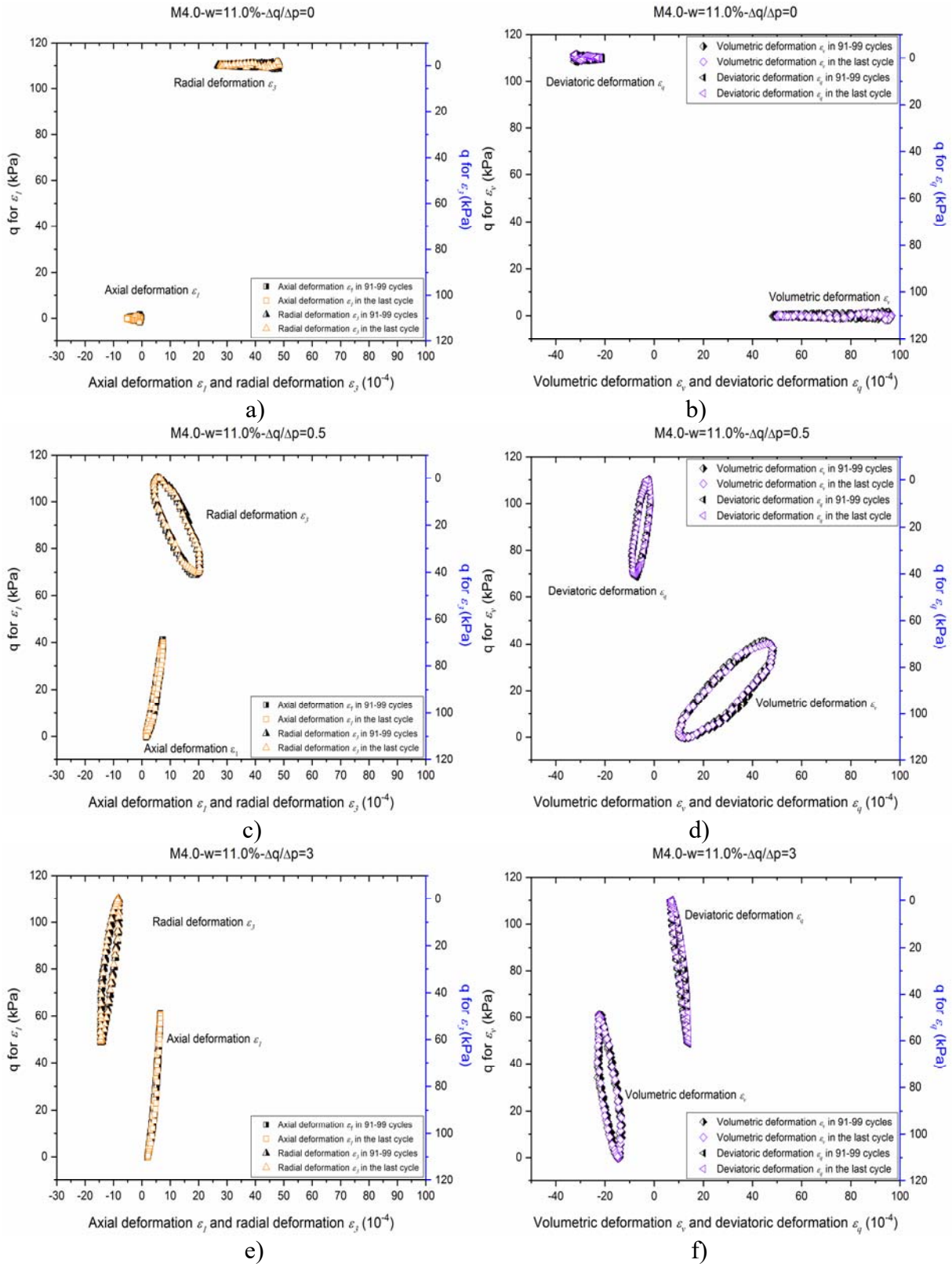

Figure IV.2. Evolution of axial deformation ε_1, radial deformation ε_3, volumetric deformation ε_v and deviatoric deformation ε_q in the last cycle and 91 th to 99 th cycles for M4.0 in stress paths of $\Delta q/\Delta p$ = 0; 0.5 and 3 with water content of 11.0%

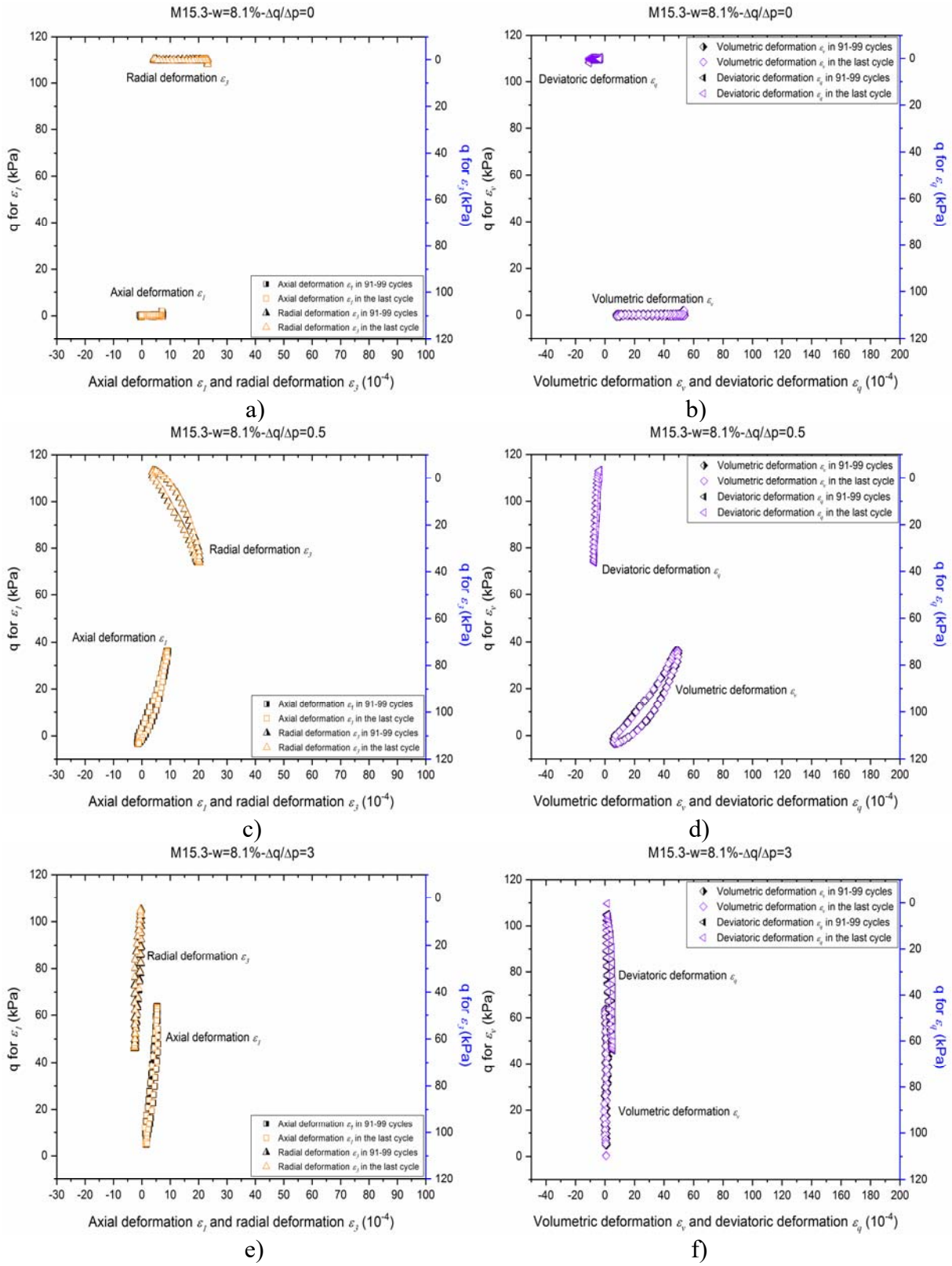

Figure IV.3. Evolution of axial deformation ε_1, radial deformation ε_3, volumetric deformation ε_v and deviatoric deformation ε_q in the last cycle and 91 th to 99 th cycles for M15.3 in stress paths of $\Delta q/\Delta p$ = 0; 0.5 and 3 with water content of 8.1%

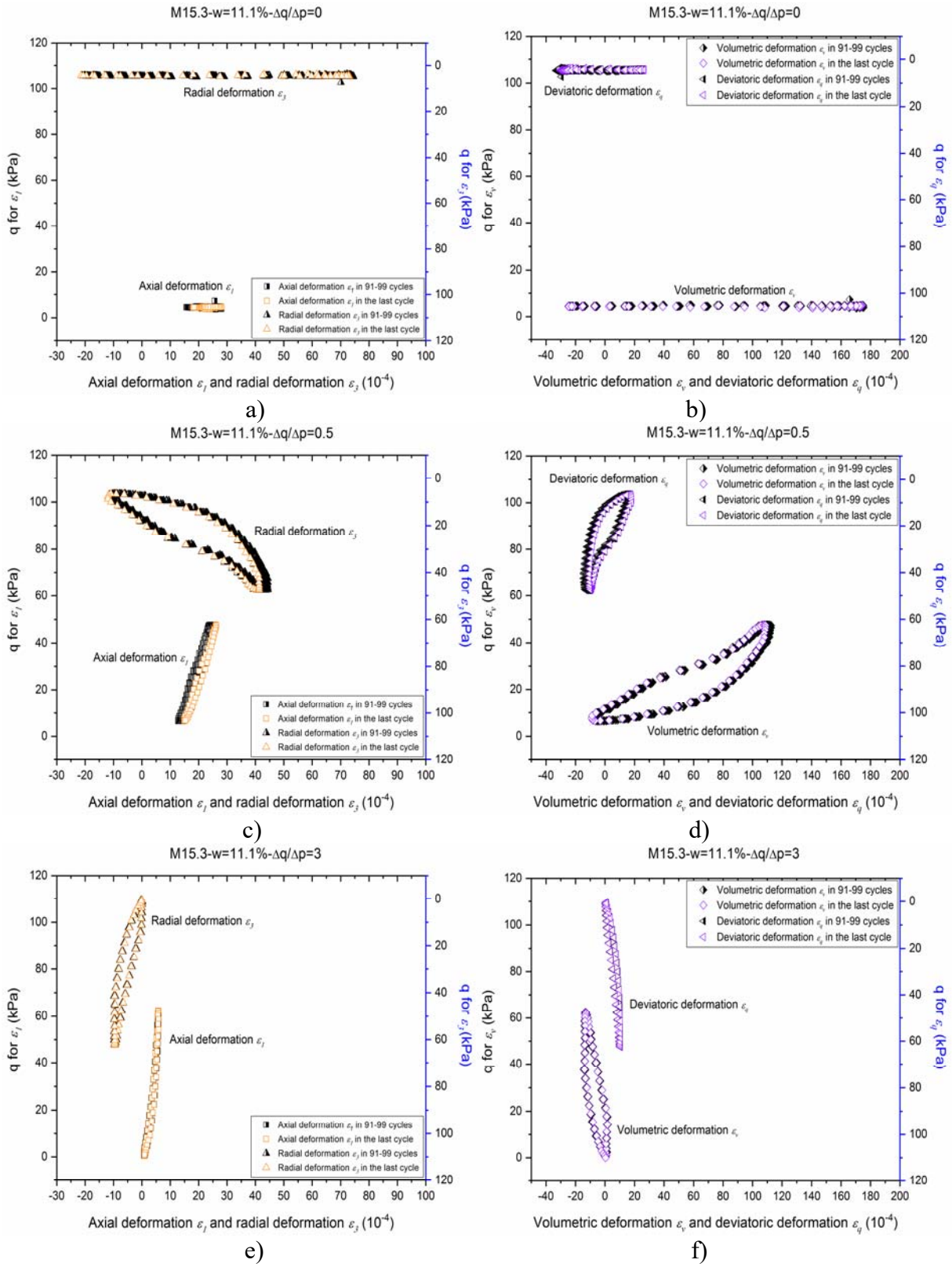

Figure IV.4. Evolution of axial deformation ε_1, radial deformation ε_3, volumetric deformation ε_v and deviatoric deformation ε_q in the last cycle and 91 th to 99 th cycles for M15.3 in stress paths of $\Delta q/\Delta p$ = 0; 0.5 and 3 with water content of 11.1%

samples are not completely elastic, and the increase of plastic deformation still exists, but the values are small (< 5×10^{-4}).

- The variation of volumetric deformation ε_v and deviatoric deformation ε_q derived from ε_1 and ε_3 are small in the last 10 cycles. As a result, the ε_v and ε_q in the last cycle can be considered resilient in the following calculations.

IV.2.3.Resilient deformation

Figure IV.5 and *Figure IV.6* present respectively the evolution of resilient volumetric deformation ε_v^r and the resilient deviatoric deformation ε_q^r in the last cycle for three different Missillac sands (M4.0, M7.5 and M15.3) at two different water contents of 8% and 11% (approximately).

Based on the test results, following observations can be stated:

- The ε_v^r values are positive in the stress paths of $\Delta q/\Delta p$ = 0; 0.5; 1 and 2 (Contraction) while it is negative in the stress paths of $\Delta q/\Delta p$ = 3 (Dilation). The ε_q^r values are positive in the stress paths of $\Delta q/\Delta p$ = 2 and 3 and negative in the other stress paths.

- The effect of water content on resilient deformations is obvious: the higher the water content is, the higher the ε_v^r in each stress path for each material. Higher the water content is, higher the ε_q^r in each stress path for each material. For M15.3 material, there are large increases of ε_v^r and ε_q^r with an increase of water content from 10% to 11%, especially for the stress paths of $\Delta q/\Delta p$ = 0; 0.5 and 1.

- The effect of fine content on the resilient deformations is not significant when the fine content increases from 4% to 7.5%, while ε_v^r and ε_q^r increase obviously with an increase of fine content from 7.5% to 15.3% at different water contents, especially for the stress paths of $\Delta q/\Delta p$ = 0; 0.5 and 1. The ε_v^r and ε_q^r are close to 0 on the stress path of $\Delta q/\Delta p$ = 2, hence the effect of increasing fine content is not obvious as increasing water content.

- Large open loops of ε_v^r and ε_q^r can be observed for M15.3 samples at water contents of 11% in the stress paths of $\Delta q/\Delta p$ = 0; 0.5 and 1.

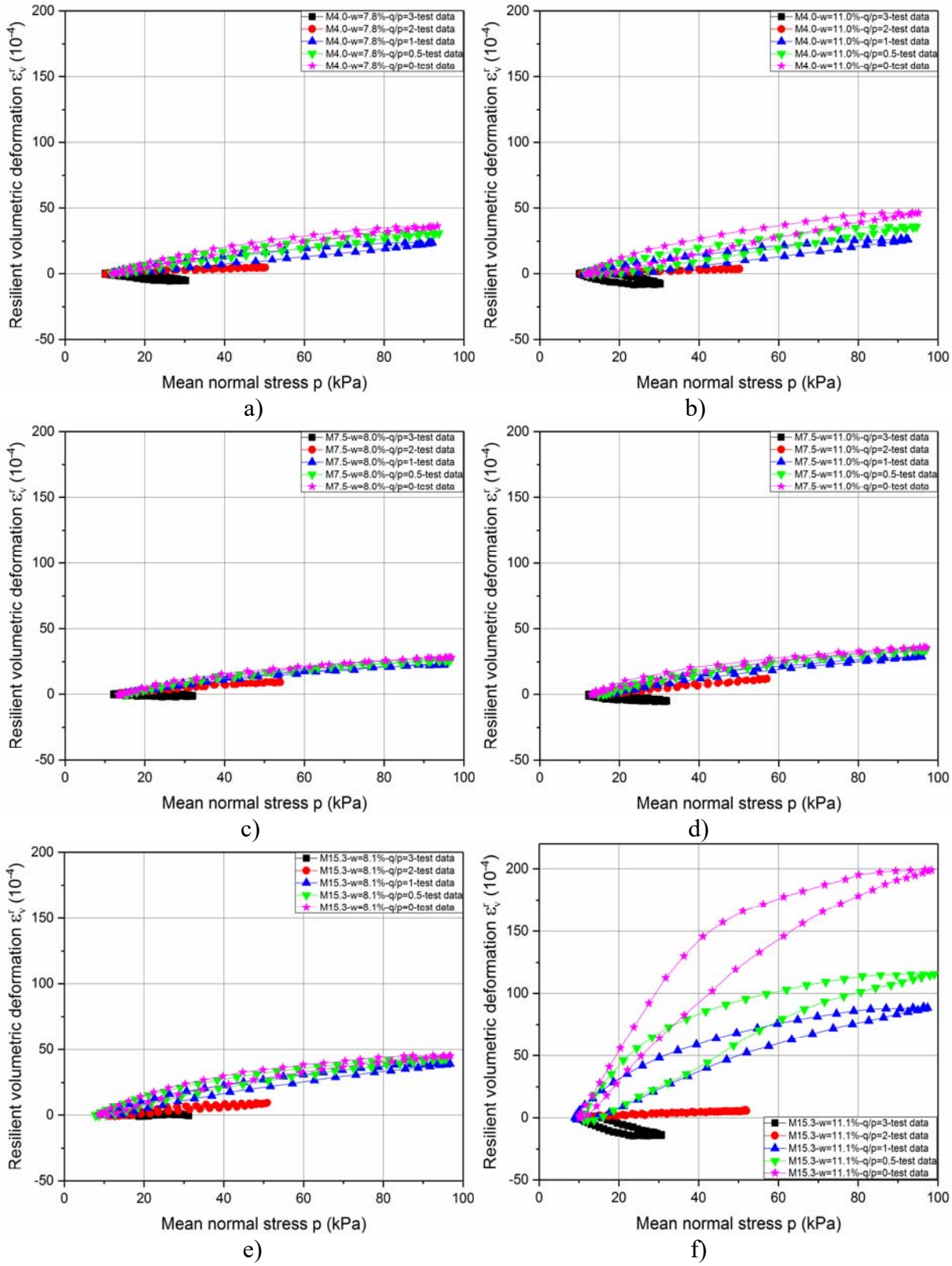

Figure IV.5. Evolution of resilient volumetric deformation ε_v^r for Missillac sand M4.0, M7.5 and M15.3 with water content of w=8% and w=11%.

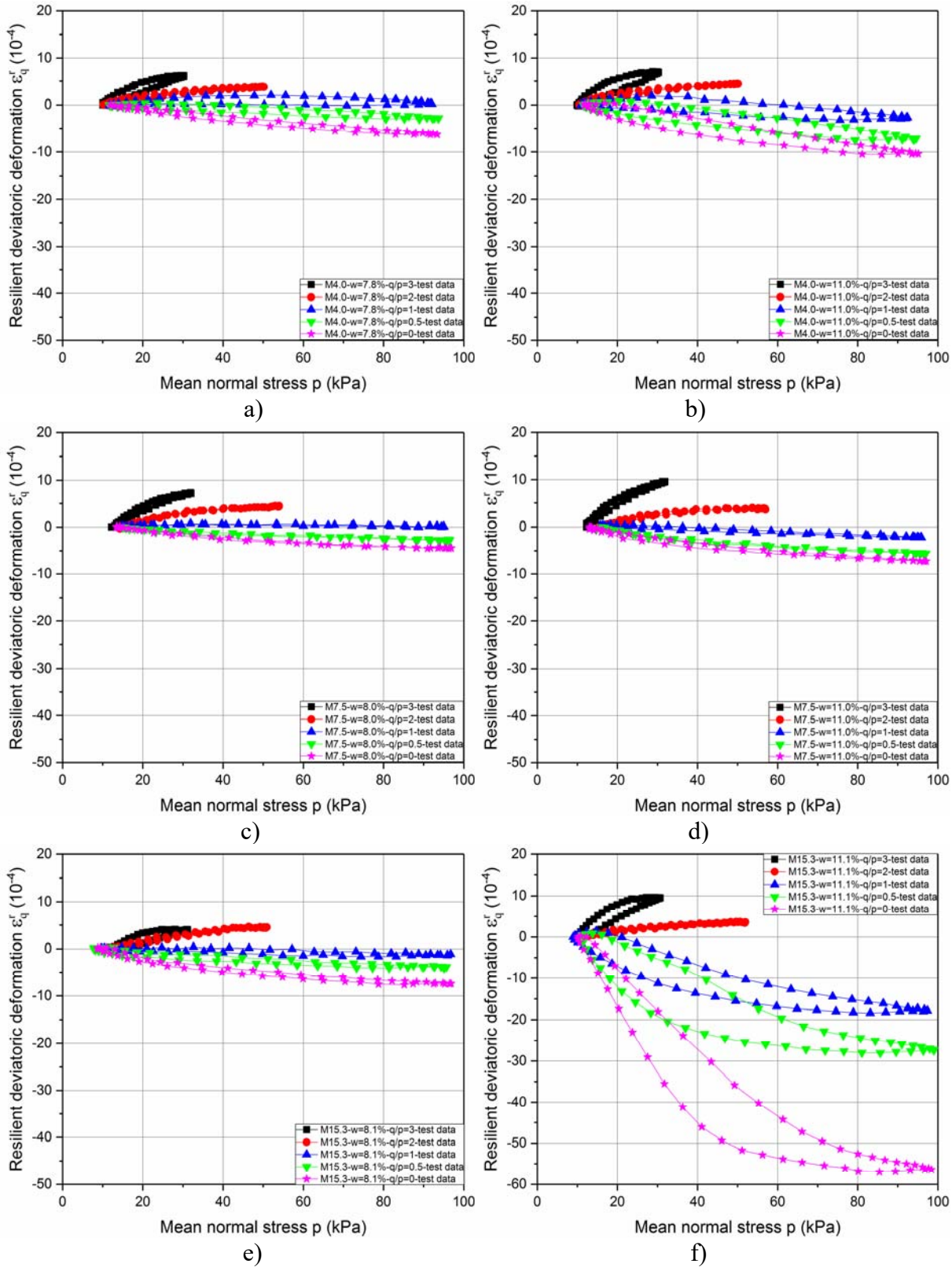

Figure IV.6. Evolution of resilient deviatoric deformation ε_q^r for Missillac sand M4.0, M7.5 and M15.3 with water content of w=8% and w=11%

IV.2.4. Maximum volumetric deformation and deviatoric deformation in s/s* plane

In Section III.2, we defined a new parameter s^* which is the suction value of the intersection point of wetting and drying paths in SWRC.

Figure IV.7 compares the maximum resilient volumetric deformation $\varepsilon_v{}^r{}_{max}$ in the last cycle of complete resilient test as a function of water content (*Figure IV.7.a*) and s/s^* value (*Figure IV.7.b*) for three materials (M4.0, M7.5 and M15.3) having a water content range of 7% to 11.3% with the stress paths of $\Delta q/\Delta p = 0$ and 3.

As shown in *Figure IV.7.a*, the $\varepsilon_v{}^r{}_{max}$ increases with the increase of water content (even the results of M7.5 are somehow scatter), which is the same as the $\varepsilon_v{}^r$ described in *Figure IV.5*. Besides, the effect of fine content as well as water content is important: the $\varepsilon_v{}^r{}_{max}$ is different for the different fine contents at a given water content.

In *Figure IV.7.b*, all $\varepsilon_v{}^r{}_{max}$ values are plotted in s/s^* plane. The lower bound of $s/(110\% \bullet s^*)$ and the upper bound of $s/(90\% \bullet s^*)$ are also illustrated in this figure to take into account the sensitivity to variation of the parameters of van Genuchten model (we think the error is lower than ±10%). From this figure, it can be stated that a simple exponential function could represent the relationship between all the $\varepsilon_v{}^r{}_{max}$ values and the s/s^* values, which is defined as:

$$\varepsilon_{v\,\max}^{r} = A \cdot e^{(-s/s^*/B)} + C \qquad \text{(IV.1)}$$

where A, B and C are constant as shown in *Figure IV.7.b*. As a result, the $\varepsilon_v{}^r{}_{max}$ could be determined by s/s^* only. These results are useful to understand the problem of dual variation of the $\varepsilon_v{}^r{}_{max}$ with the water content and the fine content.

As $\varepsilon_v{}^r{}_{max}$, the maximum resilient deviatoric deformations $\varepsilon_q{}^r{}_{max}$ are also plotted in water content plane (*Figure IV.8.a*) and s/s^* plane (*Figure IV.8.b*) respectively for three different materials (M4.0, M7.5 and M15.3) having a water content range of 7% to 11.3% in stress paths of $\Delta q/\Delta p = 0$ and 3.

In *Figure IV.8.a*, the $\varepsilon_q{}^r{}_{max}$ increases with the increase of water content. The fine content also plays an important role as to $\varepsilon_v{}^r{}_{max}$. In *Figure IV.8.b*, another simple exponential function can be observed to describe the correlation between all the $\varepsilon_q{}^r{}_{max}$ values and s/s^* values, which is defined as:

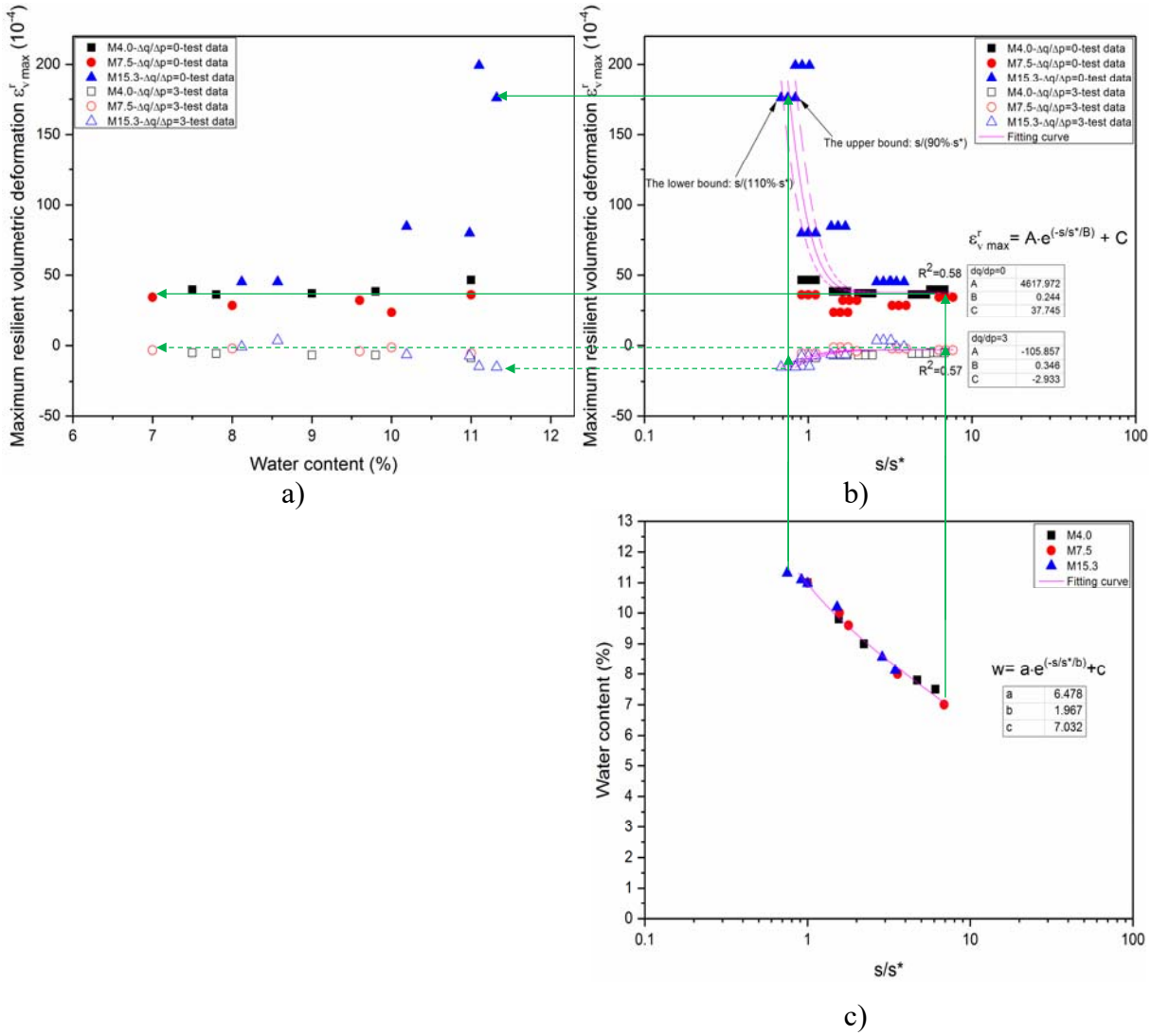

Figure IV.7. Relationship among maximum resilient volumetric deformation $\varepsilon_v{}^r{}_{max}$, water content w and s/s value*

$$\varepsilon_{q\,\max}^{r} = D \cdot e^{(-s/s^*/E)} + F \qquad \text{(IV.2)}$$

where *D*, *E* and *F* are constant as shown in Figure 8b.

Figure IV.7.c (same as *Figure IV.8.c*) also shows the evolution of water content, as a unique function of *s/s**. It can be observed that a simple exponential function could represent the relationship between *s/s** value and water content, which has been defined in Equation III.2, as shown in *Figure IV.7.c* (same as *Figure IV.8.c*). Until now, we have got a lot of unique relationship between the deformation behaviour ($\varepsilon_1{}^p$, $\varepsilon_v{}^r{}_{max}$ and $\varepsilon_q{}^r{}_{max}$) or water content with the *s/s** value at different water contents and different fine contents. This is very interesting, and in the following parts, we will try to explain more with the *s/s** value.

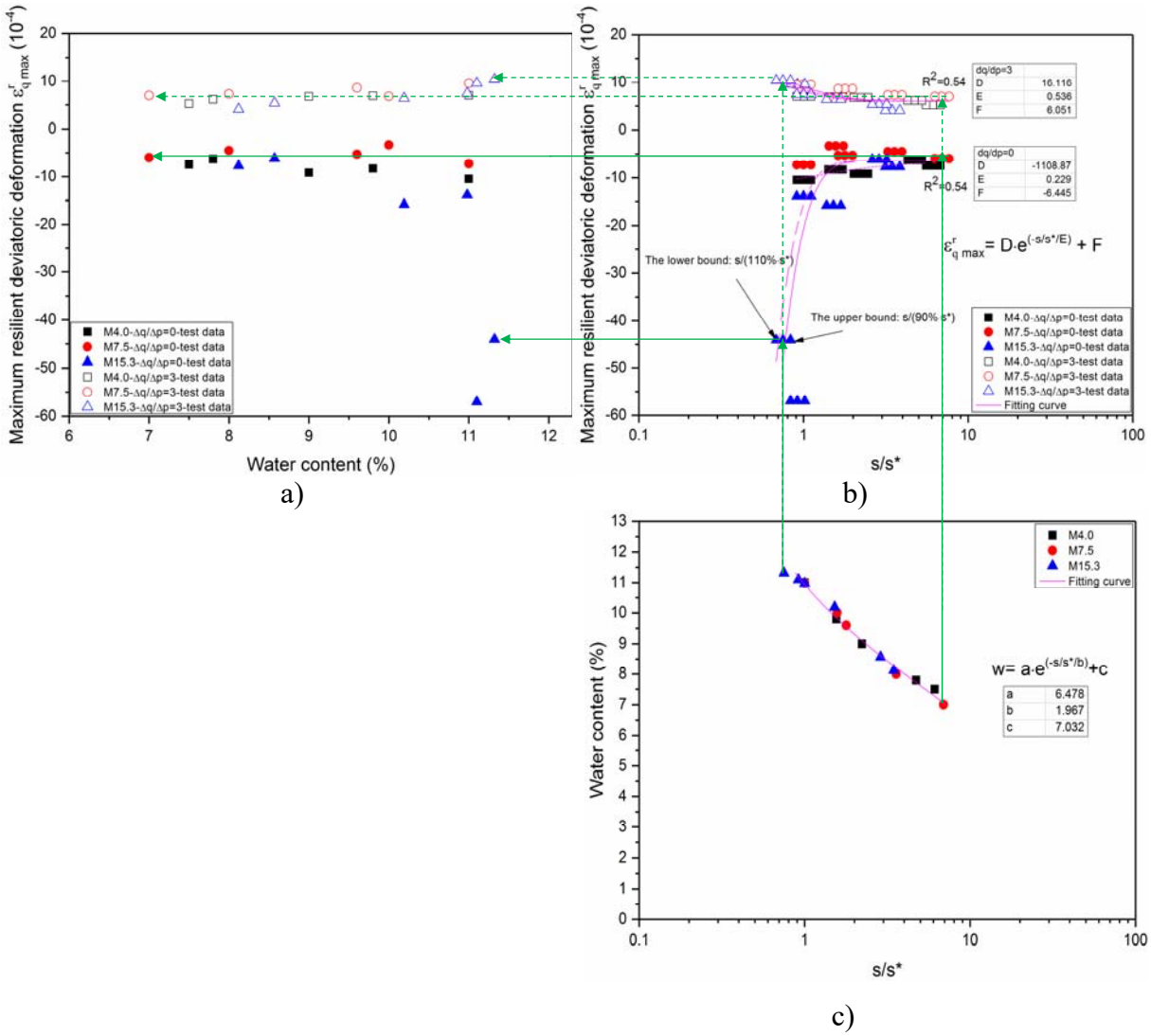

Figure IV.8. Relationship among maximum resilient deviatoric deformation $\varepsilon_q{}^r{}_{max}$, water content w and s/s value*

This result is useful to understand the maximum resilient deformations of the granular materials coupled with influence of fine content and hydraulic behaviour. It could reduce the number of tests required to predict the maximum resilient deformations of the granular materials.

IV.2.5.Anisotropy effect on resilient behaviour

In last two sections, the behaviour of volumetric deformation ε_v and the deviatoric deformation ε_q are presented, and this section will show the anisotropic behaviour represented by the difference between axial deformation ε_1 and radial deformation ε_3.

Figure IV.9 presents the final deformation ε_1 and ε_3 of M15.3 samples with different water contents after an isotropic consolidation phase ($\Delta q/\Delta p = 0$, $\sigma_3 = 10$ kPa) before conditioning.

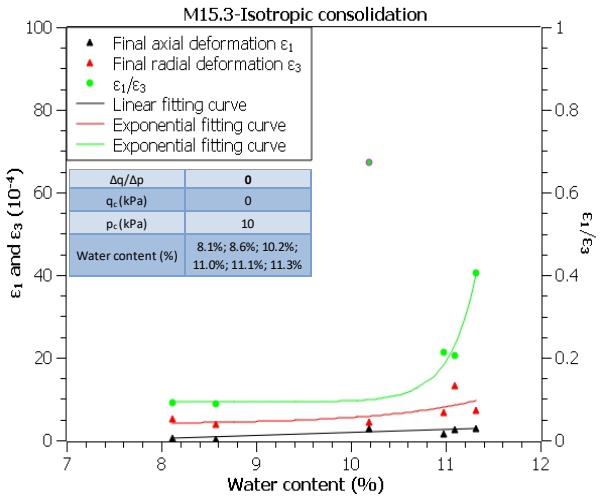

Figure IV.9. Final deformation ε_1 and ε_3 for Missillac sand M15.3 in an isotropic consolidation phase before conditioning

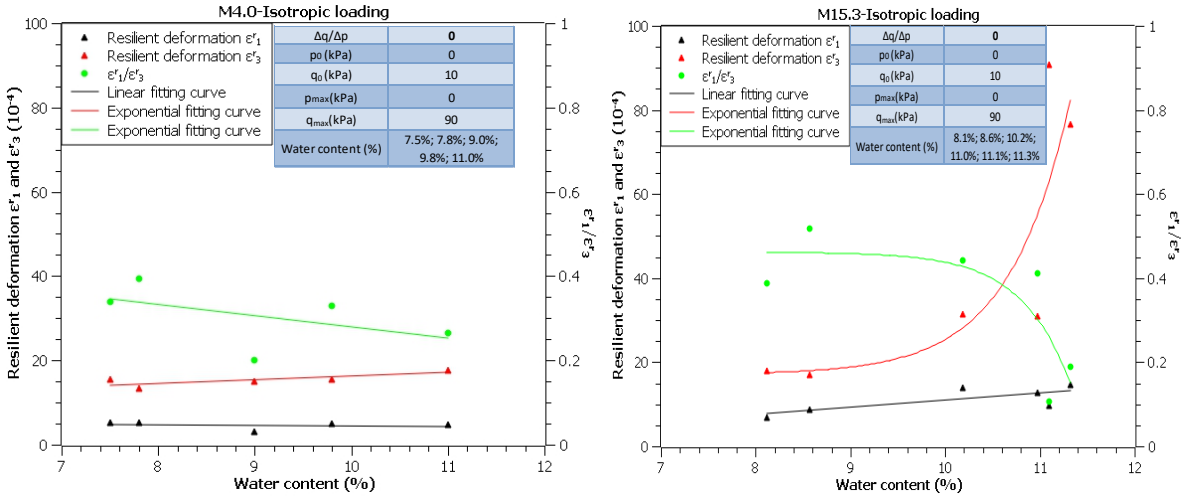

a) b)

Figure IV.10. Maximum resilient deformation ε_1^r and ε_3^r for Missillac sand M4.0 and M15.3 in the isotropic loading stress path ($\Delta q/\Delta p = 0$) in resilient test phase

It can be stated that there is an inherent anisotropy in these samples caused by compaction and the difference between ε_1 and ε_3 increases obviously as increasing of water content especially for the high saturation state (w > 10%). The results of M4.0 and M7.5 are lost in the past tests.

Figure IV.10 shows the resilient deformation ε_1^r and ε_3^r for Missillac sand M4.0 and M15.3 in the isotropic loading stress path ($\Delta q/\Delta p$ = 0, σ_3 = 90 kPa) in the resilient phase. The anisotropic behaviour can be also observed obviously as in *Figure IV.10*. The difference between ε_1^r and ε_3^r increases with an increase of water content, especially for material M15.3 which is much more obvious compared to *Figure IV.9*.

Comparing the ratio value of $\varepsilon_1/\varepsilon_3$ in *Figure IV.9* and the ratio value of $\varepsilon_1^r/\varepsilon_3^r$ *in Figure IV.10.b*, it can be stated that the anisotropic behaviour is strongly influenced by stress level and stress history. At the same time, the comparison of $\varepsilon_1^r/\varepsilon_3^r$ values between Figure *IV.10.a* and Figure *IV.10.b* shows that the anisotropic behaviour of M15.3 increases faster than M4.0 with an increase of water content from 7% to 11.3%.

Based on these results, it can be stated that the obvious inhere and developing anisotropic behaviour during loading phases shouldn't be ignored.

IV.3. Modelling with Boyce-Hornych model

IV.3.1. Boyce-Hornych model

The granular materials exhibit a complex non-linear response under repeated loading. The resilient response of these materials is usually defined by resilient modulus and Poisson's ratio or shear and bulk moduli. Boyce, (1980) proposed a stress-dependent nonlinear elastic model for predicting the resilient behaviour of granular materials as introduced as Equation I.55-57.

The hypothesis of Boyce model is isotropy. However, the anisotropy of the pavement materials was also recognized as an important parameter to model the pavement mechanical behaviour (Seyhan et al., 2005). Hornych et al., (1998) improved the Boyce model by considering the anisotropic response of granular materials and the modelling results showed a good agreement with the measured data. The improved model could be named as Boyce-Hornych model as presented as Equation I.61-62, which is recalled here as:

$$\varepsilon_v^r = \frac{p^{*n}}{p_a^{n-1}}\left[\frac{\gamma_1+2}{3\cdot K_a}+\frac{n-1}{18\cdot G_a}(\gamma_1+2)\cdot\left(\frac{q^*}{p^*}\right)^2+\frac{\gamma_1-1}{3\cdot G_a}\cdot\frac{q^*}{p^*}\right] \quad \text{(I.61)}$$

and

$$\varepsilon_q^r = \frac{2}{3}\cdot\frac{p^{*n}}{p_a^{n-1}}\left[\frac{\gamma_1-1}{3\cdot K_a}+\frac{n-1}{18\cdot G_a}(\gamma_1-1).\left(\frac{q^*}{p^*}\right)^2+\frac{2\cdot\gamma_1+1}{6\cdot G_a}\cdot\frac{q^*}{p^*}\right] \quad \text{(I.62)}$$

where,

$$p^* = \frac{\gamma_1\sigma_1+2\cdot\sigma_3}{3} \quad \text{(I.58)}$$

and

$$q^* = \gamma_1\sigma_1-\sigma_3,\ 0<\gamma_1<1 \quad \text{(I.59)}$$

In this context, as presented in *Figure IV.9* and *Figure IV.10*, the anisotropy effect on resilient behaviour of this granular material is noticeable. As a result, in the following parts, we will try to fit the resilient test results of Missillac sand with Boyce-Hornych model.

Parameter estimation

The least square method is then used to optimize the model parameters, K_a, G_a, n and γ for a given water content on five stress paths of $\Delta q/\Delta p$ = 0, 0.5, 1, 2 and 3. The Boyce-Hornych model parameters as well as the correlation coefficient values are presented in *Table IV.2* for M4.0 samples, *Table IV.3* for M7.5 samples and *Table IV.4* for M15.3 samples with different water contents.

The following points can be concluded based on the results:

- A series of good correlation coefficient values higher than 0.71 can be found for M4.0 and M7.5 samples with all the water contents (*Table IV.2 and Table IV.3*);
- For M15.3 samples, the correlation coefficient values are good at water contents of 8.1% and 8.6%, while the values are rather low for samples at water contents higher than 10% (*Table IV.4*).

Figure IV.11 and *Figure IV.12* show the modelling results of ε_v^r and ε_q^r for M4.0, M7.5 and M15.3 samples at the water contents close to 8.0% and 11.0%. As described by correlation coefficient values above, a good correspondence can be observed between the estimated and

w (%)	$\Delta q/\Delta p$	Parameters (Missillac sand, M4.0)				C_{correl}
		K_a	G_a	n	γ_1	
7.0	0; 0,5; 1; 2; 3	17.64	20.98	0.80	0.55	0.815
8.0	0; 0,5; 1; 2; 3	19.23	22.23	0.74	0.59	0.776
9.0	0; 0,5; 1; 2; 3	17.49	16.17	0.89	0.55	0.769
10.0	0; 0,5; 1; 2; 3	17.89	16.56	0.77	0.55	0.817
11.0	0; 0,5; 1; 2; 3	16.35	12.78	0.99	0.55	0.741
Average values		17.72	17.74	0.84	0.56	0.78

Table IV.2. Parameter optimization of Boyce-Hornych model for M4.0

w (%)	$\Delta q/\Delta p$	Parameters (Missillac sand, M7.5)				C_{correl}
		K_a	G_a	n	γ_1	
7.0	0; 0,5; 1; 2; 3	15.84	21.49	0.65	0.56	0.812
8.0	0; 0,5; 1; 2; 3	19.82	24.05	0.65	0.62	0.830
9.6	0; 0,5; 1; 2; 3	17.59	19.55	0.65	0.61	0.798
10.0	0; 0,5; 1; 2; 3	20.00	25.95	0.65	0.65	0.713
11.0	0; 0,5; 1; 2; 3	15.06	16.03	0.70	0.54	0.754
Average values		17.66	21.42	0.66	0.60	0.781

Table IV.3. Parameter optimization of Boyce-Hornych model for M7.5

w (%)	$\Delta q/\Delta p$	Parameters (Missillac sand, M15.3)				C_{correl}
		K_a	G_a	n	γ_1	
8.1	0; 0,5; 1; 2; 3	14.36	23.90	0.71	0.60	0.832
8.6	0; 0,5; 1; 2; 3	15.53	28.79	0.61	0.62	0.833
10.2	0; 0,5; 1; 2; 3	9.53	11.07	0.90	0.59	0.622
11.0	0; 0,5; 1; 2; 3	9.20	11.92	0.68	0.52	0.636
11.1	0; 0,5; 1; 2; 3	3.82	3.09	0.85	0.37	0.706
11.3	0; 0,5; 1; 2; 3	4.81	3.47	0.93	0.45	0.574
Average values		9.54	13.71	0.78	0.53	0.700

Table IV.4. Parameter optimization of Boyce-Hornych model for M15.3

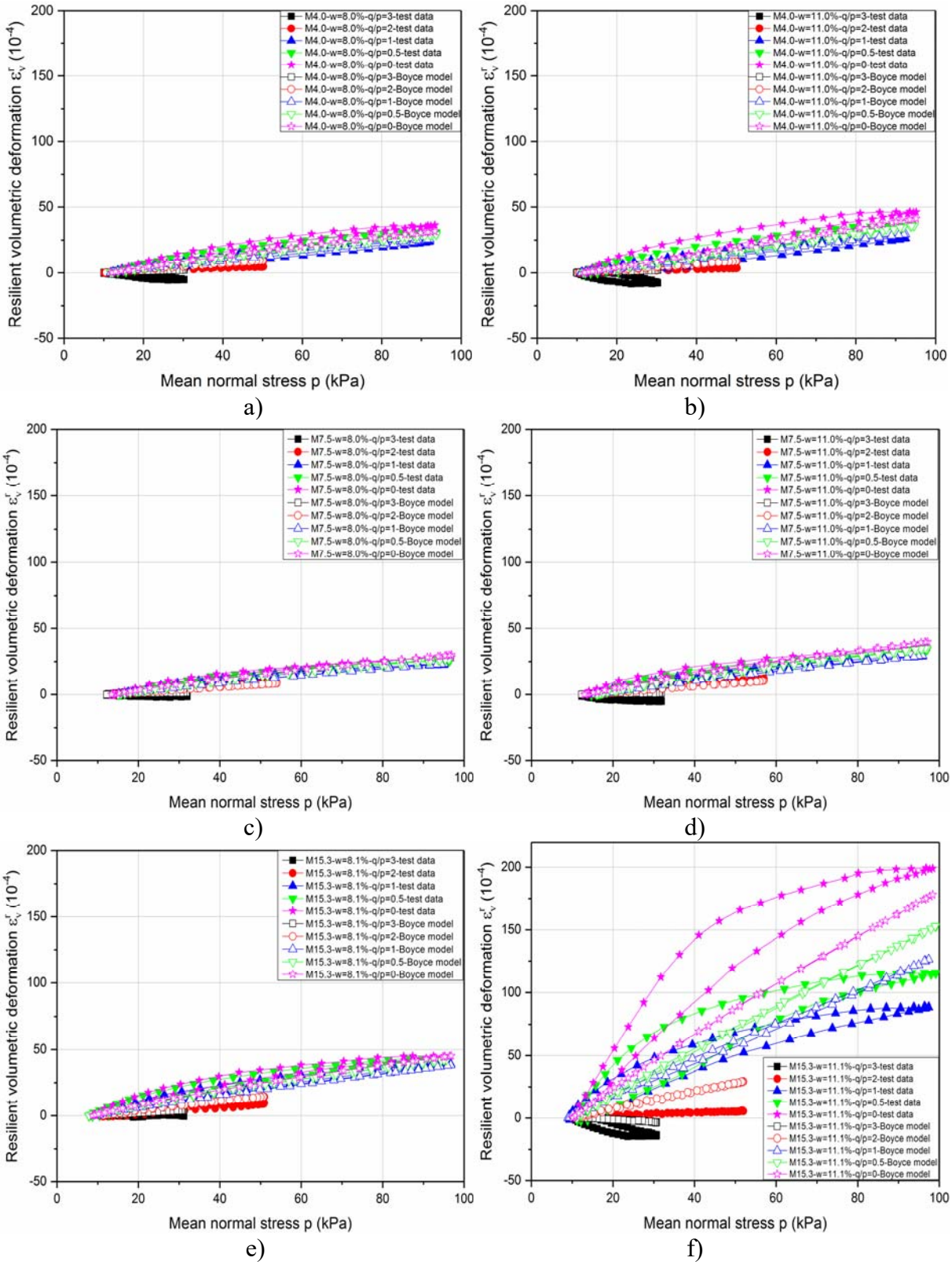

Figure IV.11. Comparison of the resilient volumetric deformation ε_v^r between the model response and the test results for Missillac sand M4.0, M7.5 and M15.3 with water contents of w=8% and w=11%

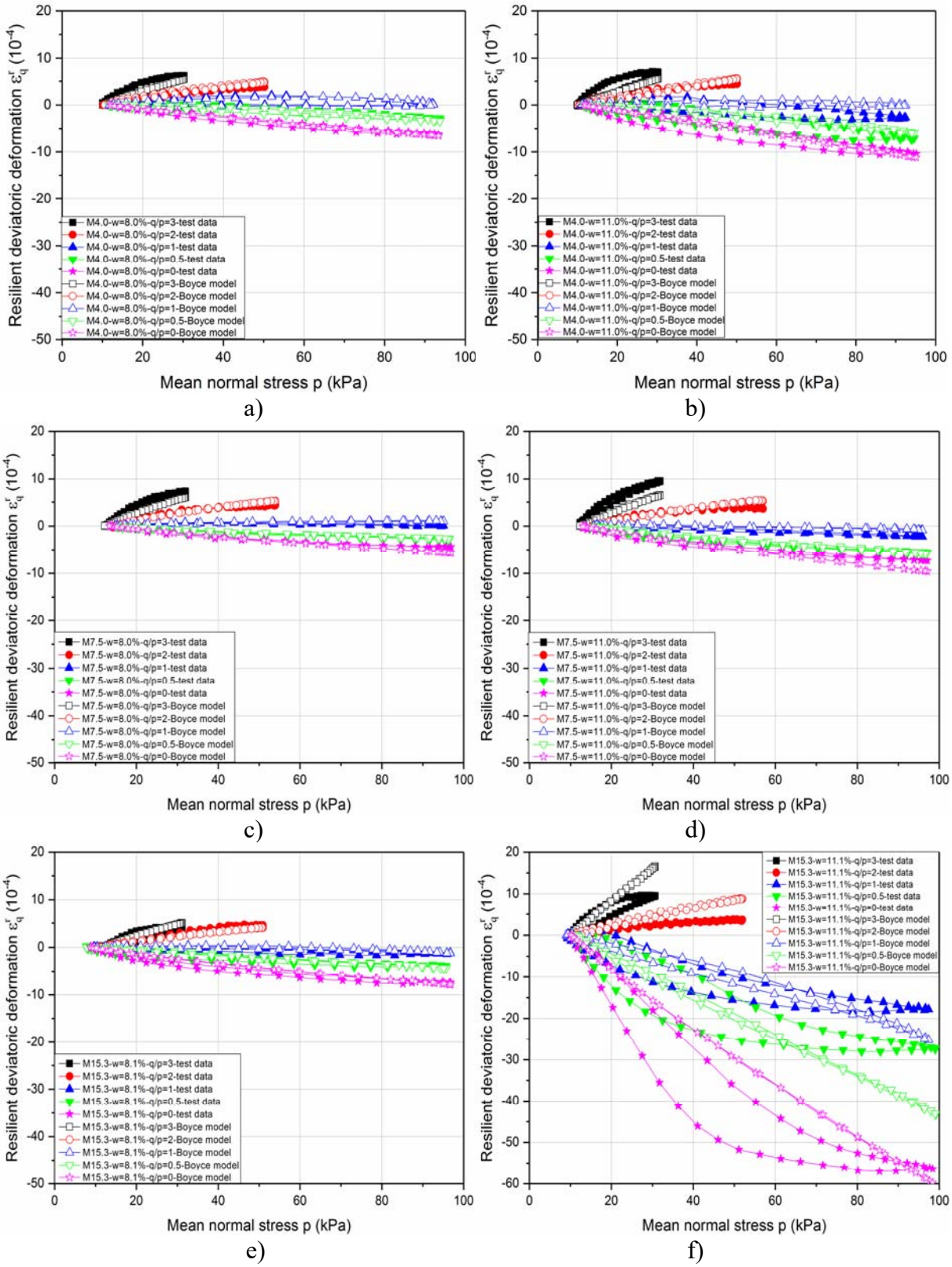

Figure IV.12. Comparison of the resilient deviatoric deformation ε_q^r between the model response and the test results for Missillac sand M4.0, M7.5 and M15.3 with water contents of w=8% and w=11%.

experimental ε_v^r and ε_q^r values for M4.0 and M7.5 samples at both water contents and M15.3 samples with water content of 8.0%. For M15.3 samples with water contents of 10% and 11%, the Boyce-Hornych model cannot fit well with the experimental ε_v^r and ε_q^r values as well as the shape (loops) in stress paths of $\Delta q/\Delta p$ = 0, 0.5, 1 even 2.

IV.3.2. Improvement of Boyce-Hornych model

As mentioned in above, the Boyce-Hornych model (Equation I.60-62) cannot predict the ε_v^r and ε_q^r values very well at a high water content (higher than 10.0%) with a high fine content (15.3%). We think that this phenomenon can be explained and improved by two following points:

- The aim of coefficient of anisotropy γ_1 is to decrease the axial stress σ_1 to fit with radial stiffness in the elastic range. However, as presented in the last section of IV.2.2, for the samples at a high water content and a high fine content with the stress paths of $\Delta q/\Delta p$ = 0 and 0.5, the axial deformation ε_1 and radial deformation ε_3 in the last 10 cycles are not completely constant and a small increase of plastic deformation still exists, especially for ε_3. It indicates that the radial deformation ε_3 maybe cannot be treated as pure elastic. Thus, the Boyce-Hornych model which is derived from elastic theory couldn't adjust $\sigma_1 \cdot \gamma_1$ values with an incompletable elastic radial stiffness to get the correct ε_1 and ε_3 values.

Besides, the difficulty to obtain accurate values of ε_3 by only one radial displacement sensor, could affect the modelling results and the two-time relation for ε_3 in Equation I.6, should be also taken into account.

In this context, we suggest replacing the coefficient of anisotropy γ_1 by γ_3, which is used to increase radial stress to fit with the axial stiffness.

The new mean normal stress p^* and the new shear stress q^* can be redefined as follows:

$$p^* = \frac{\sigma_1 + 2 \cdot \gamma_3 \sigma_3}{3} \tag{IV.3}$$

and

$$q^* = \sigma_1 - \gamma_3 \sigma_3 \text{ , } \gamma_3 > 1 \tag{IV.4}$$

The new potential function can be modified as:

$$W = \frac{\left[\frac{\sigma_1 + 2\cdot\gamma_3\sigma_3}{3}\right]^{n+1}}{{p_a}^{n-1}}\left[\frac{1}{(n+1)K_a} + \frac{1}{6G_a}\left(\frac{\sigma_1 - \gamma_3\sigma_3}{\frac{\sigma_1 + 2\cdot\gamma_3\sigma_3}{3}}\right)^2\right] \quad \text{(IV.5)}$$

The new resilient volumetric deformation $\varepsilon_v{}^r$ and new resilient deviatoric deformation $\varepsilon_q{}^r$ with anisotropy coefficient γ_3 can be also proposed by taking the derivative of potential function as:

$$\varepsilon_v^r = \frac{{p^*}^n}{{p_a}^{n-1}}\left[\frac{1+2\cdot\gamma_3}{3\cdot K_a} + \frac{n-1}{18\cdot G_a}(1+2\cdot\gamma_3).\left(\frac{q^*}{p^*}\right)^2 + \frac{1-\gamma_3}{3\cdot G_a}\cdot\frac{q^*}{p^*}\right] \quad \text{(IV.6)}$$

and

$$\varepsilon_q^r = \frac{2}{3}\cdot\frac{{p^*}^n}{{p_a}^{n-1}}\left[\frac{1-\gamma_3}{3\cdot K_a} + \frac{n-1}{18\cdot G_a}(1-\gamma_3)\cdot\left(\frac{q^*}{p^*}\right)^2 + \frac{2+\gamma_3}{6\cdot G_a}\cdot\frac{q^*}{p^*}\right] \quad \text{(IV.7)}$$

- The second reason for this incorrespondence is from the great difference of the resilient deformations between the lowest stress path of $\Delta q/\Delta p$ = 0, even 0.5 (elastoplastic behaviour) and other stress paths (pure elastic behaviour). Hence, a different anisotropy coefficient $\gamma_3{}^*$ is required for the stress path of $\Delta q/\Delta p$=0 (even 0.5).

Parameter estimation

The modified Boyce-Hornych model parameters as well as the correlation coefficient values are compared with Boyce-Hornych model (considering the anisotropy coefficient $\gamma_1{}^*$) in *Table IV.5* for M4.0 samples, *Table IV.6* for M7.5 samples and *Table IV.8* for M15.3 samples at different water contents.

The following points can be concluded based on the results:

- The good correlation coefficient values (close or higher than 0.8) can be found for M4.0 samples both in *Table IV.5.a* (with γ_1 and $\gamma_1{}^*$) and *Table IV.5.b* (with γ_3 and $\gamma_3{}^*$). The correlation coefficient values are almost same in these two models.
- The very good correlation coefficient values (higher than 0.9) can be found for M7.5 samples both in *Table IV.6.a* (with γ_1 and $\gamma_1{}^*$) and *Table IV.6.b* (with γ_3 and $\gamma_3{}^*$). The correlation coefficient values are almost same in these two models.

w (%)	Δq/Δp	Parameters (Missillac sand, M4.0)					C_{correl}
		K_a	G_a	n	Υ_1	$\Upsilon_1^{*}{}_{(q/p=0)}$	
7.5	0; 0,5; 1; 2; 3	17.88	18.95	0.77	0.51	0.56	0.839
7.8	0; 0,5; 1; 2; 3	20.01	27.52	0.56	0.56	0.58	0.767
9.0	0; 0,5; 1; 2; 3	16.30	15.48	0.62	0.42	0.46	0.869
9.8	0; 0,5; 1; 2; 3	17.87	16.00	0.74	0.54	0.60	0.841
11.0	0; 0,5; 1; 2; 3	16.48	10.60	0.88	0.46	0.53	0.794
Average values		17.71	17.71	0.72	0.50	0.55	0.822

Table IV.5.a Parameter optimization of Boyce-Hornych model for M4.0

w (%)	Δq/Δp	Parameters (Missillac sand, M4.0)					C_{correl}
		K_a	G_a	n	Υ_3	$\Upsilon_3^{*}{}_{(q/p=0)}$	
7.5	0; 0,5; 1; 2; 3	51.38	69.74	0.66	1.91	1.95	0.839
7.8	0; 0,5; 1; 2; 3	44.87	64.84	0.59	1.72	1.83	0.802
9.0	0; 0,5; 1; 2; 3	58.67	68.92	0.53	2.38	2.40	0.871
9.8	0; 0,5; 1; 2; 3	47.46	52.80	0.63	1.83	1.93	0.843
11.0	0; 0,5; 1; 2; 3	59.54	51.77	0.73	2.14	2.12	0.806
Average values		52.38	61.61	0.63	2.00	2.05	0.832

Table IV.5.b Parameter optimization of modified Boyce-Hornych model for M4.0

w (%)	Δq/Δp	Parameters (Missillac sand, M7.5)					C_{correl}
		K_a	G_a	n	Υ_1	$\Upsilon_1^{*}{}_{(q/p=0)}$	
7.0	0; 0,5; 1; 2; 3	8.49	31.91	0.23	0.52	0.48	0.914
8.0	0; 0,5; 1; 2; 3	11.97	35.47	0.27	0.60	0.57	0.931
9.6	0; 0,5; 1; 2; 3	9.29	30.15	0.22	0.58	0.53	0.902
10.0	0; 0,5; 1; 2; 3	12.77	45.25	0.22	0.68	0.62	0.942
11.0	0; 0,5; 1; 2; 3	4.15	27.10	0.11	0.46	0.36	0.939
Average values		9.33	33.98	0.21	0.57	0.51	0.926

Table IV.6.a Parameter optimization of Boyce-Hornych model for M7.5

w (%)	Δq/Δp	Parameters (Missillac sand, M7.5)					C_{correl}
		K_a	G_a	n	Υ_3	$\Upsilon_3^{*}{}_{(q/p=0)}$	
7.0	0; 0,5; 1; 2; 3	16.92	74.72	0.19	1.95	2.05	0.919
8.0	0; 0,5; 1; 2; 3	22.62	68.30	0.26	1.67	1.72	0.932
9.6	0; 0,5; 1; 2; 3	17.24	59.73	0.20	1.72	1.82	0.905
10.0	0; 0,5; 1; 2; 3	21.57	72.87	0.23	1.48	1.54	0.941
11.0	0; 0,5; 1; 2; 3	13.58	62.74	0.14	2.22	2.29	0.930
Average values		18.38	67.67	0.20	1.81	1.89	0.925

Table IV.6.b Parameter optimization of modified Boyce-Hornych model for M7.5

w (%)	Δq/Δp	Parameters (Missillac sand, M15.3)					C_{correl}
		K_a	G_a	n	Υ_1	$\Upsilon_1^{*}{}_{(q/p=0)}$	
8.1	0; 0,5; 1; 2; 3	14.46	22.01	0.74	0.59	0.64	0.836
8.6	0; 0,5; 1; 2; 3	15.78	25.78	0.66	0.61	0.67	0.838
10.2	0; 0,5; 1; 2; 3	10.90	13.51	0.99	0.64	0.53	0.631
11.0	0; 0,5; 1; 2; 3	11.03	10.13	0.91	0.54	0.51	0.645
11.1	0; 0,5; 1; 2; 3	4.90	2.95	1.00	0.38	0.30	0.721
11.3	0; 0,5; 1; 2; 3	7.86	3.03	1.17	0.45	0.20	0.606
Average values		10.82	12.90	0.91	0.54	0.48	0.713

Table IV.7.a Parameter optimization of Boyce-Hornych model for M15.3

w (%)	Δq/Δp	Parameters (Missillac sand, M15.3)					C_{correl}
		K_a	G_a	n	Υ_3	$\Upsilon_3^{*}{}_{(q/p=0)}$	
8.1	0; 0,5; 1; 2; 3	34.39	55.37	0.72	1.66	1.64	0.833
8.6	0; 0,5; 1; 2; 3	33.31	64.86	0.59	1.62	1.65	0.833
10.2	0; 0,5; 1; 2; 3	21.36	61.19	0.49	1.42	2.17	0.769
11.0	0; 0,5; 1; 2; 3	15.06	69.36	0.19	1.91	3.05	0.747
11.1	0; 0,5; 1; 2; 3	24.86	40.10	0.48	3.21	4.55	0.874
11.3	0; 0,5; 1; 2; 3	18.30	48.88	0.28	2.57	5.29	0.810
Average values		24.55	56.63	0.46	2.07	3.06	0.811

Table IV.7.b Parameter optimization of modified Boyce-Hornych model for M15.3

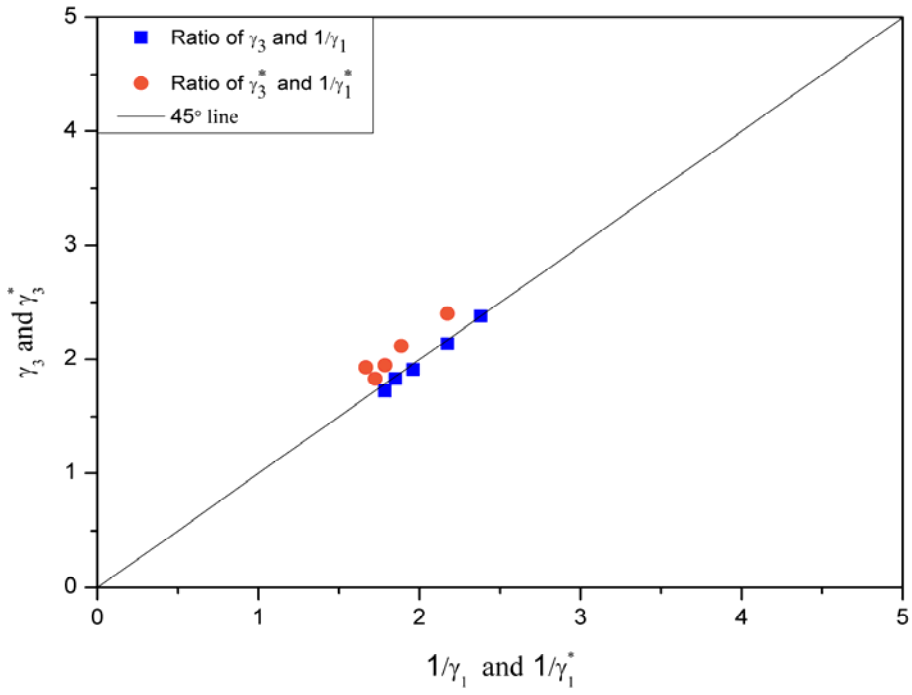

Figure IV.13. Relations between $\gamma_3$and $1/\gamma_1$ and $\gamma_3^*$and $1/\gamma_1^*$ for Missillac sand M4.0 with water contents of 7.5% to 11.0%

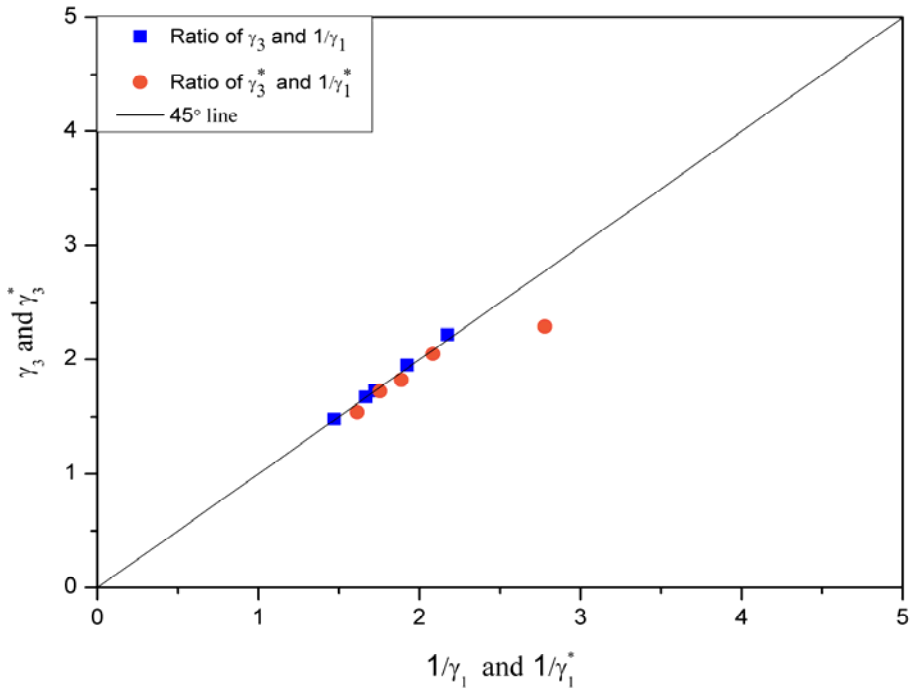

Figure IV.14. Relations between $\gamma_3$and $1/\gamma_1$ and $\gamma_3^*$and $1/\gamma_1^*$ for Missillac sand M7.5 with water contents of 7.0% to 11.0%.

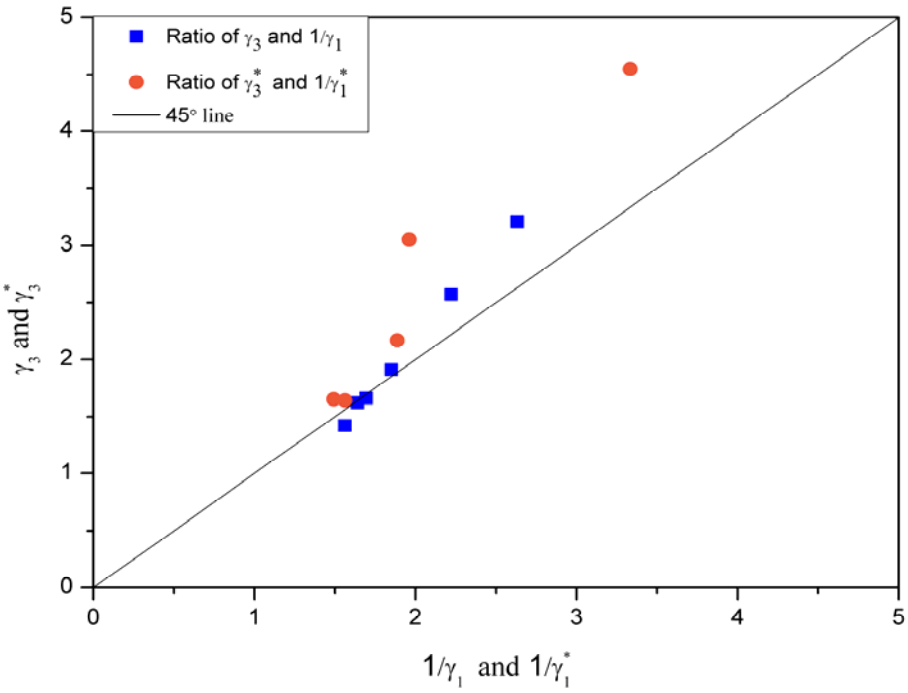

Figure IV.15. Relations between γ_3 and $1/\gamma_1$ and γ_3^* and $1/\gamma_1^*$ for Missillac sand M15.3 with water contents of 8.1% to 11.3%

- A significant improvement of correlation coefficient values for M15.3 samples at the high water contents (10.2%, 11.0%, 11.1% and 11.3%) can be observed from Boyce-Hornych model (*Table IV.7.a*) to the modified Boyce-Hornych model (*Table IV.7.b*).

- The γ_1 and γ_1^* values as well as γ_3 and γ_3^* values are almost constant or scatter in a small range for M4.0 and M7.5 samples in a water content range from 7.0 % to 11.0% (*Table IV.5* and *Table IV.6*). For M15.3 samples, the γ_1 and γ_1^* values decrease (*Table IV.7.a*) and γ_3 and γ_3^* values increase (*Table IV.7.b*) obviously with an increase of water content from 8.1% to 11.3%.

The values of γ_3 and $1/\gamma_1$ and the values of γ_3^* and $1/\gamma_1^*$ are also presented in *Figure IV.13* for M4.0 samples, *Figure IV.14* for M7.5 samples and *Figure IV.15* for M15.3 samples. The results state that the relation of $\gamma_3 = 1/\gamma_1$ and $\gamma_3^* = 1/\gamma_1^*$ can be obtained in all samples of M4.0 and M7.5 and this is normal for the pure elastic behaviour. For M15.3 samples, the relation of $\gamma_3 = 1/\gamma_1$ fits well with modelling results except for samples in water contents of 11.1% and 11.3% and the relation of $\gamma_3^* = 1/\gamma_1^*$ fits only with samples in two low water contents of 8.1% and 8.6%. It also confirms that the deformation behaviour of M15.3 samples with a high

water content cannot be described well by the Boyce-Hornych model which tries to use an elastic anisotropy coefficient γ_1 to match the incomplete elastic behaviour ε_3.

Figure IV.16 and *Figure IV.17* show the improved modelling results of ε_v^r and ε_q^r values respectively for M15.3 samples in water contents of 10.2%, 11.0%, 11.1% and 11.3% with γ_3 and γ_3^*. As described by correlation coefficient values above, a very good correspondence can be observed between the estimated and experimental ε_v^r and ε_q^r values except for the shape of open loops. In the next section, a discussion about the improved Boyce-Hornych model with effective stress conception to simulate these open loops will be introduced.

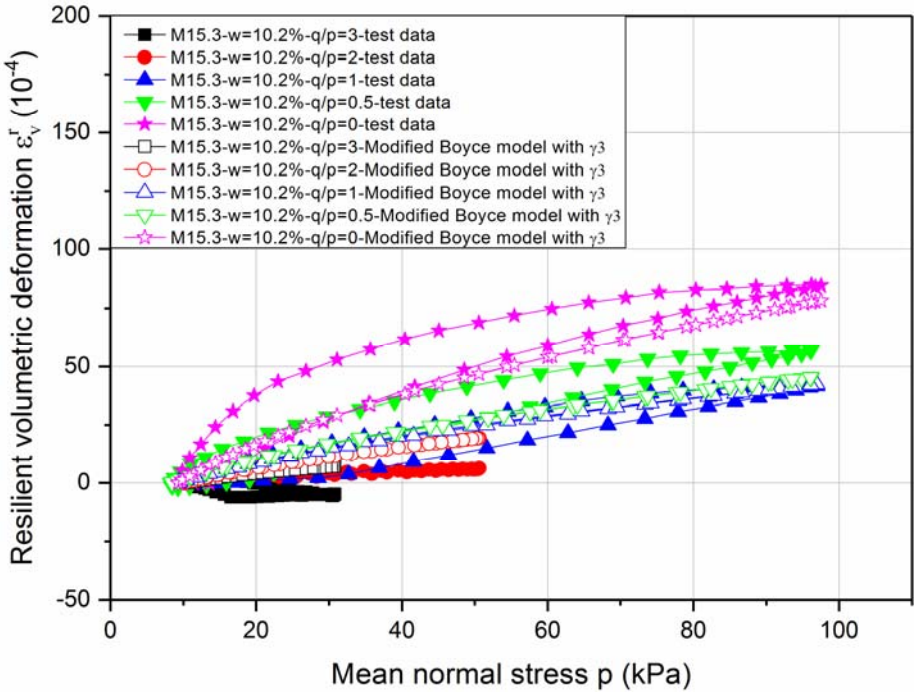

a)

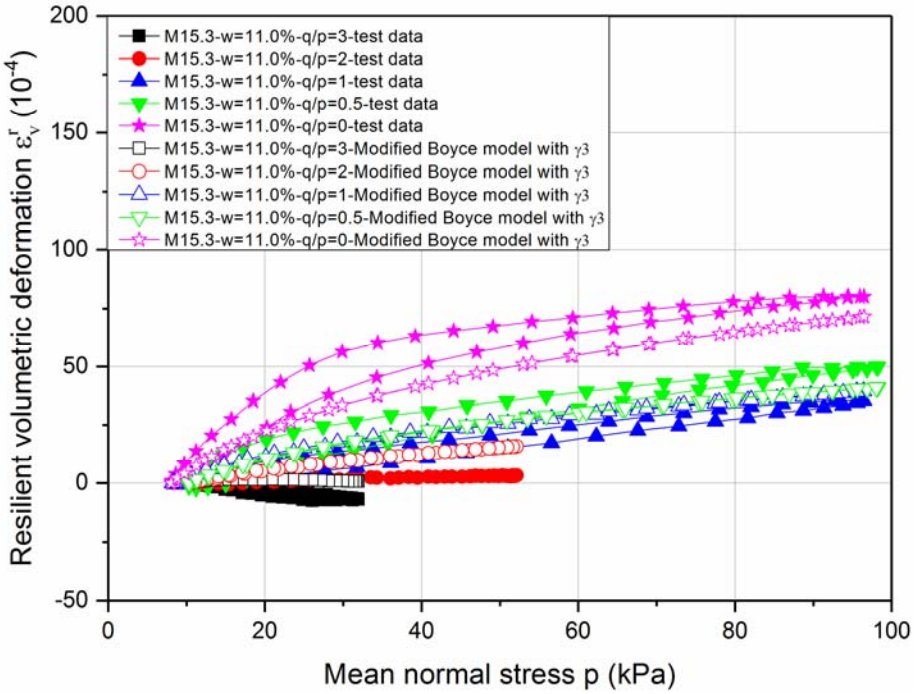

b)

Figure IV.16. Comparison of the resilient volumetric deformation ε_v^r between the model response and the test results for Missillac sand M15.3 with water content of a) w = 10.2%, b) 11.0%, c) 11.1% and d) 11.3%

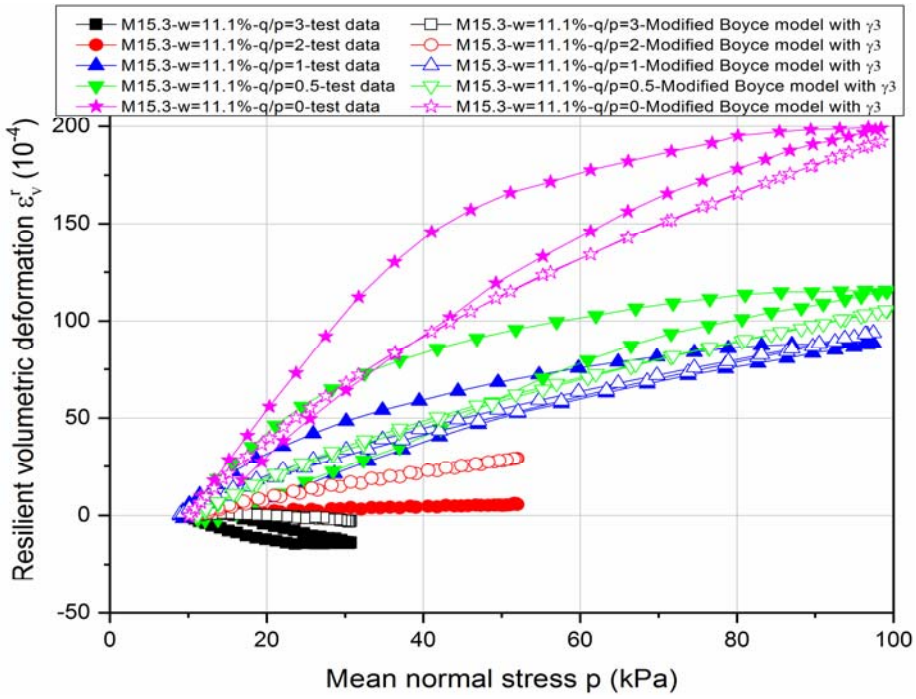

c)

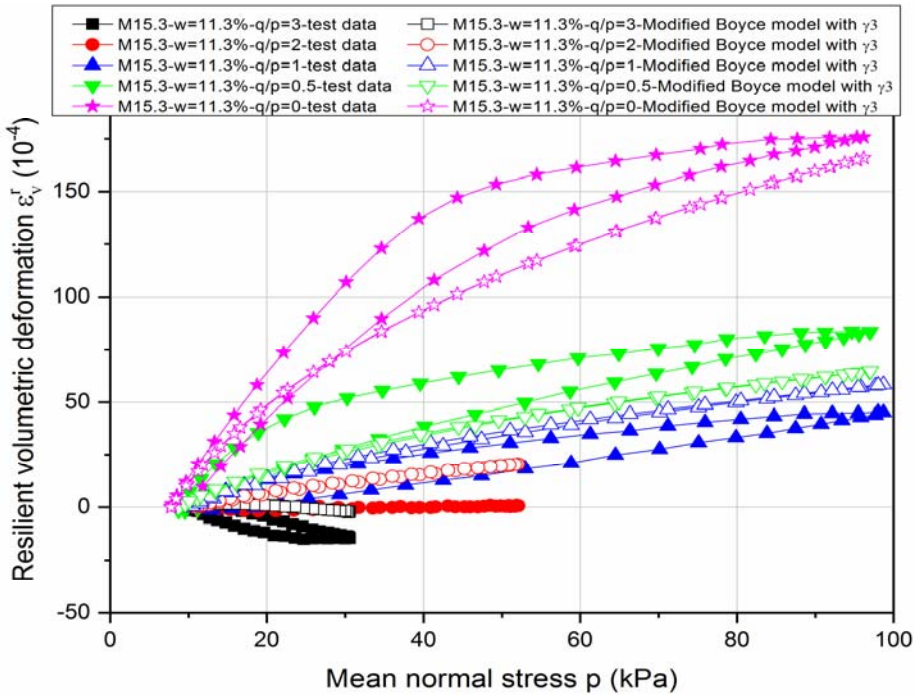

d)

Figure IV.16-Continued

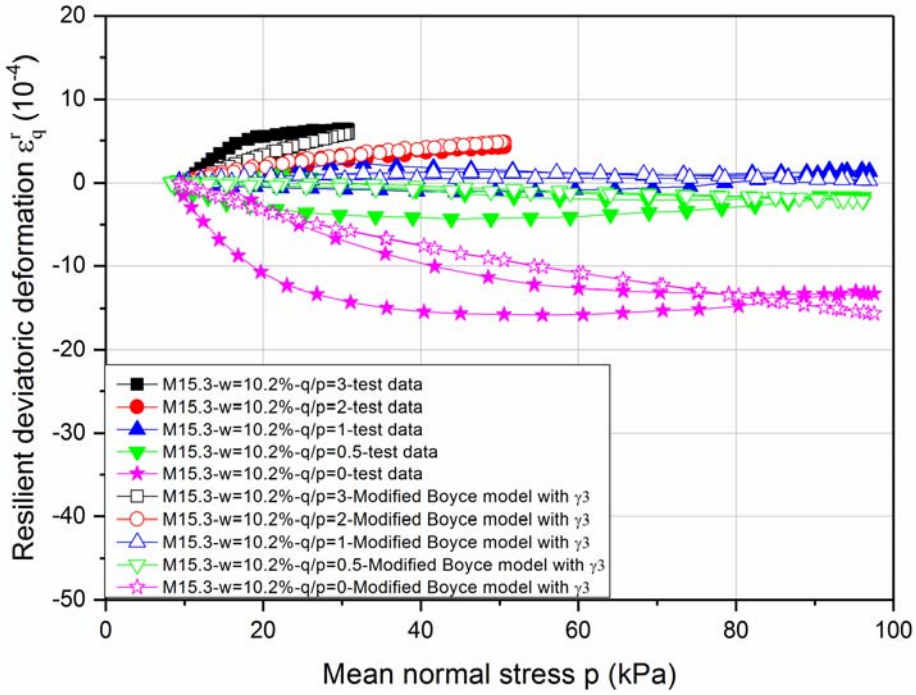

a)

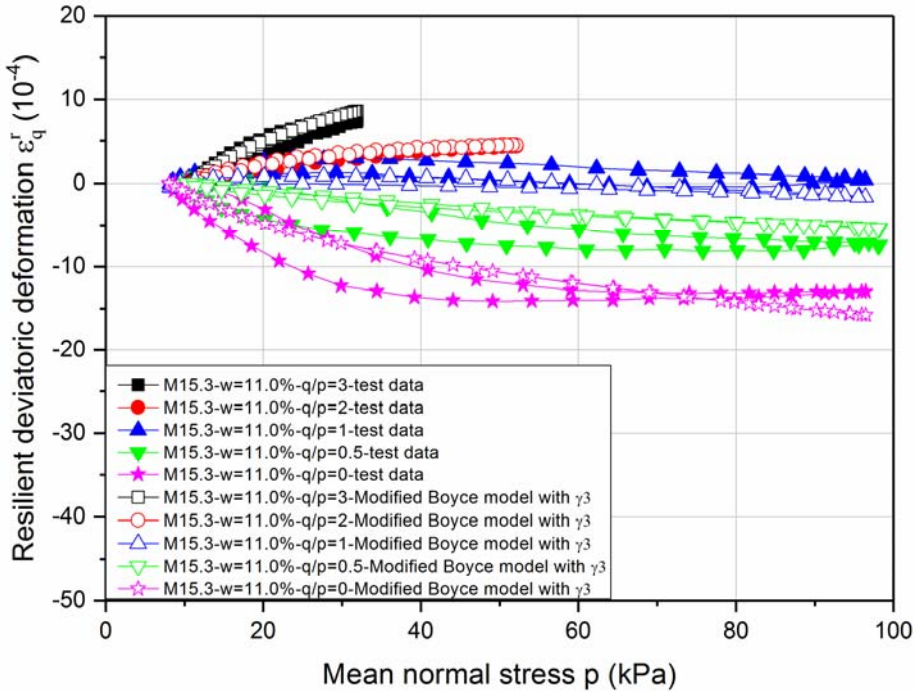

b)

Figure IV.17. Comparison of the resilient deviatoric deformation ε_q^r between the model response and the test results for Missillac sand M15.3 with water content of a) w = 10.2%, b) 11.0%, c) 11.1% and d) 11.3%

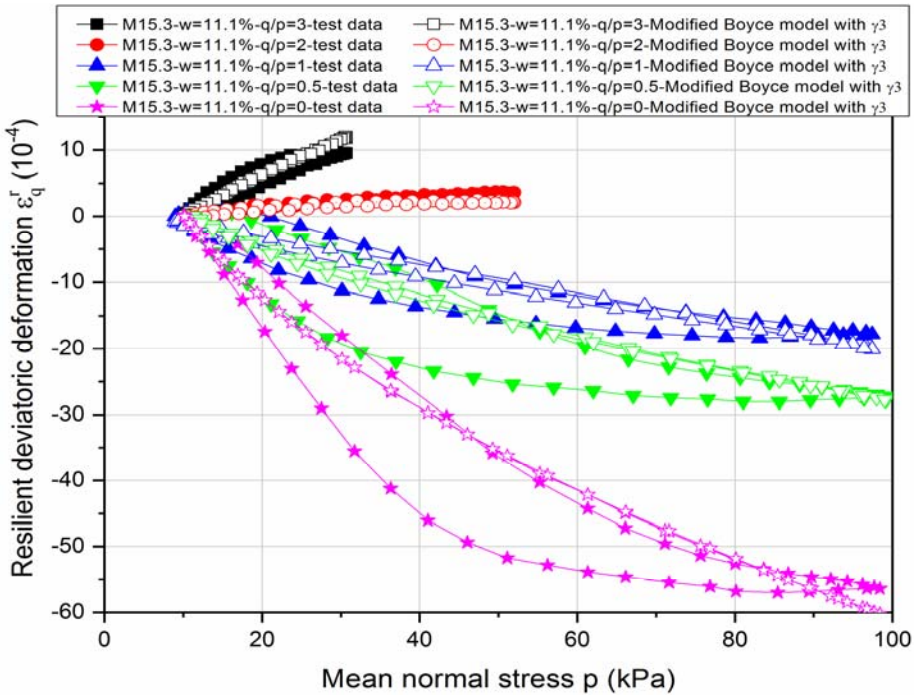

c)

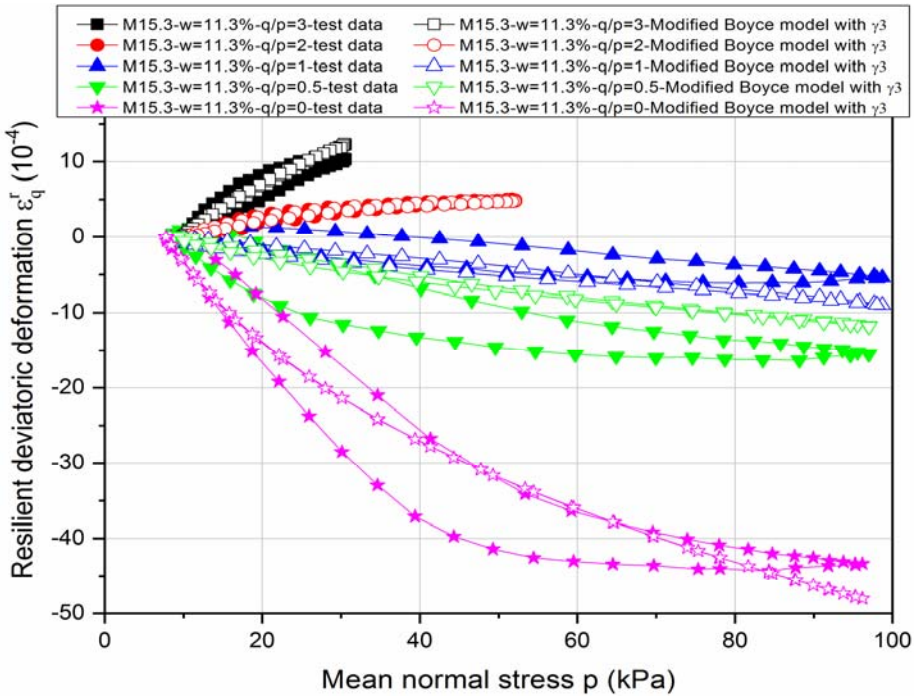

d)

Figure IV.17-Continued

IV.3.3. Discussion: Improved Boyce-Hornych model with effective stress concept

Commonly, pore air pressure is not taken into account in the resilient deformation analysis, because of relatively small deformation.

In this study, repeated shear deformation is applied to the samples with the same dry density (2.0 Mg/m^3) but different initial degrees of saturation and different fine contents under undrained condition. During the continuous loading/unloading phases, the sample volume (or soil skeleton) is changing all the time which represents the pore volume change. *Figure IV.18* and *Figure IV.19* show the changes of void ratio based on volumetric deformation ε_v from the initial state to the conditioning phase and then resilient phase for M4.0 and M15.3 materials on stress paths of $\Delta q/\Delta p = 0$ and 3.

The following points can be concluded based on the results:

- The influence of water content on void ratio changes is not obvious for Missillac sand M4.0 in both stress paths, while the void ratio of Missillac sand M15.3 decreases obviously from low to high degree of saturation ($w > 11\%$) on both stress paths.
- As the volumetric deformations have been shown in *Figure IV.5*, in the 100th resilient loading cycle, the small dilatancy can be observed in stress path of $\Delta q/\Delta p = 3$ and the contraction can be observed in stress path of $\Delta q/\Delta p = 0$ for both materials.
- *Figure IV.19.a* shows that, in the 100th resilient loading cycle, the void ratio decreases of 0.02 at the maximum, when the water content is higher than 10% in a low stress path of $\Delta q/\Delta p = 0$ for M15.3. Hence, the pore volume is compressed significantly, what is equal to the volume compression of pore air if the volume compression of solid particles and pore water are negligible. As a result, an induced increase of pore air pressure could exist with the increase of pore water pressure.

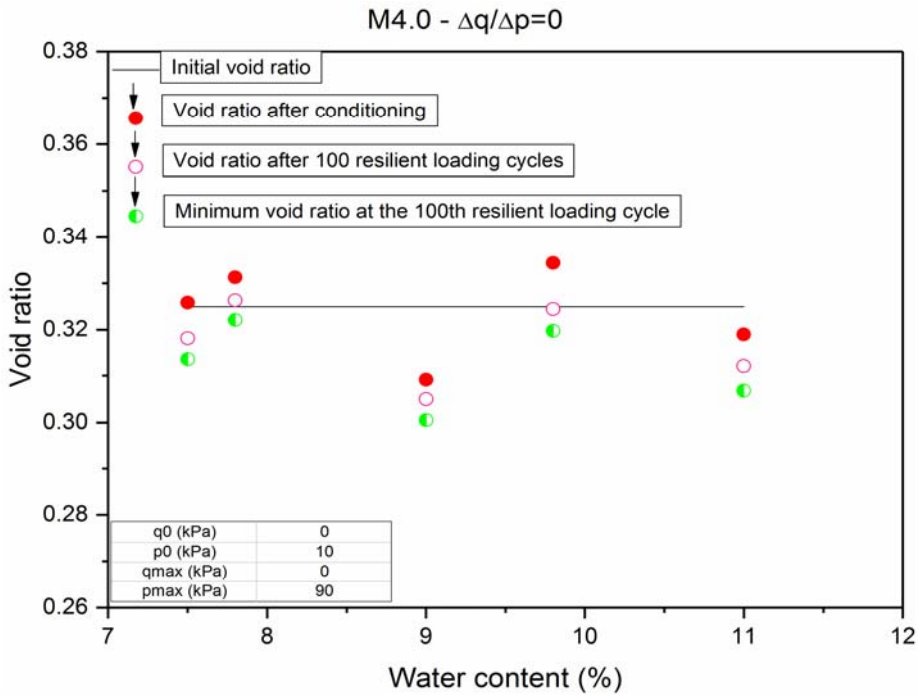

a)

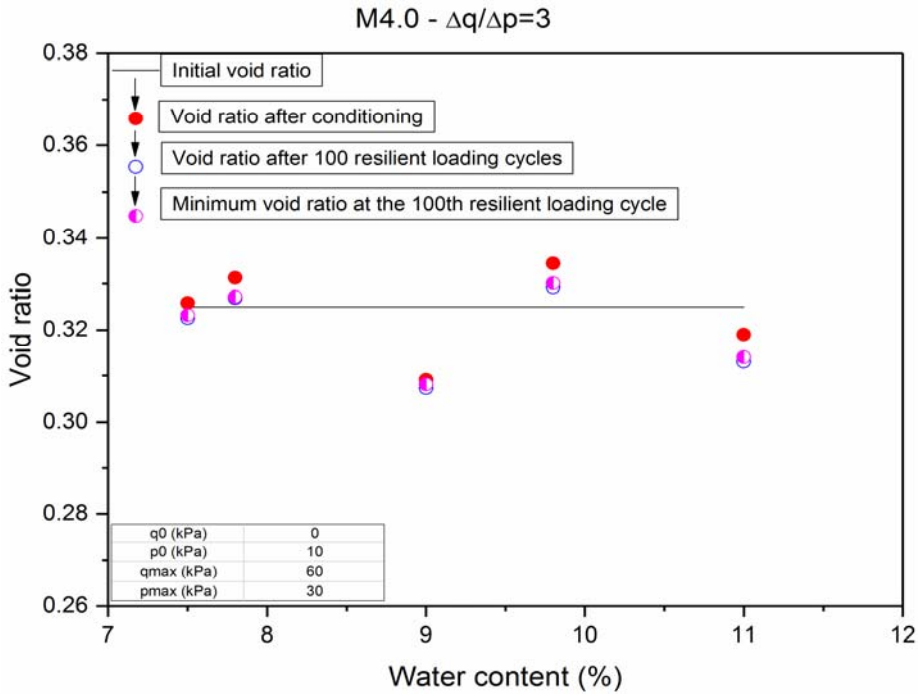

b)

Figure IV.18. Evolution of void ratio in different test phases for Missillac sand M4.0 in stress paths of Δq/Δp = 0 and 3.

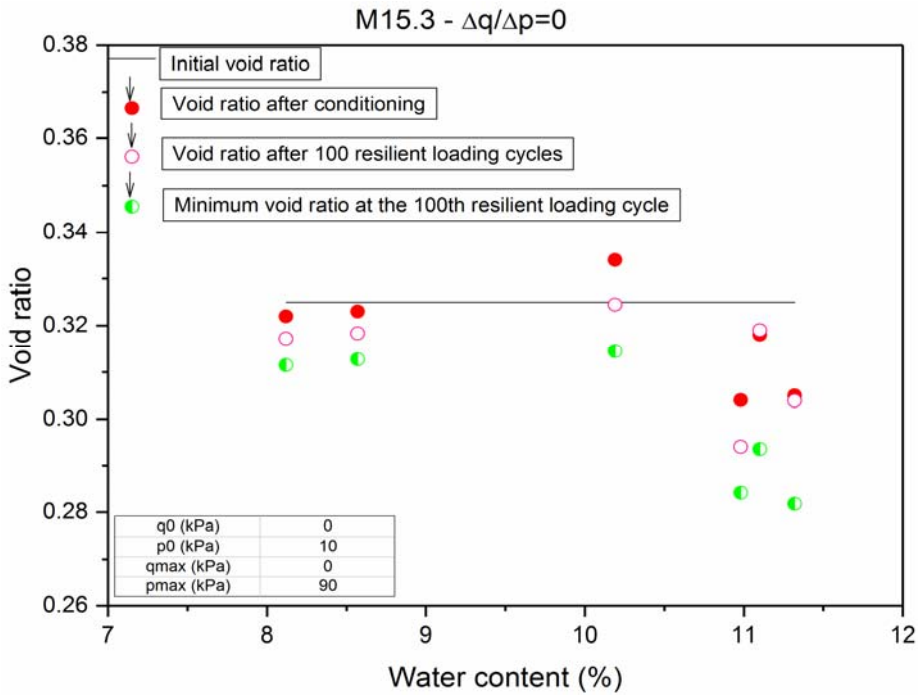

a)

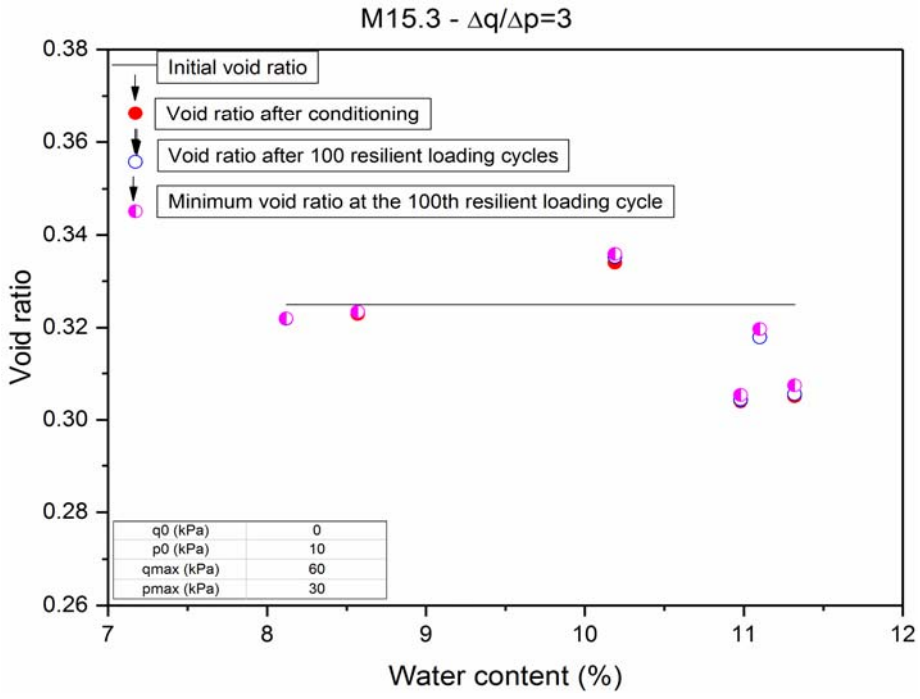

b)

Figure IV.19. Evolution of void ratio in different test phases for Missillac sand M15.3 in stress paths of Δq/Δp = 0 and 3.

Improved Boyce-Hornych model with effective stress concept

Bishop, (1963) proposed effective stress expression (Equation I.11) for unsaturated soils. In this equation, the pore water pressure (u_w), the pore air pressure (u_a) and the suction ($s = u_a - u_w$) are used to evaluate the unsaturated state. As mentioned in the literature review, the effective stress concept could be used to improve the accuracy of the evaluation of the resilient deformation behaviour.

Besides, in the study of liquefaction resistance of unsaturated sand from Unno et al., (2008), the results of the RLTTs show that (as shown in *Figure I.16*) the pore air pressure u_a and pore water pressure u_w have increased during undrained cyclic excitation. A minor change of suction is observed before the u_a reaches initial confining pressure. The similar results have been obtained by Okamura et al., (2009) and Tsukamoto et al., (2014). As a result, in an effective stress analysis for this study, the suction value could be considered as a constant value, which is obtained from SWRC.

Based on the work in the last section and the effective stress concept, the new modified Boyce-Hornych model could be proposed, which is expressed as:

$$\varepsilon_v^r = \frac{p'^n}{p_a^{n-1}}\left[\frac{1+2\cdot\gamma_3}{3\cdot K_a} + \frac{n-1}{18\cdot G_a}(1+2\cdot\gamma_3)\cdot\left(\frac{q'}{p'}\right)^2 + \frac{1-\gamma_3}{3\cdot G_a}\frac{q'}{p'}\right] \tag{IV.8}$$

$$\varepsilon_q^r = \frac{2}{3}\cdot\frac{p'^n}{p_a^{n-1}}\left[\frac{1-\gamma_3}{3\cdot K_a} + \frac{n-1}{18\cdot G_a}(1-\gamma_3)\cdot\left(\frac{q'}{p'}\right)^2 + \frac{2+\gamma_3}{6\cdot G_a}\cdot\frac{q'}{p'}\right] \tag{IV.9}$$

where,

$$p' = \frac{(\sigma_1 - u_a) + \chi s + 2\cdot(\gamma_3\sigma_3 - u_a) + 2\cdot\chi s}{3} = p^* - u_a + \chi s \tag{IV.10}$$

$$q' = (\sigma_1 - u_a) + \chi s - (\gamma_3\sigma_3 - u_a) - \chi s = \sigma_1 - \gamma_3\sigma_3 = q^* \tag{IV.11}$$

In this context, we think that the open loops or the hysteresis phenomenon of the measured ε_v^r and ε_q^r on stress paths of $\Delta q/\Delta p$ = 0 and 0.5 (even 1) for Missillac sand M15.3 with the high water contents of 10.2%, 11.0%, 11.1% and 11.3% (*Figure IV.16* and *Figure IV.17*) could be explained by the difference of effective stress between loading and unloading procedure with same mean normal stress p. It indicates that the effective stresses are larger in unloading

phase which can keep the larger ε_v^r and ε_q^r compared with loading phase. We suppose the rate of the dissipation of u_a and u_w in unloading phase is faster than the rate of the generation in loading phase with the same mean normal stress could be a reason (In this study, the u_a and the u_w are not measured because of the limitation of instruments).

As a result, before the modelling progress, we try to find a set of u_a values which could eliminate the hysteresis loops as much as possible in effective mean normal stress plane for Missillac sand M15.3 with water content of w =11.1% as shown in *Figure IV.20.* It means that the ε_v^r *and* ε_q^r could be determined only by the effective mean normal stress without hysteresis loops. The suggested u_a values are shown in *Figure IV.21.* Here, we think the significant u_a values exist only on the stress path of $\Delta q/\Delta p$ = 0 and 0.5 (even 1) with obvious open loops.

Then, we apply the same set of u_a values and the constant suction value to the Equations IV.8-11 and the model parameters are optimized by the least square method. *Figure IV.22* show the modelling results of ε_v^r and ε_q^r for Missillac sand M15.3 with water content of w =11.1%. A correct modelling results with a correlation coefficient value of R^2 = 0.73 could be obtained for all stress paths and the hysteresis loops are not very significant, especially for the stress path of $\Delta q/\Delta p$ = 0.

However, we have to note that the u_a values aren't measured and the difference of u_a is opposite to the difference of resilient volumetric compression between loading and unloading phase. Normally, a larger resilient volumetric deformation should induce higher u_a and u_w. Hence, in this context, we assume the rate of the dissipation of u_a and u_w in unloading phase is faster than the rate of the generation in loading phase. This point should be verified in the future tests and analyzed with the micro-structure evolution.

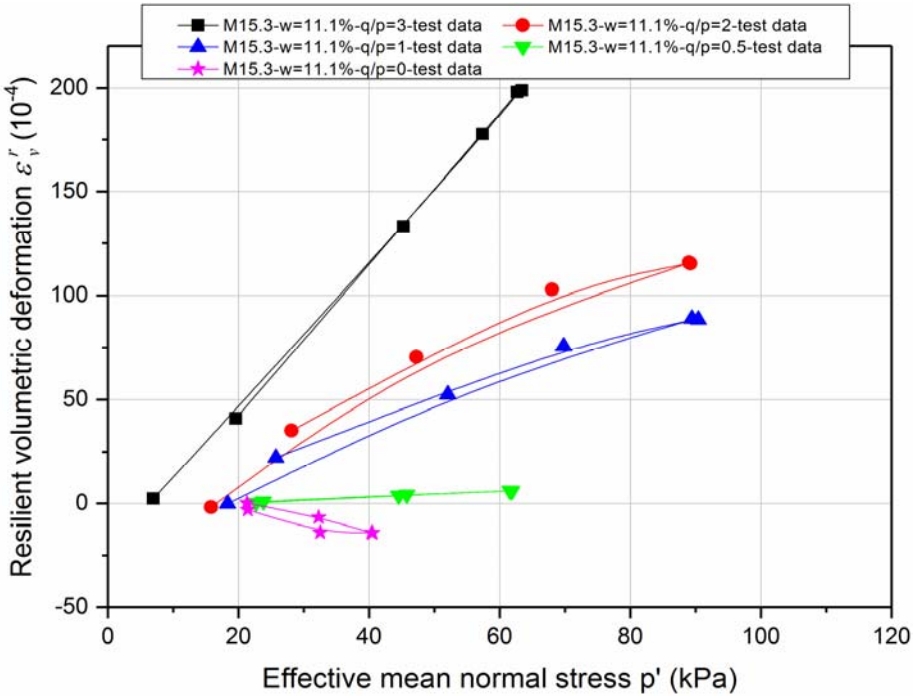

a)

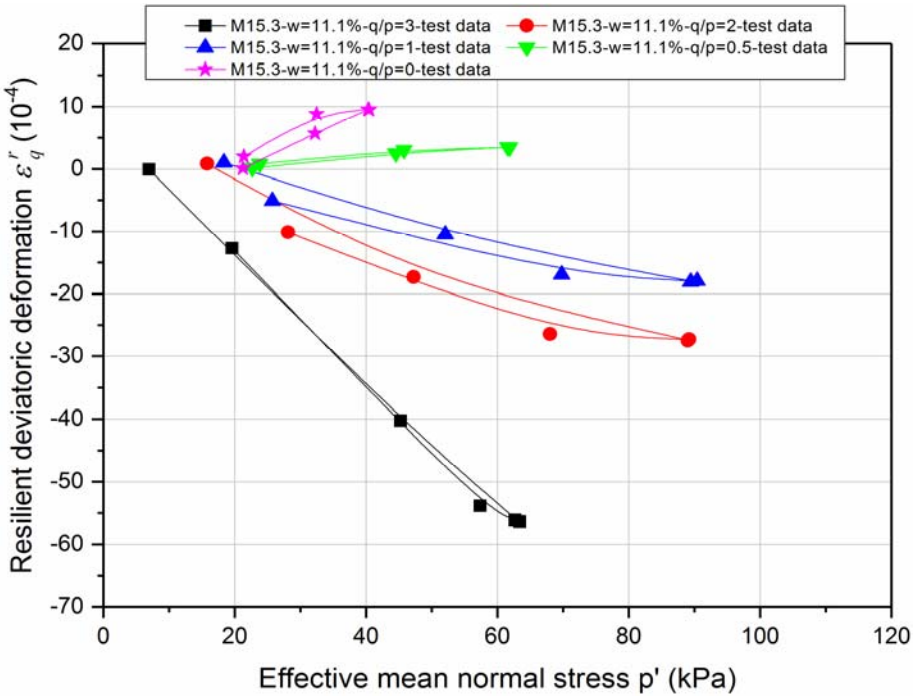

b)

Figure IV.20. Resilient volumetric deformation ε_v^r and resilient deviatoric deformation ε_q^r in effective mean normal stress plane for Missillac sand M15.3 at water content of w =11.1%

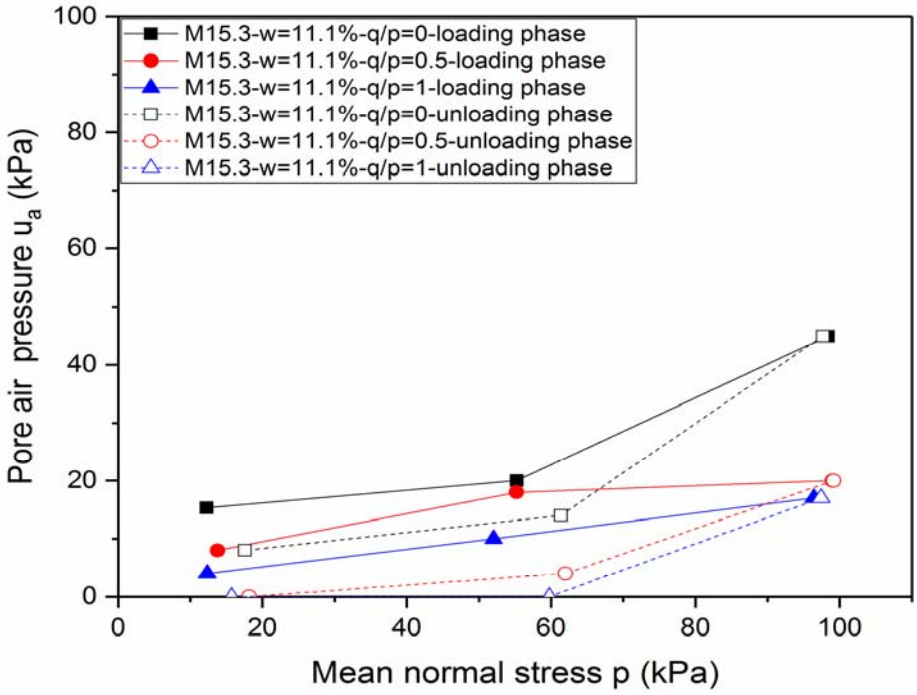

Figure IV.21. Suggested pore air pressures u_a for Missillac sand M15.3 at water content of w =11.1% in stress paths of$\Delta q/\Delta p$ = 0, 0.5 and 1

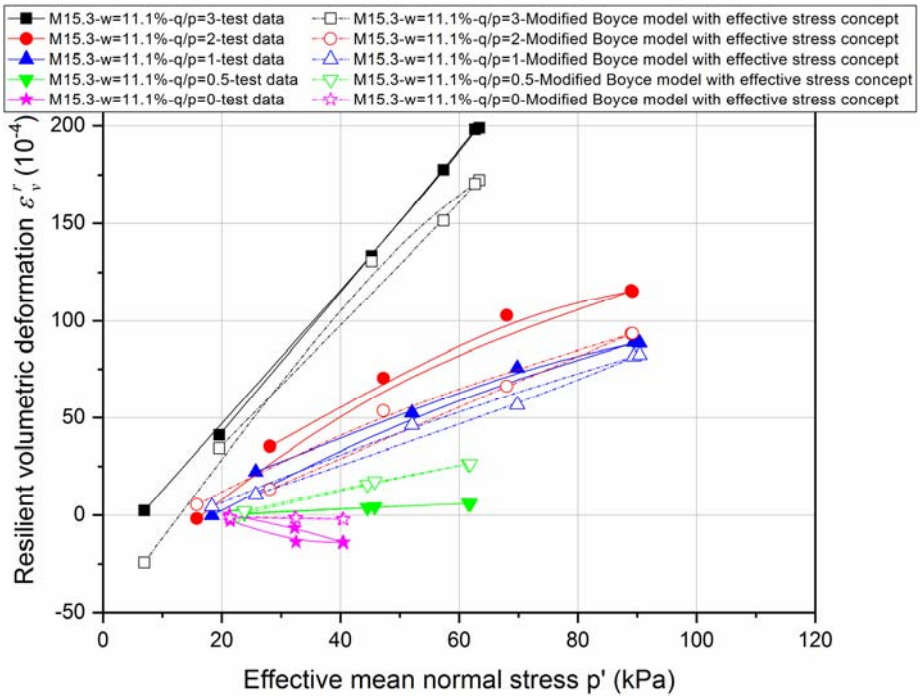

a)

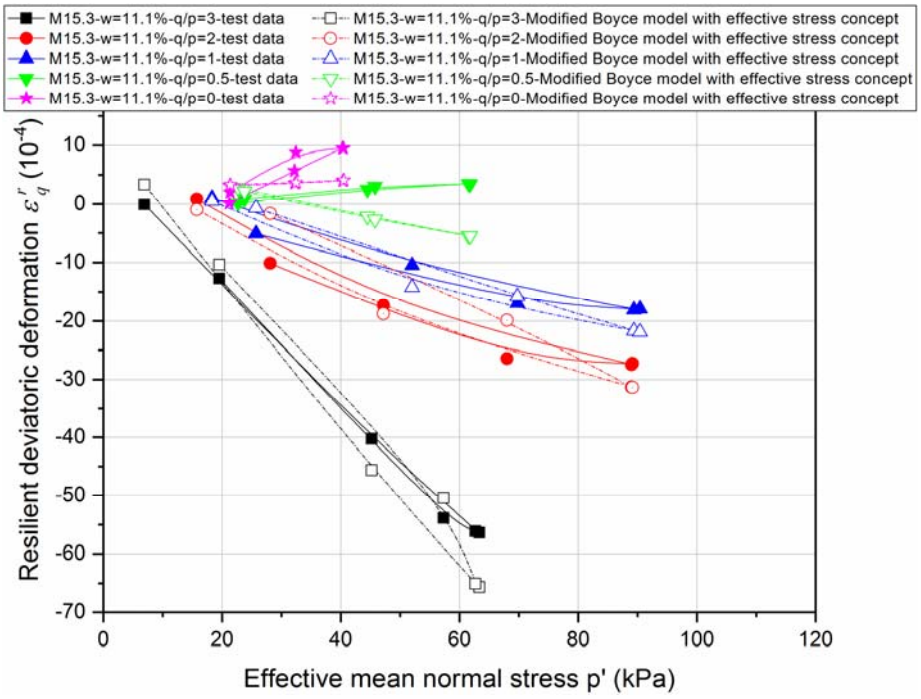

b)

Figure IV.22. Comparison of ε_v^r and ε_q^r between the effective stress model response and the test results for Missillac sand M15.3 at water content of w =11.1%

IV.4. Conclusion

This chapter presents the resilient test results of RLTTs for Missillac sand with three different fine contents. The analysis results of stabilization of the permanent deformation show the volumetric deformation ε_v and deviatoric deformation ε_q in the last cycle can be treated as resilient behaviour (ε_v^r and ε_q^r) because the variation of volumetric deformation and deviatoric deformation are small. Then, the resilient deformations, maximum resilient volumetric deformation ε_v^r and the maximum resilient deviatoric deformation ε_q^r in s/s^* plane and the anisotropy effect on the resilient behaviour are presented in detail.

In the modelling part, a modified Boyce-Hornych model was proposed with the anisotropic effect, which predicts resilient volumetric deformation and resilient deviatoric deformation correctly. At the end of this chapter, a discussion is introduced to improve the model based on effective stress concept against the problem of large open loops of resilient volumetric deformation and resilient deviatoric deformation for M15.3 samples at water contents of 10% to 11% in the stress paths of $\Delta q/\Delta p$ = 0; 0.5 and 1.

The study in this chapter is useful to understand the evolution of resilient behaviour of these granular materials coupling with effects of fine content and hydraulic behaviour. It also mentions that, the deformation of samples with a high-water content and a high fine content in low stress paths could present incompletely elastic behaviour, which means more loading/unloading cycles should be applied during the conditioning phase.

CHAPTER V. SHAKEDOWN BEHAVIOUR OF A GRANULAR MATERIAL

V.1. Introduction

The applied traffic loads on granular material layers are an important consideration in pavement design against failure. As mentioned in literature review, the mechanism of the failure of granular material layers can be explained by shakedown behaviour of the material and different approaches for determining the limited/critical stress have been developed by different researchers (Werkmeister et al., 2001; Yang & Huang, 2007; Tao et al., 2010). In this chapter, the shakedown behaviour of Missillac sand is analyzed with the effect of water content, fine content and suction based on the results of repeated load triaxial tests (RLTTs).

V.2. Shakedown analysis of single-stage RLTTs

V.2.1. Accumulated permanent axial deformation

In single-stage RLTT tests, we have observed that the permanent axial deformation increased significantly as the water content increased and the deformation hardly stabilized in a high saturation state for Missillac sand M4.0 and M15.3 as shown in *Figure III.4.a* and *Figure III.6.a.*

*Figure V.1*and *Figure V.2* present the evolution of stress–strain loop with various water contents for Missillac sand M4.0 and M15.3. It can be stated apparently that the accumulated permanent axial deformation increases with the increase of number of cycles and water content. The size of stress-strain loop is decreasing gradually as increasing number of cycles.

For Missillac sand M4.0, at water content of 7.5%, the accumulated permanent axial deformation increases rapidly at the first 1000 loading cycles and then achieves eventually a stable value. This is the typical "plastic shakedown" behaviour in Range A. The similar phenomenon could be observed with higher water contents of 7.8%, 9.0% and 9.3%. However, at water contents of 9.8% and 11.0%, the noticeable increases of the accumulated permanent axial deformation could be still observed in the last 5000 cycles and the tendency is more obvious as increasing water content. More cycles are required to estimate the deformation behaviour at these two water contents as "plastic shakedown" behaviour or others.

Similarly, for Missillac sand M15.3, the "plastic shakedown" behaviour could be observed when the water content is lower that 11% (included). Once the water content is higher than 11%, more cycles are required to decide the shakedown behaviour.

V.2.2. Permanent axial deformation rate

Figure V.3 and *Figure V.4* present the evolution of permanent axial deformation rate versus the accumulated permanent axial deformation for Missillac sand M4.0 and M15.3 at various water contents.

For Missillac sand M4.0, as shown in *Figure V.3,* based on the proposed description of shakedown categories by Werkmeister et al., (2001), here most of plots show as a convex-downwards line (Range A - plastic shakedown) with a decrease of permanent axial deformation rate less than 10^{-7}/cycle except for the sample at water content of 11.0% which doesn't show the decreasing trend further (Range B - plastic creep). It can be

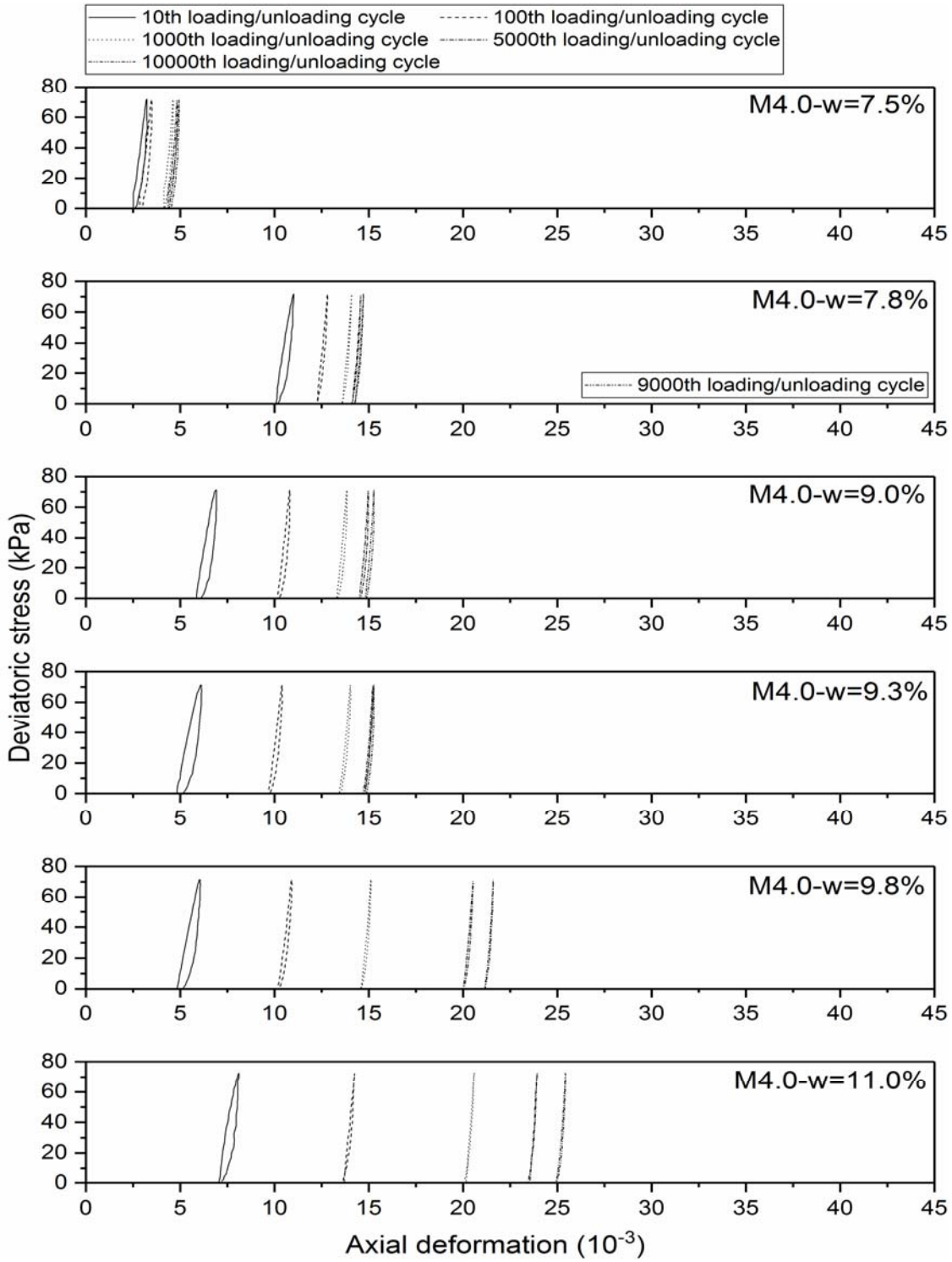

Figure V.1. Evolution of stress–strain loop at various water contents for Missillac sand M4.0

stated that the level of accumulated permanent axial deformation required to reach a stabilized permanent axial deformation, apparently depends on the water content.

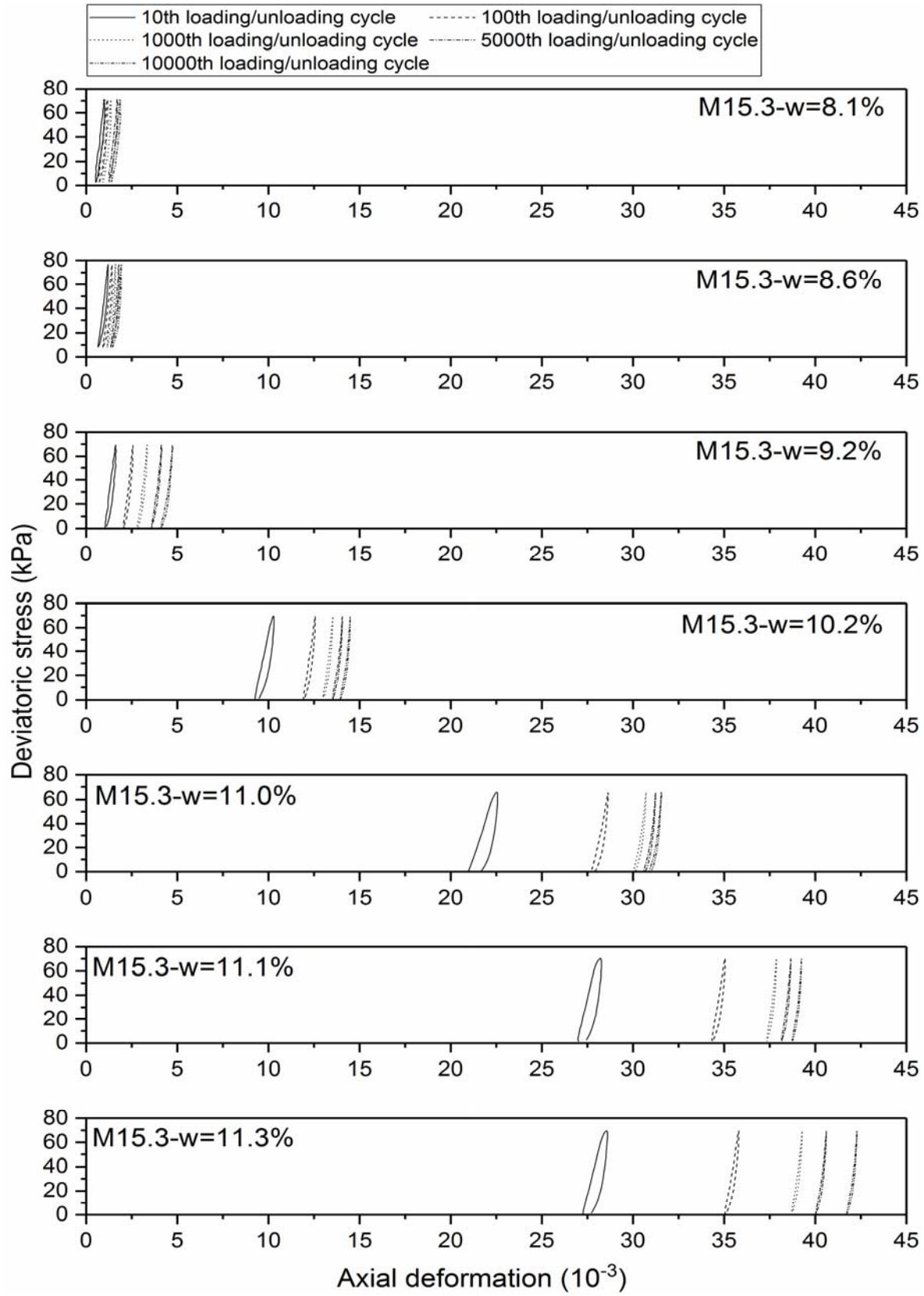

Figure V.2. Evolution of stress–strain loop at various water contents for Missillac sand M15.3

Analogously, for Missillac sand M15.3, per the plot feature, the deformation pattern could be indicated as shown in *Figure V.4*: Range A - plastic shakedown at water contents of 8.1%, 8.6%, 9.2%, Range B - plastic creep at water contents of 11.1% and 11.3%. The results at water contents of 10.2% and 11.0% could be treated as Range A or Range B.

In addition, the *s/s** value has shown the good interpretations of permanent and resilient deformation behaviour under the coupling effects of water content and fine content. Here, the minimum permanent axial deformation rates after 10,000 loading cycles are plotted in *s/s** plane for both materials at the different water contents as shown in *Figure V.5*. It can be observed that there is a unique curve following the exponential function which could be used to describe the correlation between minimum permanent axial deformation rate after a given large number of loading cycles and the *s/s** value in Range A and Range B, as expressed by:

$$\varepsilon^{p}_{1rate\text{-min}} = a \cdot e^{b\cdot(s/s*)} \tag{V.1}$$

where, *a* and *b* are parameters depending on the number of loading cycles.

This curve maybe shift a little bit if we increase the number of loading cycles because the lower permanent axial deformation rate could be achieved.

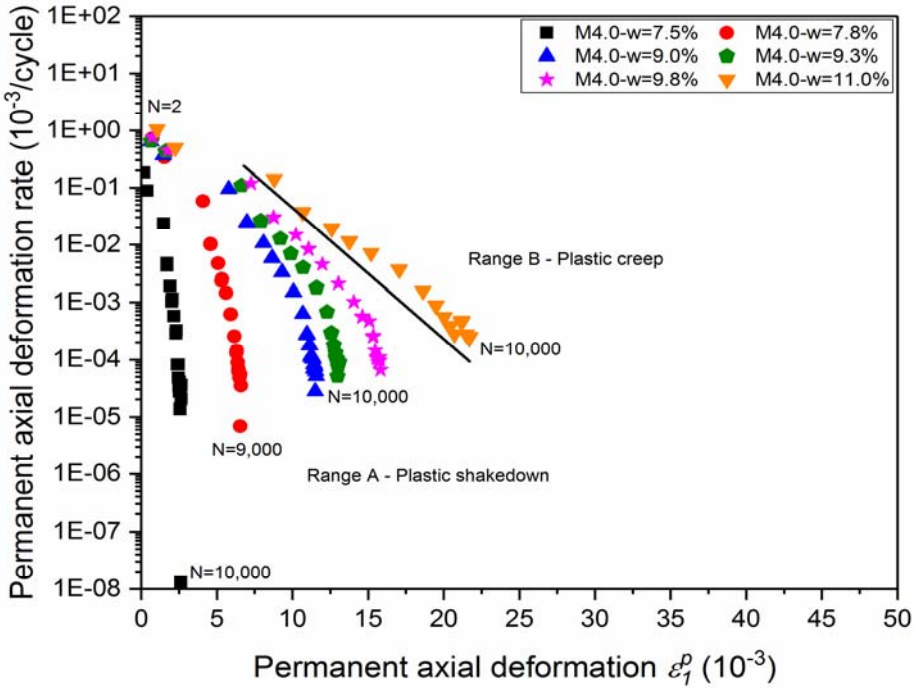

Figure V.3. Evolution of permanent axial deformation rate for Missillac sand M4.0 at various water contents

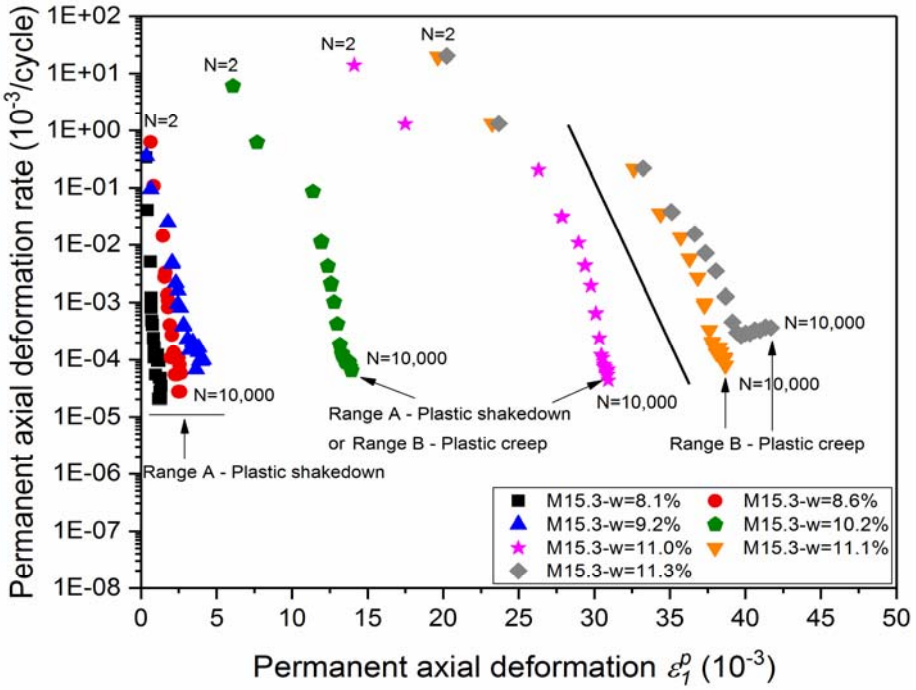

Figure V.4. Evolution of permanent axial deformation rate for Missillac sand M15.3 at various water contents

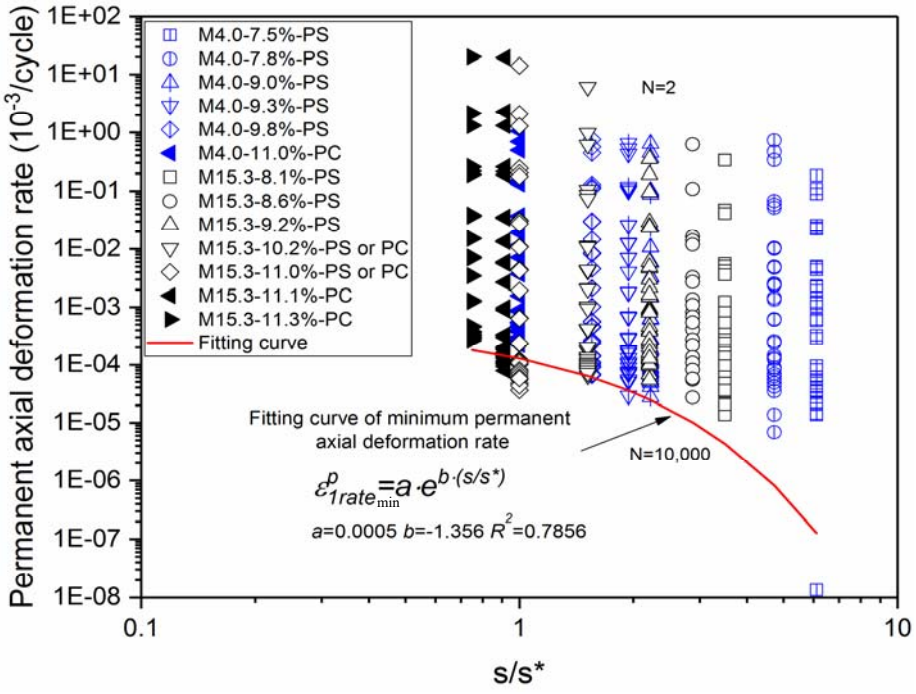

Figure V.5. Evolution of permanent axial deformation rate for Missillac sand M4.0 and M15.3 versus s/s (PS-Plastic shakedown; PC-Plastic creep)*

V.2.3. Recoverable axial deformation

Werkmeister et al., (2004) indicated that the patterns of plastic shakedown, plastic creep and incremental collapse cannot be distinguished only based on permanent deformation in some cases. The recoverable deformation behaviour could be also used to describe the shakedown behaviour as shown in *Figure I.31*.

Figure V.6 and *Figure V.7* present the evolution of recoverable axial deformation for Missillac sand M4.0 and M15.3 respectively versus number of cycles at various water contents. It can be observed that all specimens exhibit Range A or Range B behaviour with a final constant level of recoverable axial deformation after enough loading cycles (for M4.0 after 5000 cycles and for M15.3 after 2000 cycles). A significant decrease of recoverable axial deformation with increasing number of cycles as Range C presented in *Figure I.31*, cannot be seen in these results. Besides, an approximate tendency towards an increase of the recoverable axial deformation as increasing water content could be obtained in *Figure V.7* for M15.3 but it couldn't be seen in *Figure V.6* for M4.0 because of the similar deformation values for samples at various water contents.

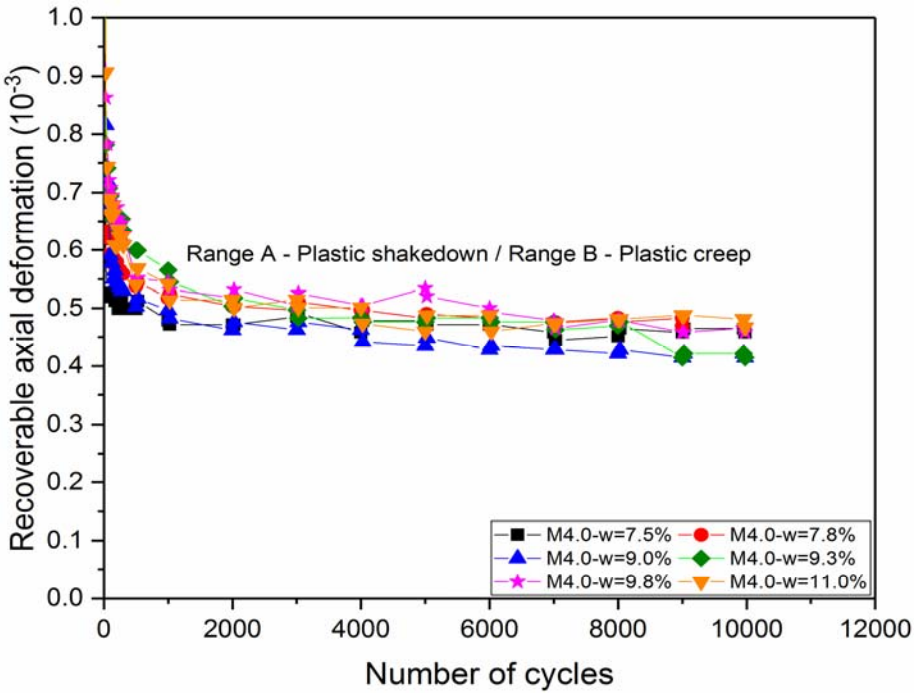

Figure V.6. Evolution of recoverable axial deformation for Missillac sand M4.0 versus number of cycles at various water contents

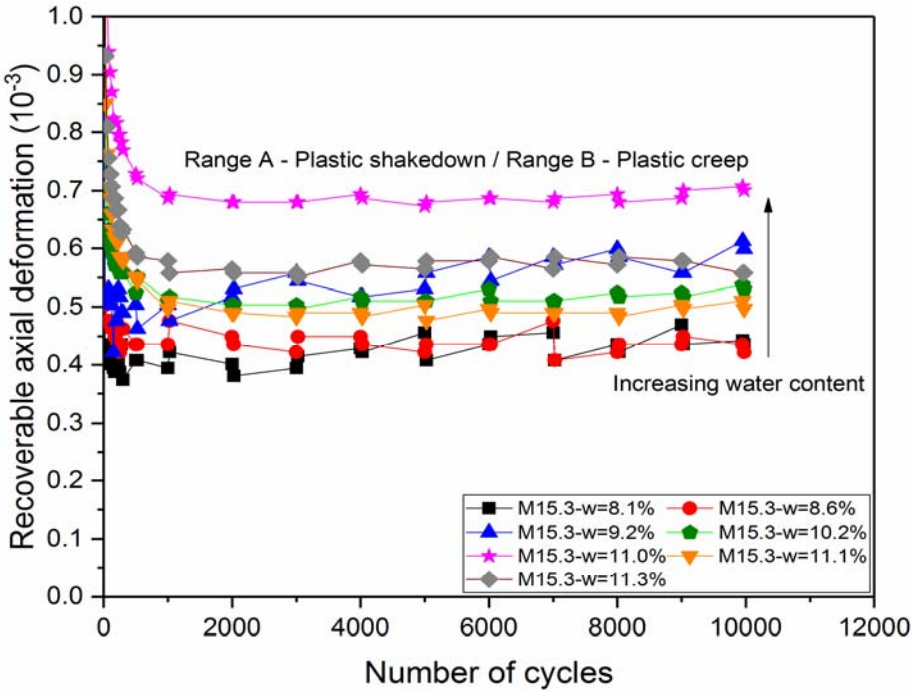

Figure V.7. Evolution of recoverable axial deformation for Missillac sand M15.3 versus number of cycles at various water contents

Based on the recoverable axial deformation behaviour presented above, it is better to compare it with the permanent axial deformation behaviour as shown in *Figure III.4.a* and *Figure III.6.a* and it seems a mirroring of permanent axial deformation with a reversed effect of water content. This means there is a correlation between the permanent axial deformation and the recoverable axial deformation which has been observed by some researchers (Puppala et al., 1999; Mohammad et al., 2006; Yang et al., 2008). The general assumption is that the higher the recoverable modulus, the less the permanent deformation, if we use recoverable modulus to represent recoverable deformation.

In this study, the relationship between the permanent axial deformation and the recoverable axial modulus M_{re} is illustrated in *Figure V.8* and *Figure V.9* for these two materials separately (for clarity purposes, we chose three water contents for each material). Based on the results, a simple exponential function is proposed as:

$$M_{re} = g \cdot e^{\left(h \cdot \varepsilon_1^p\right)} \tag{V.2}$$

The correlation coefficients are shown in *Figure V.8* and *Figure V.9.*

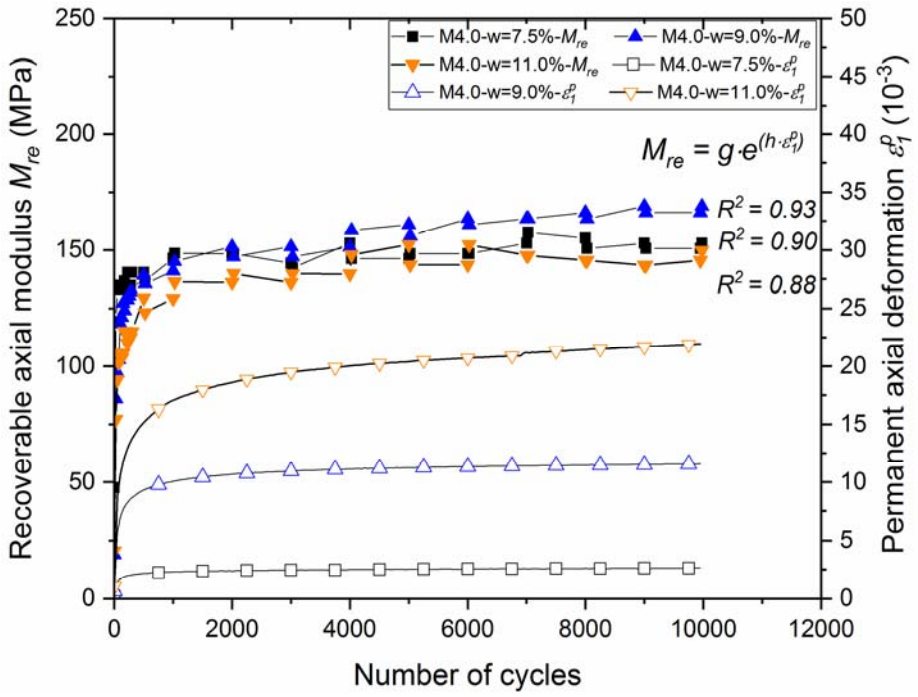

Figure V.8. Relationship between M_{re} and ε_1^p for Missillac sand M4.0 versus number of cycles

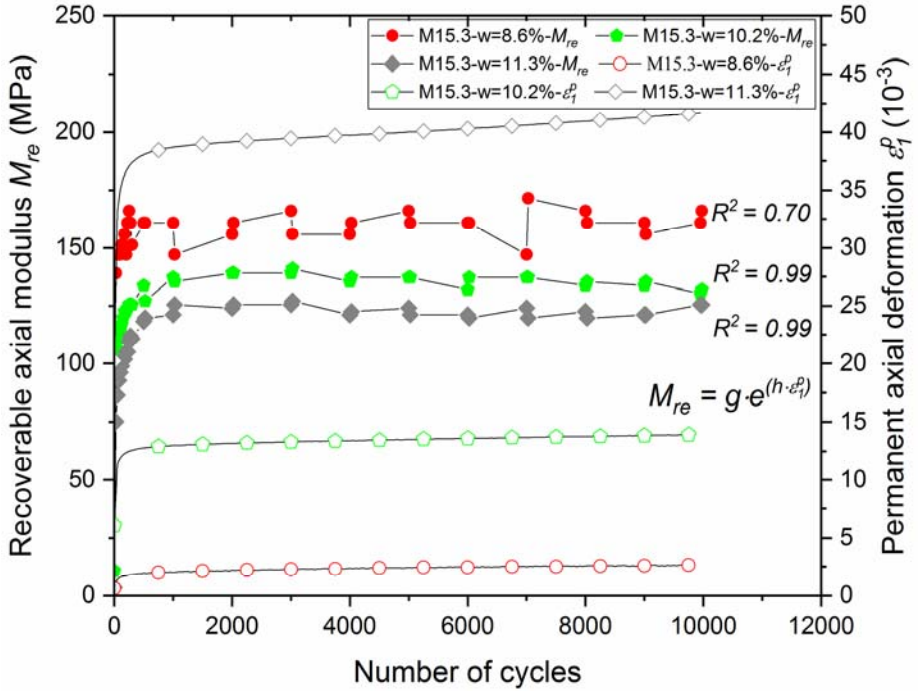

Figure V.9. Relationship between M_{re} and ε_1^p for Missillac sand M15.3 versus number of cycles

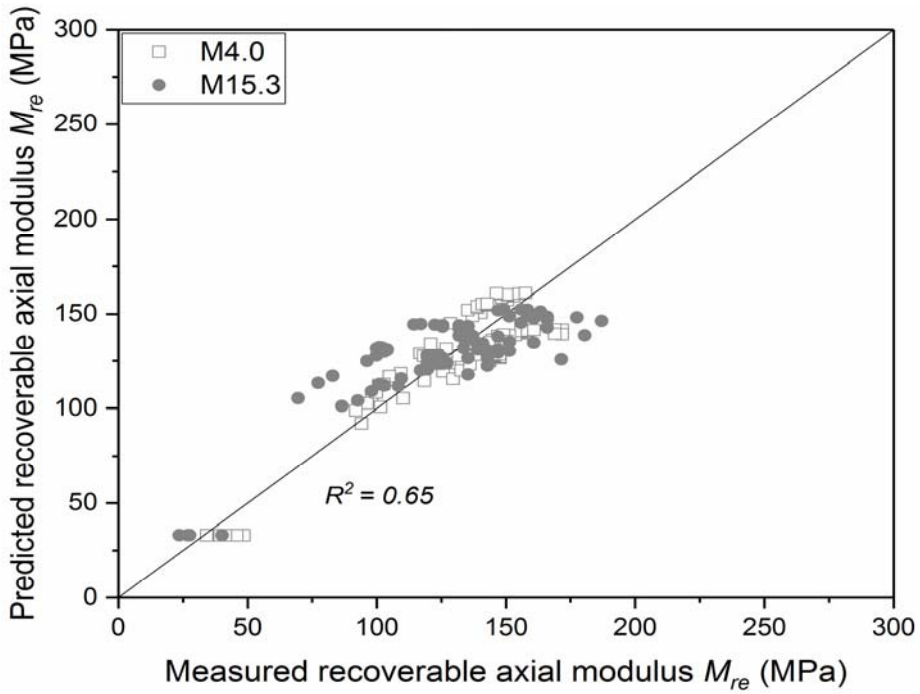

Figure V.10. Comparison between predicted and measured M_{re} for Missillac sands M4.0 and M15.3

Combine Equation V.2 and Equation III.8, the M_{re} could be described with only number of cycles and *s*/*s** values, which is expressed as:

$$M_{re} = g \cdot \mathrm{e}^{\left(h \cdot \left(\frac{s}{s^*} \right)^d \cdot \left(1 - \left(\frac{N}{N_0} \right)^{b \cdot \ln\left(\frac{s}{s_a} \right) + f} \right) \right)} \tag{V.3}$$

where, g, h, d, b, and f are parameters.

Figure V.10 illustrates the M_{re} calculated by Equation V.3 for both materials at all water contents presented. The results show that Equation V.3 could be used to predict the M_{re} values effectively. The relatively low correlation coefficient (R^2 = 0.65) could be caused by the similar M_{re} values of M4.0 samples at various water contents.

Based on the analysis of permanent axial deformation rate and recoverable axial deformation above, the shakedown categories could be defined for the single-stage test results, as shown in *Table V.1*. In general, all the samples exhibit "plastic shakedown" or "plastic creep" behaviour and they could be acceptable for base or subbase materials in pavement design. But it is important to note that the permanent axial deformation has approached or exceeded 4% for Missillac sand M15.3 at water contents of w = 11.1% and 11.3%, which should be avoided

in practice. Besides, the shakedown behaviour of Missillac sands in single-stage tests shows significant effect of water content: the increasing water content could increase permanent axial deformation and induce a less stable state. The effect of fine content on the classification of shakedown categories is not obvious in these tests.

Material	Water content (%)	Classification criterions			Shakedown behaviour
		Accumulated permanent axial deformation	Permanent axial deformation rate	Recoverable axial deformation	
M4.0	7.5	Range A	Range A	Range A or B	Range A: Plastic shakedown
	7.8	Range A	Range A	Range A or B	Range A: Plastic shakedown
	9.0	Range A	Range A	Range A or B	Range A: Plastic shakedown
	9.3	Range A	Range A	Range A or B	Range A: Plastic shakedown
	9.8	-	Range A	Range A or B	Range A: Plastic shakedown
	11.0	-	Range B	Range A or B	Range B: Plastic creep
M15.3	8.1	Range A	Range A	Range A or B	Range A: Plastic shakedown
	8.6	Range A	Range A	Range A or B	Range A: Plastic shakedown
	9.2	Range A	Range A	Range A or B	Range A: Plastic shakedown
	10.2	Range A	Range A or B	Range A or B	Range A: Plastic shakedown
	11.0	Range A	Range A or B	Range A or B	Range A: Plastic shakedown
	11.1	-	Range B	Range A or B	Range B: Plastic creep
	11.3	-	Range B	Range A or B	Range B: Plastic creep

Table V.1. Classification of shakedown behaviour for Missillac sands in single-stage tests

V.3. Shakedown analysis of multi-stage RLTTs

In this section, the shakedown analysis will be performed with Missillac sands M7.5 and M15.3 in multi-stage tests. Only the permanent axial deformation rate will be used to distinguish the shakedown categories for these two materials due to a lack of data of Missillac sand M7.5 to calculate the accumulated permanent axial deformation and recoverable axial deformation.

V.3.1. Permanent axial deformation rate

Figure V.11 present the evolution of permanent axial deformation rate with the increase of accumulated permanent axial deformation for Missillac sand M7.5 at various stress paths ($\Delta q/\Delta p$ = 1; 1.5; 2 and 3) with a given water content of w = 11%. *Figure V.12* presents the evolution of permanent axial deformation rate with the increase of accumulated permanent axial deformation for Missillac sand M15.3 at various water contents (w = 7.7%; 9.4%; 9.9% and 11.1%) under a given stress path of $\Delta q/\Delta p$ = 3.

For Missillac sand M7.5, at the water content of 11%, it is clear that the accumulated permanent axial deformation increases with the increase of stress level for each stress path and the trend is more apparent with an increase of stress path from $\Delta q/\Delta p$ = 1 to $\Delta q/\Delta p$ = 3 as shown in *Figure V.11*. In this figure, the shakedown category for each test is determined by the curve pattern. It can be stated that only plastic shakedown exists in stress paths of $\Delta q/\Delta p$ = 1 and 1.5 due to a steep decrease of permanent axial deformation rate with a small increase in permanent axial deformation for all stress levels as shown in *Figure V.11.a and Figure V.11.b*. The plastic creep and incremental collapse could happen in stress paths of $\Delta q/\Delta p$ = 2 and 3 with a high stress level, even the samples have experienced a stiffness hardening during the former loading procedures as shown in *Figure V.11.c and Figure V.11.d*.

Similarly, for Missillac sand M15.3, the accumulated permanent axial deformation increases with increasing stress level for each water content and this trend is more obvious with an increase of water content from w = 7.7% to w = 11.1% as shown in *Figure V.12*. The shakedown category for each test is indicated as well in this figure. The incremental collapse with a very slow decline of permanent axial deformation rate could be observed in all water contents with a high stress level. The required stress level inducing incremental collapse decreases apparently from Δq = 200kPa to Δq = 100kPa when the water content increases to 11.1% from the other three water contents (*Figure V.12.d)*. It means the failure line shifts down in p-q plane as increasing water content.

Based on the classification of shakedown categories, in this study, we defined the stable state with plastic shakedown behaviour and plastic creep behaviour and the unstable state with incremental collapse behaviour. The shakedown categories and the soil state of Missillac sand M7.5 and M15.3 are summarized in *Table V.2 and Table V.3* respectively.

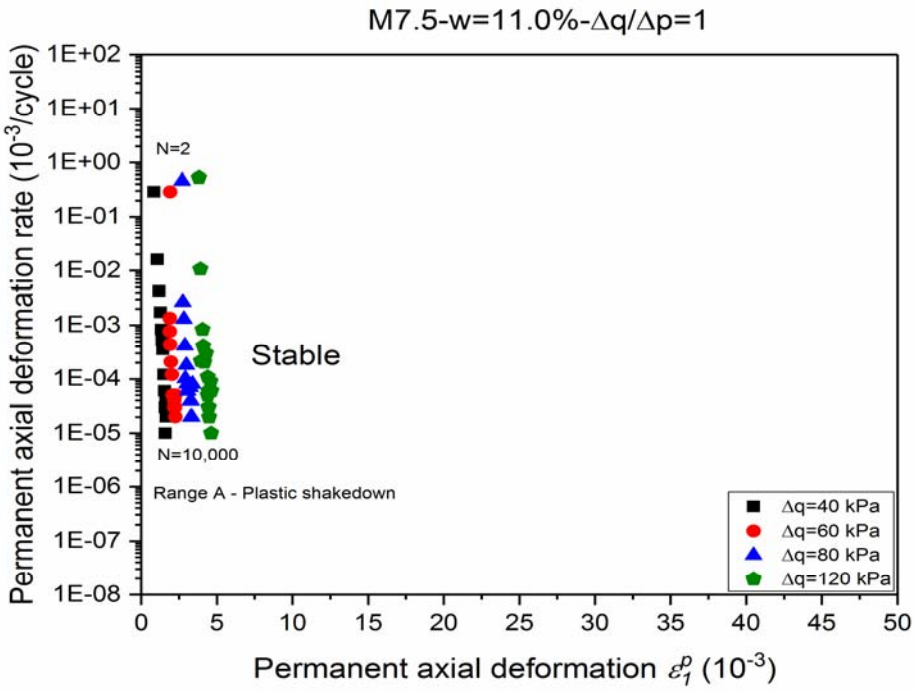

a)

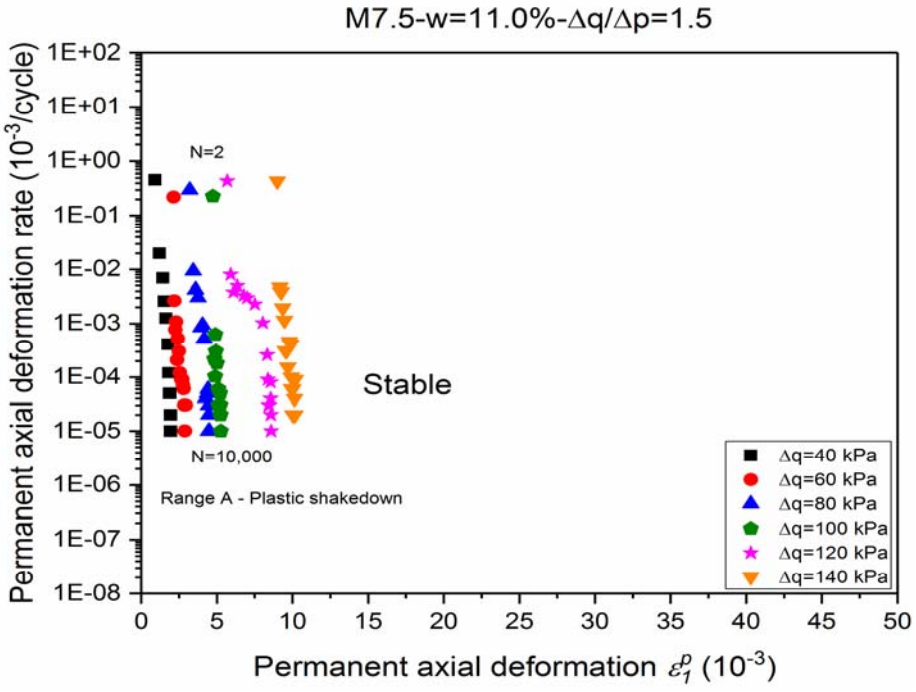

b)

Figure V.11. Evolution of permanent axial deformation rate for Missillac sand M7.5 at various stress paths a) Δq/Δp = 1; b) Δq/Δp = 1.5; c) Δq/Δp = 2; d) Δq/Δp = 3.

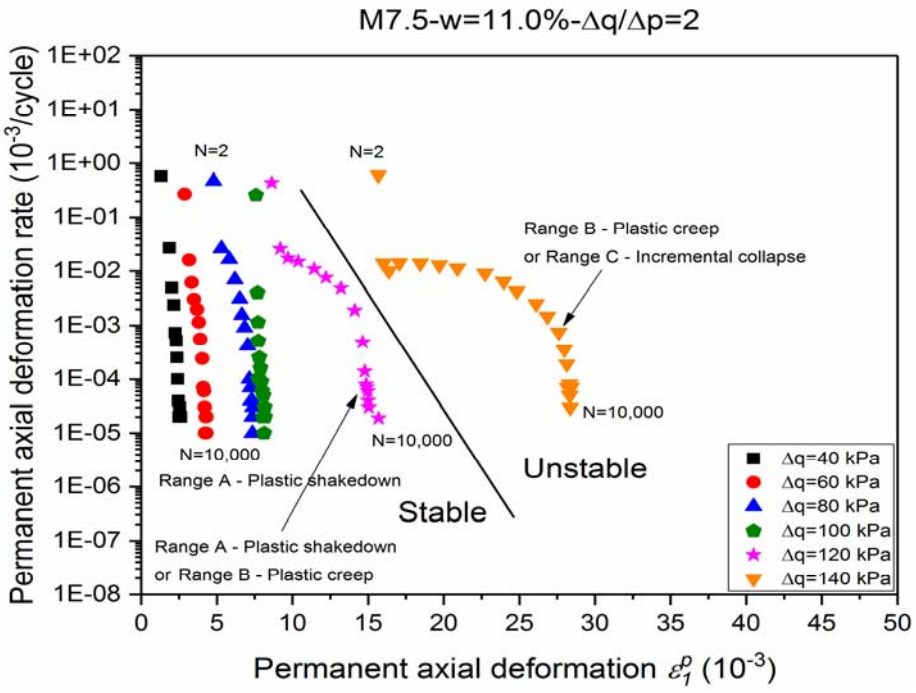

c)

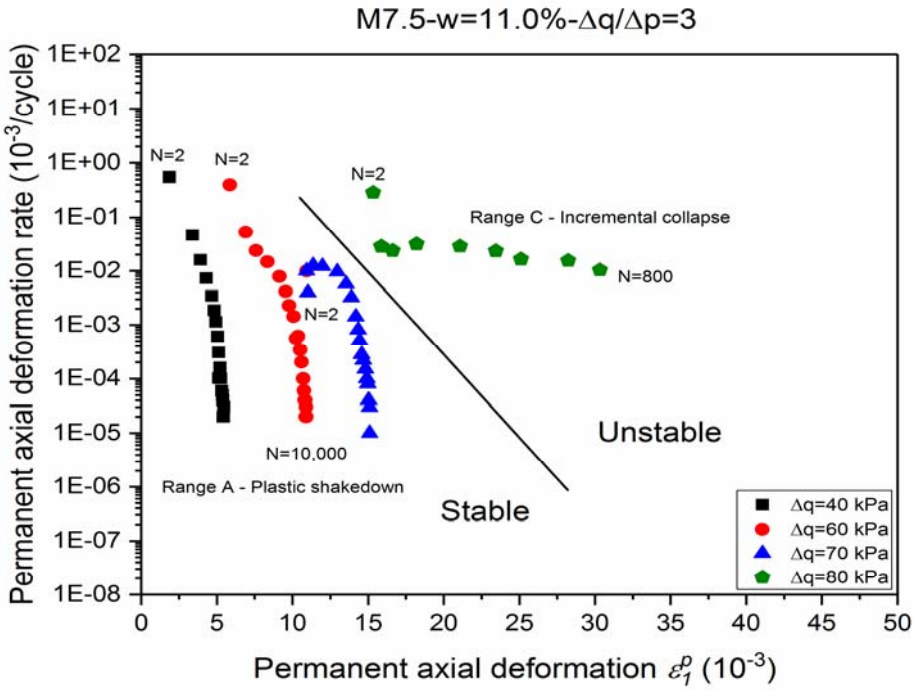

d)

Figure V.11 – Continued

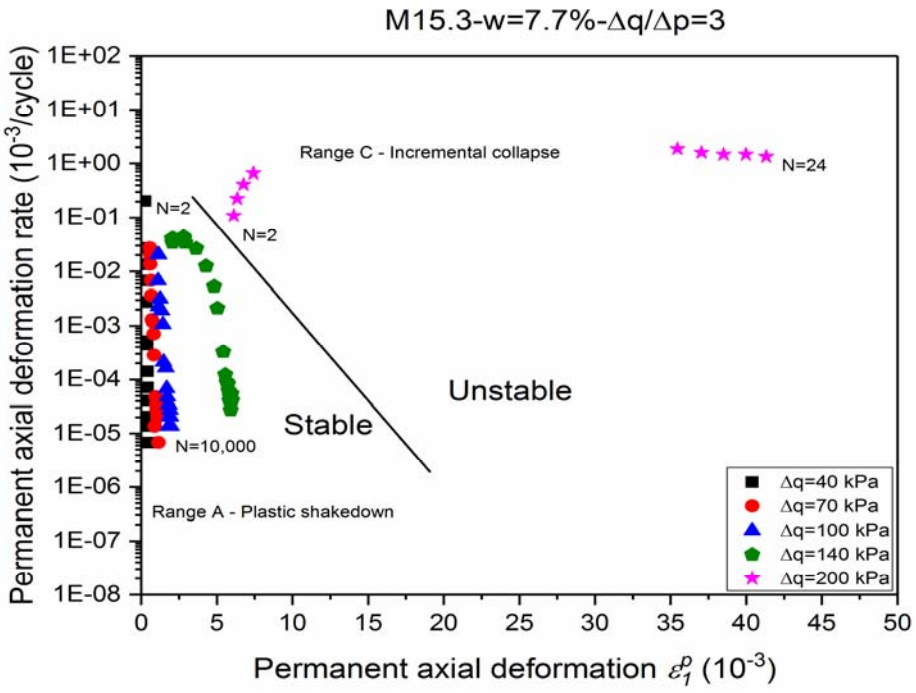

a)

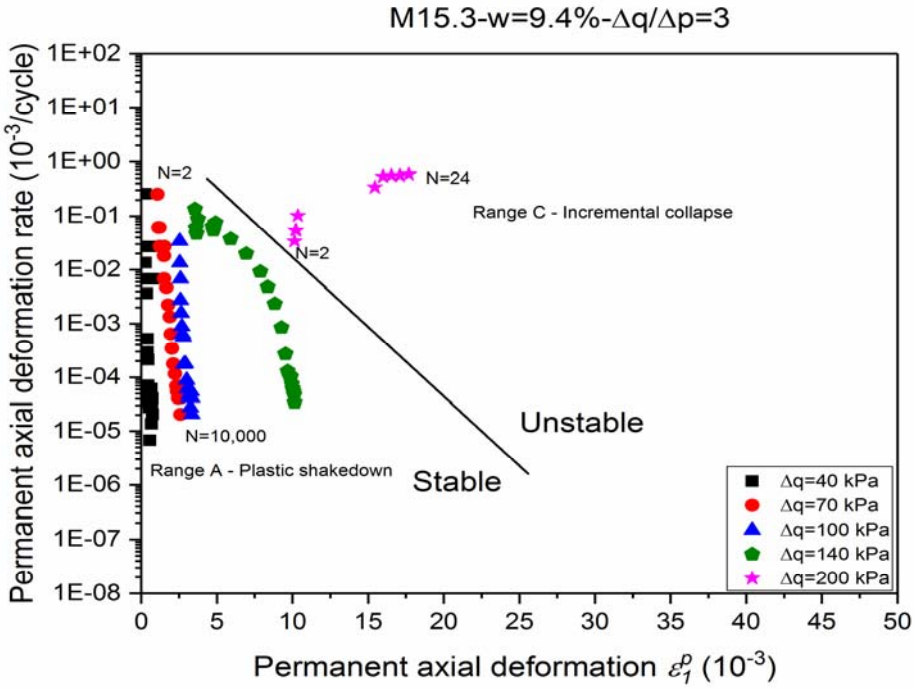

b)

Figure V.12. Evolution of permanent axial deformation rate for Missillac sand M15.3 at various water contents a) w = 7.7%; b) w = 9.4%; c) w = 9.9%; d) w = 11.1%.

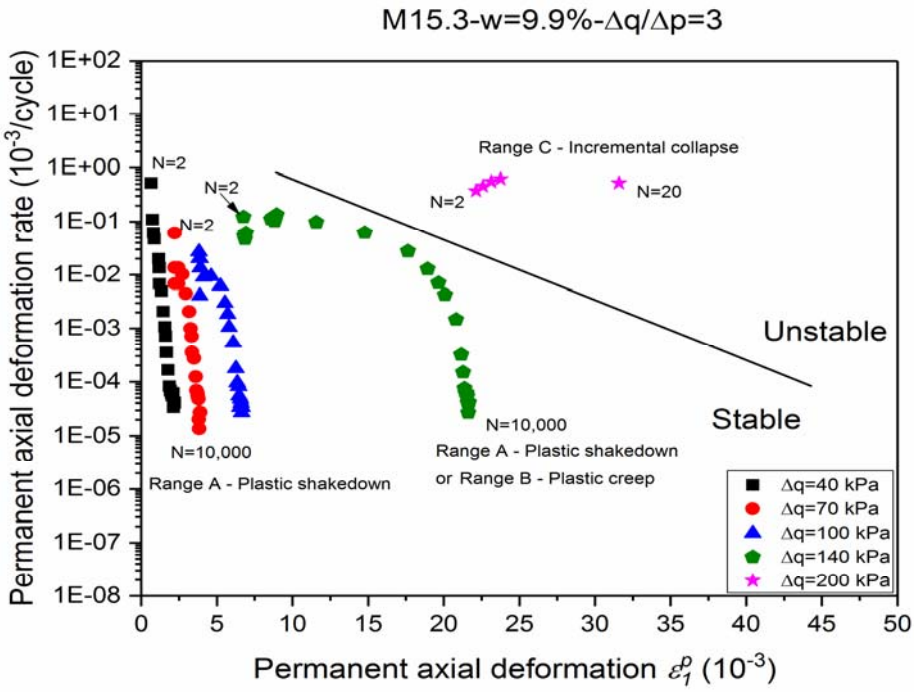

c)

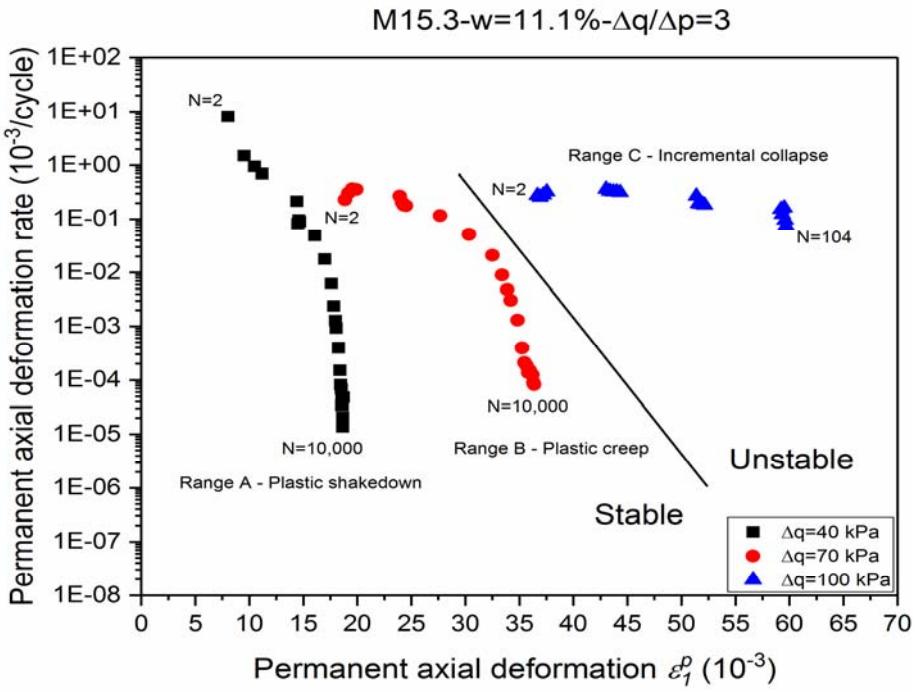

d)

Figure V.12 – Continued

Material	w	Stress path	Δq	Deformation behaviour	State
	%	/	(kPa)		
M7.5	11.0	$\Delta q/\Delta p$ =1	40	Range A: Plastic shakedown	Stable
			60	Range A: Plastic shakedown	Stable
			80	Range A: Plastic shakedown	Stable
			120	Range A: Plastic shakedown	Stable
		$\Delta q/\Delta p$ =1.5	40	Range A: Plastic shakedown	Stable
			60	Range A: Plastic shakedown	Stable
			80	Range A: Plastic shakedown	Stable
			100	Range A: Plastic shakedown	Stable
			120	Range A: Plastic shakedown	Stable
			140	Range A: Plastic shakedown	Stable
		$\Delta q/\Delta p$ =2	40	Range A: Plastic shakedown	Stable
			60	Range A: Plastic shakedown	Stable
			80	Range A: Plastic shakedown	Stable
			100	Range A: Plastic shakedown	Stable
			120	Range A: Plastic shakedown or Range B: Plastic creep	Stable
			140	Range B: Plastic creep or Range C - Incremental collapse	Unstable
		$\Delta q/\Delta p$ =3	40	Range A: Plastic shakedown	Stable
			60	Range A: Plastic shakedown	Stable
			70	Range A: Plastic shakedown	Stable
			80	Range C - Incremental collapse	Unstable

Table V.2. Classification of shakedown behaviour and state for Missillac sand M7.5 in multi-stage tests

Material	Stress path	w	Δq	Deformation behaviour	State
	/	%	(kPa)		
M15.3	$\Delta q/\Delta p=3$	7.7	40	Range A: Plastic shakedown	Stable
			70	Range A: Plastic shakedown	Stable
			100	Range A: Plastic shakedown	Stable
			140	Range A: Plastic shakedown	Stable
			200	Range C - Incremental collapse	Unstable
		9.4	40	Range A: Plastic shakedown	Stable
			70	Range A: Plastic shakedown	Stable
			100	Range A: Plastic shakedown	Stable
			140	Range A: Plastic shakedown	Stable
			200	Range C - Incremental collapse	Unstable
		9.9	40	Range A: Plastic shakedown	Stable
			70	Range A: Plastic shakedown	Stable
			100	Range A: Plastic shakedown	Stable
			140	Range A: Plastic shakedown or Range B: Plastic creep	Stable
			200	Range C - Incremental collapse	Unstable
		11.1	40	Range A: Plastic shakedown	Stable
			70	Range B: Plastic creep	Stable
			100	Range C - Incremental collapse	Unstable

Table V.3. Classification of shakedown behaviour and state for Missillac sand M15.3 in multi-stage tests

V.3.2. Discussion: the unstable state

Based on the results above, the concluded states of each stress level for all tests are plotted in Δp - Δq - s/s^* space and stable states (maximum stress level) for each test could be linked as a boundary line as shown in *Figure V.13*. This boundary line is very meaningful, because it could be used to distinguish the stable and unstable state for these two materials with different

fine contents at various water contents and various stress states (stress path and stress level). We can also imagine that, if more test results with different fine contents, different water contents and different stress states can be added to what we have tested, the boundary line will become a boundary surface separating the space as stable and unstable state.

In addition, we know that there is no significant difference of stabilized permanent axial deformation between a stress level in multi-stage tests and this stress level applied directly as a single-stage test based on Gidel's study, but it is still important to note that the unstable state could be postponed in practice due to the stiffness hardening during the loading procedures with different stress levels. This influence can be eliminated by some additional single-stage tests.

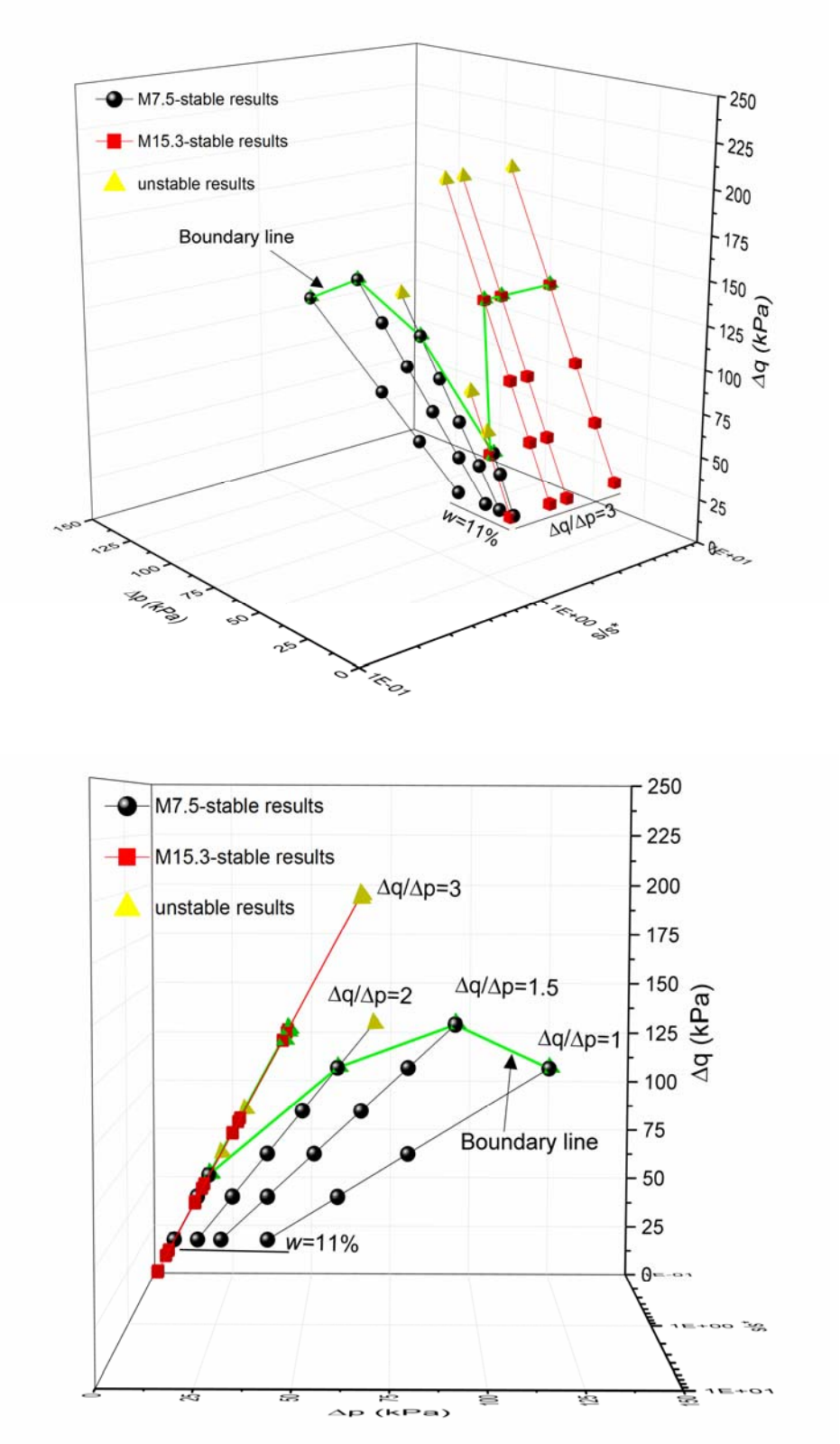

Figure V.13. Soil states in Δp - Δq - s/s space*

V.4. Conclusion

This chapter presents the shakedown analysis for Missillac sand with three different fine contents at various water contents based on the single-stage and multi-stage tests. The results led to the following findings:

- It is possible to classify the shakedown categories for permanent axial deformation behaviour based on the criterions like: the accumulated permanent axial deformation, the permanent axial deformation rate and the recoverable axial deformation.
- A proposed exponential function can describe the correlation between the minimum permanent axial deformation rate after a large number of loading cycles and the s/s^* value correctly.
- The strong relationship between permanent axial deformation and the recoverable axial deformation is observed. As a result, the M_{re} can be predicted effectively as a function of the number of cycles and the s/s^* value.
- Based on the shakedown categories, the stable and unstable states are defined and a boundary line between these two states is found in Δp - Δq - s/s^* space. This boundary line can be compared also to the static rupture line. In the future, the soil state may be determined only by the stress state and the suction value and this finding can reduce the number of tests required to predict the pavement rutting.

CONCLUSIONS AND PERSPECTIVES

In practice, low-traffic pavements are subjected to variable mechanical and hydraulic loadings. Under the successive loading and unloading cycles, particles damage may accidentally occur which leads to fine content changes and the various moisture content may cause unsaturated state changes. However, most current pavement design methods do not consider the variations above which have a significant influence on the stiffness of the granular material layers in low traffic pavements.

In this context, we try to estimate the hydromechanical behaviour (deformation behaviour mainly) of granular materials under repeated loading and unloading cycles taking into consideration the coupled effects of water content and fine content representing different unsaturated states.

The repeated load triaxial test (RLTT) is widely used to study the granular materials in pavement. In this study, a series of RLTTs are conducted with the different remolded Missillac sand samples at different water contents and fine contents to characterize the permanent and resilient deformation behaviour.

Besides, the soil water retention curves (SWRCs) of Missillac sands with different fine contents are investigated by the measurement of soil suction. Based on the SWRCs, a suction value corresponding to the intersection point of wetting and drying paths is defined as s^* which is related to fine content. The results show that the SWRCs for three different fine contents coincide together in wetting path in the s/s^* plane.

Based on the characterization of hydromechanical behaviour of Missillac sand under repeated loading by RLTTs and measurement of soil suction, the findings are summarized as follows:

- Permanent deformation behaviour of a granular material
    - The permanent axial deformation increases with the increase of the water content, while the influence of fine content depends on the initial water content and the water sensitivity of fine particles. Increasing the stress path and the stress level leads to an increase of the permanent axial deformation.
    - The permanent axial deformation could be related to suction values: a unique curve defining the variation of the permanent axial deformation with s/s^* value is proposed.
    - A new proposed empirical-analytical model taking into account the effects of water content, fine content and number of cycles and stress state shows a good capacity to evaluate the permanent axial deformation.
    - Another proposed empirical-analytical model based on the suction value has similar accuracy but two less parameters comparing with the above-mentioned model which depends on water content and fine content.

These findings are helpful for an easier interpretation of dual variation of the permanent axial deformation with the water content and the fine content in unsaturated soil. These two proposed models could reduce the number of tests required to predict the soil permanent axial deformation.

- Resilient deformation behaviour of a granular material
    - The resilient volumetric and deviatoric deformation increase with the increase of water content, especially for the high fine content samples.

- The effect of fine content on resilient deformation behaviours is not significant when the fine content increases from 4% to 7.5%, while resilient volumetric and deviatoric deformation increase obviously with an increase of fine content from 7.5% to 15.3%.
- The maximum resilient volumetric and deviatoric deformation could be predicted by the exponential functions respectively based on the *s*/*s** values.
- A modified Boyce-Hornych model is proposed with the anisotropy effect caused by incomplete elastic behavior, which accommodates to a larger scope of fine content and water content.
- A discussion is introduced to improve the modified Boyce-Hornych model based on effective stress concept for predicting resilient volumetric and deviatoric deformation.

The findings are useful to understand the evolution of resilient deformation behavior of unsaturated granular materials with the coupled effects: water content, fine content. The proposed models can describe resilient deformation behavior effectively.

- Shakedown behaviour of a granular material
  - The shakedown categories of permanent axial deformation bahviour can be classified based on the criterions such as: the accumulated permanent axial deformation, the permanent axial deformation rate and the recoverable axial deformation.
  - A proposed exponential function could describe the correlation between minimum permanent axial deformation rate after a large number of loading cycles with s/s* values.
  - Based on the classification shakedown categories, the boundary separates the stable and unstable states is obtained in Δp - Δq - *s*/*s** space.

These findings are meaningful to control and limit the pavement rutting. Furthermore, the soil state could be determined only by the stress state and the suction value.

As summarized above, this research has resulted in a better understanding of the deformation behaviour of an unsaturated granular material under repeated loading. However, there are still some potential future studies to be continued:

- As shown in previous permanent deformation behaviour, the fine particles are very sensitive to water content changes and to avoid the controversial effect of the water sensitivity, the determination of the optimum fine content (especially close to saturated state) may be helpful for the pavement design.
- The *s*/*s** values shows good interpretations in permanent and resilient deformation behaviour instead of water content and fine content. However, the definition of *s** needs more clarification.
- The developed models of short term and long term deformation behaviour should be implemented in finite element modelling together to predict the evolution of pavement rutting.
- The coupled effects on hydromechanical behaviour of unbound granular material (UGM) should be studied following the same methods and compared with Missillac sand.

BIBLIOGRAPHY

Allen, J. (1973). The effect of non-constant lateral pressures of the resilient response of granular materials. Doctoral thesis, University of Illinois at Urbana-Champaign.

Allen, J. J., & Thompson, M. R. (1974). Resilient response of granular materials subjected to time dependent lateral stresses. Transportation Research Record, 510, 1-13.

Allou, F. (2006). Un modèle élastoplastique pour la modélisation de l'orniérage des chaussées a faible trafic. Doctoral thesis, University of Limoges.

Allou, F., Petit, C., Chazallon, C., & Hornych, P. (2010). Shakedown approaches to rut depth prediction in low-volume roads. Journal of Engineering Mechanics. 136(11), 1422–1434.

Alonso, E. E., Pereira, J. M., Vaunat, J., & Olivella, S. (2010). A microstructurally based effective stress for unsaturated soils. Géotechnique, 60(12), 913–925.

Araya, A. A. (2011). Characterization of unbound granular materials for pavements. Doctoral thesis, Delft University of Technology.

Arsenie, I. M. (2009). Interprétation en contraintes effectives du comportement réversible des matériaux granulaires compactés non-saturés sous sollicitations triaxiales cycliques. Projet de fin d'etudes. INSA-Strasbourg.

Balay, J., Correia, A. G., Jouve, P., Hornych, P., Paute J. L. (1998). Etude expérimentale et modélisation du comportement mécanique des graves non traitées et des sols supports de chaussées. Dernières avancées, Bulletin Des Laboratoires Des Ponts Et Chaussees, 216, 3–18.

Barksdale, R. D. (1972). Laboratory evaluation of rutting in basecourse materials. Proceeding of 3rd International Conference on the Structure Design of Asphalt Pavements, London, 161–174.

Barksdale, R. D., & Itani, S. Y. (1989). Influence of aggregate shape on base behaviour. Transportation Research Record, 1227, 173–182.

Barksdale, R. D. (1991). The aggregate handbook. National Stone Association, Washington, D.C.

Bear, J. (1969). Dynamics of fluids in porous media. Elsevier, Amsterdam.

Benahmed, N., Nguyen, T. K., Hicher, P. Y., & Nicolas, M. (2015). An experimental investigation into the effects of low plastic fines content on the behavior of sand/silt mixtures. European Journal of Environmental and Civil Engineering, 19(1), 109–128.

Benmahmoud, A. (2010). Modélisation des chaussés construites par des matériaux granulaires compactés non saturés. Master's thesis. University of Nancy.

Bilodeau, J. P., & Doré, G. (2012). Water sensitivity of resilient modulus of compacted unbound granular materials used as pavement base. International Journal of Pavement Engineering, 13(5), 459–471.

Bishop, A. W., & Blight, G. E. (1963). Some aspects of effective stress in saturated and unsaturated soils. Géotechnique, 3, 177–197.

Bonaquist, R. F., & Witczak, M. W. (1997). A comprehensive constitutive model for granular materials in flexible pavement structures. Proceeding Eighth International Conference on Asphalt Pavements, Seattle, Washington. 1, 783–802.

Boyce, J. R., Brown, S. F., & Pell, P. S. (1976). The resilient behaviour of a granular material under repeated loading. Proceeding of the Eighth ARRB Conference: Materials Construction & Maintenance, 8, Part 3, 1–12.

Boyce, H. R. (1980). A non-linear model for the elastic behaviour of granular materials under repeated loading. Proceeding of International Symposium on Soils under Cyclic and Transient loading, Swansea, UK, 285-294.

Brooks, R.H., & Corey, A.T. (1964). Hydraulic properties of porous media. Hydrology paper, No. 3 Fort Colins, Colo: The Department of Civil Engineering, Colorado State University.

Brown, S. F., & Hyde, A. F. L. (1975). Significance of cyclic confining stress in repeated load triaxial testing of granular material. Transportation Research Record, 537, 49–58.

Brown, S. F., & Pell, P. S. (1967). An experimental investigation of the stresses, strains and deflections in a layered pavement structure subjected to dynamic loads. Proceeding of the Second International Conference of Structure Design of Asphalt Pavements, Ann Arbor, USA, 487-504.

Caicedo, B., Coronado, O., Fleureau, J. M., & Correia, A. G. (2009). Resilient behavior of non standard unbound granular materials. Road Materials and Pavement Design, 10(2), 287–312.

Cary, C. E., & Zapata, C. E. (2011). Resilient modulus for unsaturated unbound materials. Road Materials and Pavement Design, 12(3), 615–638.

Cerni, G., Corradini, A., Pasquini, E., & Cardone, F. (2015). Resilient behaviour of unbound granular materials through repeated load triaxial test: influence of the conditioning stress, Road Materials and Pavement Design, 16(1), 70–88.

Chan, F. W. K. (1990). Permanent deformation resistance of granular layers in pavements. Doctoral thesis, Department of Civil Engineering, University of Nottingham at Nottingham, England.

Chang, D. S., Zhang, L. M., & Xu, T. H. (2012). Laboratory investigation of initiation and development of internal erosion in soils under complex stress states. Proceedings of the 6th Conference on Scour and Erosion, Paris: 895–902.

Chazallon, C., Koval, G., Hornych, P., Allou, F., & Mouhoubia, S. (2009). Modelling of rutting of two flexible pavements with the shakedown theory and the finite element method. Computers and Geotechnics, 36(5), 798–809.

Chen, Q. M., Abu-Farsakh, M., Voyiadjis, G. Z., & Souci, G. (2013). Shakedown analysis of geogrid-reinforced granular base material. Journal of Materials in Civil Engineering, 25(3), 337–346.

Childs, E. C. (1969). An introduction to the physical basis of soil water phenomena. A Wiley-Interscience Publication, JOHN WILEY & SONS, INC.

Collins, I. F., Wang, A. P., & Saunders, L. R. (1993). Shakedown theory and the design of unbound pavements. ARRB, Road and Transport Research, 2(4), 28-37.

Coronado, O., Fleureau, J. M., Gomes-Correia, A., & Caicedo, B. (2004). Influence de la succion sur les propriétés de matériaux granulaires routiers. 57e Congrès canadien de géotechnique.

Coronado, O., Caicedo, B., Taibi, S., Gomes-Correia, A., Souli, H., & Fleureau, J. M. (2016). Effect of water content on the resilient behavior of non standard unbound granular materials. Transportation Geotechnics, 7, 29-39.

Coussy, O., & Dangla, P. (2002). Mécanique des sols non saturés, Chapter 4-Approche énergétique du comportement des sols non saturés, 137-174.

Dash, H. K., Sitharam, T. G., & Baudet, B. A. (2010). Influence of non plastic fines on the response of a silty sand to cyclic loading. Soils and Foundations, 50, 695-704.

Davalle, E. M. (1991). Modèle numérique du comportement d'un sol liquéfiable sous sollicitations dynamiques. Doctoral thesis, Ecole Polytechnique Fédérale de Lausanne, EPFL.

Dawson, A. R. (1990). Introduction to soils & granular materials. Lecture Notes from Residential Course, Bituminous Pavements: materials, design and evaluation, University of Nottingham at Nottingham, England.

Dehlen, G. L. (1969). The effect of non-linear material response on the behaviour of pavements subjected to traffic loads. Doctoral thesis, University of California.

Delage, P., & Cui, Y. J. (2000). L'eau dans les sols non saturés. Article Technique de l'ingénieur. RÉF: C301 V1.

Duong, T. V., Tang, A. M., Cui, Y. J., Trinh, V. N., Dupla, J. C., Calon, N., Canou, J., & Robinet A. (2013). Effects of fines and water contents on the mechanical behavior of interlayer soil in ancient railway sub-structure. Soils and Foundations, 53(6), 868–878.

Duong, T. V., Cui, Y. J., Tang, A. M., Dupla, J. C., & Calon, N. (2014). Effect of fine particles on the hydraulic behavior of interlayer soil in railway substructure. Canadian Geotechnical Journal, 51(7), 735–746.

Duong, T. V., Cui, Y. J., Tang, A. M., Dupla, J. C., Canou, J., Calon, N., & Robinet, A. (2016). Effects of water and fines contents on the resilient modulus of the interlayer soil of railway substructure. Acta Geotechnica, 11(1), 51–59.

Dunlap, W. A. (1963). A report on a mathematical model describing the deformation characteristics of granular materials. Technical report No. 1, Project 2-8-62-27, Texas Transportation Institute.

Fleureau, J. M., Hadiwardoyo, S., & Gomes Correia, A. (2003). Generalised effective stress analysis of strength and small strains behaviour of a silty sand, from dry to saturated state. Soils and Foundations, 43(4), 21–33.

Fredlund, D. G., & Morgenstern, N. R. (1977). Stress state variables for unsaturated soils. Journal of the Geotechnical Engineering Division- ASCE, 103(5), 447–466 .

Fredlund, D. G., & Rahardjo, H. (1993). Soil mechanics for unsaturated soils. A Wiley-Interscience Publication, JOHN WILEY & SONS, INC.

Fredlund, D. G., & Xing, A. (1994). Equations for the soil-water characteristic curve. Canadian Geotechnical Journal, 31(4), 521–532.

Gardner, R. (1958). Some steady state solutions of unsaturated moisture flow equations with applications to evaporation from a water table. Soil Science, 85(4), 228–232.

Gidel, G., Breysse, D., Hornych, P., Chauvin, J. J., & Denis, A. (2001). A new approach for investigating the permanent deformation behavior of unbound granular material using the repeated load triaxial apparatus. Bulletin Des Laboratoires Des Ponts Et Chaussees. 233, 5–21.

Gidel, G., Breysse, D., & Denis, A. (2002). Influence de l'état hydrique et des sollicitations routières sur l'évolution du comportement des graves non traitées calcaires utilisées en assise de chaussée. Revue Française De Génie Civil, 6(5), 789–799.

GOMES CORREIA, A. (1985). Contribution a l'étude mécanique des sols soumis a des chargements cycliques. Doctoral Thesis. Ecole National des Ponts et Chaussées.

Han, Z., & Vanapalli, S. K. (2015). Model for predicting resilient modulus of unsaturated subgrade soil using soil-water characteristic curve. Canadian Geotechnical Journal, 52,1–15.

Han, Z., & Vanapalli, S. K. (2016). State-of-the-Art: Prediction of Resilient Modulus of Unsaturated Subgrade Soils. International Journal of Geomechanics, 16(4), 1–15.

Haynes, J. G., & Yoder, E. J. (1963). Effects of repeated loading on gravel and crushed stone base course materials used in the AASHO Road Test. Highway Research Record, No. 39.

Hicks, R. G. (1970). Factors influencing the resilient properties of granular materials. Doctoral thesis, University of California.

Hicks, R. G., & Monismith, C. L. (1971). Factors influencing the resilient properties of granular materials. Highway Research Record, No. 345,15–31.

Ho, X. N. (2013). Comportement hydromécanique des matériaux granulaires compactés non saturés. Doctoral thesis, University of Strasbourg.

Ho, X. N., Nowamooz, H., Chazallon, C., & Migault, B. (2014a). Effect of hydraulic hysteresis on low-traffic pavement deflection. Road Materials and Pavement Design, 15(3), 642–658.

Ho, X. N., Nowamooz, H., Chazallon, C., & Migault, B. (2014b). Effective stress concept for the effect of hydraulic hysteresis on the resilient behavior of low traffic pavements. International Journal of Pavement Engineering, 16(9), 842–856.

Ho, X. N., Nowamooz, H., Chazallon, C., & Migault, B. (2014c). Influence of fine content and water content on the resilient behavior of a natural compacted sand. Road Materials and Pavement Design, 15(3), 606–621.

Hornych, P., Corte, J. F., & Paute, J. L. (1993). Etude des déformations permanentes sous chargements répétésde trois graves non traitées. Bulletin Des Laboratoires Des Ponts Et Chaussees, 184, 45–55.

Hornych, P., Kazai, A., & Piau, J. M. (1998). Study of the resilient behavior of unbound granular material. In: Proceedings 5th conference on bearing capacity of roads and airfields, Trondheim, 3, 1277–1287.

Hornych, P., Kazai, A., & Quibel, A. (2000). Modeling a full-scale experiment of two flexible pavement structures. Unbound Aggregates in Road Construction, Rotterdam, 359-367.

Hornych, P., Chazallon, C., Allou, F., & Abd, El, A. (2007). Prediction of permanent deformations of unbound granular materials in low traffic pavements. Road Materials and Pavement Design, 8(4), 643–666.

Jennings, J. E. B., & Burland, J. B. (1962). Limitations to the use of effective stresses in partly saturated soils. Géotechnique, 1, 125–144.

Jing, P., Nowamooz, H., & Chazallon, C. (2017 in press). Permanent deformation behaviour of a granular material used in low traffic pavements. Road Materials and Pavement Design. DOI: 10.1080/14680629.2016.1259123

Johnson, K. L. (1986). Plastic flow, residual stresses and shakedown in rolling contacts. Proceedings of the 2nd International Conference on Contact Mechanics and Wear of Rail/Wheel Systems, University of Rhode Island, Waterloo Ontario.

Jorenby, B. N., & Hicks, R. G. (1986). Base course contamination limits. Transportation Research Record, 1095, 86–101.

Kamal, M. A., Dawson, A. R., Farouki, O. T., Hughes, D. A. B., & Sha'at, A. A. (1993). Field and laboratory evaluation of the mechanical behaviour of unbound granular materials in pavements. Transportation Research Record, 1406, 88–97.

Karasahin, M. (1993). Resilient behaviour of granular materials for analysis of highway pavements. Doctoral thesis, University of Nottingham.

Khalili, N., & Khabbaz, M. H. (1998). A unique relationship for x for the determination of shear strength of unsaturated soils. Geotechnique, 48(5), 681–688.

Khedr, S. (1985). Deformation characteristics of granular base course in flexible pavement. Transportation Research Record, (1043), 131–138.

Kolisoja, P. (1997). Resilient deformation characteristics of granular materials. Doctoral thesis. Tampere University of Technology.

Kolisoja, P., Saarenketo, T., Peltoniemi, H., & Vuorimies, N. (2002). Laboratory testing of suction and deformation properties of base course aggregates. Transportation Research Record: Journal of the Transportation Research Board, 1787, 83-89.

Kool, J. B., & Parker, J. C. (1987). Development and evaluation of closed-form expressions for hysteretic soil hydraulic properties. Water Resources Research. 23(1), 105–114.

Korkiala-Tanttup, L. (2005). A new material model for permanent deformations in pavements. In 7th Conference on Bearing Capacity of Roads and Airfields, V1–V12.

Lashine, A. K., Brown, S. F., & Pell, P. S. (1971). Dynamic properties of soils. Report No. 2 Submitted to Koninklijke/Shell Laboratorium, Department of Civil Engineering, University of Nottingham at Nottingham, England.

Lee, I. K. (1968). Soil mechanics - selected tropics. Butterworth, London, England, 67–73.

Lekarp, F. (1997). Permanent deformation behaviour of unbound granular materials; Licentiate Thesis, Kungl Tekniska Högskolan.

Lekarp, F., & Dawson, A. (1998). Modelling permanent deformation behavior of unbound granular materials. Construction and Building Materials, 12(1), 9–18.

Lekarp, F., Isacsson, U., & Dawson, A. (2000a). State of the Art. I: Resilient response of unbound aggregates. Journal of Transportation Engineering, 126(1), 66–75.

Lekarp, F., Isacsson, U., & Dawson, A. (2000b). State of the Art. II: Permanent strain response of unbound aggregates. Journal of Transportation Engineering, 126(1), 76–83.

Liang, R. Y., Rabab'ah, S., & Khasawneh, M. (2008). Predicting moisture-dependent resilient modulus of cohesive soils using soil suction concept. Journal of Transportation Engineering, 1(34), 34–40.

Likos, W. J., & Lu, N. (2004). Hysteresis of capillary stress in unsaturated granular soil. Journal of Engineering Mechanics. 130(6), 646 –655.

Mckee, C. R., & Bumb, A. C. (1984). The importance of unsaturated flow parameters in designing a hazardous waste site. In Hazardous Waste and Environmental Emergencies, Hazardous Materials Control Research Institute National Conference, Houston, Tex., 12–14 March 1984. Hazardous Materials Control Research Institute, Silver Spring, Md. 50–58.

Mckee, C. R., & Bumb, A. C. (1987). Flow-testing coalbed methane production wells in the presence of water and gas. Society of Petroleum Engineers (SPE) Formation Evaluation, Richardson, Tex. 599–608.

Mitry, F. G. (1964). Determination of the modulus of resilient deformation of untreated base course materials. Doctoral thesis, University of California at Berkeley.

Mohammad, L. N., Herath, A., Rasoulian, M., & Zhang, Z. J. (2006). Laboratory evaluation of untreated and treated pavement base materials: repeated load permanent deformation test. Transportation Research Record: Journal of the Transportation Research Board, 1967, 78–88.

Monismith, C. L., Seed, H. B., Mitry, F. G., & Chan, C. K. (1967). Prediction of pavement deflections from laboratory tests. Proceeding of Second International Conference Structure Design of Asphalt Pavements, Ann Arbor, USA, 109–140.

Morgan, J. R. (1966). The response of granular materials to repeated loading. Proceeding of 3rd International Conference ARRB, 1178-1192.

Ng, C. W. W., Zhou, C., Yuan, Q., & Xu, J. (2013). Resilient modulus of unsaturated subgrade soil: experimental and theoretical investigations. Canadian Geotechnical Journal, 50(2), 223–232.

Nowamooz, H., Chazallon, C., Arsenie, M. I., Hornych, P., & Masrouri, F. (2011). Unsaturated resilient behavior of a natural compacted sand. Computers and Geotechnics, 38(4), 491–503.

Nowamooz, H., Ho, X. N., Chazallon, C., & Hornych, P. (2013). The effective stress concept in the cyclic mechanical behavior of a natural compacted sand. Engineering Geology, 152(1), 67–76.

Nur, A., & Byerlee, J. D. (1971). An exact effective stress law for elastic deformation of rock with fluids. Journal of Geophysical Research, 76(26), 6414–6419.

Odermatt, N., Wiman, L. G., Arm, M., & Magnusson, R. (2004). Deformation of unbound pavement materials – heavy vehicle simulator and cyclic load triaxial tests. 2nd International Conference on the Accelerated Pavement Testing, Minneapolis. 20p

Okamura, M., & Noguchi, K. (2009). Liquefaction resistances of unsaturated non-plastic silt. Soils and Foundations, 49(2), 221–229.

Pappin, J. W. (1979). Characteristics of granular material for pavement analysis. Doctoral thesis, Department of Civil Engineering, University of Nottingham, England.

Parker, J. C., & Lenhard, J. R. (1987). A model for hysteretic constitutive relations governing multiphase flow, 1. Saturation pressure relations. Water Resources Research, 23(12), 2187–2196.

Pereira, J. H. F., & Fredlund, D. G. (2000). Volume change behavior of collapsible compacted gneiss soil. Journal of Geotechnical and Geo Environmental Engineering, 126, 907–916.

Puppala, A. J., Mohammad, L. N., & Alen. A. (1999). Permanent deformation characterization of subgrade soils from RLT test. Journal of Materials in Civil Engineering, 11, No. 4, 274–282.

Puppala, A. J., Saride, S., & Chomtid, S. (2009). Experimental and modeling studies of permanent strains of subgrade soils. Journal of Geotechnical and Geoenvironmental Engineering, 135(10), 1379–1389.

Raad, L., Weichert, D., & Haidar, A. (1989). Shakedown and fatigue of pavements with granular bases. Transportation Research Record, 1227, 159–172.

Robinson, R. G. (1974). Measurement of the elastic properties of granular materials using a resonance method. TRRL Supplementary Report. No. 111UC.

Salour, F., & Erlingsson, S. (2015a). Resilient modulus modelling of unsaturated subgrade soils: laboratory investigation of silty sand subgrade. Road Materials and Pavement Design, 16(3), 553–568.

Salour, F., & Erlingsson, S. (2015b). Permanent deformation characteristics of silty sand subgrades from multistage RLT tests. International Journal of Pavement Engineering. doi:10.1080/10298436.2015.1065991.

Seed, H. B., Mitry, F. G., Monismith, C. L., & Chan, C. K. (1967). Prediction of flexible pavement deflections from laboratory repeated load tests. The National Cooperative Highway Research Program (NCHRP) Report. No. 35.

Seif El Dine, S., Dupla, J., Frank, R., Canou, J., & Kazan, Y. (2010). Mechanical characterization of matric coarse-grained soils with a large-sized triaxial device. Canadian Geotechnical Journal, 47(4), 425–438.

Seyhan, U., Tutumluer, E., & Yesilyurt, H. (2005). Anisotropic aggregate base inputs for mechanistic pavement analysis considering effects of moving wheel loads. Journal of Materials in Civil Engineering, American Society of Civil Engineers, 17(5), 1–8.

Sharp, R. W., & Booker, J. R. (1984). Shakedown of pavements under moving surface loads. Journal of Transportation Engineering, 110(1), 1–14.

Sharp, R. (1985). Pavement design based on shakedown analysis. Transportation Research Board, 1022, 99–107.

Skempton, W. A. (1961). Effective stress in soils, concrete and rocks. Conference on Pressure and Suction in Soils, London, 4–16.

Smith,W. S., & Nair, K. (1973). Development of procedures for characterization of untreated granular base course and asphalt-treated base course materials. Federal Highway Admin., Report No. FHWA-RD-74-61, Washington, D.C.

Soliman, H., & Shalaby, A. (2015). Permanent deformation behavior of unbound granular base materials with varying moisture and fines content. Transportation Geotechnics, 4(C), 1–12.

Song, Y., & Ooi, P. (2010). Interpretation of shakedown limit from multistage permanent deformation tests. Transportation Research Record: Journal of the Transportation Research Board, 2167, 72–82.

Sweere, G. T. H. (1990). Unbound granular bases for roads. Doctoral thesis, University of Delft.

Tao, M., Mohammad, L. N., Nazzal, M. D., Zhang, Z., & Wu, Z. (2010). Application of shakedown theory in characterizing traditional and recycled pavement base materials. Journal of Transportation Engineering, 136(3), 214–222.

Terzaghi, K. (1923). Die Berechnung der Durchl¨assigkeitsziffer des Tones aus dem Verlauf der hydrodynamische Spannungserscheinungen, Sitzber. Akad. Wiss. Wien, Abt. IIa, 132, 125–138.

Thom, N. H., & Brown, S. F. (1987). Effect of moisture on the structural performance of a crushed-limestone road base. Transportation Research Record, 1121, 50–56.

Thom, N. H., & Brown, S. F. (1988). The effect of grading and density on the mechanical properties of a crushed dolomitic limestone. Proceeding of 14th ARRB Conference, Part 7, 94–100.

Toll, D. G. (2012). The behaviour of unsaturated soils. Chapter 5 in Handbook of Tropical Residual Soil Engineering, (eds. Huat, B.B.K., Toll, D.G. & Prasad, A.) London: Taylor and Francis.

Trinh, V. N., Tang, A. M., Cui, Y. J., Dupla, J. C., Canou, J., Calon, N., et al. (2012). Mechanical characterisation of the fouled ballast in ancient railway track substructure by large-scale triaxial tests. Soils and Foundations, 52(3), 511–523.

Trollope, E. H., Lee, I. K., & Morris, J. (1962). Stresses and deformation in two-layer pavement structures under slow repeated loading. Proceeding of ARRB, 1, Part 2, 693–718.

Tsukamoto, Y., Kawabe, S., Matsumoto, J., & Hagiwara, S. (2014). Cyclic resistance of two unsaturated silty sands against soil liquefaction. Soils and Foundations, 54(6), 1094–1103.

Unno, T., Kazama, M., Uzuoka, R., & Sento, N. (2008). Liquefaction of unsaturated sand considering the pore air pressure and volume compressibility of the soil particle skeleton. Soils and Foundations, 48(1), 87–99.

Uthus, L., Hermansson, Å., Horvli, I., & Hoff, I. (2006). A study on the influence of water and fines on the deformation properties and frost heave of unbound aggregates. Cold Regions Engineering, 1–13. doi: 10.1061/40836(210)65.

Uthus, L. (2007). Deformation properties of unbound granular aggregates. Doctoral thesis. Norwegian University of Science and Technology.

Uzan, J. (1985). Characterization of granular material. Transportation Research Record, 1022, 52-59.

van Genuchten, M. T. (1980). A closed-form equation for predicting the hydraulic conductivity of unsaturated soils. Soil Science Society of America Journal, 44(5), 892–898.

van Niekirk, A. A. (2002). Mechanical behaviour and performance of granular bases and sub-bases in pavements. Doctoral thesis, Delft University of Technology.

Veverka, V. (1979). Raming van de spoordiepte bij wegen met een bitumineuze verharding. De Wegentechniek. XXIV(3), 25-45.

Vuong, B. (1992). Influence of density and moisture content on dynamic stress-strain behaviour of a low plasticity crushed rock. Road and Transport Research, 1(2), 88–100.

Werkmeister, S., Dawson, A. R., and Wellner, F. (2001). Permanent deformation behavior of granular materials and the shakedown concept. Transportation Research Record: Journal of the Transportation Research Board, 1757, 75–81.

Werkmeister, S., Numrich, R., Dawson, A. R., & Wellner, F. (2003). Design of granular pavement layers considering climatic conditions. Transportation Research Record: Journal of The Transportation Research Board, 1837, 61–70.

Werkmeister, S., Dawson, A. R., & Wellner, F. (2004). Pavement design model for unbound granular materials. Journal of Transportation Engineering, 130(5), 665–674.

Werkmeister, S., Dawson, A. R., & Wellner, F. (2005). Permanent deformation behaviour of granular materials, Road Materials and Pavement Design, 6(1), 31–51.

Wheeler, S. J., Sharma, R. J., & Buisson, M. S. R. (2003). Coupling of hydraulic hysteresis and stress-strain behavior in unsaturated soils. Geotechnique, 53(1), 41–54.

Williams, J., Prebble, R. E., Williams, W. T., & Hignett, C. T. (1983). The influence of texture, structure and clay mineralogy on the soil moisture characteristic. Australian Journal of Soil Research, 21, 15–32.

Yang, S. R., Huang, W. H., & Tai, Y. T. (2005). Variation of resilient modulus with soil suction for compacted subgrade soils. Transportation Research Record, 1913, 99–106.

Yang, S. R., & Huang, W. H. (2007). Permanent deformation and critical stress of cohesive soil under repeated loading. Transportation Research Record: Journal of The Transportation Research Board, 2016, 23-30.

Yang, S. R., Huang, W. H., & Liao, C. C. (2008a). Correlation between resilient modulus and plastic deformation for cohesive subgrade soil under repeated loading. Transportation Research Record: Journal of the Transportation Research Board, 2053, 72–79.

Yang, S. R., Lin, H. D., Johnson, H. S., & Huang, W. H. (2008b). Suction-controlled laboratory test on resilient modulus of unsaturated compacted subgrade soils. Journal of Geotechnical and Geoenvironmental Engineering, 134(9), 1375–1384.

Youd, T. L. (1972). Compaction of sands by repeated shear straining. Proceeding of ASCE, Journal of Soil Mechanics and Foundation Division, 98, No.SM7, 709–725.

STANDARD

AASHTO T 307-99. (2003). Determining the resilient modulus of soils and aggregate materials.

ASTM D2487-06. (2006). Standard practice for classification of soils for engineering purposes (Unified soil classification system).

ASTM D5298-10. (1995). Standard test method for measurement of soil potential (suction) using filter paper.

NF EN 13286-4. (2003). Mélanges traités et mélanges non traités aux liants hydrauliques. Méthodes l'essai pour la masse volumique de référence et la teneur en eau en laboratoire – Marteau vibrant.

NF EN 13286-7. (2004). Melanges avec ou sans liant hydraulique Essai triaxial sous charge cyclique pour melanges sans liant hydraulique.

NF P11-300. (1992). Exécution des terrassements – Classification des matériaux utilisables dans la construction des remblais et des couches de forme d'infrastructures routières.

NF P94-068. (1993). Sols: reconnaissance et essais – Mesure de la quantité et de l'activité de la fraction argileuse – Détermination de la valeur de bleu de méthylène d'un sol par l'essai à la tache.

NF P98-230-1. (1992). Préparation des matériaux traités aux liants hydrauliques ou non traités. Fabrication des éprouvettes par vibrocompression. 8p.

SETRA-LCPC. (1994). Conception et Dimensionnement des structures de chaussées. Guide technique, France.

XP P94-041. (1995). Sols: reconnaissance et essais-Identification granulométrique-Méthode de tamisage par voie humide.

APPENDIX A. IMPROVEMENT OF RLTT MEASUREMENT DEVICE FOR UGM

In this study, we developed a set of new fixing devices for the displacement transducers on the UGM samples to fit the larger particles comparing with the sand samples.

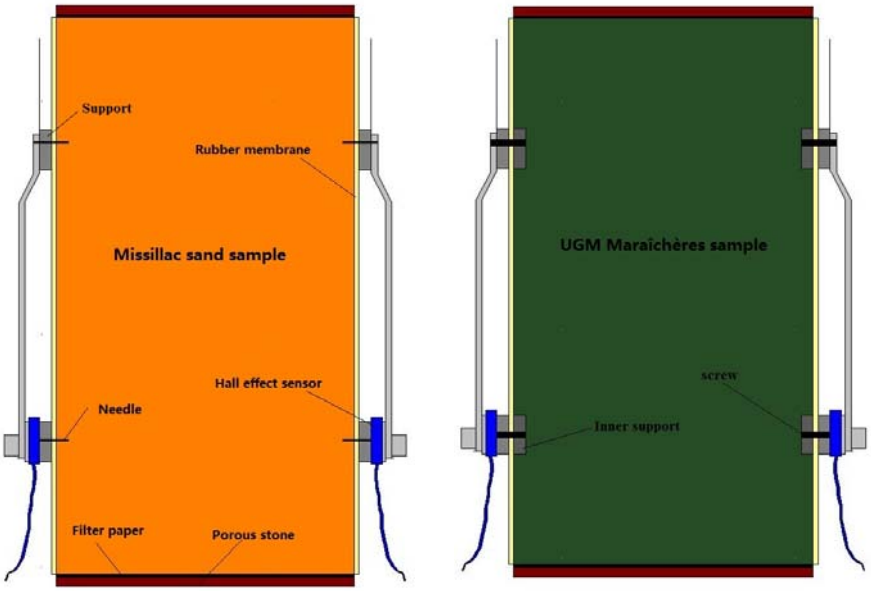

Figure A.1. Comparison of the RLTT measurement devices between the sand sample and the UGM sample

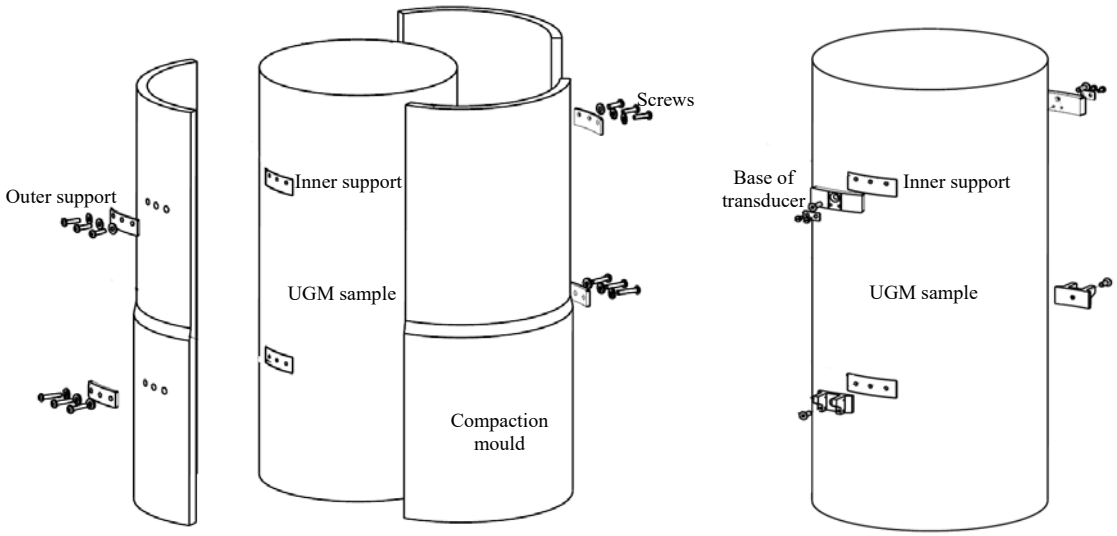

Figure A.2. Design of the fixing devices for the displacement transducers on the compaction mould and the UGM sample

Figure A.3. Photos of the fixing devices for the displacement transducers on the compaction mould

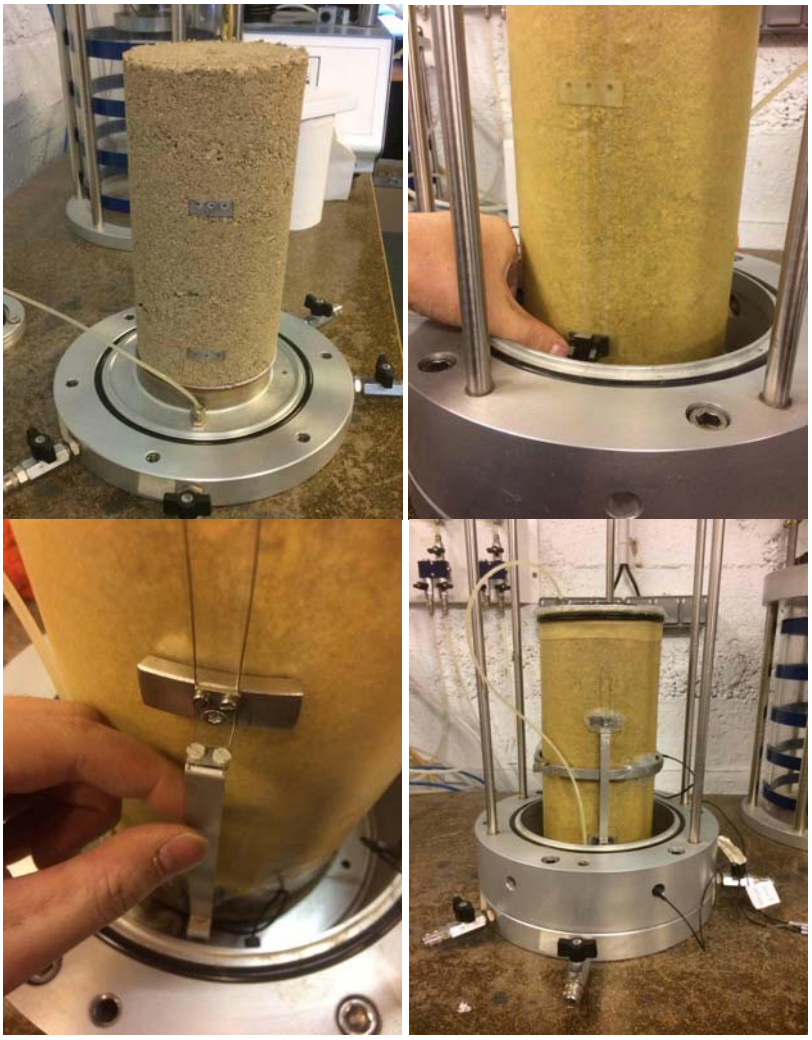

Figure A.4. Photos of the fixing devices for the displacement transducers on the UGM sample

APPENDIX B. RESULTS OF MEASUREMENT OF SOIL SUCTION AND RLTTS FOR UGM MARAICHERES

APPENDIX B.1 Results of measurement of soil suction

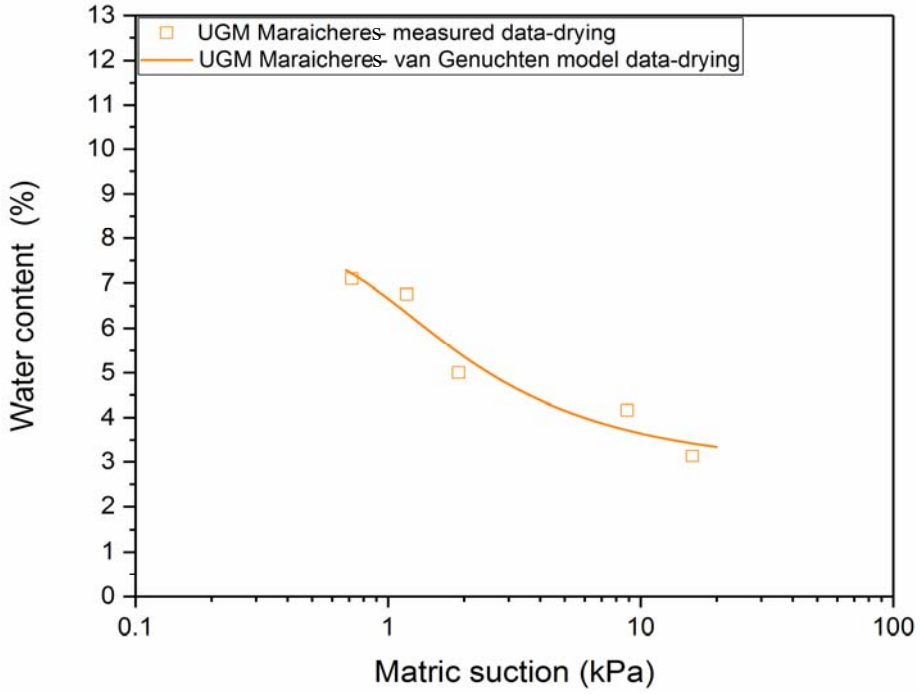

Figure B.1. Matric suction obtained by the filter paper method as well as the model prediction (UGM Maraîchères)

Parameters of van Genuchten model	Drying
α	1.252
n	2.441
m	0.318
w_s (%)	8.0
w_r (%)	3.0

Table B.1. Parameters of van Genuchten model (UGM Maraîchères)

APPENDIX B.2 Results of RLTTs

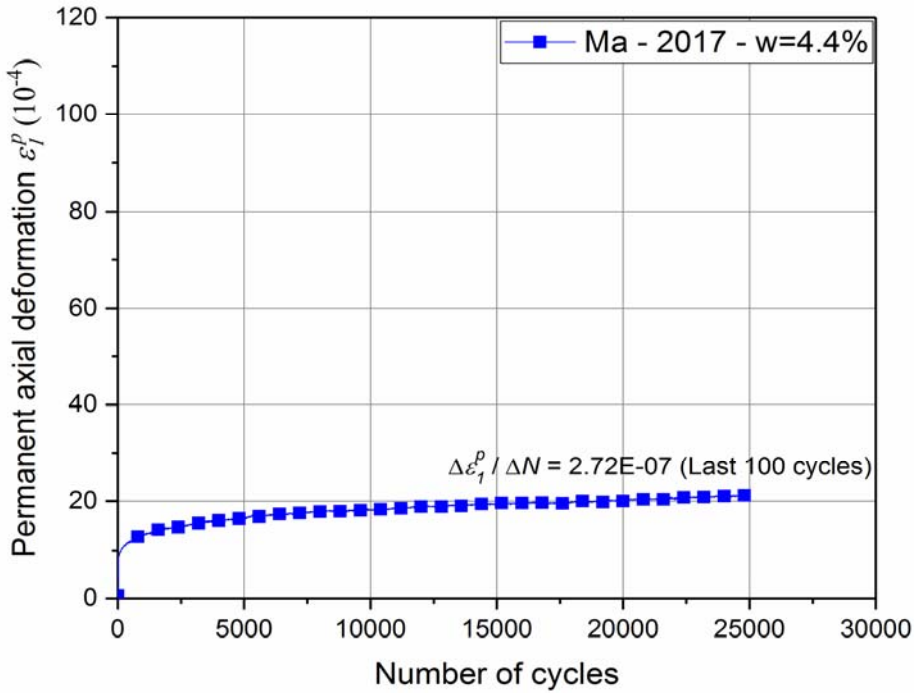

a)

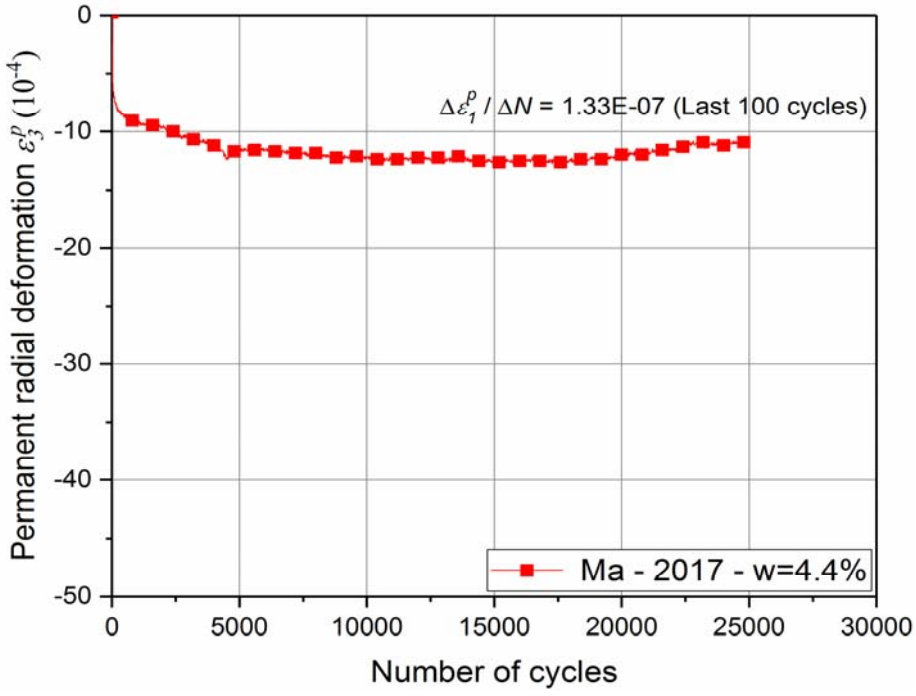

b)

Figure B.2. Evolution of permanent axial deformation ε_1^p (a) and permanent radial deformation ε_3^p (b) for UGM Maraîchères in conditioning phase

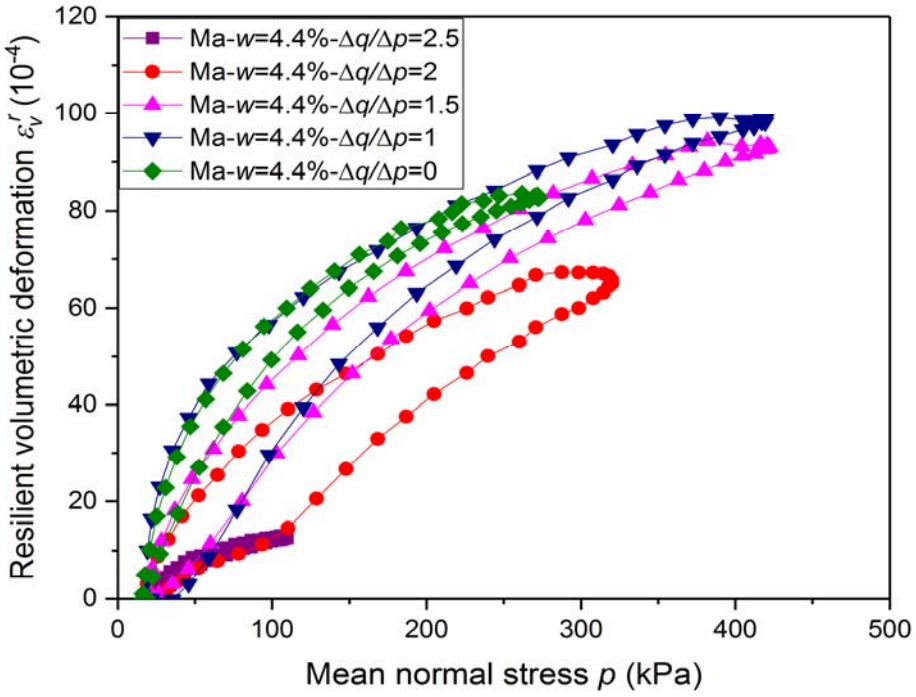

a)

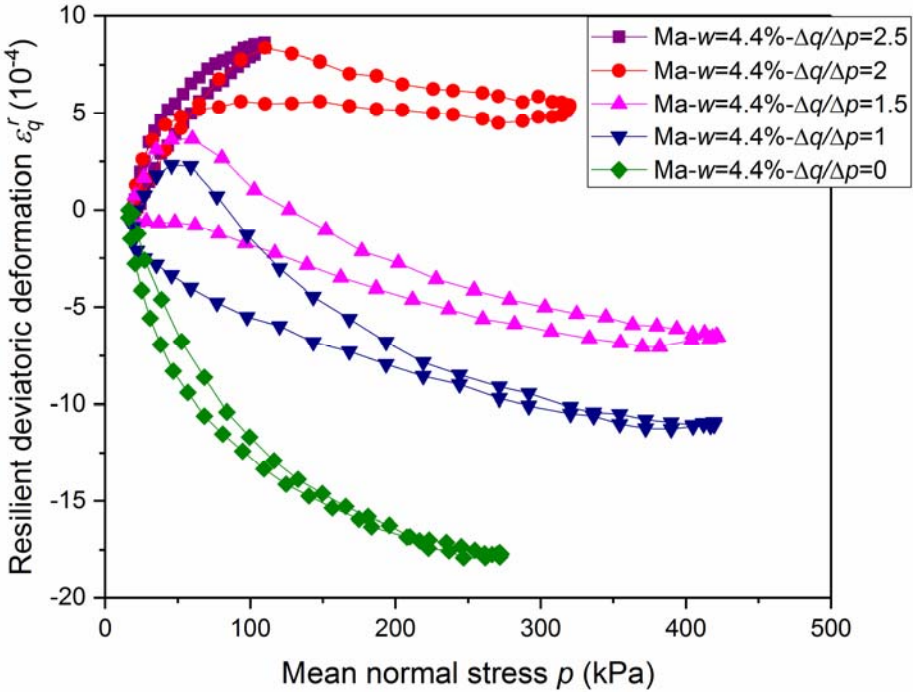

b)

Figure B.3. Evolution of resilient volumetric deformation ε_v^r (a) and resilient deviatoric deformation ε_q^r (b) for UGM Maraîchères in resilient test phase

ETUDES DE L'EFFET DES FINES ET DE LA TENEUR EN EAU SUR LE COMPORTEMENT HYDROMECANIQUE DES MATERIAUX GRANULAIRES

Doctorant: Peng JING

Directeur de Thèse: Cyrille CHAZALLON

Co-directeur de Thèse: Bernard MIGAULT

Encadrant: Hossein NOWAMOOZ

Laboratoire: Laboratoire des sciences de l'ingénieur, de l'informatique et de l'imagerie (ICube, UMR 7357, CNRS), INSA de Strasbourg, 67084, Strasbourg Cedex, France

Résumé étendu

Les matériaux granulaires sont souvent utilisés dans les chaussées à faible et moyen trafic, pour la réalisation des couches d'assise, des couches de forme et de la couche de sol support. Les sollicitations dues au trafic sont les principales causes d'endommagement de ces chaussées et conduisent à deux modes de dégradation: l'orniérage à grand rayon et la fissuration par fatigue de la couverture bitumineuse. La teneur en fines des matériaux granulaires joue un

rôle très important sur la rigidité mécanique et la résistance à l'endommagement des structures de chaussées soumises aux chargements répétés du trafic. L'état non saturé pour les sols, globalement défini par la pression interstitielle négative ou la succion, a une influence majeure sur les modes de dégradation des chaussées.

Objectifs de la thèse

La méthode de dimensionnement des chaussées neuves en France ne permet pas de prendre en compte correctement l'effet de la teneur en fines ou l'effet de la teneur en eau.

Dans ce contexte, nous nous sommes premièrement intéressés à l'effet de la teneur en fines sur le comportement mécanique en déformations permanentes des matériaux granulaires de chaussées soumis à des chargements triaxiaux répétés, au moyen des essais de caractérisation du comportement hydromécanique. Puis, pour la modélisation analytique, nous proposons des modèles empiriques-analytiques qui permettent de prédire correctement les déformations permanentes.

Dans un deuxième temps, nous allons étudier le comportement mécanique en déformations résilientes des matériaux granulaires de chaussées soumis également à des chargements triaxiaux répétés. Par la suite, à l'aide de résultats expérimentaux, nous modifions le modèle de Boyce-Hornych pour l'adapter à toutes les teneurs en eau et les teneurs en fines.

Finalement, nous analysons les déformations permanentes, le taux de variation des déformations permanentes et les déformations réversibles pour caractériser le comportement de l'état limite des matériaux granulaires étudiés.

Organisation du mémoire

Ce mémoire a été organisé en cinq chapitres:

Le premier chapitre est essentiellement consacré à l'étude bibliographique des propriétés et du comportement hydromécanique des matériaux granulaires compactés non saturés sous l'effet des chargements répétés: le mécanisme de non saturation et le comportement cyclique des sols granulaires, les facteurs influençant le comportement permanent et le comportement résilient, les modèles classiques du comportement permanent et du comportement résilient des matériaux granulaires. La théorie de l'état limite est également introduite dans ce chapitre.

Le deuxième chapitre présente premièrement les caractéristiques des matériaux granulaires étudiés. Ensuite, l'essai de succion et l'essai triaxial à chargements répétés (TCR) sont présentés pour étudier le comportement hydromécanique cyclique des matériaux granulaires: la méthode d'essai, la préparation de l'échantillon, la description des appareils et le mode opératoire des essais.

A l'aide des résultats TCR, le troisième chapitre présente l'effet de la teneur en fines et de l'état non saturé sur le comportement permanent en déformations axiales des matériaux granulaires. Pour la modélisation analytique, nous utilisons l'approche proposée par Hornych et al., 1993 pour les essais à unique palier et le cadre de Gidel et al., 2001 pour les essais à plusieurs paliers afin d'estimer la variation des déformations axiales permanentes du sable de Missillac. Deux approches sont proposées pour prédire le comportement permanent des matériaux granulaires: la première est basée sur la teneur en eau et la teneur en fines, puis la seconde est fondée sur la valeur de succion.

Le quatrième chapitre présente le comportement résilient des matériaux granulaires avec trois pourcentages de fines différents: la stabilisation de la déformation permanente, le comportement résilient, les déformations volumétrique maximales et déviatorique maximales dans le plan s/s*, ainsi que l'effet de l'anisotropie sur le comportement résilient. Pour la modélisation

analytique, un modèle de Boyce-Hornych modifié a été proposé incluant l'effet de l'anisotropie, qui prédit la déformation volumique et la déformation déviatorique. Une discussion est menée à la fin du chapitre sur le concept de contraintes effectives afin d'améliorer le modèle.

Dans le dernier chapitre, la déformation permanente, le taux de variation des déformations permanentes et réversibles a été utilisé pour caractériser le comportement de l'état limite des matériaux granulaires de chaussées. Des approches pour déterminer la contrainte critique, qui définit la limite entre des conditions stables et instables sous charges répétées, ont été développées.

Un chapitre supplémentaire 'Conclusion et perspectives' contient un résumé des conclusions de chaque chapitre et propose des perspectives à ce travail.

Un dispositif triaxial amélioré pour des graves non traitées est présenté dans l'Annexe A. La détermination des paramètres du modèle de van Genuchten pour la courbe de rétention et le comportement mécanique en déformations soumis à des chargements triaxiaux répétés pour des graves non traitées sont introduits dans l'Annexe B.

Comportement permanent en déformations d'un matériau granulaire

Les résultats d'essais triaxiaux à chargements répétés du sable de Missillac montrent que la déformation axiale permanente augmente avec l'augmentation de la teneur en eau, tandis que l'effet de la teneur en fines dépend de la teneur initiale en eau et de la sensibilité à l'eau des particules fines. L'augmentation du niveau de contrainte entraîne aussi une augmentation de la déformation axiale permanente.

Pour décrire la déformation axiale permanente, nous proposons une première loi empirique-analytique en prenant en compte l'effet de la teneur en eau et de la teneur en fines sur la base du modèle de Hornych (1993) et du modèle de Gidel

(2001). La bonne correspondance entre les résultats expérimentaux et les résultats de simulation montre bien la pertinence des approches proposées.

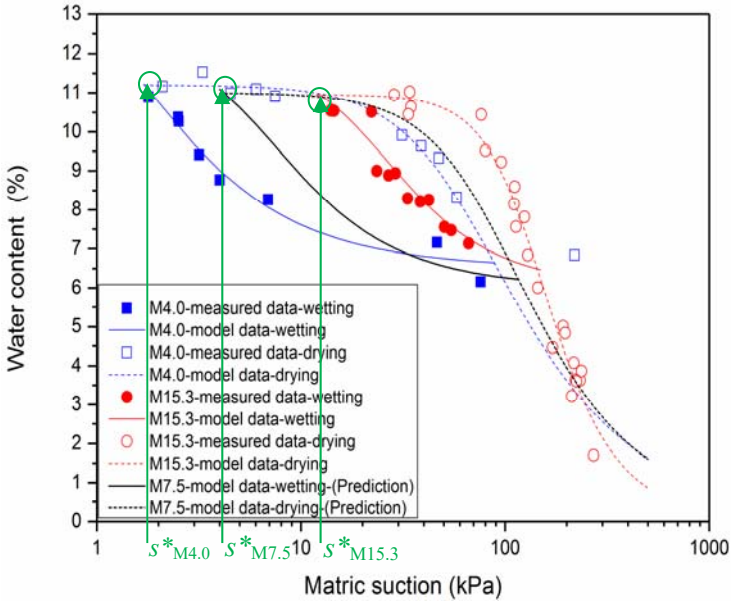

Figure 1. Courbes de rétention expérimentales et calées par le modèle de van Genuchten pour le sable de Missillac (M4.0, M7.5 et M15.3)

Les courbes de rétention sont également obtenues par la méthode du papier filtre pour le sable de Missillac à des teneurs en fines différentes (Figure 1). Le nouveau paramètre (s^*) est défini comme la valeur de succion correspondant à l'intersection des courbes de rétention en dessiccation et en humidification (Figure 1). Ensuite, on a développé une seconde loi de comportement avec la succion normalisée (s/s^*) qui présente moins de paramètres. Une corrélation satisfaisante a été obtenue entre les résultats expérimentaux et les résultats de simulation.

Ces deux lois proposées peuvent réduire le nombre de tests nécessaires pour prédire la déformation axiale permanente du sol.

Comportement résilient en déformations d'un matériau granulaire

Les valeurs des déformations résilientes dans les derniers cycles montrent la stabilisation de la déformation volumétrique (ε_v) et de la déformation déviatorique (ε_q). Une corrélation satisfaisante a été obtenue entre les déformations résilientes et la succion normalisée (s/s^*). Ensuite, l'effet marqué de l'anisotropie (Figure 2) sur le comportement résilient a été observé pour les deux sables M4.0 et M15.3: la différence entre la déformation axiale résiliente (ε_1^r) et la déformation radiale résiliente (ε_3^r) augmente avec la teneur en eau dans la phase de chargement isotropique ($\Delta q/\Delta p = 0$, $\sigma_3 = 90$ kPa), en particulier pour le sable M15.3 (Figure 2).

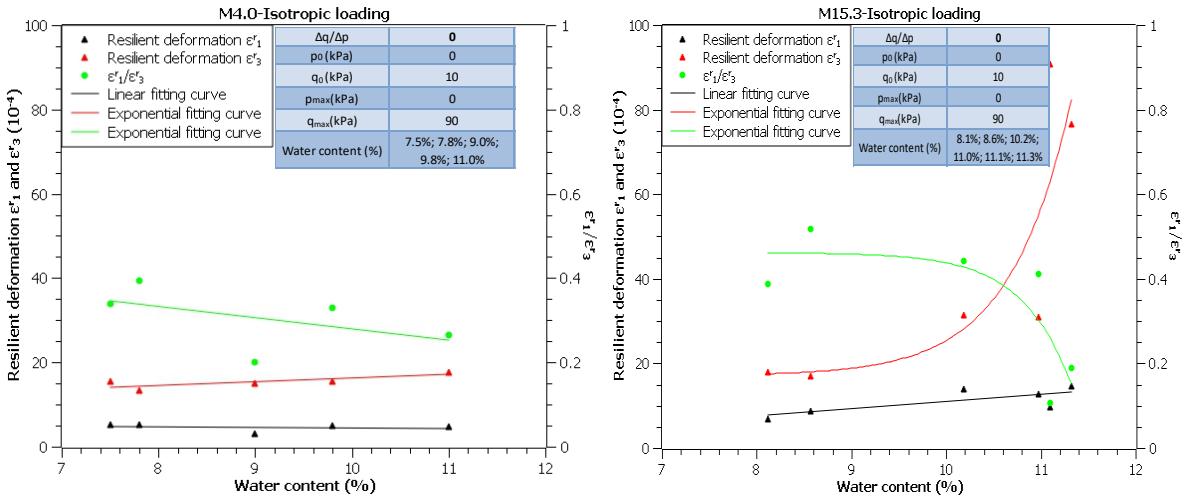

a) b)

Figure 2. Déformations résilientes (ε_1^r et ε_3^r) dans la phase de chargement isotropique ($\Delta q/\Delta p = 0$) pour le sable de Missillac M4.0 a) et M15.3 b)

Considérant l'effet de l'anisotropie, la loi de Boyce-Hornych (Hornych et al., 1998) a été modifiée dans un premier temps pour prédire la déformation volumétrique résiliente et la déformation déviatorique résiliente correctement. Dans un second temps, cette loi a été employée en introduisant le concept de contrainte effective pour les sols non saturés, en expliquant le phénomène des

grandes boucles ouvertes de déformation résiliente pour le sable M15.3 à des teneurs en eau importante (10 ou 11%) sous les faibles chemins de contraintes ($\Delta q / \Delta p = 0$; 0,5 et 1).

Comportement de l'état limite d'un matériau granulaire

Les résultats expérimentaux dans le cadre de la théorie de l'état limite montrent que les états limites peuvent être évalués en analysant la déformation permanente, le taux de variation de la déformation permanente et de la déformation réversible. De bonnes corrélations ont été obtenues entre la déformation permanente et la déformation réversible, confirmant les résultats obtenus dans la littérature. De plus, il a été observé que la succion normalisée (s/s^*) peut être utilisée pour évaluer la variation du module réversible avec le nombre de cycle de chargement. Finalement, en se basant sur la théorie de l'état limite, une frontière entre un état stable et un état instable est identifiée, correspondant à la courbe de rupture statique (Figure 3). Par conséquent, on peut distinguer un état stable et un état instable des matériaux granulaires par leurs teneurs en eau, leurs teneurs en fines et leurs états de contrainte.

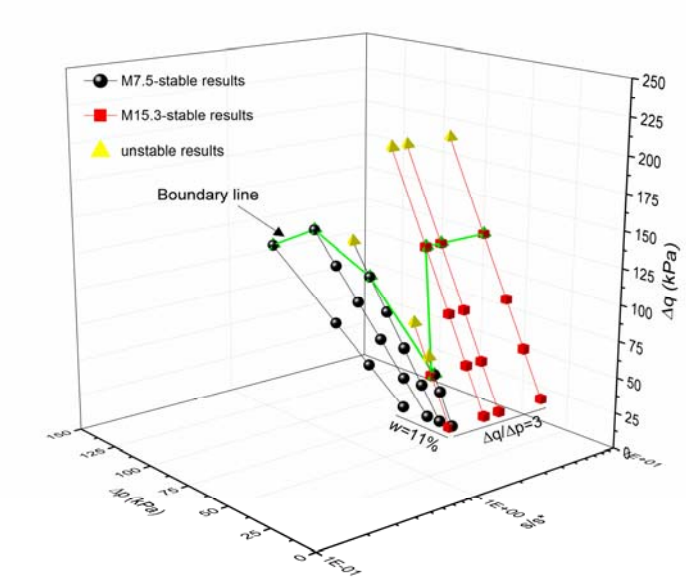

Figure 3. État de stabilisation du sol dans l'espace: Δp - Δq - s/s space*

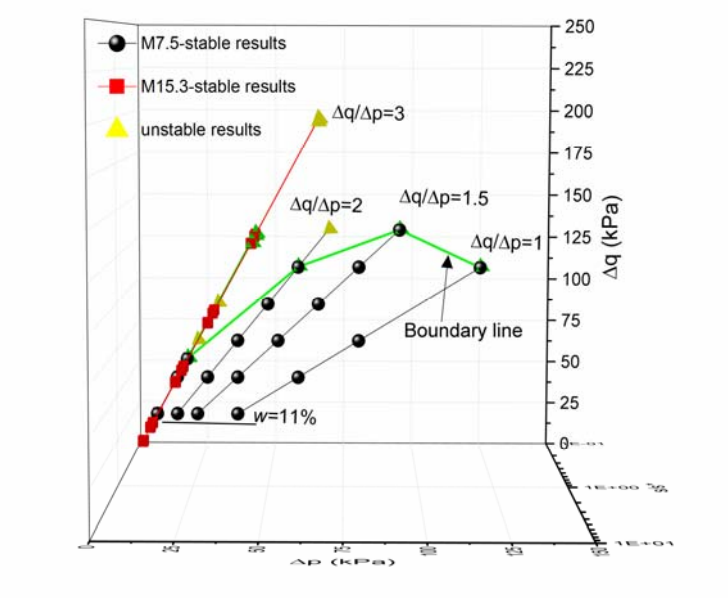

Figure 3-Continus

Conclusions et perspectives

Dans ce contexte, les résultats sont utiles pour une interprétation plus facile du comportement hydromécanique (comportement de déformation principalement) des matériaux granulaires dans des cycles de chargement et de déchargement répétés avec les variations doubles des teneurs en eau et teneurs en fines (représentant les différents états non saturés). Les modèles proposés peuvent montrer la bonne correspondance entre les résultats expérimentaux (déformation permanente et déformation résiliente) et les résultats de simulation. Ils peuvent réduire le nombre de tests nécessaires pour prédire le comportement permanant et résilient des matériaux granulaires.

En perspective, un certain nombre de points reste à traiter:

• La succion normalisée ($s/s*$) montre de bonnes interprétations du comportement de déformations permanentes et résilientes au lieu de la teneur en eau et la teneur en fines. Cependant, la définition de s * doit être clarifiée.

• Les modèles développés pour le comportement à court et long termes devraient être mis en œuvre dans la modélisation par éléments finis afin de prédire l'évolution de l'orniérage des chaussées.

• L'effet de la teneur en eau et de la teneur en fines sur le comportement hydromécanique des graves non traitées (GNT) doit être étudié selon les mêmes méthodes et comparés avec le sable de Missillac.

Bibliographie

Boyce, H. R. (1980). A non-linear model for the elastic behaviour of granular materials under repeated loading. Proceeding of International Symposium on Soils under Cyclic and Transient loading, Swansea, UK, 285-294.

Ho, X. N., Nowamooz, H., Chazallon, C., & Migault, B. (2014a). Effect of hydraulic hysteresis on low-traffic pavement deflection. *Road Materials and Pavement Design*, 15(3), 642–658.

Ho, X. N., Nowamooz, H., Chazallon, C., & Migault, B. (2014b). Effective stress concept for the effect of hydraulic hysteresis on the resilient behavior of low traffic pavements. *International Journal of Pavement Engineering*, 16(9), 842–856.

Ho, X. N., Nowamooz, H., Chazallon, C., & Migault, B. (2014c). Influence of fine content and water content on the resilient behavior of a natural compacted sand. *Road Materials and Pavement Design*, 15(3), 606–621.

Hornych, P., Corte, J. F., & Paute, J. L. (1993). Etude des déformations permanentes sous chargements répétés de trois graves non traitées. *Bulletin Des Laboratoires Des Ponts Et Chaussees*, 184, 45–55.

Hornych, P., Kazai, A., & Piau, J. M. (1998). Study of the resilient behavior of unbound granular material. In: Proceedings 5th conference on bearing capacity of roads and airfields, Trondheim, 3, 1277–1287.

Gidel, G., Breysse, D., Hornych, P., Chauvin, J. J., & Denis, A. (2001). A new approach for investigating the permanent deformation behavior of unbound granular material using the repeated load triaxial apparatus. *Bulletin Des Laboratoires Des Ponts Et Chaussees*. *233*, 5–21

Nowamooz, H., Chazallon, C., Arsenie, M. I., Hornych, P., & Masrouri, F. (2011). Unsaturated resilient behavior of a natural compacted sand. *Computers and Geotechnics*, 38(4), 491–503.

Nowamooz, H., Ho, X. N., Chazallon, C., & Hornych, P. (2013). The effective stress concept in the cyclic mechanical behavior of a natural compacted sand. *Engineering Geology*, 152(1), 67–76.

Werkmeister, S., Dawson, A. R., and Wellner, F. (2001). Permanent deformation behavior of granular materials and the shakedown concept. Transportation Research Record: Journal of the Transportation Research Board, 1757, 75–81.

Publications principales

Journaux

1. Jing, P., Nowamooz, H., & Chazallon, C. (2017 in press). Permanent Deformation Behaviour of a Granular Material Used in Low Traffic Pavements. Road Materials and Pavement Design. Published online: 08 Dec 2016. DOI: 10.1080/14680629.2016.1259123.

Conférences

1. Jing, P., Nowamooz, H., & Chazallon, C. (2016). Influence of Fine Content and Water Content on the Permanent Mechanical Behaviour of a Granular Material Used in Low Traffic Pavements. Proc.Geo-China 2016, 215-223.

2. Jing, P., Chazallon, C., & Nowamooz, H. (2017). Unsaturated resilient strain behaviours of a granular material. BCRRA 2017. Full paper accepted: 16/01/2017.

荆鹏

细粒及含水量对非粘结性颗粒材料的水力特性影响研究

摘要

非粘结性颗粒土通常作为基层和底基层材料应用于低交通量道路结构中。而在实际的服役过程中，道路结构往往承受着循环的，变化的水力条件。随着循环次数的增加，颗粒材料不可避免地发生着破裂和退化，从而改变了土体的粒径分布，增加了土体的细粒含量。此外，处于非饱和状态下的道路土体也会受到季节变化，降水等因素的影响，使得土体含水量发生变化，进而改变基质吸力条件。然而，目前在法国及欧洲使用的大多数的道路设计方法并不考虑细粒以及含水量的变化对于颗粒土的水力特性的影响。

在本论文中，考虑细粒含量，含水量，以及非饱和状态变化的前提下，更好地理解颗粒土在循环荷载作用下的水力特性（主要是变形特性）是本文的主要研究目标。为此，一系列的循环三轴实验被用来确定 Missillac 砂这种颗粒材料在不同细粒含量，不同含水量下的塑性和弹性变形行为。此外，不同细粒含量下，Missillac 砂的土水特征曲线也通过吸力实验获得了。

基于这些实验结果，既有的塑性和弹性变形预测模型被修改和改进，从而能够有效的适用于变化的细粒及含水量条件。最后，基于安定理论的分析方法也被应用在 Missillac 砂的变形特性上。

关键词: 颗粒材料, 循环三轴实验, 永久（塑性）变形, 弹性变形, 含水量, 细粒含量, 基质吸力, 安定理论.

Peng JING

ETUDES DE L'EFFET DES FINES ET DE LA TENEUR EN EAU SUR LE COMPORTEMENT HYDROMECANIQUE DES MATERIAUX GRANULAIRES

Résumé

Les matériaux granulaires sont souvent utilisés dans les chaussées à faible trafic, pour la réalisation des couches d'assise non liées. Dans la pratique, les chaussées à faible trafic sont soumises à des charges mécaniques et hydrauliques variables. Dans le cadre des cycles de chargement et de déchargement successifs, des particules endommagées peuvent se produire accidentellement conduisant aux modifications de la teneur en fines. De plus, les différents taux d'humidité peuvent provoquer des changements d'état insaturé. Cependant, actuellement la plupart des méthodes de dimensionnement des chaussées ne tient pas compte des variations précédemment citées ayant une influence significative sur la rigidité des couches de matériaux granulaires dans les chaussées à faible trafic.

L'objectif de la thèse est une meilleure compréhension du comportement hydromécanique (comportement en déformation principalement) des matériaux granulaires insaturés sous charge répétée en tenant compte des différents effets couplés: teneur en eau et teneur en fines. Une série d'essais triaxiaux à chargements répétés (TCR) est réalisée avec les différents échantillons de sable de Missillac remodelés à différentes teneurs en eau et en fines pour caractériser les comportements de déformation permanent et résilient. En outre, les courbes de rétention des sables de Missillac avec différentes teneurs en fines sont obtenues par des essais de succion.

Puis, sur la base des résultats expérimentaux, les modèles de déformations permanentes et réversibles existants sont améliorés pour prendre en compte les teneurs en fines et en eau variables. Finalement, le comportement de l'état limite du sable Missillac est estimé avec les effets des teneurs en fines et en eau.

Mots-clés: matériaux granulaires, triaxial à chargements répétés, déformation permanente, déformation réversible, teneur en eau, teneur en fines, succion matricielle, théorie de l'état limite.

Abstract

Granular materials are often used in low traffic pavement structures as unbound granular base and sub-base layers. In practice, low traffic pavements are subjected to variable mechanical and hydraulic loadings. Under the successive loading and unloading cycles, particles damage may accidentally occur which leads to fine content changes and the various moisture content may cause unsaturated state changes. However, most current pavement design methods do not consider the variations above which have a significant influence on the stiffness of the granular material layers in low traffic pavements.

The objective of this context is a better understanding of hydromechanical behaviour (deformation behaviour mainly) of the unsaturated granular materials under repeated loading taking into consideration the various coupled effects: water content and fine content. A series of RLTTs are conducted with the different remolded Missillac sand samples at different water contents and fine contents to characterize the permanent and resilient deformation behaviour. Besides, the soil water retention curves (SWRCs) of Missillac sands with different fine contents are obtained by suction tests.

Then, based on the experimental results, the existing permanent and resilient deformation models are improved to accommodate to the changeable fine content and water content. In the end, the shakedown behaviour of Missillac sand is estimated with the effects of fine content and water content.

Keyword: granular material, repeated load triaxial test, permanent deformation, resilient deformation, water content, fine content, matric suction, shakedown theory.